Cellular and Molecular Studies of the Ras-like GTPase MglA and its interplay with the bactofilin BacM of *Myxococcus xanthus*

Submitted to the University of Sheffield for the degree of Doctor of Philosophy

by

Koen Semeijn

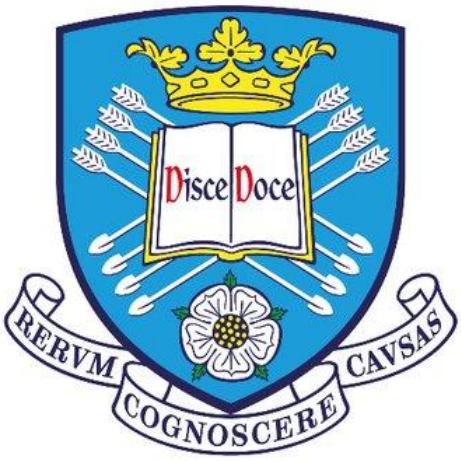

Thesis Supervisor

Dr. Egbert Hoiczyk

Department of Molecular Biology & Biotechnology

University of Sheffield

Firth Court

Western Bank S10 2TN

September 2019

Table of Contents

List of Abbreviations and Acronyms

BLAST	: basic local alignment tool
BSA	: bovine serum albumin
COPI	: coat protein complex I
COPII	: coat protein complex II
CTPM	: casitone, tris, magnesium sulphate, and potassium phosphate media
CTT	: casitone, tris media
EM	: electron microscopy
eYFP	: enhanced yellow fluorescent protein
GAP	: GTPase-activating protein
GEF	: guanine exchange factor
IPTG	: Isopropyl β- D -1-thiogalactopyranoside
kDa	: kilo Dalton
LB	: Luria-Bertani media
Lg-bit	: Large-bit
OD	: optical density
ON	: overnight
PBS	: phosphate buffer saline
PBSTB	: phosphate buffer saline + TWEEN-20 + bovine serum albumin
PCR	: polymerase chain reaction
SDS-PAGE	: sodium dodecyl sulphate polyacrylamide gel electrophoresis
Sm-bit	: small-bit
TPM	: tris, potassium phosphate, magnesium sulphate media
TWEEN-20	: polysorbate-20
WT	: wild-type

Acknowledgements

Firstly, I would like to thank Dr. Egbert Hoiczyk for offering me the opportunity to carry out this interesting PhD project under his supervision. I appreciate all his patience, guidance, and full support throughout this journey.

Secondly, I would like to thank Jeffery So, for his unwavering support and being my day-to-day lab buddy. Without his friendship, this journey would have been a lot more difficult.

Thirdly, I would like to thank Egbert Hoiczyk, Jeffery So, Eleojo A Nwokeoji, Mohsen MA Almakrami, and all the current and past members of the Hoiczyk lab, for making the lab such a lively, vibrant, safe, and happy place to work. This lab environment was not only important for my scientific development, but also my personal growth. I would like to thank all the students that I have supervised over the course of four years, for their efforts and input. These students include: Gregory Gilmour, Max Larkinson, Eleanor J. Taylor-Chilton, Maria Demou, Harry Mcdowell, Lydia S. Rawson, Benjamin Garforth, Ritika Bhaskar and Soubash Tirougnanam. Special thanks go to the two internship students from Singapore: Cherie Hong Yi Xin and Maxino Leanette Torres, for their hard work and friendship. Last but not least I thank Felicity Powell, Arthur Sonnemans, Niek de Lange, Chris James Munn and Emily Hunt for their friendship and support. In addition, I would like to thank Felicity Powell, Corinna Snashall, and Elizabeth Lees for proof reading my English.

Finally, my gratitude goes to my parents (Marjolein Semeijn-Visser and Jaap Semeijn), sister (Merel Semeijn), and brother (Rik Semeijn) for their love, encouragement and support.

Abstract

The small Ras-like GTPase MglA, the master regulator of myxobacterial A- and S-motility, was identified as a novel interaction partner of the bactofilin BacM, a morphologically important cytoskeletal protein. Initially, this interaction was confirmed using several independent methods and expanded to additionally test any interactions of MglA with the cytoskeleton protein MreB. Among others, these experiments identified a number of novel interactions between Ras-like GTPases and bactofilins, namely between MglA-BacM, MglA-BacO, and SofG-BacO. In addition, a previously published interaction between MglA and MreB could not be confirmed, despite the use of different experimental approaches, including a novel two-hybrid system in *M. xanthus*. Protein expression experiments indicated that MglA in *M. xanthus* is post-translationally modified, although the precise nature of this modification was not identified so far.

Detailed biochemical characterisations of MglA and BacM provided new insights into the nature of the interaction between these two proteins and their potential function(s) within the cell. MglA and/or BacM-associated cellular responses included: cell elongation, growth, hyper-reversals, adhesion, and spreading on hard agar. Importantly, the experimental results shed new light on the link between MglA-induced focal adhesion clusters and adventurous motility, indicating that these cell envelope-associated attachment sites may not be motor complexes, but instead areas of cell attachment that actually slow the cells down.

Finally, using pulldown-assays a number of novel interaction partners were identified for BacM, that point to the possibility that this morphogenetic cytoskeleton protein is an important platform for the orchestration of various cellular responses besides cell motility which range from the control of the cell morphology to the ability of the cells to respond to cold shock. Future research will need to elucidate these individual responses and to study whether they are more directly linked or only rely on BacM as assembly platform.

Chapter I

1. Introduction

Cytoskeletal proteins are structural components responsible for the shape of cells as well as the building blocks of cilia and flagella. In eukaryotes, they are filamentous proteins or protein assemblies that are composed of three major classes of proteins, namely, tubulin (the protein component of microtubules), actin (the component of microfilaments) and intermediate filaments (the components of connective tissue). Besides of their function in maintaining cell shape, cytoskeletal proteins also play important roles in other cellular processes such as cell cycle progression, intracellular organelle transport and motility to name a few (Shih & Rothfield, 2006). The discovery of FtsZ, the first bacterial cytoskeletal protein, twenty years ago heralded a new age of cell biology greatly expanding our understanding of the role and function of these important proteins (E. F. Bi & Lutkenhaus, 1991). Since then a large number of additional new bacterial cytoskeleton proteins have been identified including homologues of all three eukaryotic cytoskeletal protein classes. Even more surprisingly, recent research has revealed that prokaryotes possess many cytoskeletal proteins that are neither structurally nor functionally related to these three classes representing unique prokaryotic cytoskeletal elements. Nonetheless, like in eukaryotes bacterial cytoskeletal proteins contribute to many different cellular processes including cell morphogenesis, cell motility, cell division, and intracellular transport (Löwe & Amos, 1998; Van den Ent et al., 2001; Ausmees, Kuhn, & Jacobs-Wagner, 2003). They can function as scaffolds positioning specific target proteins to subcellular locations and thereby coordinating the recruitment of further proteins and spatially organize the cellular content (Coulombe & Wong, 2004; Fletcher & Mullins, 2010)

1.1 Bacterial cytoskeletal proteins

Within bacteria several cytoskeletal proteins including FtsZ (tubulin-like homologue), MreB (actin-like homologue) and crescentin (intermediate filament-like homologue) were found to have a scaffolding function at different positions within the cell. These three cytoskeletal elements are currently the best-characterized bacterial cytoskeletal proteins (Ingerson-Mahar & Gitai, 2012).

1.2 Bacterial tubulin homologs

In eukaryotes, microtubules are involved in the segregation of chromosomes, form the backbone of cilia and flagella, and act as tracks for intracellular transport. Tubulins form dynamic filaments that are instable meaning that they can rapidly switch from addition to subtraction of monomers in the filament. In eukaryotic cells, tubulins attach to the centromere during mitosis. Upon binding to the kinetochore they pull the chromosomes apart through depolymerisation (Wade, 2009). Biochemically, tubulins are GTP-binding proteins that consist of α and β subunits. Structurally, these subunits form protofilaments, which in turn form hollow tubular structures (microtubules) through the lateral interaction of thirteen protofilamants. Hydrolysis of the bound GTP is not required for normal polymerisation but is essential for tubulin de-polymerization (Hyman et al., 1992; Cabeen & Jacobs-Wagner, 2010). For a long time, tubulins were thought to be exclusively present in eukaryotes until the discovery of the distant tubulin homologue FtsZ revealed that homolog proteins also exist in bacteria (Harold P. Erickson, 1997). Other, more recently discovered, tubulin-like prokaryotic proteins are TubZ, required for plasmid stability in *Bacillus thuringiensis* (Larsen et al., 2007), and BtubA/B from *Prosthecobacter* species (Jenkins et al., 2002). TubZ is the motor component for the DNA positioning system (Larsen et al., 2007).

This system is involved in the maintenance of the virulence plasmids in *Bacillus* and *Clostridium.* Ensuring the inheritance of the plasmids by daughter cells during cell division (Baxter & Funnell, 2014). The exact function of the BtubA/B polymers is currently unknown (Pilhofer et al., 2011).

1.2.1 FtsZ, a tubulin homologue involved in cell division

FtsZ is a distant tubulin-like homologue that is involved in chromosome decatenation, the process that separates the two linked chromosomes during replication in bacteria. For that, FtsZ polymerizes in a GTP-dependent fashion into a structure called the Z-ring at the future division site located at mid-cell. GTP hydrolysis promotes the breakup of long FtsZ polymers *in vitro* and leads to Z-ring subunit turnover *in vivo* (Stricker, Maddox, Salmon, & Erickson, 2002; Mateos-Gil et al., 2012). The movement of FtsZ polymers at bacterial Z-rings is driven by GTP-hydrolysis and is essential for cell division and cell wall synthesis (Huecas et al., 2017). Functionally, the Z-ring is a highly dynamic structure that, besides of FtsZ, consists of at least 14 other different proteins, which form a complex often referred to as the divisome. Divisome formation starts In *E. coli* with the binding of FtsZ, FtsA, and ZipA, the three proteins that assemble into a proto-ring. At a later stage the rest of the divisome proteins are incorporated into this multiprotein complex, which controls the modification and synthesis of peptidoglycan at mid cell (Jiménez et al., 2011). FtsA is a member of the actin family that has a conserved amphipathic helix with which it tethers the Z-ring to the membrane (Pichoff & Lutkenhaus, 2005, 2007), while ZipA contains an N-terminal helix by which it is associated to the membrane. ZipA also binds to the cytoplasmic domain of FtsZ *via* a flexible linker (Hale & De Boer, 1999; Mosyak et al., 2000). Both FtsZ and ZipA have been shown to be involved in lipid vesicle deformation and cell membrane invagination in *in vitro* assays that mimic the more complex processes during cell division (Cabré et al., 2013). Based on super resolution light and cryo-EM microscopy, two contrasting models have been suggested to explain bacterial cell division.

The first model, was proposed based on electron cryotomography studies of *Caulobacter crescentus* and *E. coli,* which support the existence of long, continuous FtsZ filaments. According to this model, FtsZ forms a closed ring, which initiates the constriction of the cell. The overlapping filaments of the FtsZ ring then slide along each other to further decrease the ring's diameter to further constrict the cell (Szwedziak et al., 2014; **Figure 1B/C**). The second model is based on newly mounting evidence that support a fragmented morphology of the FtsZ ring in many bacterial species (Lyu et al., 2016). The evidence for this morphology mainly comes from super resolution fluorescent microscopy studies of fluorescently labelled FtsZ, FtsZ- or divisome-associated proteins as well as immune-fluorescence imaging of native FtsZ. Three-dimensional super resolution PALM (photoactivated localization microscopy) imaging was used to study the formation of the Z-ring upon expression of wildtype FtsZ and a FtsZ GTPase mutant D212A. The D212A mutation leads to a reduction of GTPase activity to ~7% of WT levels (Lyu et al., 2016). It was found that the *in vivo* organisation of the Z-ring is largely dependent on the intrinsic polymerisation properties of FtsZ and these in turn are influenced by the GTPase-activity and concentration of FtsZ (Lyu et al., 2016). Accordingly, the model supports a Z-ring organisation in which the ring is composed of loosely associated heterogeneously distributed FtsZ clusters (Lyu, Coltharp, Yang, & Xiao, 2016; **Figure 1A**). Fluorescently tagged FtsZ clusters were measured and are 118.3 ± 41.3 nm long and 86.3 ± 22.5 nm wide (Söderström et al., 2018). These FtsZ clusters are connected by few lateral contacts and irregularly distributed around the division plane (Holden et al., 2014).

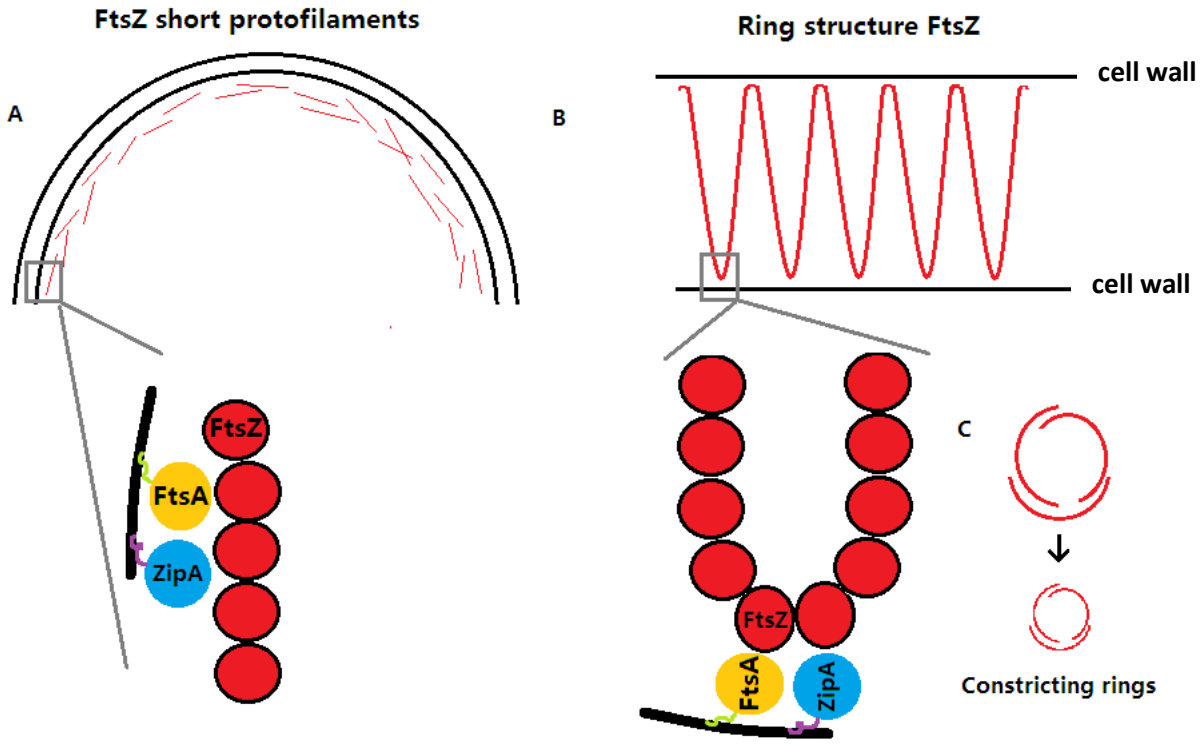

Figure 1. Two models of the Z ring. (A) *FtsZ protofilament formation: The Z ring consists of short overlapping filaments. These overlapping filaments have a thickness of 3 to 9 protofilaments. FtsZ is tethered to the membrane by binding to both FtsA (yellow) and ZipA (blue). FtsA is attached to the membrane via its C-terminal amphipathic helix (green). ZipA is attached to the membrane via its N-terminal transmembrane anchor domain (purple).* ***(B)*** *FtsZ ring structure model: During constriction, the ring develops into two helical spirals, leading to forces pushing the membrane inwards.* ***(C)*** *Constriction force generation and filament sliding. (Modified from Szwedziak, Wang, Bharat, Tsim, & Lowe, 2014).*

1.2.2 Mid-cell localisation of the FtsZ ring

In vitro experiments support the idea that FtsZ forms 30-50 subunits-long single-stranded filaments (Huecas et al., 2008; H. P. Erickson, Anderson, & Osawa, 2010). The process of filament formation starts with the dissociation of GDP from the FtsZ monomers, which initiates FtsZ dimerization. These FtsZ dimers then further polymerise into filaments (Chen et al., 2004). Based on these data, FtsZ could, at least in theory, form filaments throughout the cell. In reality however, FtsZ forms a single ring-like structure at mid-cell, so the stability and formation of the FtsZ filaments is spatially highly regulated within the cell. Several processes are involved in preventing erroneous FtsZ ring formation or activity. Some bacteria use DNA-binding proteins like SlmA and Noc, which inhibit FtsZ filament formation in a process termed nucleoid occlusion to ensure faithful chromosome segregation (Wu & Errington, 2012).

Another mechanism is based on the spatial tethering of the FtsZ ring (Martos et al., 2015). One protein involved in FtsZ tethering is FtsA. FtsA fulfils this function through two distinct processes, namely through the formation of FtsZ/FtsA co-polymers and its ability to destabilise formed FtsZ polymers. This destabilisation causes FtsZ monomers to detach from the filament in a process that, based on fluorescence microscopy and biochemical perturbations, supports a model of dynamic filament re-organisation ("movement") that is most likely based on tread-milling (Loose & Mitchison, 2014). FtsZ monomers were found to be immobile, when attached to the membrane, which is most likely the consequence of their binding to ZipA (Loose & Mitchison, 2014). ZipA and another protein, ZapA are membrane proteins that increase FtsZ polymerization. ZipA functions by promoting FtsZ monomer binding to the membrane, while ZapA is proposed to be involved in the alignment of FtsZ clusters (Buss et al., 2013). A third mechanism that bacteria use for focussing of the FtsZ ring are spatial gradients of proteins involved in de-polymerisation. In *E. coli* a reaction-diffusion system is in place to regulate the FtsZ gradient. This mechanism relies on three components MinC, MinD and MinE. MinC binds to MinD and is involved in the depolymerisation of FtsZ. MinD is an adenosine triphosphatase (ATPase) that dimerizes in the presence of ATP and binds to the lipid membrane, while MinE binds to membrane-bound MinD and induces ATP-hydrolysis by MinD. The ATP hydrolysis leads then to the detachment of MinD/MinE from the membrane (LaBreck et al., 2019). Together the function of these proteins are causing them to oscillate between the cell poles, thereby creating a gradient with a MinC minimum at mid-cell (Raskin & de Boer, 1999; Zieske & Schwille, 2014). A similar system is in place in *Myxococcus xanthus*, where the formation of the FtsZ-ring at mid-cell is driven by the positioning of the PomXYZ complex at the future division site on the nucleoid. The mid-cell positioning of the PomXYZ complex is itself driven by PomZ fluxes (Schumacher et al., 2017).

1.3 Bacterial actin homologs

One of the most important and highly conserved components of the eukaryotic cytoskeleton is actin. Monomeric (G-actin) polymerizes into filamentous actin (F-actin) within the cell. Filamentous actin consists of two proto-filaments which are twisted around one another forming a right-handed double helix (Holmes et al., 1990). In eukaryotic cells, actin transitions between its monomeric and filamentous state and these dynamics are controlled through nucleotide hydrolysis, ion concentrations and a large number of actin-binding proteins (Carlier, 1992). Polymerised actin has many functions in eukaryotic cells including cell shape determination, cell motility, cell polarity and regulation of transcription (Dominguez & Holmes, 2011). Alignment studies and X-ray crystal structures showed that actin, hexokinase and hsp70 protein share common conserved residues in five sequence motifs, which are involved in ATP-binding. Using these conserved amino acid patterns, database searches were performed that revealed that the proteins MreB, FtsA and StbA contained similar motifs indicating that they may represent bacterial actin homologues (Bork et al., 1992; Van den Ent et al., 2001).

1.3.1 MreB, an actin homologue important for the rod-shape of bacteria

In eukaryotes, actin is known to be essential for cellular processes such as sensing environmental forces, surface locomotion, cell division, internalization of membrane vesicles, and maintenance of cell shape (Ingerson-Mahar & Gitai, 2012; Pollard & Cooper, 2009). Similarly, MreB, a bacterial actin homologue is involved in cell shape maintenance through the incorporation of new peptidoglycan. MreB polymerizes into dynamic actin-like filaments in the presence of ATP (Garner et al., 2011; Van den Ent et al., 2001).

Patches of these MreB actin-like filaments have been observed to move circumferentially along the cell envelope in super resolution light microscopy studies (Dominguez-Escobar et al., 2011; Garner et al., 2011). In many species, MreB is an essential protein that localizes underneath the bacterial cell membrane through direct interaction with the membrane (Dempwolff et al., 2011). In *E. coli* and *T. maritima* it was found that this association to the membrane is facilitated by a membrane-binding N-terminal amphipathic helix (Salje et al., 2011). Upon binding to the membrane, MreB forms a complex with MreC and MreD (Kruse et al., 2005). MreC is a periplasmic protein that is involved in the spatial orientation of penicillin-binding proteins (PBPs) and a lytic transglycosylase, while MreD is essential for peptidoglycan synthesis through its interaction with the precursor-synthesizing enzymes MurG and MraY (White et al., 2010). Moreover, important connections were found between MreB proteins and a range of broadly conserved proteins that also contribute to the determination and maintenance of cell shape. Examples of these proteins are several PBPs including PBP2, which is involved in lateral cell wall elongation and PbP1A, which is a general PG synthase (Typas et al., 2011). Other protein interactors of MreB are MurG, RodZ and MraY (P. L. Graumann, 2004; Mohammadi et al., 2007; Margolin, 2009). MraY and MurG are lipid II synthesis enzymes, while MurG is also known to play a role as a scaffold for peptidoglycan synthesis (Favini-Stabile et al., 2013; Typas et al., 2011). In contrast, RodZ is bound to MreB *via* a cytoplasmic helix-turn-helix motif located at its N-terminus and attaches MreB to the cytoplasmic membrane (van den Ent et al., 2010). Studies in *E. coli* and *B. subtilis* have shown that MreB is essential for determining the characteristic rod-shape of these bacteria. Upon deletion of the *mreB* gene, cells tend to inflate, become round-shaped and eventually burst (L. J. F. Jones et al., 2001; Wachi et al., 1987). Finally, in 2013 a yeast-two-hybrid study found that MreB interacts with the tubulin-homologue FtsZ (see above). This interaction appears to be essential for septum synthesis and cell division in *E. coli*, thereby coupling bacterial cell division to cell elongation (Fenton & Gerdes, 2013).

1.3.2 Does MreB form helical filaments or patches?

Early work on MreB localization showed that the protein may form elongated filaments that follow a helical path perpendicular to the long axis of the cell. This arrangement was based on several studies using immunofluorescence with affinity-purified antibodies; the detection of epitope-tagged MreB by a fluorescent monoclonal antibody; and the detection of GFP-tagged Mbl, an MreB-like protein in *B. subtilis*. It was proposed that the MreB helices localize the cell wall synthesis enzymes thereby directing cell wall growth in a helical pattern (Daniel & Errington, 2003). Since 2011, a series of papers have been published that challenged this cell-spanning arrangement of the MreB filaments (reviewed in Errington, 2015). Importantly, it was discovered that MreB polymerizes on membranes as short anti-parallel filaments with an average length of ca. 200-300 nm substantially shorter than previously thought (Salje et al., 2011; van den Ent et al., 2014). Additional evidence for this new arrangement came from the observation that the originally reported MreB helices in *E. coli* were artifacts caused by the N-terminal yellow fluorescent protein tag. Native, untagged MreB expressed at the same level did not form extended helices and filaments. When instead an mCherry tag was added to an internal loop, MreB did not form helices in the cell (Swulius & Jensen, 2012). Finally, *in vivo* studies of MreB motion in *B. subtilis* and *Salmonella typhimurium* showed that MreB forms short filament patches that move around the cell circumference (Garner et al., 2011; Dominguez-Escobar et al., 2011). These movements of MreB patches were found to be driven by cell wall synthesis. Upon deletion or inhibition of cell wall-synthesizing enzymes, the MreB patches did no longer show motion (Garner et al., 2011; Dominguez-Escobar et al., 2011; S. van Teeffelen et al., 2011). In summary, this research indicates that MreB may tend to form disconnected patches rather than extended helices and filaments. Consequently, earlier research on the proposed cellular functions of MreB as extended helices and filaments requires careful re-evaluation.

1.4 Bacterial intermediate filament homologs

1.4.1 Crescentin, an intermediate filament-like homologue required for the curved shape of *C. crescentus*

Intermediate filaments in eukaryotes are characterized by coiled-coil-rich regions, which are flanked by N- and C-terminal sequences (Parry, 2005). Unlike actin and tubulin, intermediate filament proteins assemble nucleotide-independently into highly elastic fibers (Herrmann & Aebi, 2004). These fibers are involved in many physiological cellular processes including signal transduction, cell polarity, distribution of organelles and gene regulation (Iwatsuki & Suda, 2010). In 2003, a genetic screen identified in *C. crescentus* crescentin, the first bacterial intermediate filament-like homologue (Ausmees et al., 2003). It was found that in this widely-studied model organism, crescentin is essential for the characteristic curved shape of the cells. Interestingly, in exponentially growing cultures the protein forms a continuous filamentous structures on the inner side of the curved cells, while in stationary cultures the cells become helical and crescentin organizes into a helical structure (Ausmees et al., 2003; Briegel et al., 2006). Deletion of *crescentin* results in a loss of cell curvature leading to straight rod-shaped cells (Charbon et al., 2009). Using electron microscopy, quantitative rheology and fluorescence recovery after photo-bleaching experiments (FRAP), it was found that crescentin forms *in vivo* filamentous structures that undergo slow remodeling dynamics (Esue et al., 2010). Despite its importance in cell wall shape, it is currently not completely known how crescentin causes the observed cell curvature. One idea is that its physical presence at the inner curvature of the cells results in anisotropic peptidoglycan synthesis thereby preventing cell wall formation on the inner side of the crescent-shaped cell.

1.5 Bactofilins, a new family of cytoskeletal proteins

As discussed above, one recent surprising finding in the field of bacterial cytoskeleton protein research is that bacteria actually possess more rather than less diversity of these proteins than eukaryotes, and one of those new classes of bacterial cytoskeletal proteins is bactofilins. Bactofilins like intermediate-like filaments polymerize in a nucleotide-independent fashion into filaments. They are widely conserved within the bacterial kingdom and predominantly found in prokaryotes (Kühn et al., 2010; Deng et al., 2019). Bioinformatically, bactofilins can be easily identified by their conserved DUF583 domain, which is flanked by short variable N- and C-terminal regions. Recently, the atomic structure of this domain was determined by solid-state NMR showing that DUF583 is formed by a right-handed β helix with six turns surrounding a triangular hydrophobic core (C. Shi et al., 2015). Cryo-EM analysis of the bactofilin from *Thermus thermophilus* revealed that protofilaments are formed through end to end association of the beta-helical domains (Deng et al., 2019) (**Figure 2**).

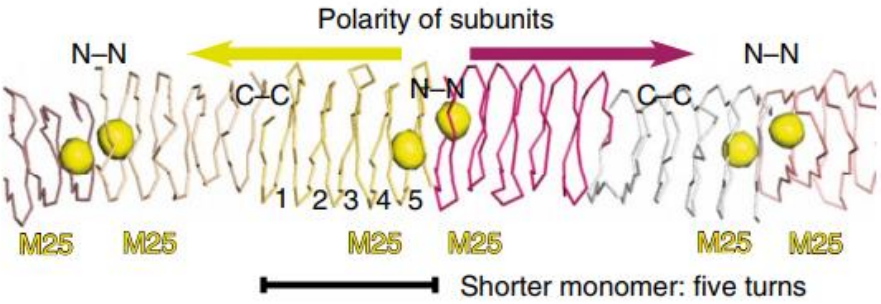

Figure 2. Crystal structure of ΔN-terminus Thermus thermophilus bactofilin. *Structure was solved using SeMet single-wavelength anomalous diffraction (SAD) phasing. The results indicating a non-polar head-to-head and tail-to-tail arrangement (Taken from Deng et al., 2019).*

The first ever identified bactofilin was CcmA (**c**urved **c**ell **m**orphology **A**) from *Proteus mirabilis*. Using a transposon-based genetic screen CcmA was shown to play a role in morphology as cells expressing a truncated version of the protein displayed high cell curvature. This curvature was higher in cells expressing a truncated form of CcmA then in those lacking the protein entirely.

In contrast, overexpression of CcmA resulted in enlarged and ellipsoidal cells in both *E. coli* and *P. mirabilis* (Hay et al., 1999). Since then homologues of CcmA have been studied in a number of other bacteria including *C. crescentus*, *Helicobacter pylori,* and *M. xanthus*. In all three bacteria, CcmA homologues were found to be involved in controlling cell morphology (Kühn et al., 2010; Sycuro et al., 2010; Koch et al., 2011). In *H. pylori,* CcmA was identified to be essential for the cell's characteristic helical cell shape. Together with three other proteins, Csd1-3 (**c**ell **s**hape **d**eterminant) CcmA appears to direct peptidoglycan synthesis to generate helical curvature. Upon deletion of any of these genes, the cells lose their helical shape and show different levels of curvature. The Csd1-3 proteins are peptidoglycan endopeptidase homologues containing conserved LytM domains and are thought to be directly involved in the remodeling of peptidoglycan. As CcmA does not contain a LytM domain or any other endopeptidase motif it was hypothesized to directly or indirectly interact with Csd1-3 at the membrane to influence cell shape morphology (Sycuro et al., 2010). CcmA has been shown to interact with Csd5 which is another cell shape promoting protein in *H. pylori* (Blair et al., 2018). Additionally, CcmA plays a role in cell swarming. A transposon mutant and a CcmA null mutant both formed elongated cells that were irregular curved and unable to swarm. Using immunogold labelling it was shown that CcmA attaches itself to the membrane (Hay et al., 1999).

In *B. subtilis,* the bactofilins BacE and BacF appear to be involved in the process of flagellar hook and filament assembly (Rajagopala et al., 2007). Their corresponding genes *bacE/bacF,* previously termed *yhbE/yhbF,* are highly conserved in most *Bacillus* species and a double deletion mutant displays reduced motility. Similarly, in *Treponema pallidum yhbE* and *yhbF* paralogues were found to interact with FliY and FliS, two proteins that are important for flagella formation. While FliY is located in the basal body complex of the flagellum, FliS functions as a chaperone of flagellin. Flagellin is the main structural protein forming the hollow cylinder structure of the flagellar filament (Rajagopala et al., 2007; El Andari et al., 2015). Deletion of both of these genes leads to reduced motility (Rajagopala et al., 2007).

Another set of bactofilins, called BacA and BacB, where discovered in *C. crescentus* and shown to be involved in cell morphology. BacA and BacB were found to form membrane-associated polymeric sheets that recruit PbpC (**p**enicillin **b**inding **p**rotein C) to the stalked cell pole to support the formation of the stalk, an elongated tube-like outgrowth of the cell body. Both, a *bacA* deletion and a *bacA/bacB* double deletion led to a reduced length of the stalk probably through the absence of PbpC (Kühn et al., 2010).

1.6 Bactofilins in *Myxococcus xanthus*

1.6.1 *Myxococcus xanthus*

M. xanthus is a heterotrophic, rod-shaped Gram-negative soil bacterium with an approximate length of 4-6 µm and a width of 0.5 µm (Kaiser, Manoil, & Dworkin, 1979; Blackhart & Zusman, 1985). Due to its complex life style, *M. xanthus* has become a model organism to study complex cellular and physiological processes such as biofilm formation (Palsdottir et al., 2009), changes in cell morphology (Licking et al., 2000), kinship (Dey et al., 2016), predation (Müller et al., 2016), altruism (Pathak et al., 2013), and cell fate determination (Arias Del Angel et al., 2018). These unusually evolved behaviors are most likely the consequence of the complex developmental life cycle of this quasi multicellular bacterium. This developmental life cycle consists of a vegetative growth cycle during which the cells move cooperatively as swarms and a developmental cycle in which, upon starvation, large numbers of cells (~10^5) coalesce into macroscopically visible fruiting bodies (Kuner & Kaiser, 1982). (**Figure 3**).

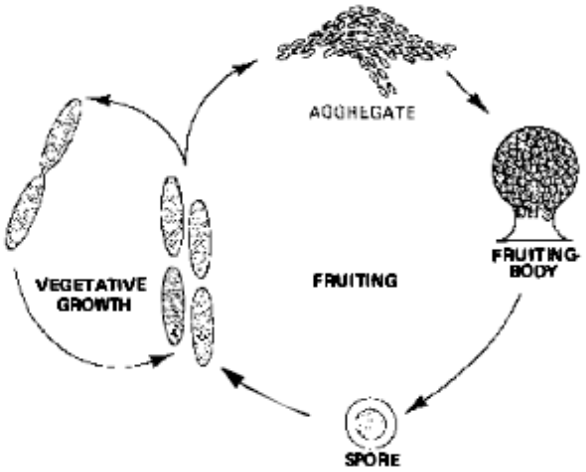

Figure 3. Developmental and vegetative growth cycles of M. xanthus (Taken from Kaiser, Manoil, & Dworkin, 1979)

1.6.2 Gliding motility in M. xanthus

Myxococcus xanthus cells move using two different types of motility, adventurous (A-) motility and social (S-) motility (Jonathan Hodgkin & Kaiser, 1979). A-motility facilitates single cell movement, while S-motility allows groups of cells to move together (W. Shi & Zusman, 1993). On hard agar (1.5%) A-motility is the dominant form of movement, while on soft agar (0.3-0.5%) the cells use S-motility. Both motility systems are coordinated, as the swarm expansion rate of S^+A^+ wild type cells is greater than the sum of the expansion rates of S^+A^- and S^-A^+ swarms (Dale Kaiser & Crosby, 1983).

1.6.3 Social motility

Three components are necessary for S-motility in *M. xanthus*: type IV pili, extracellular matrix exopolysacharides (EPS) and lipopolysaccharide (LPS) (H. Lancero et al., 2002; A. Lu et al., 2005). Type IV pili are slender protein projections, typically 5-7 nm in diameter that can extend up to 5 µm or more in length (Mattick, 2002). These pili power S-motility through repeated cycles of extension, binding and retraction, which pull the cells forward. *M. xanthus* has between 1-4 type IV pili at the leading cell pole (Y. Li et al., 2003), which generate an average retraction force of about 150 pN making them one of the strongest biological motors (Clausen et al., 2009). Both the extracellular polysaccharides (also referred to as fibrils) as well as LPS are thought to mediate the binding of the type IV pili during force generation (Y. Li et al., 2003).

Ten core proteins form the type IV pili machinery, pilA, pilB, pilC, pilD, pilM, pilN, pilO, pilP, pilQ, and pilT (Nudleman & Kaiser, 2004). Together they form a complex structure that spans the entire cell envelope and consists of four sub-complexes: the pilus, the outer membrane complex, the motor and the alignment complex. The up to 5 µm long pilus is composed of a single small protein PilA. The addition and removal of pilA subunits at the base of the pilus facilitates the extension and retraction of the pilus fiber (Jakovljevic et al., 2008). The outer-membrane complex consists of the PilQ oligomer, which forms the secretin channel through which the pilus can cross the outer membrane (Wall et al., 1999). The motor complex is composed of three proteins, PilB, PilC and PilT. PilB and PilT are two ATPases, that provide the energy for type IV pili extension and retraction cycles (Jakovljevic et al., 2008). Both, PilB and PilT bind to PilC, which is an inner membrane platform protein (Takhar et al., 2013). Finally, the alignment complex connects the outer membrane and motor complexes and is composed of PilM, N, O, and P (Leighton et al., 2016).

1.6.4 Adventurous motility

In contrast to S-motility, the motor of A-motility is less well understood. Nonetheless, several key features have been associated with A-motility in *M. xanthus*. One of these features is the secretion of slime. Although the precise function of slime in A-motility is still debated, it appears to play an important role in the process (Reichenbach & Dworkin, 1981; Wolgemuth et al., 2002; R. Yu & Kaiser, 2007). Another feature is the observation that A-motility uses the proton motive force (PMF) as an energy source. More specifically, it uses the pH gradient across the inner cytoplasmic membrane, which was demonstrated through the treatment of cells with nigericin, a substance that functions as an ionophore dissipating the PMF. Three proteins, AglQ, R and S appear to form a proton-conducting channel that is essential to harness the PMF for A-motility (B. Nan et al., 2011; Sun et al., 2011). Additional features are the synergism between A- and S-motility and the crucial role of MreB in A-motility (Dale Kaiser & Crosby, 1983; Treuner-Lange et al., 2015b).

Two models have been proposed to explain A-motility in *M. xanthus*. The first model suggests that the secretion of slime from arrays of nozzle complexes that are concentrated at both cell poles provides the propulsive force (Wolgemuth et al., 2002). Theoretic calculations showed that slime secretion would generate sufficient power to move the cells at the observed speeds (Wolgemuth et al., 2002). Importantly, during gliding the slime is secreted only at the lagging pole, which could propel the cell into the opposite direction (Hoiczyk, 2000; Hoiczyk & Baumeister, 1998).

The second model, termed the focal adhesion model is based on the formation of areas of contact between the cell surface and the substrate ("focal adhesions") which are crucial for motility (T. Mignot, 2007). The formation of these focal adhesions starts at the leading cell pole, where they bind at fixed positions to the underlying substrate. As the proteins forming the complexes are envelope-spanning, they are able to connect the substrate to the MreB cytoskeleton and upon binding start to move from the leading to the lagging cell pole. This movement is thought to drive the cell forward as the focal adhesions stay anchored in place thereby pushing against the secreted slime (T. Mignot, 2007).

1.6.5 The myxobacterial bactofilins BacM, N, O, and P

Four bactofilins are encoded in the genome of *M. xanthus*. BacM (MXAN_7475), and three homologues (BacN-P; MXAN_4637–4635) which are encoded by adjacent genes in a different operon. The deletion mutants of the *bacNOP* genes in *M. xanthus* resulted in no obvious phenotype. The deletion of BacM however lead to cells having a crooked cell morphology and becoming more susceptible to cell-wall targeting antibiotics (Koch et al., 2011). Following this initial characterization, a follow up study reported more detailed structural and functional data about BacM, one of the four initially discovered bactofilins (Zuckerman et al., 2015). In particular, it was shown that BacM forms *in vivo* electron microscopically visible fibers that could be isolated from cells.

These fibers were 0.2-8 µm long and 6-8 nm wide and composed of thinner, 3 nm wide filaments. BacM (MXAN_7475), the only protein component of the filaments and fibers is a 150 amino acids long protein that exist in the cell in two forms, a full-length form (16 kDa) and an N-terminally cleaved form (13 kDa) (Koch et al., 2011). Although the precise role of the N-terminal cleavage process is currently unknown, one possibility is that the cells may use the process to control the polymerization of the protein inside the cell as to prevent unproductive polymer formation.

BacP was shown to interact with SofG, which is a small Ras-like GTPase. BacP was found to localize at the subpolar region at both cell poles. SofG would bind to BacP and appears to use it as a track to reach the cell pole where it localizes two ATPases PilB and PilT. MglA, another Ras-like GTPase sorts PilB and PilT to the opposite poles (Bulyha et al., 2013). PilB and PilT enable the extension and retraction of type IV pili, thereby regulating S-motility (Jakovljevic et al., 2008). In 2017, an article was published showing that BacP was found to form a complex with BacO and BacN (Lin et al., 2017). The BacNOP complex interacts with a *parS*-binding protein ParB (MXAN_7476) and a DNA-partitioning ATPase ParA (MXAN_7477). The DNA-partitioning ATPases ParA was additionally found to interact with PadC (MXAN_4634). The integrity of these complexes was shown to be essential for proper nucleoid morphology and chromosome segregation. Important to notice is that PadC is located in the same operon as *bacNOP* and that ParA and ParB are located in the same operon as BacM (Lin et al., 2017). Previous deletion of BacM or MXAN_7474 did not affect chromosome segregation or cell growth (Koch et al., 2011).

1.7 Ras-like GTPases

1.7.1 Eukaryotic Ras proteins

Ras proteins heavily influence cellular organization and signalling (Rojas et al., 2012). They achieve this, by having a conserved GTP-binding domain, combined with highly divergent sequences and functions of the rest of the Ras protein (Jiang & Ramachandran, 2006). The G-domain contains six central β-sheets and five α-helices. It has a high affinity for GDP and GTP and almost none for GMP (Kjeldgaard et al., 1996). Concentrations of GTP and GDP in tissues and cells typically range between 0.3-0.5 mM and 0.03-0.06 mM, respectively (Karl, 1978). The G-domain contains five conserved fingerprint motifs that are located in five loops labelled G1 to G5. These loops are clustered around the nucleotide-binding site. The first loop, G1 is called the P-loop (GxxxxGKS/T), which is the glycine-rich phosphate-binding loop (**Figure 4**). The wrapping of the P-loop around the phosphates allows for the strong binding of the main-chain nitrogen with the negatively charged phosphate (Shalaeva et al., 2018). The lysine of the P-loop is crucial for nucleotide-binding and interacts with the β- and γ-phosphate oxygens (Schweins & Wittinghofer, 1994). G2 contains switch region I, which undergoes large conformational changes upon transition from the GDP to GTP-bound state and *vice versa* (Anand et al., 2006). There are two switch regions in the G-domain. Switch region I is involved in the exchange of GTP and GDP and is often called the effector region. The effector region binds to the effector protein upon exchange of GTP to GDP. This switch region, contains a highly conserved threonine, which is essential for binding to the γ-phosphate and contacting the magnesium ion (Spoerner et al., 2001). Magnesium plays a role in the geometry and charge of Ras-proteins during hydrolysis of GTP to GDP (Rudack et al., 2012). G3 is close to the switch II region and contains the DxxG motif. The aspartate in the G3 motif sits close to the magnesium ion in most Ras proteins. The switch II region does not have a conserved motif in Ras proteins except for a glycine (G60). This glycine is essential for effector interactions both with guanine exchange factors (GEFs) and GTPase-activating proteins (GAPs) (J. Bos et al., 2007).

G4 contains the N/TKxD motif in which the aspartate makes contact with the nitrogen atoms and the asparagine with the purine, thereby conferring specificity with the guanidiunium base (Papke et al., 2014). Finally, G5 contains the SAK motif in which the backbone amine interacts with the oxygen of the guanine. The serine side-chain stabilizes the G5 loop in a tight turn (Papke et al., 2014).

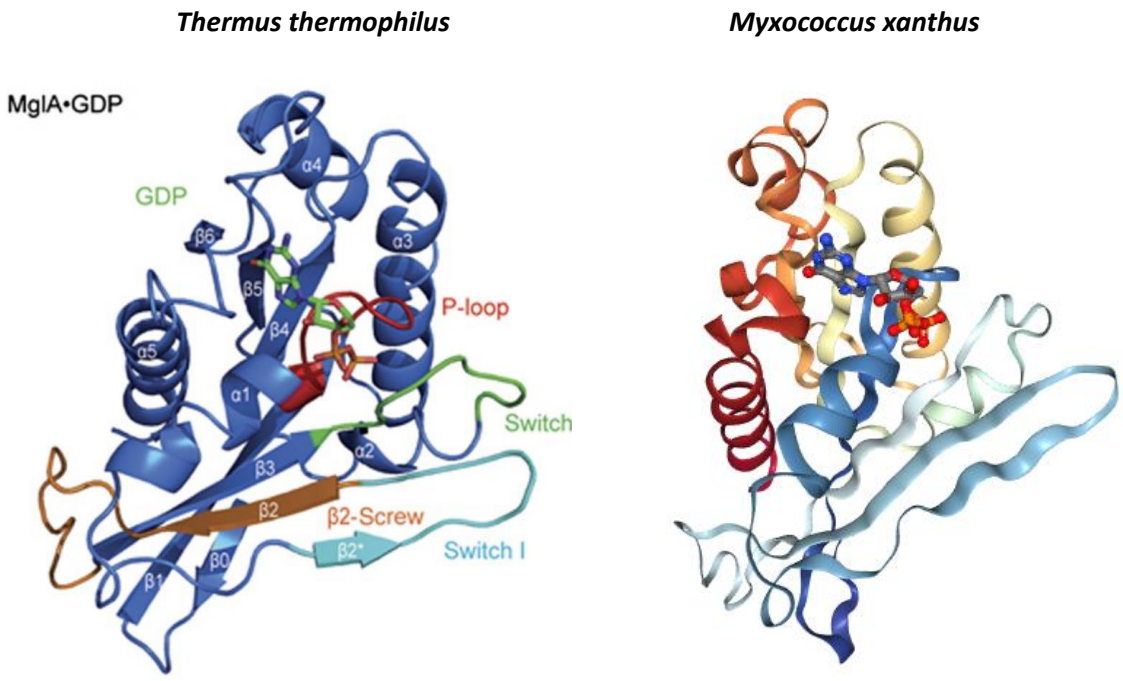

Figure 4. Structure of MglA from Thermus thermophilus (left) and Myxococcus xanthus (right). *T. thermophilus MglA has a 62% sequence identity with MglA from M. xanthus resulting in both proteins sharing a lot of structural similarity. Thermus thermophilus* MglA (red) P-loop (light blue) Switch region I (green) Switch region II (orange) β2 screw (dark blue) rest of the protein. The β2 screw moves as MglA transitions between its GTP and GDP bound form. The β2-screw movement is required to position crucial hydrophobic residues such as Leu55, Phe56, Phe57 and Phe59 involved in the MglA–MglB interface. (Taken from Miertzschke et al., 2011 (left) and *Galicia et al., 2019 (right)*).

1.7.2 Ras protein families

Based on their sequences and interaction with various other proteins, Ras proteins are divided into five subfamilies Rho, Ran, Arf/Sar, Rab, and Ras. They function, as signalling nodes and are triggered by both internal and external stimuli (Rojas et al., 2012). Ras proteins regulate intracellular signalling, which indirectly influences gene transcription. This in turn influences important cellular processes including cell growth, proliferation, differentiation, morphology, and apoptosis (Yamamoto, Taya, & Kaibuchi, 1999; Shao et al., 2000; Overmeyer, 2011).

1.7.2.1 Rho protein family

The Rho family is involved in cell cycle progression, gene expression and the regulation of actin (Marinissen, Chiariello, & Gutkind, 2001; Sit & Manser, 2011; David, Petit, & Bertoglio, 2012). This family of small RasGTPases is widely conserved having numerous family members in various species like *Saccharomyces cerevisiae* (7 genes), *Caenorhabditis elegans* (9 genes), and *Homo sapiens* (23 genes). The 23 genes from *H. sapiens* result in the formation of 26 different proteins due to alternative splicing. These 26 proteins are divided into six subfamilies, namely: Rho, Rac, Cdc42, Rnd, RhoBTB and RhoT/Miro. The RhoBTB and RhoT proteins are also referred to as atypical, due to their alternative function and structure (Bustelo et al., 2007). Rho/Rac proteins are controlled through a number of regulatory steps, which include: control of nucleotide-binding by GEFs and GAPs, regulation of subcellular localization, modulation of protein expression levels, and other regulatory events (Etienne-Manneville & Hall, 2002). Most Ras proteins require the docking onto the cell membrane in order to exert their function. Rho/Rac proteins achieve this by using a CAAX lipobox. The cysteine residue in this lipobox gets geranyl-geranylated or farnesylated (Maurer-Stroh et al., 2003).

Attachment of the isoprenoid group facilitates the localization of the GTPase to the endoplasmic reticulum, where the AAX region is proteolytically cleaved (Boyartchuk et al., 1997). After this step, the α-carboxyl group of the C-terminal cysteine gets methylesterified. In some of the Rho/Rac GTPases additional cysteines are palmitoylated. The isoprenyl group attached to the CAAX box plays a crucial role for the subcellular localization of these proteins (Michaelson et al., 2005). RhoB for example, localizes to endomembranes, when geranyl-geranylated and the plasma membrane, when farnesylated (Lebowitz et al., 1995). Upstream of the CAAX box is a polybasic region that is responsible for subcellular localization of several Rac proteins. Small changes in this region leads to differences in localization of these proteins. Rac1, Rac2 and RhoG localize to lipid rafts, endosomes, and caveolar vesicles, respectively (Filippi et al., 2004; Prieto-Sánchez & Bustelo, 2003).

Interestingly, in the case of Rac1, a proline-rich domain is located near the CAAX box, which is essential for the localization of this protein to focal adhesion complexes (Ten Klooster et al., 2006). The proline-rich domain interacts with an SH3 domain protein β-Pix. β-Pix is the Rac1 GEF protein, that is constitutively located at these focal adhesion sites. Important to mention is that some Rho/Rac proteins also undergo phosphorylation, which may influence their interaction with RhoGDIs (Rho guanine dissociation inhibitor) (Dermardirossian et al., 2004), stability in the membrane (Forget et al., 2002), and effector functions (Lang et al., 1996).

1.7.2.3 Ran protein family

Ran GTPases are involved in nuclear import and export processes. The regulators of Ran are asymmetrically localized, with the GEF (RCC1) in the nucleus and the GAF RanGAP1 in the cytosol (Ki & Ying, 2009). The asymmetrical localization of these proteins, creates a gradient of Ran-GTP across the nuclear envelope, which dictates the direction of the nuclear transport (Izaurralde et al., 1997; Nachury & Weis, 1999). Binding of Ran-GTP to importin β triggers the displacement and release of cargo into the nucleus (Lange et al., 2007). The export complex in the nucleus consists of the cargo-containing exportin1 (export signal) and Ran-GTP. Ran-GTP is hydrolyzed to Ran-GDP upon reaching the cytoplasm, due to the activity of RanGAP1, while the exportin1 is recycled (J. Bos et al., 2007).

1.7.2.4 Arf/Sar protein family

The Arf and Sar proteins are regulators of vesicle biogenesis in intracellular trafficking (Chavrier & Goud, 1999). The Arf1 and Sar1 proteins bi-directionally manage vesicular trafficking, between the ER and the golgi. The pathway from the ER to the golgi depends on Sar1 (Barlowe et al., 1994), while the pathway from the golgi to the ER depends on Arf1 (Lu et al., 2001).

These vesicles move protein and lipids between the ER and the golgi. Sar1 and Arf1 proteins are responsible for the recruitment of COP (coat proteins complex) proteins to the membrane and the initiation of the formation of COP-mediated vesicles. COPI coated vesicles are formed at the Golgi and traffic to the ER, while COPII coated vesicles are formed at the ER and go to the Golgi. Sar1 and Arf1 have both an α-helix at their N-terminus that is comprised of 20 hydrophobic and 20 hydrophilic amino acids, thereby creating an amphiphatic helix (Carlos et al., 1994). In the inactive GDP-bound form the amphiphatic helix is not exposed, however, due to a conformational change upon GTP-binding the amphiphatic helix is removed from its hydrophobic pocket (Bruno Antonny et al., 1997). Because of the amphiphatic helix, Arf1 and Sar1 stably associate with the membrane vesicle (Pasqualato et al., 2002). In addition, the N-terminal helix is involved in deformation of the membrane. Liposomes were shown to be highly deformed, when mixed with purified Arf1/Sar1 protein (Beck et al., 2008). Arf family proteins undergo myristioylation at the N-terminal helix. This modification is essential for the function and membrane-association of these proteins (Liu et al., 2009).

In contrast, Sar1 does not undergo myristoylation. The Sar1 GEF protein Sec12 is essential for the ER localization of Sar1 (d'Enfert et al., 1992). In contrast to Sar1, Arf1 has more diverse GEF proteins (Donaldson & Jackson, 2011). Sec23 is the GAP protein of Sar1 and forms a complex with Sar1 together with Sec24, termed the pre-budding complex. The pre-budding complex recruits Sec13/31 heterotetramer complexes, which are involved in linking the pre-budding complexes *via* polymerization. Sec13/31 complexes self-assemble into spherical lattice like structures in solution (Bhattacharya et al., 2012). Sec31 functions in this complex as the GAP stimulator of Sec23 (X. Bi et al., 2007). Importantly, Sec31 has a C-terminal proline-rich domain as the GAP stimulator. Within the complex the proline-rich domain binds both the surface of Sec23 and Sar1. It reaches the active site of Sar1, which optimizes the orientation of a catalytically important histidine residue of Sar1 (X. Bi et al., 2007).

For Arf1 the α, β', ε-COP forms the complex essential for the outer layer coat, that resembles the Sec13/31 structures (Hsia & Hoelz, 2010). However, the COPI coat does not possess GAP function, so the mechanism of Arf1 GAP activation remains to be elucidated.

1.7.2.5 Rab protein family

Rab GTPases are the largest family of small GTPases and are known as the master regulators of intracellular membrane trafficking (Diekmann et al., 2011). Different Rab GTPases localize to different subcellular localizations, thereby controlling specificity and directionality of membrane trafficking pathways (Hutagalung & Novick, 2011). Rab GTPases exist in both a soluble and membrane bound form. Membrane association is caused by the post-translational modification of C-terminal cysteine residues with one or two lipophilic geranylgeranyl groups (Pfeffer & Aivazian, 2004). The addition of geranyl groups is mediated by RABGGTB (GGTase II; geranylgeranyl transferase II) in cooperation with REP (Rab escort protein) (Ka et al., 2007). GDI is the GDP dissociation inhibitor of Rab-GTP and mediates the dissociation of membrane-bound Rab-GTP (Pfeffer & Aivazian, 2004). Similar to Rho proteins, compartment-specific GEFs seem to play a crucial role in defining the precise localization of Rab-GTPases. Rab-GTPases have been found to be essential for both exocytic and endocytic vesicle transport (Das & Lambright, 2016; Klinkert et al., 2016). Due to their role in vesicle transport a lot of Rab-GTPases control specialized structures including: lipid droplets, cilia, autophagosomes, tight junctions, inter-organelle membrane contact sites and focal adhesions (Marzesco et al., 2002; Martin & Parton, 2008; Deretic, Saitoh, & Akira, 2013). Membrane traffic has an impact on several cellular functions and therefore, Rab-GTPases indirectly control cell signalling, polarity, migration and division (Militello et al., 2013; de Franceschi et al., 2015).

1.7.3 Ras-like GTPases in *M. xanthus*

M. xanthus was the first bacterium, in which a Ras-like GTPase, termed MglA, was discovered (P. Hartzell & Kaiser, 1991). Using a genetic transposon-based screen, MglA was identified as a protein of unknown function, which later turned out to be important for both A- and S-motility (Jonathan Hodgkin & Kaiser, 1979; K. Stephens, Hartzell, & Kaiser, 1989; P. Hartzell & Kaiser, 1991). MglA is the only protein known to be essential for both types of motility in *M. xanthus* and is therefore termed the master regulator of myxobacterial motility (Jonathan Hodgkin & Kaiser, 1979; P. Hartzell & Kaiser, 1991). The active form of MglA (MglA-GTP) accumulates at the leading pole, where it spawns the formation of focal adhesion clusters involved in A-motility, while MglA-GDP, the inactive form, is found diffusely in the cytosol (Leonardy et al., 2010; Y. Zhang, Franco, Ducret, & Mignot, 2010; Miertzschke et al., 2011). MglB is the GAP protein of MglA and localizes to the opposite pole of the cell, where it functions in inactivating GTP-bound MglA through its conversion into MglA-GDP (Leonardy et al., 2010b; Y. Zhang et al., 2010). Sequence analyses showed, that MglA contains a variable N- and C-terminus and a conserved G-domain. This G-domain contains most of the conserved residues required for guanine binding and GTP hydrolysis. One minor difference is the replacement of an aspartate residue for a threonine in the conserved G4 motif. A more pronounced difference is the extra-long switch I region, which indicates MglA to be more closely related to the Arf subfamily (Miertzschke et al., 2011). Another Ras-like GTPase in *M. xanthus*, termed SofG, has been found to be essential for S-motility. SofG plays a role in the polar localization of two ATPases, PilB and PilT. PilB and PilT are essential for the extraction and retraction, respectively, of type IV pili. The type IV pili function as the motor complexes for S-motility in *M. xanthus* (Bulyha et al., 2013; Chang et al., 2016). Finally, the third RasGTPase in *M. xanthus* is the protein MXAN_2694. No clear phenotype has been found, when *MXAN_2694* was mutated or deleted in *M. xanthus* and therefore its function is currently unknown (Bulyha et al., 2013).

1.8 Scope of work

Preceding this work pulldown assays had identified the small RasGTPase MglA (K. Stephens et al., 1989, **Chapter II 2.3.1 Page 46**) as a potential interaction partner for the bactofilin BacM (Koch et al., 2011). Although interesting no direct study had been performed at the time to confirm or validate this important potential interaction between the master regulator protein of myxobacterial A- and S-motility MglA and the morphologically important cytoskeleton protein BacM. Therefore, the initial scope of this work was to confirm this interaction and to test whether MglA, as had been previously reported, also interacted with the cytoskeleton protein MreB (Mauriello et al., 2010).

To study the potential MglA-BacM interaction, the two proteins as well as a number of other bactofilins and small RasGTPases from *M. xanthus* were analysed using an *E. coli*-based bacterial two-hybrid system. The results of these studies confirmed the initial observation of the MglA-BacM interaction, while simultaneously showing that a previously described interaction between MglA and MreB could not be confirmed. Moreover, the other tested combinations of various bactofilins such as BacN, O, and P and small RasGTPases SofG and MglA showed that the employed assay was able to successfully reproduce previously published interactions between these two important groups of proteins (Bulyha et al., 2013). Although these two-hybrid results confirmed the initial discovery, it was difficult to determine whether the studied proteins were correctly folded inside the *E. coli* host environment. To address this problem, it was next tested whether the interactions could also be observed using a *M. xanthus*-based two-hybrid system. To establish such a novel two-hybrid system suitable plasmids were generated and introduced into *M. xanthus*. Moreover, to increase the sensitivity of detection the two-hybrid system was designed in such a way as to use a luciferase-based read out that substantially increased its detection limit. Using this novel engineered system, it was again confirmed that MglA and BacM interact directly with each other, but that the previously published interaction between MglA and MreB could not be confirmed. Therefore, it was concluded that MglA in *M. xanthus* binds to BacM but not to MreB.

During the course of these studies, detailed biochemical characterisations of MglA and BacM were performed that provided new insights into the nature of the interaction between these two proteins and their potential function(s) within the cell. Importantly, the experimental results shed new light on the link between MglA-induced focal adhesion clusters and adventurous motility indicating that these cell envelope-associated attachment sites may not be motor complexes. Intriguingly, these new results directly contradict the current proposed model that claims MglA-induced focal adhesion clusters are the molecular motors driving A-motility. Moreover, the investigation of BacM and MglA also indicated that these two proteins appear to be part of an output pathway that regulates the length of the cells. However, how this is accomplished is not yet clear. Finally, using pulldown-assays a number of novel interaction partners were identified for BacM that point to the possibility that this morphogenetic cytoskeleton protein is an important hub for the orchestration of various cellular responses ranging from the control of the cell morphology to the ability of the cells to respond to cold shock. Future research will be needed to elucidate these individual responses and to study whether they are more directly linked to BacM or only rely on BacM as assembly platform.

Chapter II

2. Identification and validation of cytoplasmic and membrane-associated interaction partners of BacM

2.1 Introduction

In the last decade, many advances have been made in terms of understanding the different functions associated with bactofilins across prokaryotes. Beginning with the finding that the bactofilin CcmA from *P. mirabilis* and BacM from *M. xanthus* are important for cell shape and multicellular swarming (Hay et al., 1999; Koch et al., 2011) to the understanding that binding of BacA and BacB to the stalk of the cell in *C. crescentus* is involved in recruiting the peptidoglycan synthase PbpC, which in turn plays a role in the extension of this part of the cell (Kühn et al., 2010). A similar morphological role is played by CcmA from *H. pylori* (Sycuro et al., 2010), which is essential for the helical cell morphology of the organisms that allows the cells to colonise the mucosal lining of the stomach. In contrast, the bactofilins BacE and BacF of *Bacillus subtilis* play a role in motility through the control of the assembly of the flagellar hook (El Andari et al., 2015) and LbbD, one of five bactofilins of *Leptospira biflexa* is essential for motility, although it also plays a role in establishing the periodicity of the helical cell and the integrity of the cell wall (Jackson, Schwartz et al., 2018). While BacM in *M. xanthus* plays mainly a role in morphology, the bactofilins BacN, O and P were shown to form a complex essential for both chromosome segregation and type IV pili-driven motility (Bulyha et al., 2013; Lin et al., 2017). Based on these observations, bactofilins seem to be involved in a multitude of important cellular functions including cell morphology, motility, and cell division.

In this chapter, the experiments will be described that were undertaken to identify potential interaction partners of BacM, one of four bactofilins in *M. xanthus*. Using two pulldown assays, one with soluble cytoplasmic proteins and the other with membrane-associated proteins, earlier findings of a postdoc, Dr David Zuckerman were confirmed as well as several interaction partners of BacM were validated. One of those interaction partners is MglA, the master regulator of A- and S-motility in *M. xanthus* (Jonathan Hodgkin & Kaiser, 1979; P. Hartzell & Kaiser, 1991). MglA is a small RasGTPase that is known to localise in clusters at the cell pole, which eventually brake up into smaller sub-clusters that travel on a helical track along the long axis of the cell (Patryn et al., 2010). During these intracellular movements, MglA is suggested to be part of membrane-bound complexes called focal adhesions. These focal adhesion complexes move along the cell membrane and are thought to be the motors driving A-motility (Mignot et al., 2007). To generate the force for A-motility, the focal adhesion complexes have been suggested to move along cytoskeletal proteins, a process that is powered by the proton motive force (B. Nan et al., 2011). Subsequent research identified the cytoskeletal protein MreB, an actin homologue as the interaction partner of MglA and this interaction was proposed to be essential for the formation of focal adhesion complexes as well as their movements (Mauriello et al., 2010). Based on this research, it was suggested that MglA binds to MreB and uses polymers of this protein as tracks. Intriguingly, previous pulldown experiments in our lab had indicated that MglA in pull down essays was found to bind to BacM. Therefore, experiments were designed to clarify whether MglA binds to BacM, or to MreB or to both proteins using pulldown assays as well as interaction assays of these three proteins.

2.2 Materials and methods

2.2.1 Bacterial strains and growth conditions

In all experiments the strains and growth media were prepared and used as described below. The wild-type strain was *M. xanthus* WT (DK1622). *M. xanthus* cells were grown in CTT medium (1% casitone, 1 mM K_2PO_4, 8 mM $MgSO_4$, 10 mM Tris/HCl, pH7.6) (J. Hodgkin & Kaiser, 1977). For the maintenance of cells on solid medium and the preparation of agar plates, 1.5% agar was added to the CTT medium. Antibiotics were added to the CTT medium and CTT agar after autoclaving. Antibiotics and media used in this research are listed in **Table 1**. The solutions were either autoclaved at 120˚C for 20 minutes or sterile filtered using a Millipore 0.22 µM filter. For *E. coli* strains, vectors were maintained in DH5α cells (Invitrogen) and proteins expressed in BL21 (DE3) or Rosetta$_{TM}$ cells (Invitrogen). The growth medium for *E. coli* cells was Lennox lysogeny broth (LB: 10 g/L tryptone, 5 g/L yest extract, 5 g/L NaCl) with 1.0% agar added for LB agar plates.

Table 1: Antibiotics and suplements used in this study

Suplements and antibiotics	**Solvent**	**Stock concentration** (mg/ml)	**Working concentration** (µg/ml)
Ampicilin (Amp)	dH_2O	100	100
Kanamycin (Km)	dH_2O	100	50
Tetracycline (Tc)	70%[a] Ethanol	20	10
Chloramphenicol	ddH_2O	25	25
Isopropyl-β-D-galactopyranoside (IPTG)	ddH_2O	1 M	1 mM
Vanillate	ddH_2O	25 mM	5, 50, 500 µM

a: percentages are weight per volume

2.2.2 Cloning

The pET-DUET plasmid was used for the expression of different combinations of our genes of interest under the T7 promoter in *E. coli*. This vector contains two multiple cloning sites, which are both preceded by a T7 promoter, lac operator and a ribosome binding site. The vector carries a pBR322-derived ColE1 replicon, *lacI* gene and ampicillin resistance gene. Genes cloned into the multiple cloning site one were sequenced using the pET upstream primer in combination with the DuetDOWN1 primer. Genes cloned into the second multiple cloning site were sequenced using the DuetUP2 primer in combination with the T7 terminator primer. The pMR3679 plasmid was used for the expression of MglA in *M. xanthus*. The pMR3679 vector contains a kanamycin resistance gene, a vanillate promoter and a 1.38 Kbp region, allowing it to incorporate in the *M. xanthus* genome at the *attB* site. Plasmids used in this chapter are listed in **Table 2**.

Table 2: Strains used in this chapter

Strains for expression in *E. coli*	**Expression**	**Reference**
pET-DUET $BacM_{28\text{-}150}$	BL21 cells	This study
pET-DUET $BacM_{28\text{-}139}$	BL21 cells	This study
pET-DUET $BacM_{28\text{-}134}$	BL21 cells	This study
pET-DUET MreB	$Rosetta_{TM}$ cells	This study
pET-DUET MglA	Bl21 cells	This study
pET-DUET MglA	$Rosetta_{TM}$ cells	This study
Strains for expression in *M. xanthus*	**Expression**	**Reference**
pMR3679 MglA	WT (DK1622)	This study

2.2.3 Overexpression of proteins in *E. coli* and *M. xanthus*

The N-terminus of BacM in purified filaments had previously been identified to begin with amino acid 28 (Koch et al., 2011). Therefore, it was decided to express BacM and the C-terminal truncated versions of BacM starting from serine 28. $BacM_{28\text{-}150}$, $BacM_{28\text{-}139}$, $BacM_{28\text{-}134}$, MreB and MglA were cloned into the pET-DUET vector (Invitrogen) and DNA fragments were amplified by PCR using purified *M. xanthus* WT (DK1622) genomic DNA as a template. For the amplification of the DNA fragments, the primers listed in **Table 3** were used. The fragments were isolated using a gel extraction kit (GeneJET gel extraction kit; Thermo Scientific) and then subsequently cloned into the pET-DUET or pMR3679 plasmid. PCR fragments and plasmids were digested with the appropriate restriction enzymes for 1 hour at 37 °C. To the plasmids 1 µl of phosphatase was added and left incubating for 30 minutes at 37 °C. Both the plasmids and PCR fragments were PCR purified using a PCR purification kit (Qiaquick PCR purification kit; Qiagen). PCR fragments were ligated (Rapid Ligation Kit, Roche) into their respective plasmids. Plasmids were used to transform heat shock competent *E. coli* DH5α cells, by incubating the cells with the plasmids for one minute at 42 °C. The identity of the insert in each vector construct and the correct nucleotide sequence were confirmed by automated sequencing at the Core Genomic Facility of the University of Sheffield. Plasmids for the expression in *E. coli*, confirmed by sequencing, were transformed into heat shock competent BL21 or Rosetta$_{TM}$ cells at 42 °C. Positive clones were picked from LB agar plates containing kanamycin or ampicillin. Plasmids for the expression in *M. xanthus*, confirmed by sequencing, were transformed into competent *M. xanthus* cells using electroporation. Around 1000 ng of plasmid was added to 50 µl of competent *M. xanthus* cells. The *M. xanthus* cells were added to a electroporation cuvette. Cells were electrocuted using an electroporator at 0.65 volt. After electroporation 1 ml of CTT medium was added and the cells are transferred to a sterile Eppendorf tube. Cell suspension is left shaking for 4 hours or overnight at 30 °C. The *M. xanthus* cells were mixed with CTT soft agar containing the appropriate antibiotic and then plated on CTT agar plates containing the appropriate antibiotic. Colonies were picked once they reached the surface of the plate and started spreading.

Table 3: Primer list

Primers	**Description** **Forward primer (F)** **Reversed primer (R)**	**Sequence 5' to 3' end**
M. xanthus		
Mx_MglA_F_XbaI	Fwd primer *M. xanthus* MglA gene; XbaI; Mxan_1925	**ATCGC** *TCTAGA* ATGTCCTTCATCAATTACTCATC
Mx_MglA_R_EcoRI	Rev primer *M. xanthus* MglA gene; EcoRI; Mxan_1925	**ATATA** *GAATTC* CGCTTGCTTCAACCACC
E. coli		
Ec_MreB_F_NdeI	Fwd primer *E. coli* MreB gene; NdeI; NC_000913.3	**CACAT** *CATATG* GGATTATCCCTTAGTATGTTG
Ec_MreB_R_XhoI	Rev primer *E. coli* MreB gene; XhoI; NC_000913.3	**TATAT** *CTCGAG* TTACTCTTCGCTGAACAGGTC
Ec_MglA_F_XbaI	Fwd primer *M. xanthus* MglA gene; NdeI; Mxan_1925	**ATCGC** *CATATG* ATGTCCTTCATCAATTACTCATC
Ec_MglA_R_XhoI	Rev primer *M. xanthus* MglA gene; XhoI; Mxan_1925	**ATATA** *CTCGAG* CGCTTGCTTCAACCACC
Ec_BacM_F_NdeI	Fwd primer *M. xanthus* BacM gene; NdeI; Mxan_7475	**ATATA** *CATATG* TCTGGTGAGGTCCAC
Ec_ BacM_R_XhoI	Rev primer *M. xanthus* BacM gene; XhoI; Mxan_7475	**ATATA** *CTCGAG* CTACTTCTTCTCGCCACC
Plasmid primers		
pET upstream	For sequencing multiple cloning site 1	ATGCGTCCGGCGTAGA
DuetDOWN1	For sequencing multiple cloning site 1	GATTATGCGGCCGTGTACAA
DuetUP2	For sequencing multiple cloning site 2	TTGTACACGGCCGCATAATC
T7 Terminator	For sequencing multiple cloning site 2	GCTAGTTATTGCTCAGCGG

For the overexpression in *E. coli,* cells were grown ON (overnight) in 10 ml LB with kanamycin added. This overnight culture was then added to 1 L LB, which was grown until the cells reached an OD_{600} = 0.4-0.6. IPTG was added to a final concentration of 1 mM and *E. coli* cells were induced overnight at 37 °C shaking at 200 rpm. Cells were harvested by centrifugation using a JA-500 rotor at 8000 rpm for 10 minutes at 4 °C. For the overexpression in *M. xanthus,* cells were grown ON in 25 ml CTT with kanamycin added. This overnight culture was then added to 1 L CTT, which was grown ON to a high cell density. The expression using the pMR3679 plasmid was induced using 500 µM vanillate ON at 30 °C shaking at 200 rpm in a baffled flask. Cells were harvested by centrifugation using a JA-500 rotor at 8000 rpm for 10 minutes at 4 °C.

2.2.4 Isolation BacM, BacM$^{\Delta C139\text{-}151}$, BacM$^{\Delta C134\text{-}151}$

BacM was overexpressed using the pET-DUET system as described above. The resulting cell mass was weighted and resuspended in 20 mM Tris/HCl, pH 7.6, at 1 ml/mg cell dry weight. Next, the cell suspension was sonicated on ice using a sonic dismembrator model 505 (Fisher Scientific), using 30 second pulses 3-9 times. Cell breakage was montitored using an AX10 Zeiss light microscope. To the broken cells urea to a final concentration of 1 M was added. 500 µL of this solution was added on top of 2 ml of a cesium chloride gradient in a SW55 tube. The cesium chloride gradient solution contained 1.35 mg/ml cesium chloride, 1 M urea, 0.5% β-dodecyl maltoside in 20 mM Tris HCl, pH 7.6. This solution was spun at 55,000 rpm in an SW55-TI rotor for 15 hours at 4 °C. The BacM protein filaments formed a cloudy white layer in the middle of the cesium chloride gradient. This layer was carefully isolated using a gradient fractionator (Buchler Instruments auto DENSI-FLOW II C). The isolated protein was dialyzed against 1 M urea, 20 mM Tris/HCl, pH 7.6 for at least 4 hours at 4 °C. The BacM protein solution was then loaded on a sucrose gradient containing 40% sucrose and spun in an SW41-TI rotor for 15 hours at 4 °C. BacM protein filaments were isolated and dialyzed as described above. BacM filaments were run again on a cesium chloride gradient as described above.

The purified proteins were dialyzed against 20 mM Tris/HCl, pH7.6 for at least 4 hours at 4 °C and the purity of the proteins were checked using SDS-PAGE (**Figure 7**) and electron microscopy.

2.2.5 Additional isolation methods BacM

Isolation 1.

The BacM band from an SDS gel was cut out and put in 20 mM Tris/HCl, pH 7.6 buffer inside a dialysis bag. The BacM band was run off the SDS gel, by putting the dialysis bag in a gel tray and running it at 100 volt. The BacM isolated this way was checked for filament formation using electron microscopy. This isolation resulted in the reformation of BacM filaments, indicating how robust this protein is in its ability to repeatedly form filaments even after denaturation.

Isolation 2.

E.coli cells with overexpressed BacM were re-suspendid in about 50 ml 50 mM Tris pH 7.0. Cells were sonicated 3x for 20 seconds using a sonic dismembrator (model 505 Fisher Scientific). The cell suspension was centrifuged at 12.000 g for 5 minutes. The cell free extract was separated and sonicated 3x for 10 seconds. Ammonium sulphate was added to the cell free extract to a final concentration of 1.7 M. The cell free extract was spun at 43,000 g for 10 minutes. The pellet was re-suspended in 3 ml of 8 M urea, 50 mM HEPES pH 7.0 and was stirred for 1 hour at room temperature. This solution was spun at 70.000 g for 20 minutes and the supernatant was applied onto a gel filtration column (Superdex 200). The isolated fractions containing BacM were collected and applied onto Q-HP and SP-HP columns. The columns were washed with 8 M urea, 50 mM HEPES pH 7.0, then with the same buffer containing 1 M NaCl. Fractions containing BacM were isolated and concentrated using VivaSpin columns.

2.2.6 Isolation of membrane-associated proteins from *M. xanthus*

For the pulldown experiment membrane-associated proteins were isolated and solubilized. *M. xanthus* cells were spun down at 8000 rpm in a JA-500 rotor for 10 minutes at 4 ^{o}C. The cells were re-suspended in deionized H_2O containing 5 mM N-ethylmaleimide, which was first dissolved in ethanol. The addition of ethyl maleimide was aimed at preventing the autolysins in *M. xanthus* from breaking down the membrane. Cells were spun at 10.000 rpm for 10 minutes at 1 ^{o}C. The cells were broken using the cell mill for 5 minutes at 4 ^{o}C. Unbroken cells and cell envelopes were harvested at 10.000 rpm for 10 minutes at 1 ^{o}C. These steps were repeated 3 times. After the third round of cell milling only membranes were left. This pellet was dissolved in 20 mM Hepes pH 8.3 containing 0.5% dodecyl maltoside. This solution was spun initially at 10.000 rpm and after that at 25.000 rpm JA-25 rotor for 10 minutes each at 1 ^{o}C. The dissolved membrane-associated proteins were used for the pulldown.

2.2.7 Pulldown of BacM mixed with solubilized membrane proteins

Isolated BacM filaments were dissolved in 0.1 M $NaHCO_3$, 100 mM NaCl, 20 mM Tris/HCl, pH 8.5. Cyanogen-bromide activated resin (GE Healthcare Life Sciences) was washed and swollen using ice-cold 1 mM HCl for 30 minutes. A total of 200 ml ice-cold HCl was added to 1 gram of dry gel in aliquots. The supernatant was removed by gentle filtration between each aliquot addition. The resin was washed with 10x columnn volume of deionized H_2O, before being washed with $NaHCO_3$/NaCl coupling buffer (5 ml per gram dry gel). The resin was then immediately transferred and mixed with the BacM filaments. This solution was left rocking for 2 hours at room temperature. BacM filaments that had not bound to the matrix were washed off using $NaHCO_3$/NaCl coupling buffer. The unreacted groups where blocked with 0.2 M glycine, pH 8.0 for 2 hours at room temperature. The blocked resin was extensively washed using initially coupling buffer and then with 0.1 M acetate buffer, pH 4.0, containing 0.5 M NaCl. This step was repeated five times.

The resin was then equilibrated with 20 mM HEPES, pH 8.3. Solubilized membrane proteins (3.5 ml) were run 3x over the cyanogen beads with the bound BacM filaments. The beads were then washed using 10x column volumes of 20 mM Hepes, pH 8.3. Onehundred microliters of beads were removed and dissolved in 100 µl SDS solubilization buffer containing 8 M urea and fresh 1mM DTT. These samples were boiled for ~ 10 minutes prior to loading 50 µl on a 4-20% tris/glycine SDS gel.

2.2.8 Isolation of MreB polymers

Two start-up cultures of the pETDUET1-MreB Rosetta$_{TM}$ strain were grown in 10 ml LB containing ampicillin 100 µg/ml and chloramphenicol 25 µg/ml. After ON growth at 37 °C these cultures were used to inoculate two 1L LB flasks containing ampicillin and chloramphenicol. These cultures were grown to an OD600 = 0.4-0.6 before the addition of 1 mM IPTG. After induction, cultures were grown ON at 37 ^{o}C while shaking at 200 rpm. The ON cell cultures were spun down at 8000 rpm in a JA-20 rotor for 10 minutes at 4 ^{o}C. Around 15 grams of cells were collected from the 2L cultures and dissolved in 15 ml of polymerization buffer (20 mM HEPES pH 7.5, 100 mM NaCl, 2 mM $MgCl_2$). Cells were sonicated using a soniprep 150+ on ice 3-9 times for 30 seconds at full power. The cell breakage was evaluated using an AX10 Zeiss light microscope. Spun the cell suspension at 75000 g for 10 minutes at 4 ^{o}C in a JA-25 rotor. This centrifugation resulted in the formation of a thick yellow/brownish pellet and a purple fluffy layer on top. The fluffy layer was dissolved in polymerization buffer containing 1M urea to a final volume of 7 ml. Next, 0.4% lauroyl sarcosinate and 0.4% Triton X-100 were added to the suspension of the fluffy later and was left rocking at 4 ^{o}C for one hour. An 85% sucrose solution in polymerization buffer was prepared and 500 µl added to an SW55-TI rotor tube. On top of this solution 2.5 ml of a 35% sucrose solution was added. Then 100 µl of a pre-prepared lipid solution (Avanti Polar Lipids, total *E. coli* lipid extract) was added on top of the 35% sucrose.

This was then carefully mixed with 1 ml of a 5% sucrose solution forming a slightly yellowish top layer. 250 µl of the pre-prepared MreB containing solution was next carefully pipeted on top of the 5% sucrose solution and sunk until it hit the 35% sucrose layer. Next, 92 µl of a 100 mM ATP solution was added to the top layer (5% sucrose layer) of the gradient ensuring the presence of an excess of ATP. The centrifuge tubes were kept standing at room temperature for 1 hour before being centrifuged at 257,000 g for 18 hours at 4 ^{o}C in an SW55-TI rotor. This centrifugation resulted in a white fluffy band on top of the 35% sucrose layer. Close underneath the white band was a yellowish band, which contained very little MreB. All the MreB that associated with the liposomes was found in the upper white band. This band was taken up and dialyzed against polymerization buffer containing 2 mM ATP. Finally, the samples were analysed using electron microscopy.

2.2.9 Isolation of native MglA

WT (DK1622) cells were grown overnight in 25 ml CTT at 200 rpm and 32 ^{o}C. This culture was used to inoculate two 1 L CTT flasks, which were left shaking ON at 30 °C. Cell cultures were centrifuged at 8000 rpm in a JA-20 rotor for 10 minutes at 4 ^{o}C. Around 10 grams of cells were collected from the 2L cultures and dissolved in 10 ml of polymerization buffer (20 mM HEPES pH 7.5, 100 mM NaCl). Cells were sonicated using a soniprep 150+ on ice 30 seconds at full power. The six times sonicated cells were centrifuged at 100,000 g for 1 hour in a SW55TI rotor. The resulting supernatant contained the soluble proteins, which were collected, while the pellets were discarded. The lysate was run over nickel beads with MglA being in the flowthrough. This solution was dialyzed against 1 M urea, 20 mM HEPES pH 7.5, 100 mM NaCl. The flowthrough containing MglA was run again over beads that were washed with 1M UREA, 20 mM Hepes pH7.5, 100 mM NaCl before being washed twice with 10 volumes of polymerization buffer until the solution became clear. Finally, MglA was eluted using 50 mM imidazole, 20 mM HEPES pH 7.5, 100 mM NaCl.

2.2.10 Isolation of overexpressed *M. xanthus* MglA

WT *M. xanthus* cells containing the pMR3679 MglA expression plasmid were grown ON in 25 ml CTT containing 100 µg/ml kanamycin, at 200 rpm and 32 ^{o}C. The ON culture was used to inoculate two flasks of 1 L CTT containing kanamycin 100 µg/ml, which were left shaking ON at 30 °C at 200 rpm. The next day, when the cultures had reached an OD_{600} = 0.6-1, the expression of MglA was induced, through the addition of vanillate at a final concentration of 500 µM. The cultures were left shaking for another 12-16 hours at 30 ^{o}C at 200 rpm. The cell cultures were harvested at 8000 rpm in a JA-20 rotor for 10 minutes at 4 ^{o}C. Around 10 grams of cells were collected from the two cultures and resuspendid in 50 mM Tris pH 8.0. The cells were sonicated six times using a soniprep 150+ on ice for 30 seconds at full power. The sonicated cells were centrifuged at 100,000 g for 1 hour in a SW55Ti rotor. The cell free extract was applied onto a 5 ml His-Trap column at a flow rate of 5 ml/min. A 10 column volume gradient of 0.5 M NaCl, 50 mM Tris pH 8.0 containing 0-0.35 M imidazole was applied to the column. Most MglA was in the flow-through fraction. To the flow-through 4 M NH_4SO_4 was added and spun at 43.000 g for 10 minutes. The supernatant was collected and applied onto a 5 ml Phe-HP column. Fractions containing MglA were combined and concentrated using VivaSpin columns. The collected solution was separated on a gel filtration column (Superdex 200). Fractions containing MglA were collected and applied on a Zeba column to desalt the protein solution. The purity of the protein isolated was checked using SDS-PAGE.

2.2.11 Electron microscopy

To visualize purified proteins in the electron microscope commercially available 400 mesh carbon-coated copper grids were used (Electron Microscopy Sciences, Hatfield, PA). As carbon is hydrophob, these grids had to be first glow-discharged before the sample could be evenly applied to the grid surface. Therefore, the grids were placed onto a glass slide and positioned into a vacuum chamber of a custom-build glow discharge unit (Biozentrum, University of Basel).

The discharge unit was evacuated for 5 min using a two-stage turbo pump (Edwards Vacuum, Burgess Hill, Sussex), before the high voltage power was slowly increased to about 40% output or until a plasma could be seen. After glow discharge the grids were removed and placed carbon-surface down onto drops containing the BacM or MreB samples. They were left on the samples for 1 minute, then washed twice on deionized H_2O, and negatively stained for 1 minute using unbuffered 2% uranylacetate. After that excess liquid was removed with a filter paper and the grids kept in a storage box. The grids were viewed under a Philips CM100 electron microscope at a high-tension voltage of 100 kV. Images were recorded using a CCD camera (Gatan, Milton, Abingdon) at magnifications ranging from 5 to 45,000-fold. Selected images were converted into TIF images before being further processed using Fiji.

2.2.12 Generation of 100 nm unilamellar liposomes

Total *E. coli* lipid extract from AVANTI polar lipids was used for the formation of liposomes. Using a glass Pasteur pipette, a total of 1 ml of lipid solution was added to a round bottomed flask (or conical flask). A stream of nitrogen gas was applied to evaporate the chloroform, which left a film of lipid on the glass. The lipids were left for 10 minutes under the stream of nitrogen to ensure that no chloroform was left. To the lipid film, 1 ml of polymerization buffer (20 mM HEPES pH 7.5, 100 mM NaCl, 2 mM $MgCl_2$) was added and vortexed for ~15-45 minutes until the lipid film was completely re-suspended. Once the solution had become “cloudy”, the flask was put inside a vacuum desiccator. After a vacuum had formed, the air source was closed and the flask was left for at least 1 hour. Two filter papers were soaked in polymerization buffer before the extruder was assembled and polymerization buffer was passed 2-3 times through the extruder. Then this lipid solution was taken up using a Hamilton syringe and passed through the extruder 15 times, before the liposome solution was decanted into an Eppendorf tube. For the extrusion 100 nm membranes (Avanti Polar Lipids) were used (Hope et al., 1985; Szoka & Papahadjopoulos, 1980).

2.2.13 Mass spectrometry sample preparation

The to be identified bands were cut out of the gel using a scalpel. Each of the excised bands were cut into 1–2 mm cubes, and these cubes were transferred to a microcentrifuge tube. To remove the stain from the gel, 500 µL of 50 mM ammonium bicarbonate/50 % ACN was added and the samples were incubated overnight with shaking. The supernatant was extracted and discarded. Gel samples were washed and dehydrated by repeating twice each of the following incubations for 10 min with shaking: 500 uL of 50 mM ammonium bicarbonate, 500 µL of 50 mM ammonium bicarbonate/50 % ACN and 500 uL of ACN. After each incubation, the supernatant was discarded. Next, 200 µL of 50 mM TCEP was added to the samples and they were incubated for 20 min at 70 °C. Samples were spun using a tabletop centrifuge and the liquid was discarded. Samples were cooled to room temperature. 200 µL of 50 mM IAM was added to the gel pieces and they were left in the dark for 30 min at room temperature with shaking. Samples were spun using a tabletop centrifuge and the liquid was discarded. Gel pieces were washed and dehydrated again with same steps as describe above. 200 uL of trypsin solution at 1ng/uL was added to the gel pieces. The gel pieces were left on ice until rehydrated with trypsin solution. Samples were spun briefly and incubated at 37 °C overnight. Digestion was stopped by adding 100 µL of ACN and incubating the samples at 37°C. Supernatant containing the digested peptides was transferred into a new microcentrifuge tube. Peptides were extracted from the gel pieces by the sequential addition of 50 µL of 0.5% formic acid, 100 µL of ACN, 50 µL of 0.5% formic acid, 100 µL of ACN and 100 µL of ACN and incubating the gel pieces for 15 min at RT with shaking. Supernatants were transferred and pooled together into a separate tube after each ACN extraction. Peptides were dried using a SpeedVac concentrator, then resuspended in 0.5% formic acid and used for injection in the LC-MS/MS system.

2.2.14 Liquid chromatography tandem mass spectrometry (LC-MS/MS)

Peptides were separated in a Dionex Ultimate 3000 uHPLC (Thermo Scientific) with an Acclaim™ PepMap™ 100 C18 trap column (3 µm particle size, 75 µm X 150 mm) and an EASY-Spray™ C18 column (2 µm particle size, 50 µm X 150 mm) using a 35 min gradient at 0.25 µL/min with 0.1% formic acid in water (mobile phase A) and 0.1% formic acid in 80% ACN (mobile phase B) as follows: 0-3 min, hold at 3% B; 3-21 min, from 3% B to 40% B; 21-21.1 min, from 40% B to 90% B; 21.1-26 min, hold at 90% B; 26-26.1 min, from 90% B to 3% B; 26.1-35 min, re-equilibrate at 3% B.

MS/MS analysis was performed on a LTQ Orbitrap Elite (Thermo Scientific) hybrid ion trap-orbitrap mass spectrometer equipped with an EASY-SprayTM Ion Source. MS survey scans in positive ion mode were acquired in the FT-orbitrap analyzer using an m/z window from 375 to 1600, a resolution of 60,000, and an automatic gain control target setting of 1 × 10E6. The 20 most intense precursor ions were selected for the acquisition of MS/MS spectra in the ion trap (Normal Scan Rate) using collision-induced dissociation (CID) with normalized collision energy of 35%, activation time of 10 ms, activtion Q of 0.25, isolation width of 2 Th, and automatic gain control target value of 1 × 10E4. Ions with charge state 1+ were excluded from precursor selection. Monoisotopic precursor selection was activated. Dynamic exclusion for precursor ions was applied for 45 s after 1 fragmentation count and a repeat duration of 30 s.

2.2.15 LC-MS/MS Data Analysis

For all experiments, MS/MS data files were used for protein identification using MaxQuant software (Cox and Mann, 2008) version 1.5.5.1. Default MaxQuant parameters were used except for the following: protein database was the Myxococcus xanthus Strain DK1622 Uniprot proteome (downloaded on the 15th March, 2017) or the Escherichia coli BL21-DE3 Uniprot proteome (downloaded on the 1st September, 2016) calculation of iBAQ values was selected; variable modifications, Oxidation(M), Acetyl (Protein N-term); fixed modifications, Carbamydomethylation(C). MaxQuant results were imported into Excel and subjected to interpretation.

The best hits from the hit-lists obtained, were determined based on IBAQ score (molar quantities of protein), sequence coverage, score, molecular weight matching the band in the SDS gel, and the number of peptides identified.

2.3 Results

2.3.1 Overexpression of BacM leads to *E. coli* cell chain formation

Intriguingly, overexpression of BacM in *E. coli* cells led to the formation of characteristic cell chains (**Figure 5A**). As *E. coli* does not possess any bactofilin-encoding genes in its genome, it appears to lack the mechanisms that are necessary to disassemble the cell-spanning bactofilin cytoskeleton during cell division. This deficiency allows the cells to perform cell divisions but not to resolve them, resulting in the formation of cell chains, which are not observed in un-induced cells (**Figure 5B**). BacM-overexpressing *E. coli* cells were cryo-substituted and thin sectioned (**Figure 5C/D**) so as to further test whether the chaining of the cells was indeed caused by the accumulation of BacM fibres. As can be seen in **Figure 5D**, individual cells within the cell chains were connected through a thin cytoplasmic bridge that, at higher magnification, was clearly filled with fibrillar material. Although individual BacM fibrils or filaments can not be resolved due to the intrinsic resolution limit of thin sections (ca. 5 nm), the fibrillar nature of the material together with the observation that these cell connections were missing in the absence of BacM expression strongly suggested that they were the result of the accumulation of BacM fibres that cannot be resolved by the cells during cell division.

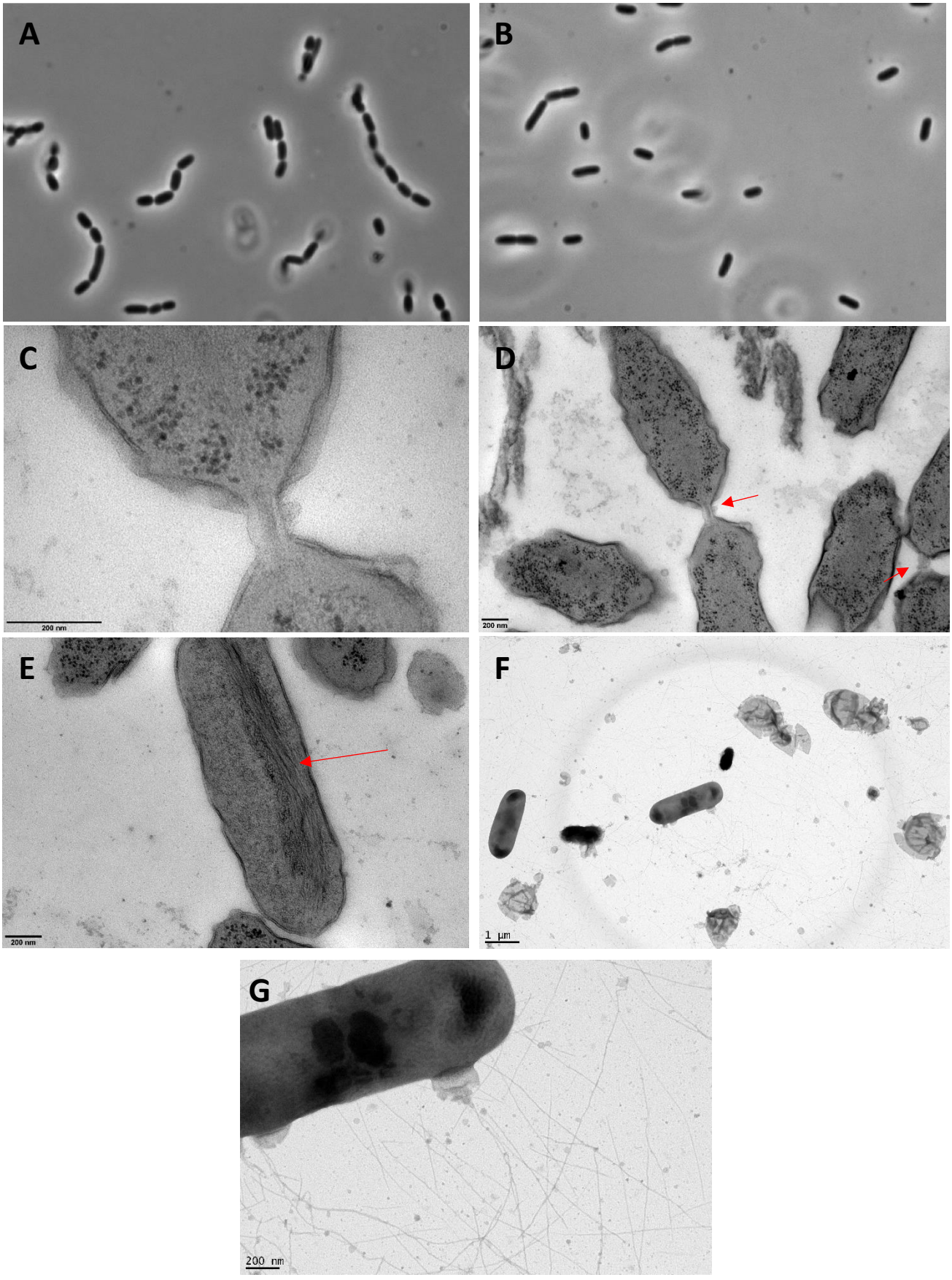

Figure 5 Overexpression BacM in E. coli cells. *(A) BacM expression leads to E. coli cell chain formation through un-resolved cell divisions. (B) Un-induced E. coli cells (C/D) Cells showing BacM fibres forming a cytoplasmic bridge between cells indicated by red arrows. (E) Intracellular bundles of BacM filaments inside an E. coli cell indicated by a red arrow (F/G) E. coli cells after sonication. The lysed cells are surrounded by liberated BacM filaments*

2.3.2 Pulldown assays of His-tagged BacM and His-tagged C-terminally truncated BacM with cell lysate

In order to identify cytoplasmic BacM-interacting proteins, a pulldown assay had been previously performed in the laboratory by Dr David Zuckerman, a former post-doctoral student (unpublished). For this assay, isolated and purified his-tagged BacM fibres were mixed with a cytoplasmic extract of vegetative *M. xanthus* cells. Since the presence of multiple proline residues at the C-terminus indicated a possible function of this part of the protein in the interaction with other proteins (Zuckerman et al., 2015), two different BacM versions were used for the pulldown. The first version of BacM fibres contained the proline-rich C-terminus ("full length"), while the second version lacked this part of the protein. Additionally, both versions lacked the first N-terminal 27 amino acids, because it had been previously shown that isolated native BacM fibres are composed of an N-terminal cleaved version of the full-length protein missing these amino acids (Koch et al., 2011). Based on the hypothesis that cytoplasmic proteins may specifically interact with the proline-rich C-terminus of BacM, this study focused primarily on bands that were only present in the pulldown with full-length BacM (**Figure 6**, lane 2), but absent in the lane showing interactions with the C-terminal truncated BacM (**Figure 6**, lane 3). All unique bands labelled A to I were identified using mass spectrometry and the *M. xanthus* genome sequence information (Goldman et al., 2006, **Table 4**).

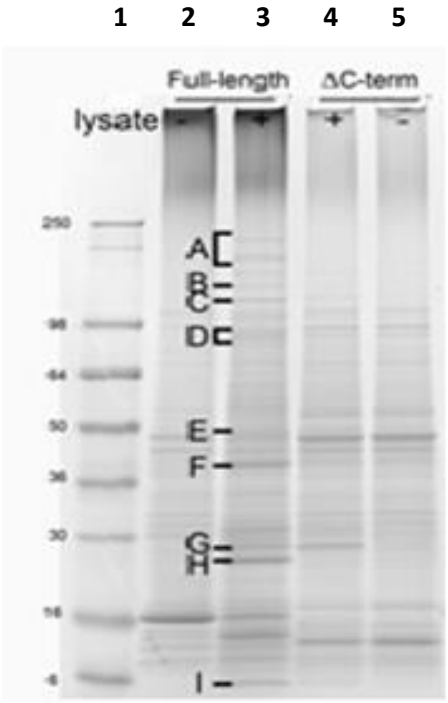

Figure 6. Pulldown of BacM fibres mixed with M. xanthus lysate. *Lane 1) see blue protein marker, Lane 2) full-length BacM without lysate, Lane 3) full-length BacM with lysate, Lane 4) ΔC-terminus BacM with lysate, Lane 5) ΔC-terminus BacM without lysate. Samples were run on a 4-20% Tris/glycine gel. Taken with kind permission from David Zuckermann.*

Table 4. Proteins found to potentially interact with the C-terminus of BacM. *MXAN numbers (left) and potential assigned functions/names of the protein(s) (right).*

Name	Function
A* MXAN_6735	CheY-like histidine kinase/response regulator
B* MXAN_4870	AgmU
C* MXAN_1450	TonB-dependent receptor
D* MXAN_2485, MXAN_4864	Type II DNA topoisomerase A, AgmV
E* MXAN_4433, MXAN_4634	S1C family peptidase, ParB
F* MXAN_4295	Patatin-like phospholipase
G* MXAN_5530	Hypothetical protein
H* MXAN_1925	MglA
I* MXAN_3345, MXAN_0672, MXAN_3582 and MXAN_6037	CspA, CspC, CspD and CspE

A careful inspection of the identified proteins revealed that they were not random but that some of them were clearly functional related. In particular, two functional groups of proteins were identified that are involved in A-motility (MglA, MXAN_1925 and the MglA-associated focal adhesion complex proteins; MXAN_4870 and MXAN_4864) and the cellular cold shock response (MXAN_3345, MXAN_0672, MXAN_3582, MXAN_6037 as well as a putative type II DNA topoisomerase, MXAN_2485). Besides these functional related protein groups a few individual, not obviously linked potential interaction partners were identified: the serine peptidase MXAN_4433, a ParB-like protein (PadC, MXAN_4634), a patatin-like phospholipase (MXAN_4295), a CheY-like response regulator (MXAN_6735), a TonB-dependent receptor (MXAN_1450), and a hypothetical protein of unknown function (MXAN_5530). The significance of the identified proteins will be discussed in the discussion section **(page 62)**.

2.3.3 Isolation of overexpressed BacM from *E. coli* BL21 cells

BacM was overexpressed using *E. coli* BL21 cells and isolated as described in **Materials and methods Chapter II 2.2.6 page 35** resulting in a very pure isolation of BacM, BacM$^{\Delta 139\text{-}151}$ and BacM$^{\Delta 134\text{-}151}$ (**Figure 7**).

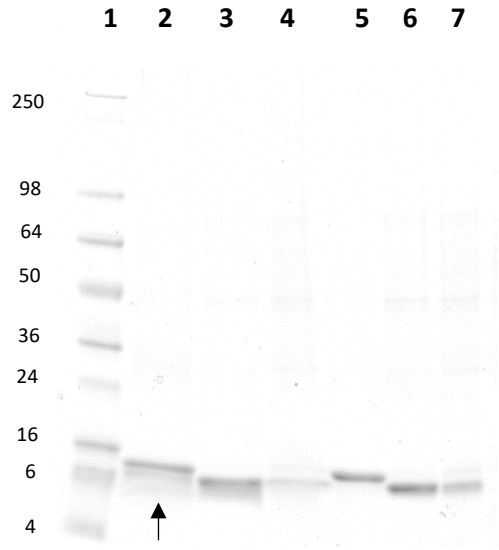

Figure 7 Two isolations of BacM, BacM NoPP and BacM STOP *Lane 1) See blue Pre-stained ladder, Lane 2) BacM, Lane 3) BacM$^{\Delta C139\text{-}151}$, Lane 4) BacM $^{\Delta C134\text{-}151}$, Lane 5) BacM, Lane 6) BacM$^{\Delta C139\text{-}151}$, Lane 7) BacM $^{\Delta C134\text{-}151}$. First isolation BacM (lane 2) showed potential degradation of BacM (indicated by the black arrow) and was not used for the pulldown. Samples were run on a 4-20% tris/glycine gel. Numbers next to the marker lane correspond to the molecular weight of the marker proteins in kilodalton.*

An experiment performed by a former postdoc David Zuckerman showed that there was no BacM concentration at which BacM does not form filaments (unpublished results). The removal of the C-terminus did not interfere with the two truncated forms of the protein BacM $^{\Delta C139\text{-}151}$ and BacM $^{\Delta C134\text{-}151}$ forming filaments/fibres. Thereby confirming previous observations that the C-terminus of BacM is dispensable for polymerization but enhances stability of the fibres (Zuckerman et al., 2015).

2.3.4 C-terminal proline rich region BacM plays a role in fiber formation in vitro

Three different versions of BacM were expressed, natively isolated, and purified for pulldown assays and protein-protein interaction assays. The tree different versions of BacM included full-length BacM, BacM $^{\Delta C139-151}$ and BacM $^{\Delta C134-151}$. The purified BacM fibres were structuraly characterized using EM and a difference was observed in the thickness of the fibres. With BacM $^{\Delta C139-151}$ and BacM $^{\Delta C134-151}$ forming thicker fibre bundles then full-length BacM (**Figure 8**). The isolation of BacM $^{\Delta C139-151}$ and BacM $^{\Delta C134-151}$ lead to the formation of fibres between 29 nm and 66 nm thickness (**Figure 8A/B/C/D**). This is substantially thicker than the 3 nm thick fibres described for the full length form of BacM (**Figure 8E**, Koch et al., 2011). Indicating that the stiff proline-rich region is involved in controlling the thickness of BacM fibre formation. At high concentrations of BacM (4 mg/ml) the protein starts forming sheets. The sheets are around 175-200 nm thick in width and 230 to 350 nm in length (**Figure 8F**).

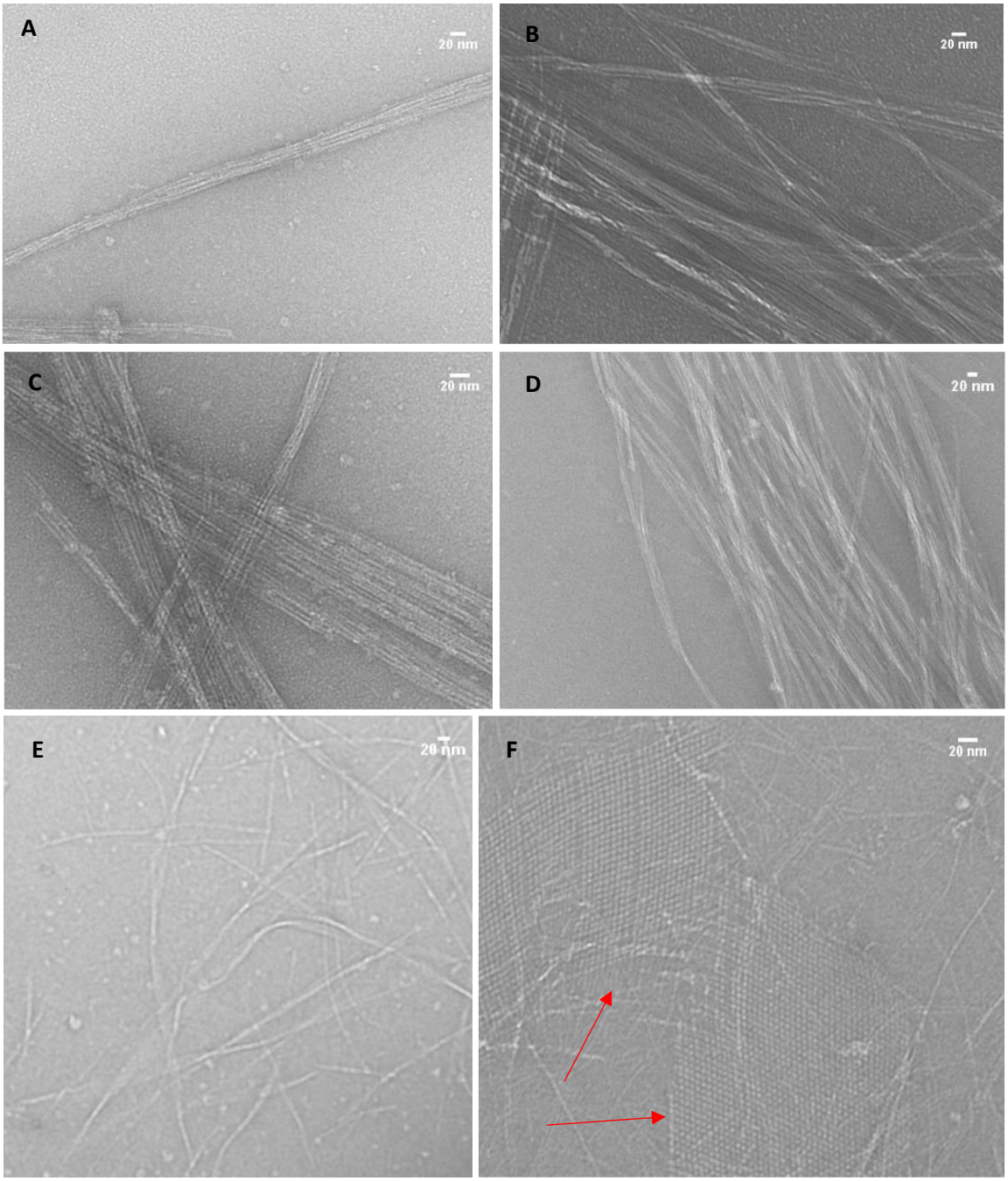

Figure 8 Electron microscopy pictures from the isolations of BacM, BacM $^{\Delta C139-151}$ and BacM $^{\Delta C134-151}$. *(A/B) BacM$^{\Delta C139-151}$ forming thick fibres. (C/D) BacM$^{\Delta C134-151}$ forming thick fibres. (E) BacM forming around 3 nm filaments and 10 nm fibres. (F) Formation of BacM sheets at high concentrations of BacM protein. Sheets are indicated by red arrows and can be recognized by their striated appearance.*

2.3.5 BacM pulldown using BacM, BacM $^{\Delta C139-151}$ and BacM $^{\Delta C134-151}$ fibres mixed and solubilized membrane extracts

In order to identify BacM-interacting membrane proteins, a pulldown assay was performed using the various natively isolated and purified BacM wild type and mutant fibres. In each assay, the BacM fibres were mixed with solubilized membrane extract of vegetative *M. xanthus* cells. Two C-terminally truncated BacM versions were generated to test whether the presence of the proline-rich region, located at the C-terminus of BacM, also plays a role in the interaction with membrane or membrane-associated proteins. The proline-rich region at the C-terminus of BacM consists of 5 prolines in a row, thereby adopting a polyproline II helix conformation (**Figure 9**). Polyproline II helixes have a single preferred conformation in solution, forming a stiff sticky arm with ϕ = -78^{o} and ψ = +146^{o} degrees of rotational freedom. The proline-rich region allows for the rapid and non-specific binding to a range of proteins (Williamson, 1994).

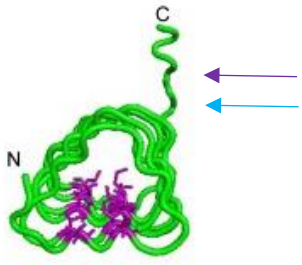

MALLGGKKDESSSKPLFRREEESVSQRSGEVHTLLGKGSEFEGKLTFEGQVRIDGKFQG
QIITKDVLVIGDGAKVQAEIQAGTVIINGQVEGNVKATQIIELKTPGRVKGNLETPSLSM
DRGVIFEGSLKMENLGTAGARPPPPPGGEKK

Figure 9 Model BacM structure + cleavage sites. *(red) the N-terminally cleaved part of BacM, (blue + purple) C-terminal cleaved part of BacM^{134} (STOP), (purple) C-terminal cleaved part of BacM^{140} (NoPP). (Zuckerman et al., 2015)*

BacM$^{\Delta C139-151}$, which stops at amino acid 139 lacks the proline-rich region, while BacM$^{\Delta C134-151}$ lacks an additional 5 amino acids (GTAGA). BacM, BacM$^{\Delta C139-151}$, and BacM$^{\Delta C134-151}$ were expressed, isolated and structurally characterized in order to ensure their proper folding (**Chapter II 2.3.2 page 49**). After the incubation of the fibres with the cytoplasmic membrane extract, the fibres were washed and samples were solubilised and run on an SDS PAGE gel.

Any differences in the pattern of protein bands observed between the BacM, BacM $^{\Delta C139-151}$ and BacM $^{\Delta C134-151}$ samples may be attributed to the absence of the proline-rich region at the C-terminus in these BacM variants. As a control sample, empty beads without bound BacM fibres were incubated with solubilized membrane extract. Any protein band(s) unique or overly associated with the various BacM samples were send for mass spectrometry analysis for identification (**Table 5**).

A total of twelve bands were identified on SDS PAGE, one of which was exclusively present in the pulldown sample of the full length BacM (**Figure 10, band J**). Most of the other bands were more associated with the BacM $^{\Delta C134-151}$ in comparison to full length BacM. This may be probably caused by the thicker fibre bundles formed by BacM $^{\Delta C134-151}$ that may result in enhanced binding of proteins. The bands labelled L and M (**Figure 10**) were both send for mass-spectrometry because of the small difference in height between the bands and how predominant the bands were in the pulldown. Most bands identified were present in all three versions of BacM.

This observation together with the BacM pulldown using cytoplasmic protein extracts indicated, that the C-terminal region appears to be mostly involved in the interaction with cytoplasmic proteins, while the DUF domain of BacM appears to be only important for the polymerisation of the protein, but plays no detectable role in the interaction with other proteins. The significance of the identified proteins will be discussed in the discussion section **(page 62)**.

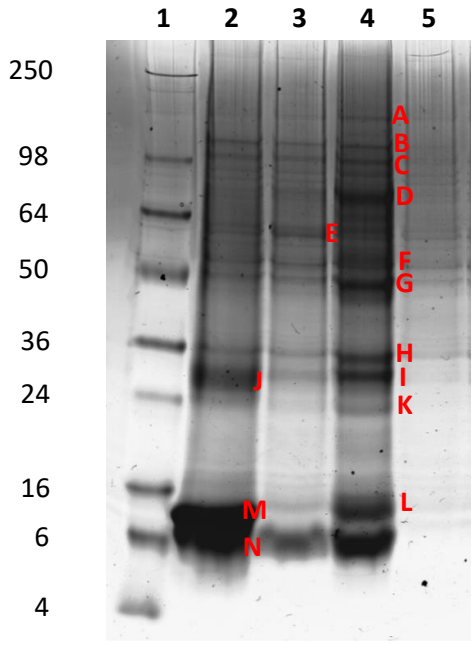

Figure 10 Pulldown assay with cyanogen beads-bound BacM, BacM$^{\Delta 139-151}$ and BacM$^{\Delta 134-151}$ fibres mixed with solubilised membrane extract from vegetative M. xanthus cells. *Lane 1: See blue pre-stained marker, lane 2 BacM + membrane extract, lane 3 BacM^{139} + membrane extract, lane 4 BacM^{134} + membrane extract, lane 5 cyanogen beads + membrane extract. Samples were run on a 4-20% tris/glycine gel. Numbers next to the marker lane correspond to the molecular weight in kilodalton.*

Table 5 Potential membrane-associated interaction partners of BacM identified by mass spectrometry.

Band	Gene name	Function	Molecular weight	Sequence coverage	Score	Q-value
A	MXAN_3564	Peptidase, M36 (Fungalysin) family	185	2.3%	113.6	0
B	MXAN_1450	TonB-dependent receptor (Oar)	122	52.6%	323.31	0
C	MXAN_6079	Putative lipoprotein;	107	28.9%	288.3	0
C	MXAN_7039	Putative molybdopterin oxidoreductase, iron-sulfur binding subunit	116	17.3%	239.5	0
D	MXAN_3539,	Succinate dehydrogenase, flavoprotein subunit sdhA;	69	26.7%	289.6	0
D	MXAN_3160	Peptidase, M13 (Neprilysin) family	78	17.4%	194.3	0
E	MXAN_6487	Outer membrane efflux protein domain protein;	50	13.5%	215.7	0
E	MXAN_0659	Putative lipoprotein	64	18.7%	54.5	0

F	MXAN_4747	Putative lipoprotein;	49	30%	108	0
F	MXAN_5030	Efflux transporter, HAE1 family, outer membrane efflux protein	49	29.4%	100.9	0
G	MXAN_2624	Putative lipoprotein;	44	44.8%	152.4	0
G	MXAN_5025	Peptidase, M36 (Fu Uncharacterized protein ngalysin) family	47	37.2%	161.9	0
H	MXAN_0976	Putative lipoprotein	33	26.4%	76.8	0
H	MXAN_6925	ATP synthase gamma chain atpG;	33	48.3%	146.2	0
I	MXAN_3698	Putative lipoprotein	29	24.1%	41.3	0
J	MXAN_4860	Uncharacterized protein (same operon as AgmX) associated with C-terminus of BacM	33	8.7%	72.5	0
K	MXAN_0512	Uncharacterized protein	27	22.4%	32.1	0
L/M/N	MXAN_7475	BacM	16	50%	222	0
L/M	MXAN_6921	ATP synthase epsilon chain atpC	15	52.9%	160.7	0
L/M	MXAN_7026	ATP synthase subunit delta atpH	20	29.7%	142.8	0
L/M	MXAN_3323	30S ribosomal protein S13	14	38.6%	28.9	0
L/M	MXAN_3306	SOS ribosomal protein L16	16	15.8%	48.2	0
L/M	MXAN_3313	30S ribosomal protein S8	15	13%	32.4	0
L/M	MXAN_6483	MotA/TolQ/ExbB proton channel family protein	25	14.6%	148.5	0
L/M	MXAN_0818	MotA/TolQ/ExbB proton channel family protein	25	14.6%	50.1	0

2.3.6 Co-expression of bactofilins and Ras-like GTPases using the pET-DUET system

To determine whether the observed interaction in the pulldown assay between BacM and MglA was not spurious, co-sedimentation assays were performed next. Both proteins were co-expressed in *E. coli* using the pET-DUET system to achieve high overexpression of the proteins (Duet™ Expression System from Novagen). After over-expression, the *E. coli* cells were lysed using sonication and the cell debris was removed through centrifugation. As bactofilins form nucleotide-independent, micrometer-long filaments, they pellet at much lower centrifugal force then the small monomeric Ras-like GTPase MglA. If, however, the two proteins interact, a large percentage of MglA should be recovered from the low speed centrifugation pellet. Unfortunately, it became clear that *E. coli* overexpressed MglA rapidly started to aggregate and consequently pelleted during centrifugation (**Figure 11**). This self-aggregation of MglA prevented the usage of co-sedimentation studies for the evaluation of a potential BacM/MglA interaction. Interestingly, these results confirmed an earlier report about the unsuitability to use *E. coli*-overexpressed MglA for X-ray crystallography (Miertzschke et al., 2011), while contradicting a paper, which reported that addition of 30 µM GDP keeps MglA in a monomeric soluble state (Treuner-Lange et al., 2015).

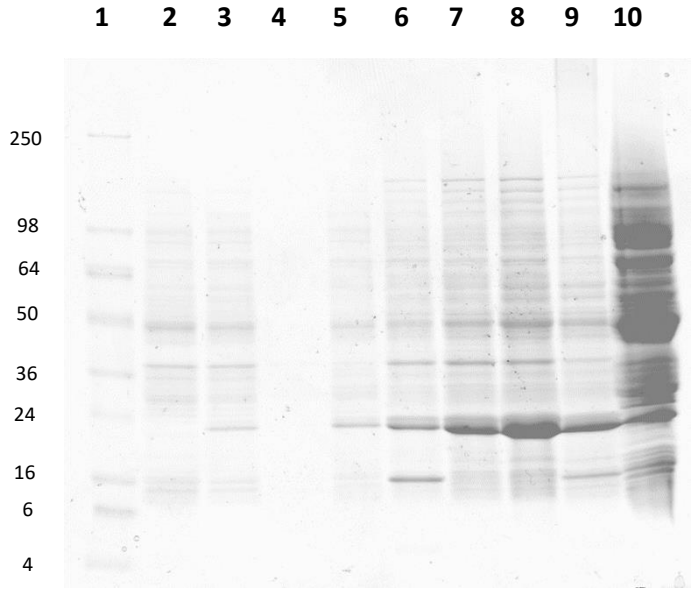

Figure 11 Overexpression of MglA in E. coli BL21 leads to non-soluble MglA *Lane 1) See blue prestained ladder, Lane 2) uninduced BL21 cells, Lane 3) induced MglA BL21 cells, Lane 4) empty lane, Lane 5) MglA pellet 0 hours after lyses of cells, Lane 6) 1 hour, Lane 7) 2 hours, Lane 8) 3 hours, Lane 9) pellet after standing overnight at 4°C, Lane 10) supernatant after standing overnight at 4°C. Samples were run on a 4-20% tris/glycine gel. Numbers next to the marker lane correspond to the molecular weight in kilodalton.*

Even addition of GDP of up to 1 mM did not suppress the previously observed aggregation of MglA after overexpression in *E. coli* (**Figure 12**). As it was not clear from these experiments whether the aggregation of MglA was due to the misfolding of the protein during expression because of the high GC content of the *M. xanthus* genome (69% *vs*. 50% in *E. coli*) or the absence of necessary chaperones, MglA was next overexpressed in rare codon-containing *E. coli* Rosetta™ cells instead. However, even the usage of these "universal" translation-competent *E. coli* cells resulted only in the recovery of aggregating MglA, indicating the possibility that the absence of certain chaperones is responsible for the observed folding deficiency. Importantly, these results may cast doubt on a previous publication using *E. coli* overexpressed MglA and MreB to demonstrate successful "binding" of these two proteins (Treuner-Lange et al., 2015).

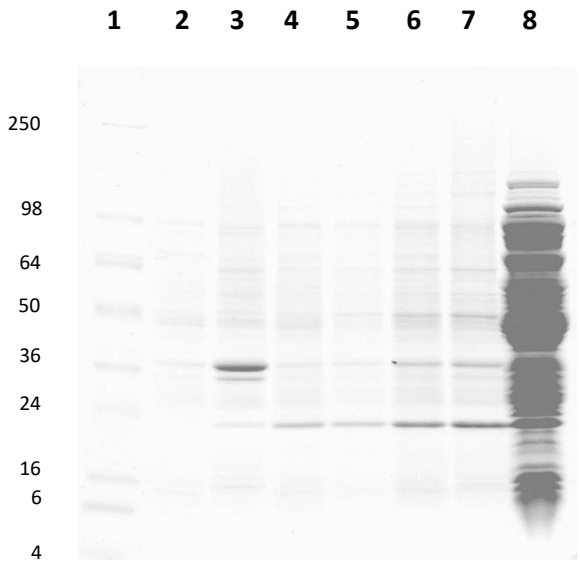

Figure 12 Overexpression of MglA in an E. coli Rosetta strain in the presence of 1 mM GDP *Lane 1) See blue prestained ladder, Lane 2) uninduced BL21 cells, Lane 3) induced MglA BL21 cells, Lane 4) MglA pellet 0 hours after lyses of cells, Lane 5) 2 hours, Lane 6) 4 hours, Lane 7) pellet after standing overnight at 4°C, Lane 8) supernatant after standing overnight at 4°C. Samples were run on a 4-20% tris/glycine gel. Numbers next to the marker lane correspond to the molecular weight in kilodalton.*

2.3.7 Isolation and overexpression of MglA in *M. xanthus*

Because it was not possible to isolate MglA expressed in *E. coli* in a physiological soluble form, MglA was next expressed in *M. xanthus*. For this purpose, the pMR3679 plasmid was used that utilises a vanillate-inducible promoter (Iniesta et al., 2012). **Figure 13** shows a representative SDS PAGE gel of the many MglA isolations that were done during the course of this work. The highly prominent band corresponds to MglA. This isolation resulted in a highly enriched MglA sample, but was not yet pure enough for the follow up experiment and therefore still needed further purification.

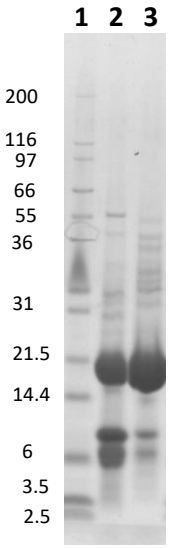

Figure 13 Isolation of overexpressed MglA from M. xanthus. *Lane 1) MARK12 ladder, Lane 2) Sample 1 MglA, Lane 3) Sample 2 MglA. Numbers next to the marker lane correspond to the molecular weight in kilodalton.*

Consequently, an alternative isolation method was developed for the purification of native MglA from *M. xanthus* cells. This isolation was based on the observation that MglA bound to nickel beads in the presence of relative low concentrations of urea (1 M), but readily washed off the beads at low concentrations of imidazole (50 mM) (**Figure 14**). In the SDS PAGE gel shown below MglA is the most pre-dominant band, but there were still quite some contaminating proteins. The second most pre-dominant band is running at around 13 kDa (**Figure 14; red arrow**).

Mass spectrometry analyis confirmed that the proteins belonging to the 13 kDa band are several soluble cytoplasmic proteins and BacM. Interestingly, the presence of BacM indicated that it was co-purified with MglA. All of the BacM filaments were pelleted in the 100,000 g centrifugation step (1 hour) prior to running the sample over nickel beads. Maybe, some of the monomeric BacM or shorter filaments were able to remain soluble, potentially by binding to MglA. To confirm that the isolated band corresponded to MglA a Western blot was run using an anti-MglA antibody on one of the samples during the isolation (**Chapter IV page 114**). The isolation of native MglA had the advantage that it retained its native activity and functional state. This would allow for an interaction assay with a biologically relevant form of the protein and determine whether MglA preferentially binds to BacM or MreB.

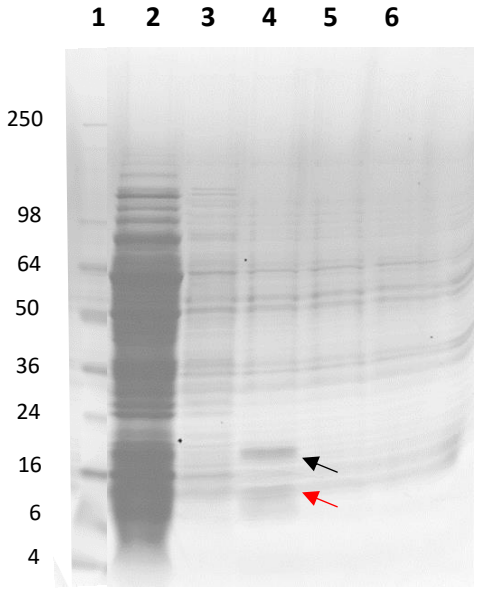

Figure 14 Isolation of native MglA from M. xanthus cells. *Lane 1) See blue prestained ladder, Lane 2) Flowthrough non-bound M. xanthus lysate, Lane 3) Washing buffer, Lane 4) 100 mM immidazole elution, Lane 5) 300 mM imidazole, Lane 6) 500 mM imidazole. MglA band present in lane 4 black arrow and a co-isolated protein red arrow. Samples were run on a 4-20% tris-glycine gel. Numbers next to the marker lane correspond to the molecular weight in kilodalton.*

2.3.8 Isolation of overexpressed MreB from *E. coli* BL21 cells

MreB was overexpressed using *E. coli* Rosetta DE3 cells. To physiologically reconstitute the MreB from the lysed Rosetta DE3 cells, liposomes were used. For this purpose, preformed liposomes were added to the lysed *E. coli* cells to initiate the binding and formation of native MreB filaments on the surface of the liposomes. The resulting short MreB filaments in these experiments should more closely reflect the currently known conformation of native MreB filaments inside bacterial cells (Dominguez-Escobar et al., 2011; Garner et al., 2011; van den Ent et al., 2014). As virtually all studied MreBs are known to anchor themselves *via* an N-terminal amphiphatic helix to the membrane (Salje et al., 2011; Fu et al., 2018), it was investigated whether the *M. xanthus* MreB contained such a putative N-terminal amphiphatic helix that could be used for direct membrane binding. After the identification of the amphiphatic helix, the direct incubation of the cell lysate and the liposomes resulted in the reconstitution of MreB filaments on the surface of liposomes. These liposomes however were structurally deformed (**Figure 15, Figure 16**), which could be the result of the way the liposomes were prepared, the presence of low amounts of Triton X-100 (>0.4%) in the reconstitution assay, or the excessive binding of large amounts of *M. xanthus* MreB. As similar membrane deformations have been described for MreB from *T. maritima* (Salje et al., 2011), it is most likely that the observed deformation in our assays are caused by the binding of excess MreB filaments. Nonetheless, the observed parallel filament structures on the surface of these liposomes were most likely MreB filaments for the following reasons: Firstly, they were parallel arranged dimeric filament structures, which are virtually identical to the described structure of MreB filaments from *T. maritima (*van den Ent et al., 2014). Secondly, the distance between the parallel filaments as well as their diameter perfectly matched the reported dimensions for *T. maritima* MreB (van den Ent et al., 2014). Likewise, the formed filaments showed the characteristic bead-like appearance of the $MreB_{Tm}$ filaments. To improve these preparations, future experiments have to aim at generating non-deformed liposomes as well as control the concentration of MreB to prevent liposome deformation to occur. Finally, the Triton X-100 could be replaced by other detergents to improve the reconstitution of the MreB filaments.

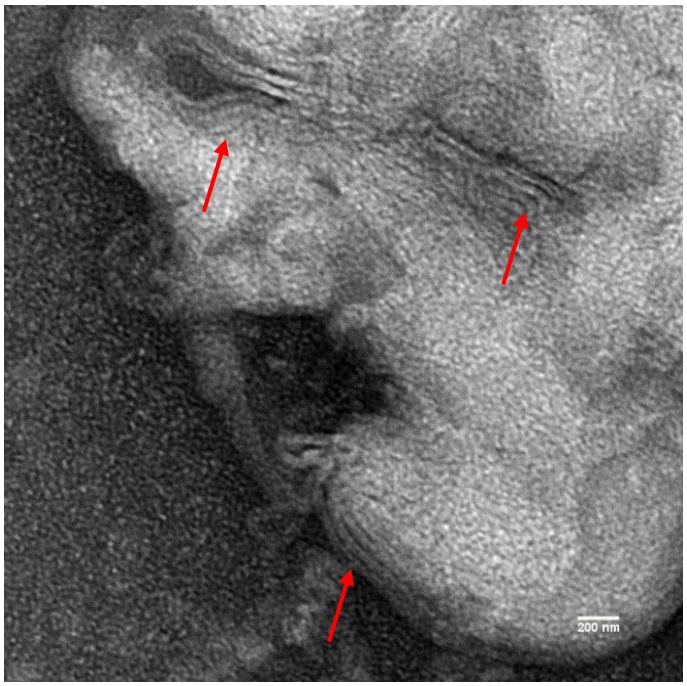

Figure 15 Electron microscopy picture of MreB filaments covering liposomes. *MreB double filaments are indicated with red arrows. The image was taken at 52K magnification.*

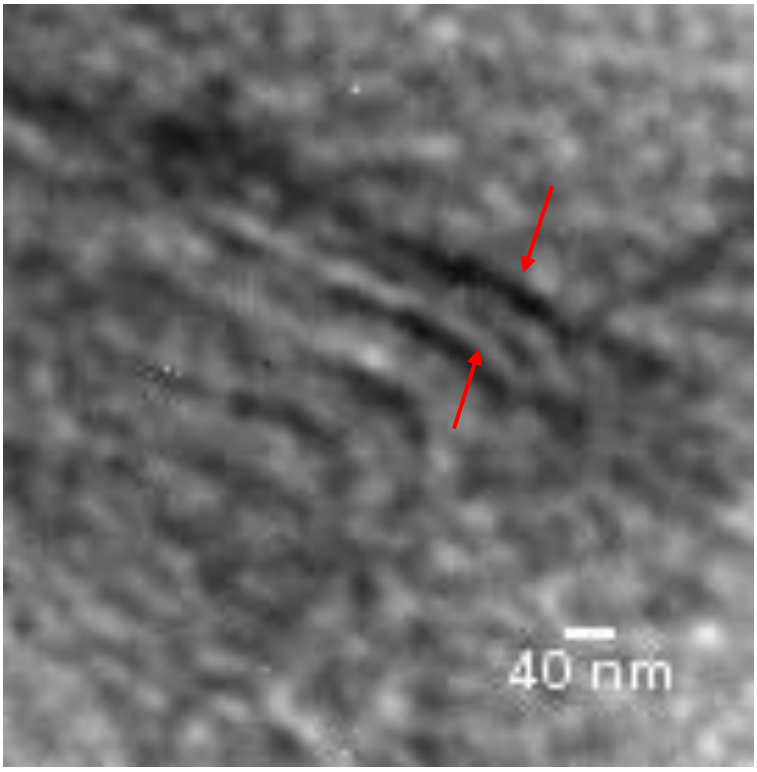

Figure 16 Electron microscopic picture of individual MreB filaments. *Individual MreB filaments are indicated with red arrows. The known bead-like structure of the filaments are clearly visible. Picture was taken at 52K magnification.*

2.4 Discussion

When analyzing the SDS PAGE from the pulldown performed by Dr. David Zuckerman MglA, MXAN_1925 (**Figure 6**; **band H**) was found to be one of the most abundant bands. This protein is a small Ras-like GTPase and has been identified as the master regulator of both adventurous and social motility (P. Hartzell & Kaiser, 1991; K. Stephens et al., 1989). Interestingly, two other identified proteins are functionally clearly linked to MglA. MXAN_4870 (**Figure 6**; **band B**) and MXAN_4864 (**Figure 6**; **band D**). MXAN_4870 and MXAN_4864 correspond to the proteins AgmU and AgmV respectively and both proteins have been identified as part of the focal adhesion complexes (Tâm Mignot, Shaevitz, Hartzell, & Zusman, 2007; Beiyan Nan, Mauriello, Sun, Wong, & Zusman, 2010; Luciano et al., 2011). Focal adhesion complexes are regularly spaced trans-envelope complexes that are thought to be the motors driving A-motility (Tâm Mignot et al., 2007). However, their role in A-motility is not undisputed as an alternative model for A-motility exist that attributes the generation of propulsive force to the secretion of slime (Wolgemuth et al. 2002). AgmU which has been found both in the cytoplasm and periplasm seems to interact with multiple other proteins associated with the focal adhesion complex including FrzCD, AglT, AglW, AgmK, AgmX and CglB (Beiyan Nan et al., 2010). AgmU is a tetratricopeptide repeat protein, a group of proteins that are typically involved in protein-protein interactions (Zeytuni & Zarivach, 2012)**.**

An MglA homologue from *Bdellovibrio bacteriovorus*, which shares 64% protein identity and 82% similarity with MglA from *M. xanthus*, has been shown to interact with the tetratricopeptide repeat containing protein, Bd2492 (Milner et al., 2014) indicating that the interaction of these proteins may be shared across different delta-proteobacteria. This reported interaction may point to the possibility that AgmU does not bind directly to BacM, but may interact with the bactofilin indirectly by binding to MglA.

The second large group of identified interactors are the cold shock proteins. These proteins play a central role in bacteria in the adaptation to low temperatures that impact the fluidity of membranes as well as the transcription of DNA. Cold shock proteins modulate membrane lipid composition to maintain membrane fluidity appropriate for necessary processes and appear to change DNA supercoiling to allow transcription to occur at low temperatures (Los, 2004). However, what function their potential interaction with BacM in the cold shock response may play is unclear as this response has been much less studied than the heat shock response. The identified type II DNA topoisomerase MXAN_2485 (**Figure 6**; **Band D**) was included in this group of potential cold shock response-related proteins as it has been shown that a similar protein, a gyrase DNA type II topoisomerase is involved in the cold shock response in *E. coli* (P. G. Jones et al., 1992). It is therefore possible that MXAN_2485 is functionally related to the cold shock proteins identified in the pulldown.

Similarly, other identified proteins have potential links to bactofilins. For example, the serine peptidase MXAN_ 4433 (**Figure 6**; **Band E**) could potentially function as the protease involved in the N-terminal cleavage of BacM (Koch et al., 2011). Although of potential significance this finding was not been further pursued in this thesis. The ParB-like protein PadC MXAN_ 4634 (**Figure 6**; **Band E**) is located in the same operon that contains the other three bactofilins (BacN, O, and P). Moreover, PadC has been found to interact *via* its ParB-like domain with the BacN, O, P scaffolds that stretch along the subpolar region of the cell, specifically binding to BacO and BacP (Lin et al., 2017). Accordingly, PadC is essential for proper chromosome structure and segregation as it plays a vital role in the recruitment of ParA to the BacN, O, P scaffolds (Lin et al., 2017). Interestingly, the operon encoding BacM contains a gene encoding for a different other ParB protein, but this protein was surprisingly not identified in the pulldown. Based on the structural similarity between the bactofilins, and the fact that PadC has been found to interact with both BacP and BacO (Lin et al., 2017), it seems likely that it could also interact with BacM.

In contrast, the remaining identified proteins have no obvious recognizable link to bactofilins. MXAN_4295 is a patatin-like phosphatase (**Figure 6; Band F**). These phosphatases are storage proteins that function in catalysing the cleavage of fatty acids from membrane lipids (Banerji & Flieger, 2004). MXAN_6735 contains a CheY-like domain. These domains are often found in signalling proteins like FrzE and FrzZ, both of whom interact with AglZ, a protein involved in the regulation of A-motility. In *M. xanthus,* FrzE and FrzZ are involved in the control of reversal frequency, but how the CheY-like histidine kinase MXAN_6735 (**Figure 6**; **Band A**) is linked to BacM is currently unclear (Bustamante et al., 2004; Inclán, Vlamakis, & Zusman, 2007). MXAN_1450 (**Figure 6**; **Band C**), the TonB-dependent receptor Oar (OmpA-related protein) is another such potential interacting protein that is difficult to interpret as its linkage to BacM is unclear. Oar has a β-barrel domain that anchors the protein in the outer membrane and its extracellular TonB domain shares similarities with other TonB proteins that are involved in transmembrane transport (Martinez-Canamero et al., 1993; Bhat et al., 2011). As Oar is one of the most abundant proteins of the outer membrane of *M. xanthus* its appearance in the pulldown assay could be the result of spurious contamination with outer membrane fragments. Even less is currently known about MXAN_5530, a hypothetical protein that was identified in the assay and for which no data exist that would allow a functional characterisation let alone allow an assessment about its potential interaction with BacM.

When analyzing the SDS PAGE from the pulldown using solubilized membrane-associated proteins, the most predominant band uniquely identified in the full length BacM fraction corresponded to MXAN_4860 (**Figure 10; Band J**). MXAN_4860 is an uncharacterised hypothetical protein, which is encoded by a gene that is located in close proximity to the A-motility gene cluster MXAN_4862 to MXAN_4870 and could potentially be a structural component of the focal adhesion complexes. All other identified proteins appeared to bind independent of the presence and absence of the C-terminus to BacM. MXAN_1450, the TonB-dependent receptor Oar (**Figure 10; Band B**) was also identified in pulldowns using cytoplasmic protein extracts (**Chapter II 2.3.1 Page 46**).

According to sequence analysis, the beta barrel part of Oar is formed by a 22-stranded β-barrel (Gómez-Santos et al., 2019). Based on published research it is known that Oar is involved in cellular adhesion, required for fruiting body formation and additionally plays a role in the secretion of the protease PopC (Bhat et al., 2011; Martinez-Canamero et al., 1993). PopC is a 50.8 kDa protein that is secreted by starving *Myxococcus* cells and cleaves with its C-terminal subtilisin domain the cell-surface exposed p25 protein. This cleavage generates the cell-surface exposed p17 protein fragment, the C-signal, an important initiator of fruiting body-dependent cell aggregation (S. K. Kim & Kaiser, 1990; Rolbetzki et al., 2008). As Oar was also found in pulldowns using cytoplasmic protein extracts it is questionable whether its appearance in pulldowns using membrane protein extracts is more meaningful. As pointed out before, as Oar is one of the most abundant membrane proteins in *M. xanthus* the most likely explanation for its occurrence in these pulldowns may be contaminations of the assays by small amounts of the abundant protein. Two membrane efflux pumps, MXAN_6487 and MXAN_5030 were identified in the pulldown (**Figure 10; Bands E/F**). Efflux pumps are located in the plasma membrane of the bacterium and are responsible for the recognition and transportation of toxic compounds to the external environment (Amaral et al., 2014). Some of the membrane efflux pumps belong to the group of ABC transporters and are known to function together with certain TonB-dependent receptors in the uptake of nutrients including carbohydrates, vitamin B12, iron complexes, and nickel chelates (Cascales et al., 2007; Schauer et al., 2007; Schauer, Rodionov, & de Reuse, 2008). Whether these efflux pumps really interact with BacM however, is an open question as so far, no function has been attributed to any bactofilin in the uptake or export of substances. Therefore, it is most likely the case that these hits are wrong positives. Likewise, a MotA/TolQ/ExbB proton channel family protein (MXAN_6483) was identified that is intriguingly present in the same operon encoding MXAN_6487 and a TonB-1 protein (**Figure 10; Bands L/M**).

In the pulldown six putative lipoproteins were identified (MXAN_3698, MXAN_7039, MXAN_0659, MXAN_4747, MXAN_2624 and MXAN_0976), that could potentially facilitate or play a role in the uptake of iron or certain other compounds using a TonB-dependent pathway. Whether the identification of these proteins, however, indicates that they truly interact with BacM is however very difficult to ascertain and they may again be only the result of unspecific hydrophobic interactions. Several other identified proteins like MXAN_3539 (succinate dehydrogenase) and MXAN_6079 (molybdopterin oxidoreductase, iron-sulfur binding subunit) are linked to the electron transport chain (**Figure 10; Bands C/D**). The electron transport chain allows for the formation of a transmembrane proton electrochemical gradient between the inner membrane and the periplasmic space (Anraku, 1988). Another identified protein, MXAN_3539 (**Figure 10; Band D; SdhA**) is a succinate dehydrogenase, which can convert succinate to fumarate. This reaction is part of the citric acid cycle and converts flavin adenine dinucleotide (FAD) into $FADH_2$ (Yankovskaya et al., 2003). One of the identified proteins MXAN_6079 is a putative molybdopterin oxidoreductase and contains an iron-sulfur-binding subunit (**Figure 10; Band C**).

The identification of these proteins is difficult to reconcile with our current knowledge of BacM. Although it cannot be completely ruled out that BacM may serve as a platform for the assembly of protein complexes of the electron transport chain it is not clear what the functional significance of such an interaction would be (Feniouk, Suzuki, & Yoshida, 2007; Hosking et al., 2006).

Additionally, three ATP synthase proteins were identified in the pulldown, AtpG (MXAN_6925), AtpC (MXAN_6921) and AtpH (MXAN_7026) (**Figure 10; Bands H/L/M**). As these proteins would normally be expected to be part of the ATP synthase complex, their association with BacM is difficult to interpret. Although a role of BacM in the assembly of the ATP synthase complex or transport of nutrients (Gómez-Santos et al., 2019; Perkins-Balding et al., 2004; Schauer et al., 2008) cannot be ruled out *a priori*, no effect on the energetic state of the cells has been observed in ΔBacM cells. Therefore, it is more likely that these hits are also false positives.

Like in the pulldowns using cytoplasmic proteins, peptidases were identified among the membrane-bound proteins potentially interacting with BacM. In particular, two peptidases, MXAN_3564 (**Figure 10; Band A**) belonging to the M36 fungalysin family and MXAN_3160 (**Figure 10; Band D**) belonging to the M13 Neprilysin family were identified. The M36 fungalysin proteases are known to be secreted outside of the cell in *Aspergillus fumigatus* and can hydrolyse laminins, elastin and collagen (Na Pombejra et al., 2018). In contrast, the neprilysin (M13) zinc-dependent peptidases are membrane-bound and capable of cleaving a wide variety of peptides (Bland et al., 2008). Like for the serine peptidase MXAN_4433, it is possible that one of these two peptidases may be involved in the proteolytic maturation process of BacM. However, due to the focus of the thesis on MglA, this direction of research was not further pursued.

Finally, three ribosomal proteins were identified in this pulldown MXAN_3306, MXAN_3313, and MXAN_3323(**Figure 10; Bands L/M**) as well as three uncharacterized hypothetical proteins MXAN_0512, MXAN_5025, and MXAN_4860 (**Figure 10; Bands G/J/K**). Whether any of those proteins interacts with BacM is difficult to tell, but at least two of the proteins MXAN_5025 and MXAN_4860 have links to other identified proteins in our pulldown experiments.

MXAN_5025 is present in the same operon as MXAN_5030, which is one of the outer membrane efflux proteins identified in this pulldown (**Figure 10; Bands F**), while MXAN_4860 is encoded by a gene just outside of an operon containing a gene cluster involved in A-motility (Luciano et al., 2011). Two proteins of this cluster, AgmU and AgmV were identified in the BacM pulldown with cytoplasmic *M. xanthus* lysate (**Chapter II 2.3.1 Page 46**).

Using pull down assays with cytoplasmic and membrane-associated proteins, a wide range of potential interaction partners for BacM were identified. Among the identified membrane-associated proteins only one, MXAN_4860 was identified to be potentially interacting with the proline-rich region at the C-terminus of BacM. This finding supports the idea that the C-terminus of BacM is mainly involved in the binding of cytoplasmic proteins, while the DUF583 domain seems to be more responsible for the binding to membrane-bound proteins. MXAN_4860 was previously identified as an extracellular matrix protein and its disruption resulted in a 24 h delay in cell aggregation and sporulation in a *ΔpilA* background (Curtis et al., 2007). Of note, the disruption of the gene in wt cells had no effect on aggregation and sporulation. Biochemically, MXAN_4860 is a lipoprotein, although it misses the typical C-terminal lipobox region (LxxC). This lipobox region is essential for lipidation and anchoring of the mature protein to the membrane (Denham et al., 2008). As no further characterisation of MXAN_4860 was done, it is difficult to determine whether the protein is truly lipidated and whether it indeed interacts with BacM. One possibility for such an interaction would be that BacM functions as a scaffold for the binding of MXAN_4860 before it is translocated across the membrane. Interestingly, MXAN_4860 is located in close proximity to an operon containing an A-motility gene cluster (Luciano et al., 2011). Therefore, the observed delay in aggregation and sporulation of *ΔpilA* mutant strains of MXAN_4860 could indicate that the protein may be linked to cell motility.

Among the BacM-binding cytoplasmic proteins, MglA is by far the most prominent one. MglA is the master regulator of motility in *M. xanthus* and mutant strains form *E. coli*-like colonies that show no spreading on agar surfaces (Hodgkin & Kaiser, 1979). MglA binds to and is known to be essential for the localisation of FrzS and AglZ, two proteins that are important for the regulation and control of A- and S-motility (Mauriello et al., 2010). As such MglA forms a direct link between A- and S-motility.

MglA additionally has been described to interact with a wide range of other proteins including: MglB, MreB, MasK, RomR, RomX and potentially BacM (Thomasson et al., 2002; Mauriello et al., 2010; Miertzschke et al., 2011; Y. Zhang et al., 2012; Szadkowski et al., 2019). MglB is the GAP protein of MglA and is located in the same operon as MglA and their interaction in *T. thermophilus* has been shown by co-crystallization of the two proteins (Miertzschke et al., 2011). MreB has been identified as a potential interaction partner of MglA through a co-sedimentation assay in *M. xanthus* and their interaction has been suggested to be essential for the assembly of the focal adhesion complexes driving A-motility (Treuner-Lange et al., 2015). MasK is a tyrosine kinase receptor and its interaction with MglA is essential for motility and development (Thomasson et al., 2002). A mutant of *masK* at the 3'end of the gene, led to a gain-of-function in ΔMglA cells. The ΔMglA cells had an increased production of extracellular fibrils. In addition, this mutant resulted in the restoration of type IV pili-mediated motility and starvation-induced development. The interaction between these two proteins was identified through bacterial two hybrid screens in *E. coli* (Thomasson et al., 2002). RomR is a response regulator essential for the regulation of cell polarity by interacting with both MglA and MglB. The interaction of RomR with MglA and MglB was identified through affinity chromatography of soluble extracts containing RomR-His_6 (Keilberg et al., 2012). RomX has been shown to form a complex with RomR that functions as the MglA GEF. It catalyses the conversion of the GDP-bound form of MglA to the GTP-bound one. Thereby, RomX stimulates the formation of focal adhesion complexes composed of the Agl-Glt proteins through the formation of a pool of MglA-GTP at the leading pole (Szadkowski et al., 2019). However, the previously measured interaction between RomR and MglA was deemed weak and the difference between the RomR-based data (Keilberg et al., 2012) and the RomX-based data (Szadkowski et al., 2019) was later attributed to the different used protein purification methods. Based on the newly acquired RomX-based data, no interaction between RomR and MglA is thought to exist (Szadkowski et al., 2019).

Yet another Ras protein, SofG in *M. xanthus* has been described to interact with the bactofilin BacP (Bulyha et al., 2013), the finding of a potential link between MglA and BacM is not as unexpected as initially thought. Quite to the contrary, these results may indicate that the binding of small RasGTPases is a novel functional feature of bactofilins.

From the A-motility gene cluster previously identified by Sodergren & Kaiser, 1983 two proteins, AgmU and AgmV were identified in the pulldown using his-tagged BacM fibres mixed with cytoplasmic extract. AgmU has been shown to interact with multiple other focal adhesion complex-associated proteins including: AglZ, FrzCD, AglT, AglW, AgmK, AgmX and CglB (Beiyan Nan et al., 2010). AgmV might interact directly or indirectly with AglZ as in a *ΔagmV* mutant AglZ-GFP was found to localize diffusively instead of forming lateral clusters (Beiyan Nan et al., 2010). The identification of three proteins essential for A-motility in the pulldowns strongly suggest that BacM plays an important role in the assembly of focal adhesions complexes and potentially A-motility.

The BacM pulldown lead to the identification of many other proteins involved in the protein secretion pathway, the electron transport chain, the generation of ATP, and ribosomal proteins such as the TonB-dependent receptor Oar (MXAN_1450; Gómez-Santos et al., 2019), the succinate dehydrogenase MXAN_3539, the molybdopterin oxidoreductase MXAN_6079 (Bradbeer, 1993; Maloney, Kashket, & Wilson, 1974), and the three ATP synthase proteins AtpG, AtpC, and AtpH (Junge, 2002; Oster & Wang, 2003) and the ribosomal proteins MXAN_3306, MXAN_3313, and MXAN_3323. Whether any of these proteins indeed interact with BacM under physiological condition is without additional experiments difficult to decide. One possibility for an interaction between (some of) these proteins and BacM could be that the bactofilin fibres may be used as scaffolds for the assembly of cellular complexes and multiprotein machines and as such individual protein components of these machines or complexes may interact with BacM.

In total three peptidases were identified in our pulldowns: the serine peptidase S1C, an M36, and an M13 peptidase. Whether any of those three peptidases indeed interacts with BacM is without further experiments difficult to decide. One potential reason for an interaction could be the fact that BacM is posttranslational modified through a proteolytic maturation step (Koch et al., 2011). Therefore, one of these three peptidases could be actually involved in the maturation process through the cleavage of BacM before serine 28. Although the discovery of the responsible BacM-specific protease would be important, this aspect was not further investigated.

Another interesting identified protein in the pulldown was PadC (MXAN_4634), a protein located in the same operon as the other three bactofilins (BacN, O, and P). PadC functions in proper chromosome structure and segregation and therefore does not seem to be linked to the other identified proteins.

However, the identification of PadC as an interaction partner of BacO and BacP (Lin et al., 2017) and the structural similarity between the bactofilins makes it likely that PadC may interact with BacM as indicated by the observed potential interaction in our assay.

Several of the identified potential binding partners are involved in the cellular cold shock response (CspA, CspC, CspD and CspE). Cold shock proteins (Csp) are nucleic acid-binding proteins ranging in size from 65-75 amino acids. They have a highly conserved domain called the cold shock domain (CSD), which functions in the binding of nucleic acids (P. Graumann & Marahiel, 1996). Cold shock proteins are involved in counteracting harmful effects caused by a decrease in temperature. Some of these harmful effects include a decrease in membrane fluidity, reduced mRNA translation and transcription, inefficient folding of proteins, and reduced ribosome function (Phadtare, 2004). These effects are mostly caused by the stabilization of nucleic acid secondary structures. The cold shock proteins play a role in the unwinding of these secondary structures (Phadtare, 2011). Some cold shock proteins are non-cold inducible and have been implicated in cellular functions related to normal growth and stress adaptation. These Csps contribute to osmotic, oxidative, starvation, pH and ethanol stress tolerance (Loepfe et al., 2010; Wang, Wang, & Wu, 2014).

Unfortunately, how Csps precisely contribute to these non-cold induced stress adaptation responses is not yet clear. If the identified cold shock proteins bind to BacM then they could potentially facilitate proper protein folding and ribosomal function at the membrane, by unwinding nuleic acid secondary structures. In addition, a cold shock protein UNR (upstream of N-RAS) was identified as a regulator of N-Ras expression (Boussadia et al., 1997; Jeffers et al., 1990). Another publication revealed the mutual regulation of the cold shock protein YB-1 and the Ras/ERK/RSK signalling pathway in prostate cancer progression (Imada et al., 2013).

We were unable to isolate soluble overexpressed MglA from *E. coli* cells. Importantly, neither changes in expression temperature (from 37 ^{o}C to 20 ^{o}C) nor switching to *E. coli* Rosetta^{TM} cells prevented MglA aggregation. Intriguingly, previous works had reported the purification of soluble MglA-his from *E. coli* C41 DE3 cells by adding 30 µM GDP during the isolation procedure (Treuner-Lange et al., 2015). However, in our experiments the addition of GDP (even at concentrations of up to 1 mM) did not prevent the protein from aggregating. The reasons for these differences are currently unclear and may have to do on the usage of different plasmids for the expression process or slightly different procedures of cell breakage and protein handling. Importantly, we were able to immediately isolate overexpressed soluble MglA from *M. xanthus* without addition of GDP. This observation supports the idea that our isolation protocol was not the reason for failure but the lack of a suitable expression host.

The isolation of BacM has been optimized to the point where very pure samples are reproducibly obtained. Using electron microscopy, the characteristic BacM filament/fibres were observed. The formation of very thick fibres upon the deletion of the C-terminal region of BacM indicated the importance of the proline-rich region in controlling BacM fibre formation in addition to playing a role in cytoplasmic protein interactions. The isolation of MreB seems to be successful, but needs some further optimization. By decreasing the amount of MreB protein isolated per liposome we might be able to obtain short MreB filaments on the liposomes suitable for the pulldown with MglA and BacM.

Together the identification of these proteins supports the idea that BacM may be involved in multiple processes including the secretion of certain proteins/peptidases, generation of PMF, ATP synthesis and *M. xanthus* motility. Whether the identified proteins in the BacM pulldown are linked processes meaning that the generation of PMF and ATP in turn drives the translocation/secretion of proteins across the membrane and/or provides the energy to drive motility remains an open question. Based on these results, however, BacM seems to function as a hub for the binding and potential localization of multiple proteins involved in a range of different functions.

2.5 Conclusion and Outlook

The identification of multiple potential BacM-interacting cytoplasmic and membrane-associated proteins opens up numerous new avenues for investigating the molecular output pathways of this bactofilin. Although whether all of the identified proteins indeed interact with BacM is questionable, certain proteins appear to be prime candidates. For example, the identification of three proteins directly involved in motility and one additional protein (MXAN_4860) linked to an A-motility gene cluster suggests that BacM may be involved in A- and/or S-motility either through the formation of focal adhesion complexes or the coordination of both types of motility. However, based on our current knowledge it seems unlikely that BacM is directly involved in motility due to the observation that a deletion of the protein shows morphological defects but no obvious disruption of A- or S-motility. Far more likely BacM functions like a scaffold for either the regulation, adhesion or specific cellular localization of these proteins to the membrane where they in turn can exert their function (Koch et al., 2011; Vasa et al., 2015).

As steady progress has been made in the expression and purification of MglA, BacM and MreB, it will soon be able to perform direct interaction assays using the physiologically active versions of these proteins. In these assays, the three proteins will be mixed in MreB polymerization buffer (**see Materials and Methods Chapter II Page 30**) with added ATP and GTP.

ATP to facilitate MreB filament formation and GTP to keep MglA in its active form. This protein mixture will then be injected into the sub-phase of a sucrose cushion (**see Materials and Methods Chapter II Page 30**). If MglA binds to liposome-bound MreB, as has been claimed, it should rise to the top of the sucrose cushion, while BacM-bound MglA will stay in the sub-phase of the cushion. Upon fractionation, the preferred binding partner of MglA should be evident and this identification will be essential for our understanding of A-motility.

As A-motility has been claimed to be the result of PMF-powered movement of motor complexes along cytoskeletal filaments (B. Nan et al., 2011). If MglA binds to MreB, then this would support the current focal adhesion model. However, if MglA binds to BacM then this opens up new questions about how this protein interaction is related to A-motility.

Chapter III

3. Development of a novel luciferase system for the identification of protein-protein interactions in *M. xanthus*.

3.1 Introduction

A large number of protein-protein interactions in *M. xanthus* have been identified using either *E. coli*-based bacterial two-hybrid systems (Beiyan Nan et al., 2015), yeast two-hybrid systems (Lancero et al., 2005; Whitworth et al., 2008) or direct protein-protein interaction assays (Mauriello et al., 2010; Beiyan Nan et al., 2010). On closer inspection, however, some of these identified protein-protein interactions appear to be somewhat uncertain. For example, the observed auto-aggregation of *E. coli*-expressed MglA has been observed by at least three groups independently (including our laboratory as discussed in Chapter 2), but has not been taken into account in protein-protein interaction assays performed in other labs (Leonardy et al., 2010b; Patryn et al., 2010). Moreover, some proteins like SofG were used in these assays after extensive modifications for example, to generate a soluble overexpressed version of SofG in *E. coli*, the authors not only had to remove the N-terminal first 17 amino acids, but also had to add a MalE tag to the C-terminus (Bulyha et al., 2013). Consequently, protein-protein interactions identified with those extensively modified protein versions in pulldown assays or bacterial two-hybrid systems must be carefully assessed. Importantly, *E coli* does not possess Ras-like GTPases or bactofilin-encoding genes in its genome. The expression of these proteins therefore, might be toxic to the cells or may lead to miss-folded products. The miss-folding thereby could be either the result of improper translation of the protein in *E. coli* due to GC content differences or due to the absence of certain chaperones necessary for the proper folding of MglA and SofG (Gasser et al., 2008). In order to prevent these issues from interfering with the planned protein-protein interaction studies of this thesis, it was decided to develop a two-hybrid system in *M. xanthus*.

Such a system should allow for the more reliable identification of protein-protein interactions through the expression of the proteins in their native host in which e.g. correct folding of the proteins should be easier achieved than in *E. coli* or yeast.

In this chapter, a novel two-hybrid system is described that was developed to re-evaluate previously identified protein-protein interactions in *M. xanthus* as well as identify novel such interactions. This two-hybrid system uses a luciferase-based assay in which the interaction of two tagged proteins catalyses a reaction leading to a measurable light output (Hall et al., 2012). The intensity of this light output is proportional to the strength of the interaction and can be used e.g. to characterise the absolute strength of the protein interactions. Furthermore, the potential use of this luciferase system to localize the protein interactions inside the cell was investigated. The identification and localization of these interactions in their native host has the potential to provide a deeper understanding of the involved molecular pathways as well as the spatial and temporal regulation of these interactions in *M. xanthus.*

3.2 Materials and Methods

3.2.1 Cloning of genes for the luciferase and bacterial two-hybrid system

The pKT25 and the pUT18C plasmids were used for the expression of different combinations of genes of interest using the bacterial two-hybrid system in *E. coli*. Genes encoding the two proteins of interest were amplified by PCR using appropriate primers and sub-cloned into the pKT25 and pUT18C vectors in frame with the T25 and T18 fragment open reading frames. For the expression of the luciferase system in *E. coli* and *M. xanthus* the pMR3679 plasmid was used. Cloning the designed luciferase fragment (**see Chapter III 3.2 Page 88**) into the multiple cloning site of the pMR3679 plasmid. The Ras-like genes were amplified using PCR and digested using KpnI and BglII (NEB). The pMR3679 luciferase plasmid was digested with KpnI and BglII, allowing for the cloning of the genes at the Sm-tag. The bactofilin genes in addition to *mreB*, *masK*, *romR* and *mglB* were PCR amplified and digested using EcoRI-HF and MluI-HF (NEB). The pMR3679 luciferase plasmid was digested with the same enzymes, allowing for the cloning of these genes at the Lg-tag. As controls, a full length luciferase and a construct expressing a non-tagged Sm and Lg were constructed. A for the controls, vectors were constructed expressing only the SmBiT and LgBiT domains. The strains and primers used in this chapter are listed below (**Table 6**, **Table 7**, **Table 8**)

Table 6: Strains used for expression BTH system in E. coli

Strains for expression BTH system in *E. coli*	**Expression**	**Reference**
pKT25 MglA pUT18C BacM	BTH101 cells	This study
pKT25 MglA pUT18C BacN	BTH101 cells	This study
pKT25 MglA pUT18C BacO	BTH101 cells	This study
pKT25 MglA pUT18C BacP	BTH101 cells	This study
pKT25 MglA pUT18C MreB	BTH101 cells	This study
pKT25 SofG pUT18C BacM	BTH101 cells	This study
pKT25 SofG pUT18C BacN	BTH101 cells	This study

pKT25 SofG pUT18C BacO	BTH101 cells	This study
pKT25 SofG pUT18C BacP	BTH101 cells	This study
pKT25 SofG pUT18C MreB	BTH101 cells	This study
pKNT25 pUT18	BTH101 cells	BACTH System Kit EUROMEDEX
pKNT25-zip pUT18-zip	BTH101 cells	BACTH System Kit EUROMEDEX

Table 7 Strains used for expression luciferase system in E. coli and M. xanthus

Strains for expression luciferase system in *E. coli* and *M. xanthus*	**Expression**	**Reference**
MglASm BacMLg	*E. coli* Dh5α cells and *M. xanthus*	This study
MglASm BacNLg	*E. coli* Dh5α cells and *M. xanthus*	This study
MglASm BacOLg	*E. coli* Dh5α cells and *M. xanthus*	This study
MglASm BacPLg	*E. coli* Dh5α cells and *M. xanthus*	This study
MglASm MreBLg	*E. coli* Dh5α cells and *M. xanthus*	This study
MglASm MasKLg	*E. coli* Dh5α cells and *M. xanthus*	This study
MglASm RomRLg	*E. coli* Dh5α cells and *M. xanthus*	This study
MglASm MglBLg	*E. coli* Dh5α cells and *M. xanthus*	This study
SofGSm BacMLg	*E. coli* Dh5α cells and *M. xanthus*	This study
SofGSm BacNLg	*E. coli* Dh5α cells and *M. xanthus*	This study
SofGSm BacOLg	*E. coli* Dh5α cells and *M. xanthus*	This study
SofGSm BacPLg	*E. coli* Dh5α cells and *M. xanthus*	This study
SofGSm MreBLg	*E. coli* Dh5α cells and *M. xanthus*	This study
SofGSm MasKLg	*E. coli* Dh5α cells and *M. xanthus*	This study
SofGSm RomRLg	*E. coli* Dh5α cells and *M. xanthus*	This study
SofGSm MglBLg	*E. coli* Dh5α cells and *M. xanthus*	This study
$BitLuc^{opt}$	*E. coli* Dh5α cells and *M. xanthus*	This study
SmLg	*E. coli* Dh5α cells and *M. xanthus*	This study

Table 8 Primer list

Plasmid + gene	Description Forward primer (F) Reverse primer (R)	Sequence 5' to 3' end
pKT25 AglZ	Mx_MglA_F_NdeI	**ATCGC** *CATATG* ATGTCCTTCATCAATTACTCATC
pKT25 AglZ	Mx_MglA_R_EcoRI	**ATATA** *GAA TTC* TCACCACCCTTCTTGAGCTC
pKT25 MglA	ΔMXAN_7475 Primer A EcoR-I	**TATAT** *GAATTC* AAGCAAGTCGCGGACAAG
pKT25 MglA	ΔMXAN_7475 Primer B	AACGCACGT- GTCCTACTC CTTCCTGAG
pKT25 SofG	ΔMXAN_7475 Primer C	GAGTAGGAC- ACGTGCGTT CCTGGAAGC
pKT25 SofG	ΔMXAN_7475 Primer D Xba-I	**TATAT** *TCTAGA* TCTCTTCTTCCTGGTCCA
pUT18c MreB	Mx6789_MreB_F_XbaI	**ATATA** *TCTAGA* TATGTTTGACTGGCTTCACAC
pUT18c MreB	Mx6789_MreB_R_KpnI	**ATATA** *GGTACC* CCCGGCTGGCAGACC
pUT18c AglZ	Mx2991_AglZ_F_XbaI	**ATATA** *TCTAGA* CGCGTTCCTCGACCGCAC
pUT18c AglZ	Mx2991_AglZ_R_KpnI	**ATATA** *GGTACC* AGGACGGTGTCCTGGAGCT
pUT18c BacM	Mx6789_BacM_F_XbaI	**ATATA** *TCTAGA* TCTGGTGAGGTCCAC
pUT18c BacM	Mx6789_BacM_R_KpnI	**ATATA** *GGT ACC* CTACTTCTTCTCGCCACC
pUT18c BacN	Mx4637_BacN_F_XbaI	**ATATA** *TCTAGA* CATGGCAACGGGTGAAAC
pUT18c BacN	Mx4637_BacN_R_KpnI	**ATATA** *GGTACC* ATGTCGTCAGGAAGCCGT
pUT18c BacO	Mx4636_BacO_F_XbaI	**ATATA** *TCTAGA* TTTGAGCTTCACGCCGCG
pUT18c BacO	Mx4636_BacO_R_KpnI	**ATATA** *GGTACC* CGCTCCTTCATGTCCATG

pUT18c BacP	Mx4635_BacP_F_XbaI	**ATATA** *TCTAGA* CGTGGCCACCGCGAAGGA
pUT18c BacP	Mx4635_BacP_R_KpnI	**ATATA** *GGTACC* CGGGTCTTCTTCTTCACCACGACC
pMR3679-lucif	LgBit without protein F	**TATAT** *GAATTC* TAGGGATCCTATAAGTTT
pMR3679-lucif	LgBit without protein R	**TATAT** *ACGCGT* TTTAAAGTTTTA
pMR3679-lucif	SmBit without protein F	**TATAT** *GGTACC* TAGGGATCCTATAAGTTT
pMR3679-lucif	SmBit without protein R	**TATAT** *CTAGATCT* ACGCGTTTTAAAGTTTTA
pMR3679-lucif	Bitlucopt F primer NdeI	**TATAT** *CATATG* GTGTTTACACTTGAAGAT
pMR3679-lucif	Bitlucopt R primer MluI	**TATAT** *ACGCGT* CTATAGAATTTCTTCAAA
pMR3679-lucif	SofG F Sm primer KpnI	**TATAT** *GGTACC* GTGAGGAGCCGGATTTCG
pMR3679-lucif	SofG R Sm primer BglII	**TATAT** *CTAGATCT* TCATCGCCCTTCTCCGCT
pMR3679-lucif	MglA F Sm KpnI	**TATAT** *GGTACC* ATGTCCTTCATCAATTAC
pMR3679-lucif	MglA R Sm BglII	**TATAT** *CTAGATCT* TCAACCACCCTTCTTGAG
pMR3679-lucif	MreB F Lg EcoRI	**TATAT** *GAATTC* ATGTTTGACTGGCTTCAC
pMR3679-lucif	MreB R Lg MluI	**TATAT** *ACGCGT* TCAGCCCGGCTGGCAGAC
pMR3679-lucif	MasK F Lg EcoRI	**TATAT** *GAATTC* ATGTCCCCCCCCCAGACG
pMR3679-lucif	MasK R Lg MluI	**TATAT** *ACGCGT* CTACTGCGTCACCCGCCA
pMR3679-lucif	MglB F Lg EcoRI	**TATAT** *GAATTC* ATGGGCACGCAACTGGTG
pMR3679-lucif	MglB R Lg MluI	**TATAT** *ACGCGT* TTACTCGCTGAAGAGGTT
pMR3679-lucif	RomR F Lg EcoRI	**TATAT** *GAATTC* ATGCCCAAGAATCTGCTG
pMR3679-lucif	RomR R Lg MluI	**TATAT** *ACGCGT* TCAGTGCTGGGTCTCTCG

pMR3679-lucif	BacM F Lg primer EcoRI	**ATATA** *GAATTC* TCTGGTGAGGTCCAC
pMR3679-lucif	BacM R Lg primer MluI	**ATATA** *ACGCGT* CTACTTCTTCTCGCCACC
pMR3679-lucif	BacN F Lg primer EcoRI	**TATAT** *GAATTC* ATGGCAACGGGTGAAACG
pMR3679-lucif	BacN R Lg primer MluI	**TATAT** *ACGCGT* TCAAATGTCGTCAGGAAG
pMR3679-lucif	BacO F Lg primer EcoRI	**TATAT** *GAATTC* TTGAGCTTCACGCCGCGC
pMR3679-lucif	BacO R Lg primer MluI	**TATAT** *ACGCGT* TCAGCGCTCCTTCATGTC
pMR3679-lucif	BacP F Lg primer EcoRI	**TATAT** *GAATTC* GTGGCCACCGCGAAGGAG
pMR3679-lucif	BacP R Lg primer MluI	**TATAT** *ACGCGT* CTAGCGGGTCTTCTTCTT

3.2.2 Bacterial two-hybrid system

The two recombinant plasmids encoding the X-T25 and Y-T18 hybrid proteins were transformed into competent BTH101 cells. Twenty µl of fresh or thawed electrocompetent BTH101 reporter cells were mixed with 5 ng of each plasmid. As a positive control, competent reporter cells were co-transformed with the control plasmids pKT25-zip and PUT18C-zip. The transformed BTH101 cells were plated on X-gal (5-bromo-4-chloro-3-indolyl-β-D-galactopyranoside, 40 µg/ml) plates containing 0.5 mM IPTG and appropriate antibiotics. The plates were incubated at 30 ^{o}C and after 1-3 days screened for blue colonies.

3.2.3 β-galactosidase assay

Bacterial cells assayed for β-galactosidase activity were grown overnight in 10 ml LB broth in the presence of 0.5 mM IPTG and appropriate antibiotics at 30 ^{o}C at 200 rpm. Aliquots (80 µL) were made of permeabilization solution in 1.5 mL eppendorf tubes.

The OD_{600} was measured of each culture and 20 µL was added to the permeabilization solution (100 mM Na_2HPO_4, 20 mM KCl, 2 mM $MgSO_4$, 0.8 mg/mL hexadecyltrimethylammonium bromide, 0.4 mg/mL sodium deoxycholate and 5.4 µL/mL β-mercaptoethanol). Next, the samples were moved with the substrate solution to 30 ^oC for 20-30 minutes. 600 µl Of the substrate solution (60 mM Na_2HPO_4, 40 mM NaH_2PO_4, 1 mg/mL o-nitrophenyl-β-D-Galactoside (ONPG), 2.7 µL/mL β-mercaptoethanol) was added to each sample and the time of addition was noted. After sufficient colour had developed, 700 µL of stop solution (1 M Na_2CO_3) was added and mixed, to halt the reaction. The time of the addition of stop solution was noted. The samples were centrifuged in a microfuge at top speed for 10 minutes. The top of the solution was transferred to cuvettes and the Abs_{420} was recorded. The miller units were calculated using the following equation (X. Zhang & Bremer, 1995):

$$1000 \times \frac{(Abs_{420})}{((Abs_{600} \text{ of culture sampled}) \times (\text{volume [0.02 ml]}) \times (\text{reaction time}))}$$

3.2.4 bitLuc^{opt} Assay

For the *M. xanthus* luciferase assay, cells from three different colonies were grown ON at 30 °C at 200 rpm until an OD_{600} of 0.4-0.6. These cells were induced using 50 µM vanillate ON. To measure luciferase activity 50 µl NanoGlo Luciferase (Promega, N112A) was added to 50 µl of culture sample. Next, 1 µl furimazine substrate (Promega, N113A) was added, which started the oxidation of furimazine. Measurements were performed in triplicate using glass tubes. Luciferase activity was determined using a Berthold LuMat-3 luminometer for 0.1 seconds. Data was normalized to culture optical density measured at 600 nm (OD_{600}). For the *E. coli* luciferase assay, cells from three different colonies were grown at 37 °C and 200 rpm until an OD_{600} of 0.4-0.6. These cells were induced using 50 µM vanillate ON. Measurement of luciferase activity was performed as described above.

3.2.5 Preparation of agar patches for fluorescent microscopy of the bitLuc^{opt} Assay

The sample preparation for fluorescence microscopy was done using TPM agar. CTT agar has fluorescent background and for this reason TPM agar was used for the fluorescent microscopy. TPM agar (1.5%) was molten using a microwave and three microscope slides were aligned in a row with four additional microscope slides aligned at a 90 ° angle on top of the three microscope slides, two at each end (**Figure 17**). This created a small open square on each of the aligned microscope slides. The molten TPM agar was pipetted into these squares and before it solidified a microscope slide was placed on top of it creating an agar patch with a smooth surface. Next, 10 µl of a culture sample was mixed with 1 µl furimazine substrate in an Eppendorf tube prior to being pipetted onto the TPM agar patch. Finally, the agar patch was covered with a cover slip and candle wax was molten and used to seal the sides of the cover slip, thereby preventing the sample from drying out. The prepared samples were incubated at 32 °C for at least one hour prior to examining them under a Nikon widefield microscope.

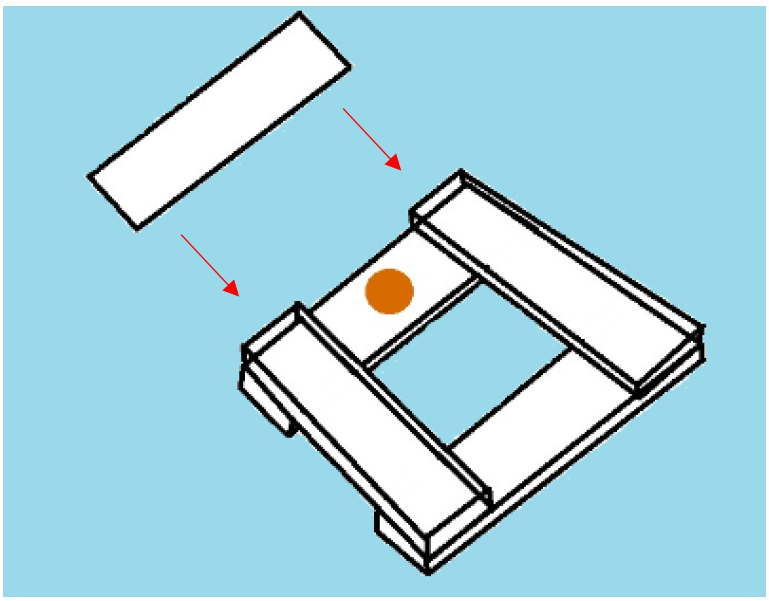

Figure 17 Preparation of agar patches. *Molten agar (brown) was pipetted into the small open square. A microscope slide was placed on top of it, to smoothen the agar.*

3.2.6 Fluorescent microscopy of bitLuc^{opt} Assay

An inverted widefield microscope (Nikon) was used for the acquisition of fluorescent microscopy data. The microscope included a 100X/1.30 NA oil PH3 objective, an X, Y motorized stage, a sCMOS camera, a light source, filters for green, red, blue-fluorescent proteins, and a temperature-controlled incubation chamber. Prior to using the microscope, the incubation chamber and the microscope were heated to 32 ^{o}C for ~1-2 hours. A drop of high quality immersion oil was added onto the lens of the objective. The objective lens was put into the stage holder and the cells were brought into focus by moving the stage in the Z-direction closer to the objective. For time-lapse experiments the duration was set to 5-10 minutes and images were recorded at time intervals of 10 seconds. Depending on the sample either FITC, DAPI or TxRED was used for the acquisition of fluorescent data. For the bitLuc^{opt} system FITC was used with an exposure time of 800 ms.

3.3 Results

3.3.1 Validation of potential interactions between MglA and BacM/BacO and SofG and MreB using a bacterial two-hybrid system.

To further investigate the pull down-identified interactions between BacM and MglA a bacterial two-hybrid assay was used next. To do so, all potential interactions between the various combinations of the two Ras-like GTPases, MglA and SofG and the cytoskeletal proteins BacM, N, O, P and MreB were tested. As demonstrated in **Figure 18**, the strongest interaction was recorded between SofG and BacP resulting in a β-galactosidase activity of 8787 miller units confirming a previous publication reporting a strong interaction between these two proteins (Treuner-Lange et al., 2015). High values were also found for the combination of MglA and BacM (5944 miller units), MglA and BacO (5331 miller units), and SofG and MreB (5652 miller units), whilst nearly all other tested combinations resulted in values around and below 2000 miller units. Values between 700-7000 units/mg are normally considered as an indication that proteins interact with each other with the higher values indicating more certainty (BACTH system kit, Euromedex). However, lower values as recorded for most of the protein combinations can be the result of prolonged expression, as it is more likely that this observed lower activity is simply the result of the accumulation of too much expressed protein inside the cell. As prolonged expression increases the chances of the pKT25 and pUT18c protein parts to arbitrarily find each other and induce the expression of the *lacZ* gene. Consequently, interactions that resulted in 5000 miller units or higher are overall encouraging results and indicative of a potential interaction. Nevertheless, these observed interactions would still have to be confirmed or evaluated further using a different two-hybrid system or other independent approach. One of the reasons for this precaution is based on the observation that overexpressed MglA and SofG in *E. coli* leads to the formation of non-soluble aggregates (**Section 2.3.6 Page 56** Bulyha et al., 2013).

The formation of these aggregates could indicate that the observed interactions in the bacterial two-hybrid system are not due to true physiologically relevant interactions between correctly folded proteins, but due to spurious interaction/aggregation of incompletely folded proteins. Consequently, the observed interactions might not be physiologically relevant or indicative of an actual interaction of these proteins inside *M. xanthus* cells.

A

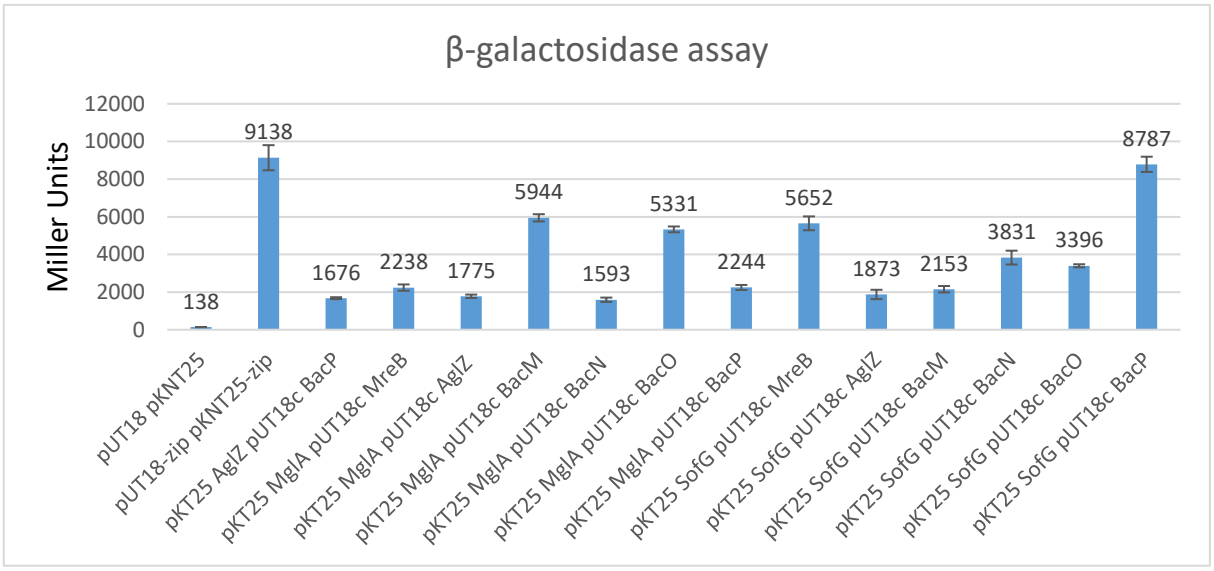

B

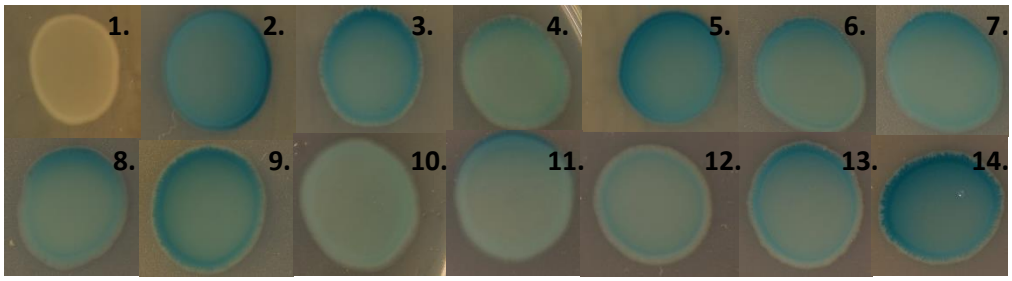

Figure 18. Bacterial two-hybrid studies in which the blue colour indicates β-galactosidase activity. *(A) β-Galactosidase activity measured in miller units. The means of the results of three independent experiments and the standard deviations of the means (error bars) are shown. (B) Colonies grown on LB plates containing Amp50 Kan25 IPTG500 and Xgal40. (1) Empty plasmids (-C), (2) +C, (3) MglA and MreB, (4) MglA and AglZ, (5) MglA and BacM, (6) MglA and BacN, (7) MglA and BacO, (8) MglA and BacP, (9) SofG and MreB, (10) SofG and AglZ, (11) SofG and BacM, (12) SofG and BacN, (13) SofG and BacO, (14) SofG and BacP. The data indicates a potential interaction between MglA and BacM, MglA and BacO, SofG and MreB, SofG and BacP.*

Because of the identified problems associated with the correct folding of *E. coli*-expressed MglA and the broader implications of potential misfolded heterologous proteins for the meaningful interpretation of two-hybrid assay results, it was decided to develop a luciferase-based expression system that would allow to perform these types of interaction assays directly in *M. xanthus* using a different independent two-hybrid assay.

3.3.2 Development of a luciferase-based two-hybrid system in *M. xanthus*

The luciferase system uses a structurally optimized luciferase subunit from the deep sea shrimp *Oplophorus gracilirostris* (Hall et al., 2012). This luciferase is referred to as N-luc (new luciferase), which was used to engineer a new complementation reporter (NanoBit). The NanoBit subunit consists of a 1.3 kDa protein, the Sm (small) bit and an 18 kDa polypeptide called the Lg (large) bit (**Figure 19**). The intrinsic binding affinity of the Sm and Lg bit is low (dissociation constant K_D = 190 µM) in comparison to the average physiological protein-protein binding, thus allowing for the screening of protein-protein interactions (Dixon et al., 2016). The Nanobit was later optimised into Bitlucopt (Bit luciferase optimized), which contains several point mutations and increased luminescence to allow the detection of even weak protein-protein interactions (Dixon et al., 2016).

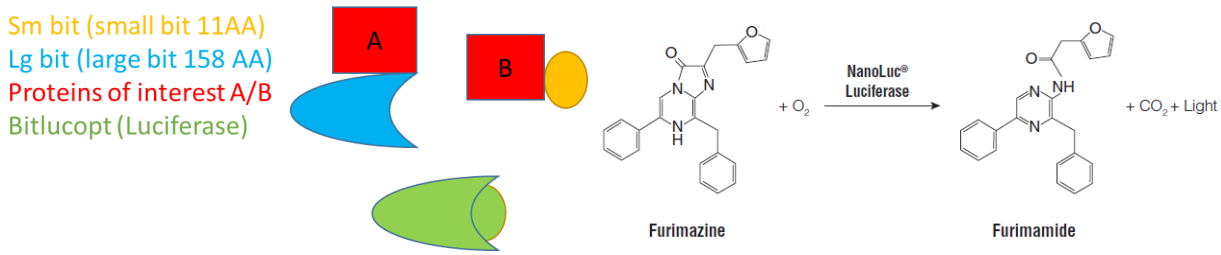

Figure 19. Bitlucopt and subunits catalysing the oxidation of furimazine to furimamide. *(Left) Luciferase system subunits of Bitlucopt (green), proteins of interest (red), Lg bit (blue), Sm bit (yellow), Bitlucopt (active luciferase enzyme, green). (Right) Bioluminescent reaction catalysed by Bitlucopt that converts furimazine to furimamide.*

The bitlucopt enzyme catalyses the oxidation reaction of furimazine to furimamide, which results in the release of carbon dioxide and the emission of light. This emission of light can be quantified using a spectrophotometer. Initially, a number of tests were performed to ensure that this system was functional in *M. xanthus*. Several luciferase constructs were transformed into *M. xanthus* and tested for bioluminescence. The full length bitLucopt was used as a positive control (PAP259 plasmid) and compared with plasmids that contained HupA with a C-terminally-tagged Sm-bit (PAP256), HupA with a C-terminally tagged Lg-bit (PAP257), and a construct, which contained a HupA protein attached to both Sm and Lg (PAP118). Pap256 and Pap257 served as negative controls. HupA is a 10 kDa bacterial chromatin-associated protein from *Clostridium difficile* that self-interacts *in vivo* (Oliveira Paiva et al., 2019). To ensure that the plasmids were taken up by *M. xanthus,* a 1.38 Kbp region was added to each of the luciferase plasmids in order for them to be incorporated at the *attB* site. Both MglA and BacM were cloned into the PAP118, PAP256 and PAP257 plasmids. MglA was C-terminally attached to the Sm bit *via* a small linker region, and BacM was cloned and C-terminally attached to the Lg bit *via* the same small linker region. Previous observations showed that *M. xanthus* grew slower in the presence of the antibiotic tetracycline as it is toxic to the cells (**Chapter IV 4.3.7 Page 125**). Unsurprisingly, when MglA and BacM were cloned and overexpressed using the tetracycline-controlled PAP118 plasmid, the cells grew poorly. More specifically, it took over a week to grow *M. xanthus* cells on hard agar plates containing 5 and 2 µg/ml tetracycline. This concentration was much lower than the 10-15 µg/ml used in several publications for growth on hard agar (Bullock et al., 2018; Yang et al., 2018). The poor growth observed during the expression of the two proteins in the presence of tetracycline made it impossible to meaningfully interpret any potential protein-protein interactions in these cells. In order to solve this problem, the bitlucopt parts, parts essential for the Sm and Lg tagging of proteins, of the PAP256, PAP257, PAP259 and PAP118 constructs were cloned into the PMR3679 plasmid (Iniesta et al., 2012).

This plasmid has a kanamycin resistance gene and a vanillate-inducible promoter and has a track record of being successfully used in *M. xanthus* (Cotter et al., 2017; Kaimer & Zusman, 2016; Vassallo et al., 2015). After successful cloning, the constructs were transformed into *M. xanthus* and checked for their ability to express luciferase (**Figure 20**). No obvious toxicity was observed during the expression of the luciferase system using the PMR3679 plasmid. The Bitlucopt construct (PAP259) showed an overload message when measured using the LUMAT3 luminometer. This result indicated that the luciferase enzyme was not only functional in *M. xanthus*, but due to its high efficiency after prolonged expression of bitlucopt in the cell would result in a light output outside of the measurement range of the luminometer (overload message). The other tested plasmids showed values between 3,000 and 13,000 relative light units (RLU). PAP118 contained both a HupA protein attached to the Sm and Lg subunit and showed a positive interaction (**Figure 20**). This was an indication that the dimeric HupA from *C. difficile* when expressed in *M. xanthus* successfully dimerizes and could function as a positive control.

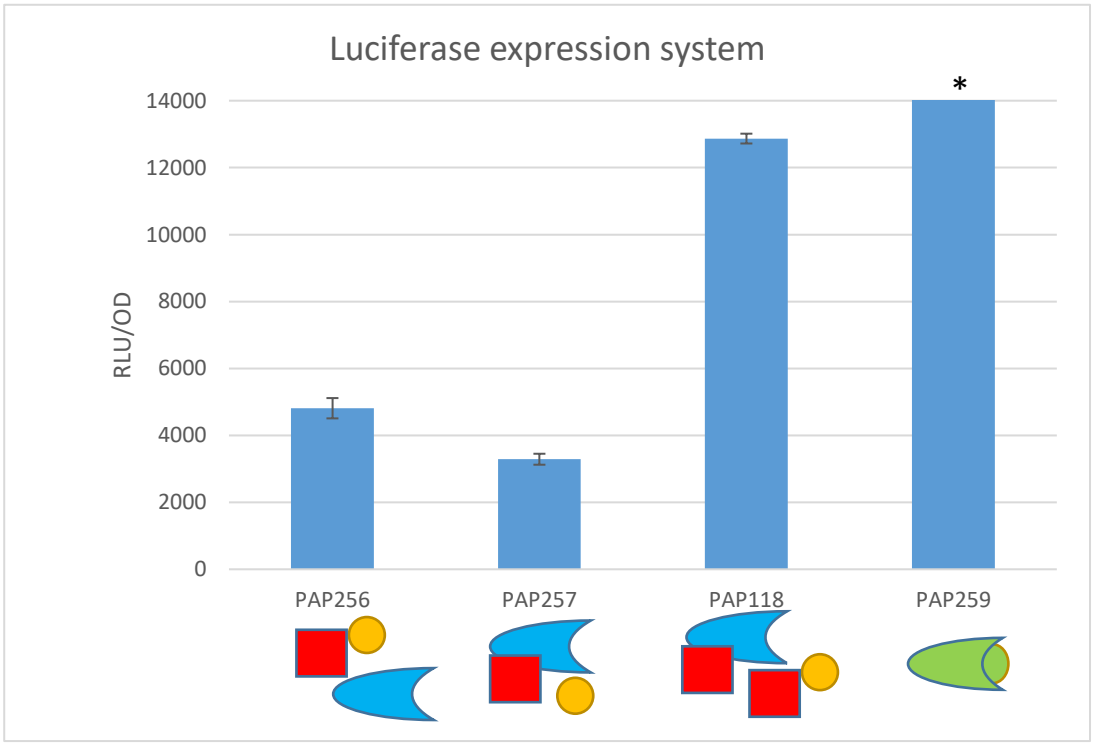

Figure 20. Expression of Bitlucopt subunits using the PMR3679 plasmid in M. xanthus. *Sm bit (Yellow), Lg bit (Blue), HupA (Red), Bitlucopt (Green). *overload message on the LUMAT3 indicating too much light. The means of the results of three independent experiments and the standard deviations of the means (error bars) are shown.*

3.3.3 N-terminally tagged Sm and Lg bit luciferase system

Based on the measured data, MglA seemed to interact with the C-terminus of BacM. This was based on MglA being present in the pulldown fraction of full length BacM, but missing from the C-terminally truncated BacM fraction (**Chapter II 2.3.1 Page 46**). Based on this result, the C-terminal tagging with the Sm and Lg bit using the PAP constructs might interfere with the identification of protein-protein interactions including BacM and MglA. In order to prevent this, a new luciferase construct was designed that would allow for the expression of proteins with an N-terminally tagged Sm or Lg bit (**Figure 21**). For the design of this construct, the restriction enzymes (NdeI, KpnI, BglII, EcoRI, MluI, and NheI, yellow) that are present in the multiple cloning site (MCS) of the PMR3679 plasmid were used. Two ribosomal binding sites (orange) were added in front of the Sm and Lg bit to ensure efficient and accurate translation of mRNA. The Sm (dark blue) and Lg (green) bit were both followed by a short flexible linker region (light blue). The amino acid sequence of this linker region is GSSGGGGSGGGGSSG in which the glycine residues provide flexibility and serine conformational and energetic stability (Argos, 1990). The linker was followed by a restriction site KpnI, a HupA sequence (purple), and a BglII site for the cloning of genes attached to the Sm bit. The second linker region was followed by an EcoRI restriction site, a HupA sequence (purple) and another restriction site MluI for the cloning of genes attached to the Lg bit. At the end of the construct a SlpA terminator region (red) was added to efficiently stop transcription.

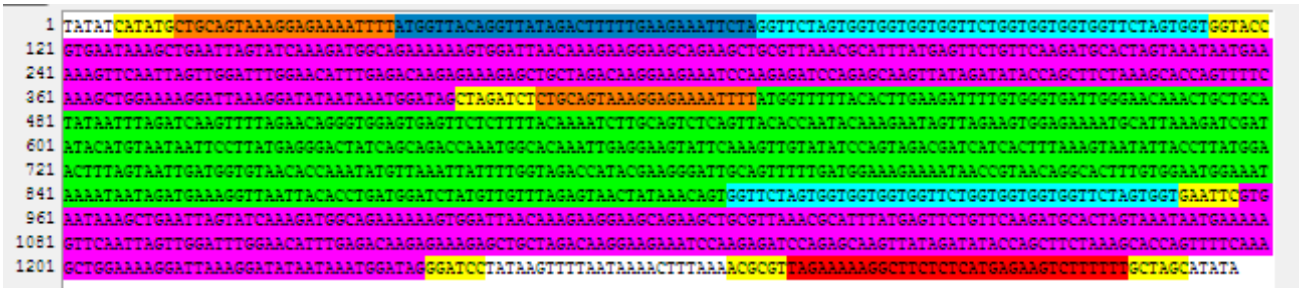

Figure 21. Luciferase system sequence for N-terminally tagged Sm and Lg bit. *restriction sites (yellow), ribosomal binding sites (orange), Sm bit (dark blue), flexible linker region (light blue), HupA (purple), Lg bit (green), SlpA terminator region (red).*

3.3.4 Identification of interaction partners of MglA using the luciferase system in *E. coli*

Two Ras-like GTPases MglA (MXAN_1925) and SofG (MXAN_6703) were cloned at the Sm position adding the 1.3 kDa Sm-tag to their N-termini. Then BacM, N, O, P, MreB, MasK, MglB and RomR were cloned at the Lg position adding the 18 kDa Lg-tag to their N-termini. The smaller Sm-tag was added to the Ras-like GTPases because MglA and SofG are prone to aggregation when overexpressed (Bulyha et al., 2013; Patryn et al., 2010). The Lg-tag was added to the bactofilins because they are known to form stable filaments; in fact, BacM even forms filaments when expressed as a red fluorescent protein fusion protein (Koch et al., 2011). By adding the Sm-tag to the Ras-like GTPases, the chances for miss-folding and hindrance of the protein-protein interactions were reduced. The constructs were then transformed into Dh5α cells and checked for luciferase expression by the addition of vanillate. At first it was checked whether there was a difference between un-induced and induced expression, and whether MglA and BacM interacted in *E. coli* using the luciferase system. There was a significant increase in RLU between MglASm BacMLg and the controls that contained the proteins individually. The SmLg (negative control) which expressed Sm and Lg separately without any attached proteins showed no significant increase in luciferase, thus indicating that the intrinsic affinity for these subunits was low when expressed in *E. coli*. The Bitlucopt (positive control) showed some light even when un-induced; this was most likely due to leaky expression. Interestingly, a significant reduction in luciferase was observed when the C-terminus of BacM was removed, confirming the previous finding that the C-terminus of BacM seemed to be crucial for the binding to MglA (**Figure 22**).

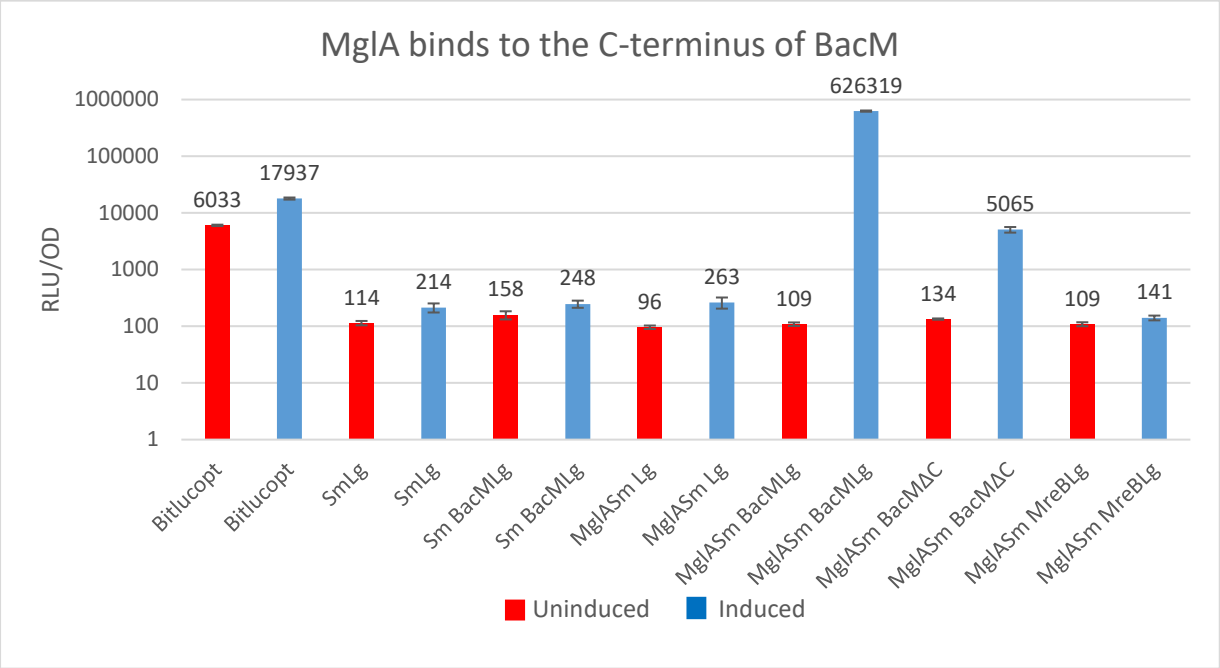

Figure 22. Un-induced (red) and induced (blue) expression of MglASm and BacMLg in E. coli. *Cultures were induced with 500 µM vanillate for 6 hours at 30 ^{o}C. Culture density was measured and diluted to an OD_{600} = 1. Y-axis are the relative light units per OD_{600} = 1. Data shown are means ± standard deviation of three biological replicates.*

Next, the remaining bactofilins plus MreB, RomR and MasK were tested for their ability to interact with MglA in *E. coli*. This resulted in the identification of a potential interaction between BacO and MglA (**Figure 23**), thus verifying the previous interaction observed between BacO and MglA using the converted bacterial two-hybrid system in *E. coli* (**Figure 18**). In these experiments MglA Sm MglB Lg was included as a positive control. MglB is the GTPase-activating protein (GAP) of MglA and therefore was expected to be able to interact with MglA as GAP proteins are responsible for the stimulation of GTPase activity of Ras-like GTPases (J. L. Bos et al., 2007). No interaction was detected between MglA and MreB, RomR or MasK. Interestingly, a recent publication had demonstrated that RomR forms a complex with RomX and that this complex then binds to MglA (Szadkowski et al., 2019). The RomR-RomX complex was suggested to function as the guanine exchange factor (GEF) of MglA.

This newly identified interaction of MglA with RomX and a previously found potential interaction of MglA with RomR was deemed weak and could explain why no interaction between these proteins were detected using the luciferase assay (Szadkowski et al., 2019). Therefore, the validity of these recently described interactions remain to be confirmed. Moreover, MasK had previously been identified using a yeast two-hybrid system to interact with MglA, an interaction that we could not confirm in our experiments (Thomasson et al., 2002). One explanation for this failure could be that the change of expression host (*E. coli* instead of yeast cells) impacted our ability to identify this interaction (Gasser et al., 2008). Alternatively, if the N-terminal region of one of these two proteins is crucial for the interaction, then the interaction could potentially be disrupted by the addition of the Sm or Lg tag. MasK is predicted to have an N-terminal cytoplasmic domain containing 6 prolines within 22 amino acids potential forming a proline-binding domain (Thomasson et al., 2002; Williamson, 1994). As a similar proline-rich C-terminal region in BacM was responsible for binding to MglA (**Chapter II 2.3.1 Page 46**), the presence of the prolines in the cytoplasmic N-terminal domain of MasK made it likely that this part of the protein was involved in the binding to MglA. If this reasoning was correct, it could offer an explanation why no interaction between these two proteins was observed with the luciferase system.

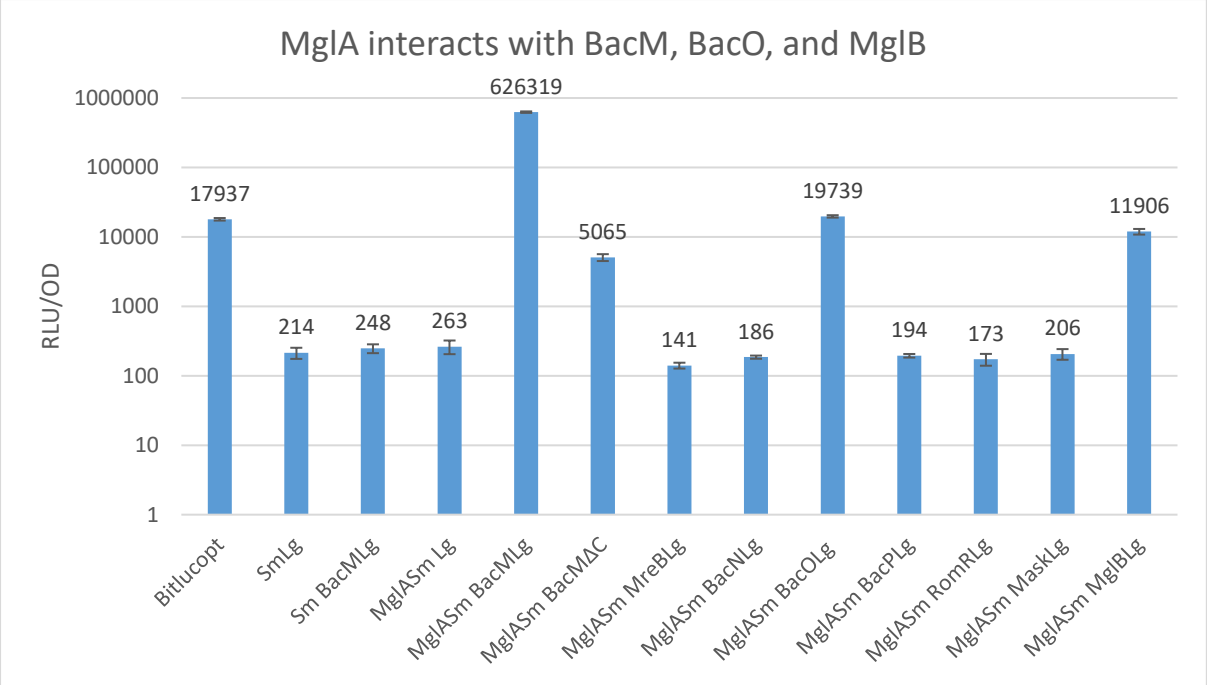

Figure 23. MglA interacts with BacM, BacO and MglB but not with BacN, BacP, MreB, RomR or MasK using the luciferase system in E. coli. *Cultures were induced with 500 µM vanillate for 12 hours at 30 °C. Culture density was measured and diluted to an OD_{600} = 1. Y-axis are the relative light units per OD_{600} = 1. Data shown are means ± standard deviation of three biological replicates.*

3.3.5 Identification of interaction partners of SofG using the luciferase system in *E. coli*

Next, all *M. xanthus* bactofilins plus MreB, RomR, MglB and MasK were tested for their abilities to interact with SofG in *E. coli.* These experiments resulted in the identification of BacO and MglB as novel potential interaction partners of SofG. In this interaction assay, the proteins were two hours longer expressed than usual, which resulted in a higher average amount of relative light units (RLU) (~1000-4400 RLU) of the non-interacting proteins in comparison to the interaction assay performed with MglA (~200 RLU **Figure 23**). The most likely explanation for the observed data is that the increased amount of Sm and Lg inside the cell lead to the coincidental binding of the two protein subunits and therefore to a higher background of light. The increased expression of the proteins was chosen as to be able to identify weaker protein-protein interaction and resulted in the discovery of a potential interaction between SofG and BacP.

The interaction between these two proteins seemed to inhibit the formation of the SmLg complex, thereby leading to a significantly reduced amount of light (RLU). Importantly this interaction had also been observed in the previous bacterial two-hybrid assay (**Figure 18**) and was also reported in a previous publication that used both a pulldown assay and co-expression in *E. coli* (Bulyha et al., 2013). An interesting finding was that SofG like MglA also seemed to interact with BacO and MglB (**Figure 24**). BacO is the smallest bactofilin (127 amino acids) and does not contain a proline rich region like BacM and BacP. Therefore, it is currently unclear how these two Ras-like GTPases and BacO interact.

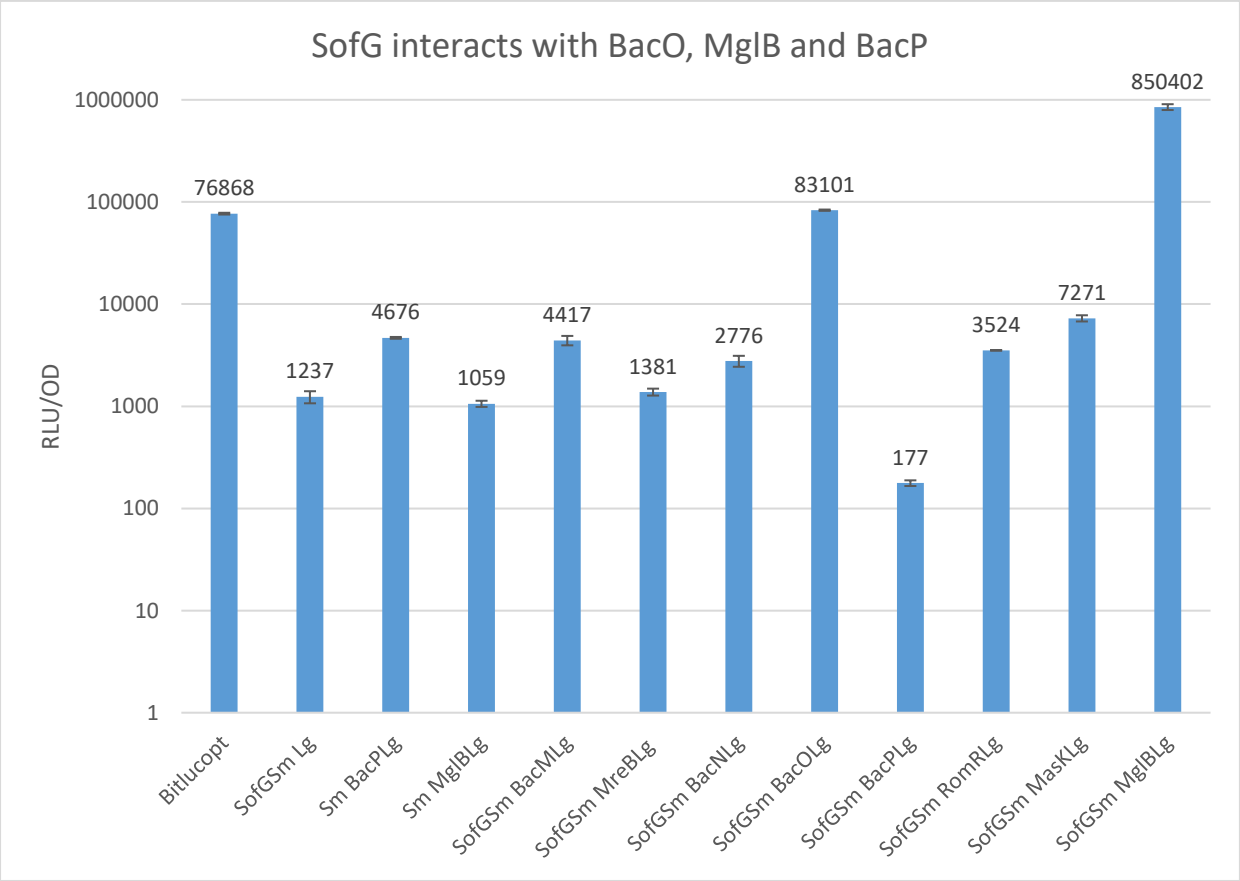

Figure 24. The RasGTPase SofG interacts with BacO, BacP and MglB, but not with BacM, BacN, MreB, RomR and MasK. *Cultures were induced with 500 µM vanillate for 14 hours at 30 °C. Culture density was measured and diluted to an OD_{600} = 1. Y-axis are the relative light units per OD_{600} = 1. Data shown are means ± standard deviation of three biological replicates.*

3.3.6 Validation of interaction partners of MglA using the luciferase system in *M. xanthus*

The *M. xanthus* bactofilins BacM, BacN, and BacO plus MreB, RomR, and MasK were tested for their ability to interact with MglA in *M. xanthus.* These experiments validated the identification of BacM, BacO, and MasK as potential interaction partners of MglA (**Figure 25**). MglASm BacPLg and MglASm MglBLg have not yet been included in this assay due to cloning issues. Using these experiments, we were able to confirm that MasK interacted with MglA when probed in the luciferase system in *M. xanthus,* a result that was not detected in *E. coli* pointing to the important possibility that some protein-protein interactions are only detectable in certain bacterial backgrounds.

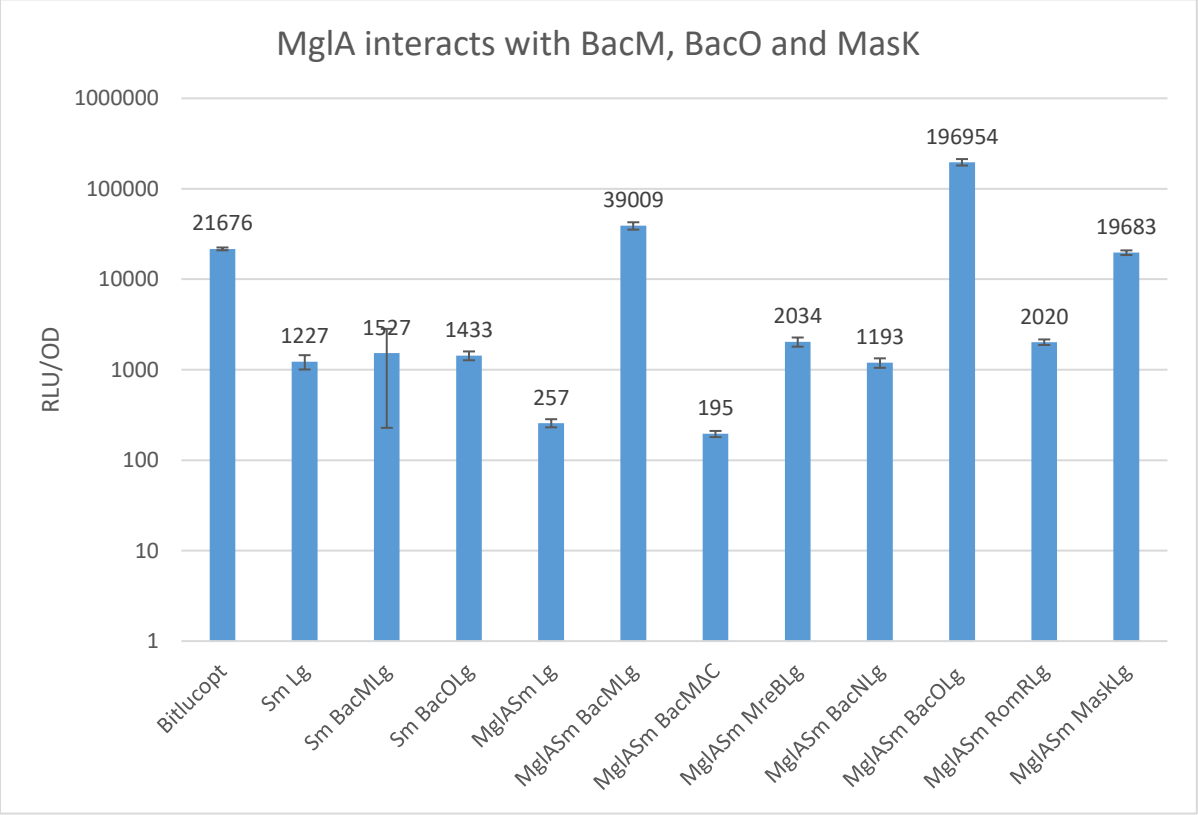

Figure 25. MglA interacts with BacM, BacO and MasK but not with BacN, BacP, MreB, or RomR using the luciferase system in M. xanthus. *Cultures were induced with 50 µM vanillate for 20 hours at 30 ^{o}C. Culture density was measured and diluted to an OD_{600} = 1. Y-axis are the relative light units per OD_{600} = 1. Data shown are means ± standard deviation of three biological replicates.*

3.3.7 Use of the luciferase system for the localization of protein-protein interactions in *M. xanthus*

The high sensitivity of the light emitting reactions of the luciferase system prompted an investigation whether one could use the system for the localization of protein-protein interactions in *M. xanthus*. Although the luciferase-emitted light is quite weak in comparison to fluorescently tagged proteins, a long enough exposure time indeed enabled the localisation of different protein-protein interactions in *M. xanthus*. Thus, allowing the system to be used not only for the identification of interactions but also for the visualisation of their cellular localisation. To adequately judge these results, it was important to keep in mind that the proteins were overexpressed and therefore may be localised in a non-physiological way. When viewed in the light microscope, most of the cells expressing MglASm BacMLg had bipolar clusters with some cells having a cluster at mid-cell (**Figure 26**). An earlier publication had shown that an N-terminally mCherry tagged BacM, which replaced the native BacM, showed irregular cytoplasmic fluorescence present in many parts of the cell, but was absent from regions stained by the DNA stain DAPI (Koch, Mchugh, & Hoiczyk, 2011). These observations are in line with the observed patterns in **Figure 26** and the observed fluorescent clusters described in **Chapter V 5.3.10 page 157**.

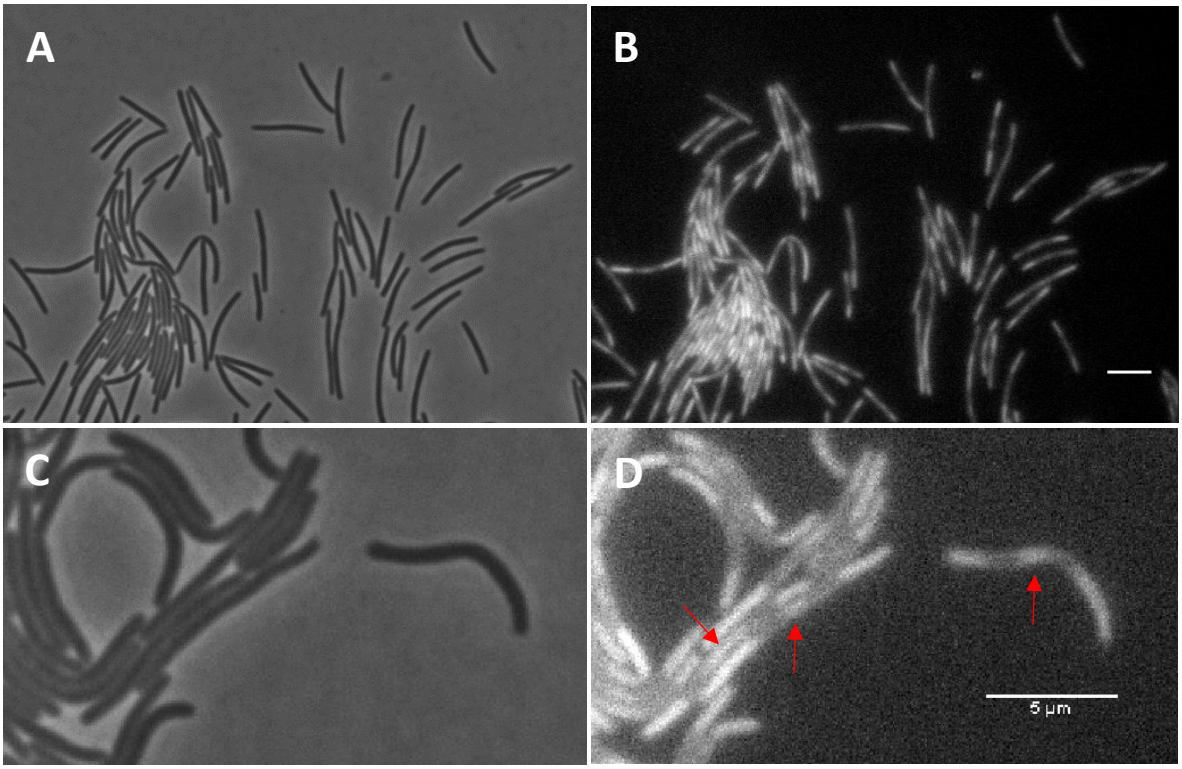

Figure 26. Localisation of MglASm BacMLg in cells grown on TPM agar. *Pictures were taken using brightfield (A/C) and FITC (B/D). Mid-cell clusters are indicated with red arrows (D). Scale bars: 5 µm.*

When MglA was co-expressed with BacM missing the C-terminus, unipolar clusters were observed in the cells (**Figure 27A**), while co-expression of MglA and MasK lead to the formation of lateral clusters (**Figure 27C/D**). Previously, a C-terminal mCherry-tagged MasK was found to form unipolar clusters at the leading pole in some of the observed cells (S. Fremgen et al., 2013). However, all the cells contained fluorescent clusters throughout the cell, which was in line with the observations in **Figure 27C/D** (S. Fremgen et al., 2013). Co-expression of MglA and BacO resulted in cells with diffuse fluorescence as well as cells with bipolar or a mid-cell cluster (**Figure 27E**). This observation was similar to the bipolar and mid-cell clusters of the BacNOP complex, observed by immunofluorescence microscopy (Lin et al., 2017). No clusters were observed when cells were viewed that expressed bitlucopt or SmLg (**Figure 27B/F**).

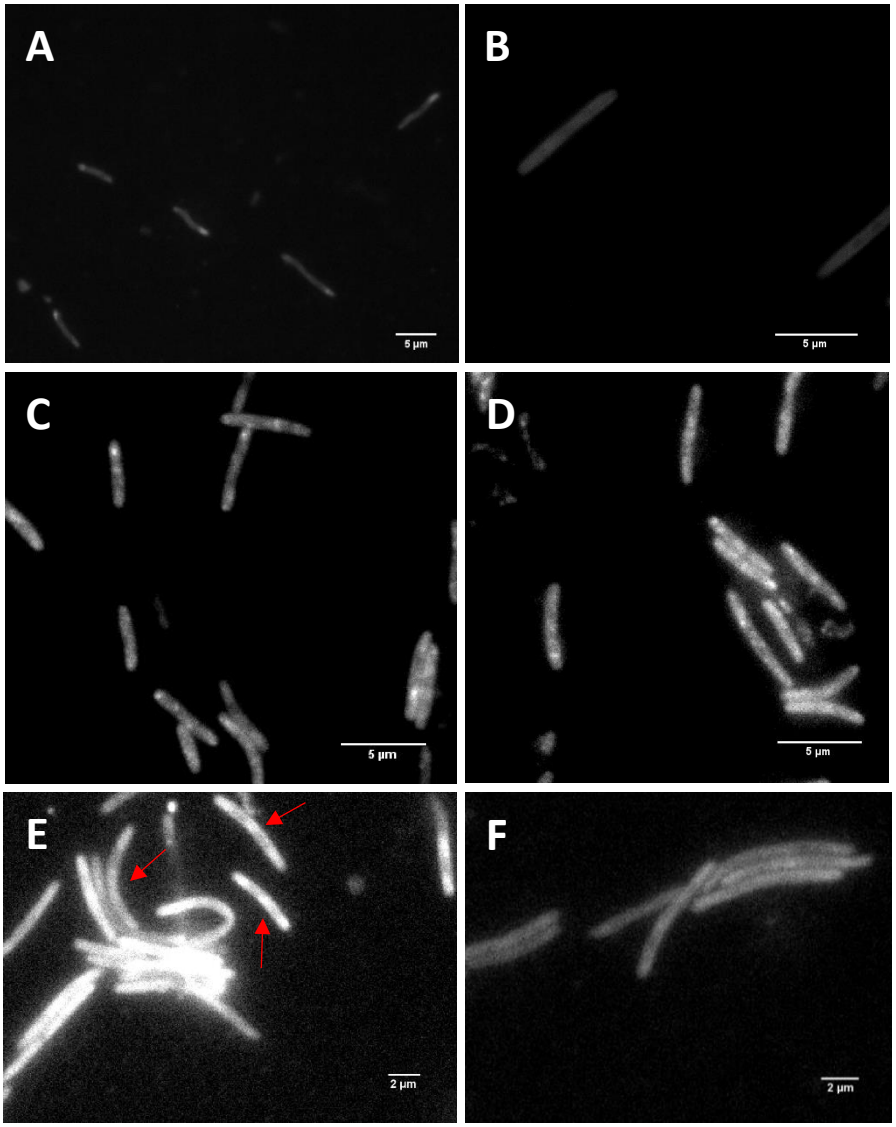

Figure 27. Localisation of MglASm and BacM$^{(codons\ 28–128)}$Lg, MglASm and MasKLg, MglASm and BacOLg and bitlucopt in TPM agar-grown cells. *(A) unipolar cluster formation in cells expressing BacM$^{(codons\ 28–128)}$Lg (B) Sm and Lg diffuse fluorescence (C/D) MasKLg forms clusters along the cell (E) clusters and diffuse fluorescence BacOLg (F) Diffuse fluorescence of bitlucopt. Mid-cell clusters are indicated with red arrows in (E).*

M. xanthus cells are known to possess background fluorescence (Parish, 1985), which made it necessary to investigate whether the observed background fluorescence interfered with the identification of bioluminescence from the luciferase assay or whether WT cells could oxidize furimazine without the presence of the luciferase enzyme. WT cells and WT cells plus furimazine showed weak diffuse fluorescence, indicating that if they could oxidize furimazine it seemed to be minimal and that the background fluorescence was low when compared to cells expressing bitlucopt (**Figure 28**). Consequently, the background fluorescence did not interfere with the localisation of the protein-protein interactions.

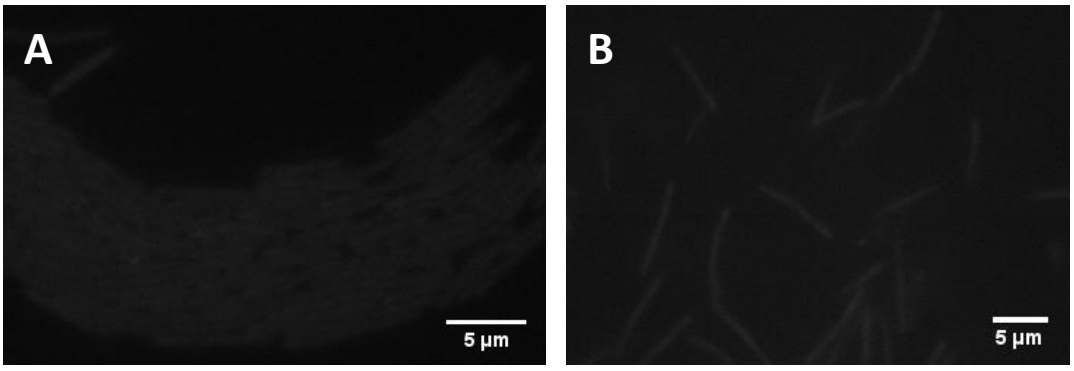

Figure 28. Background fluorescence of WT cells with and without furimazine on TPM agar-grown cells.
(A) WT cells + furimazine (B) WT cells. Both cells show very low background fluorescence.

3.4 Discussion

In this chapter, data were presented that documented that a novel luciferase-based bacterial two-hybrid system allowed for the first time to identify and validate protein-protein interactions directly in *M. xanthus*. Moreover, it was shown that this system was also functional in *E. coli* thereby allowing to directly compare interactions that were identified in both bacterial backgrounds. The new bacterial two-hybrid system relies on the enzyme luciferase that is split in two subunits (Sm and Lg) that are each attached to a protein of interest. When the two proteins interact, a functional complementation of the luciferase enzyme subunits takes place, which allows the conversion of furimazine to furimamide resulting in the emission of light (Dixon et al., 2016; Hall et al., 2012; Taylor et al., 2018).

As working in the physiological relevant bacterial background generally promised to identify potential protein-protein interactions more faithfully, the identified interactions most likely represented real interactions. Despite this advantage, several problems were identified during the course of the investigation that have to be considered when judging the results. These problems included the observed miss-folding and aggregation of proteins like MglA and SofG in *E. coli* and the expression of heterologous proteins that have no homologous counterparts in the bacterial host of choice such as Ras-like GTPases or bactofilins in *E. coli*. The latter case may be problematic as necessary chaperones are not present that will help to correctly fold these proteins.

Another important factor that can influence the outcome of the two two-hybrid assays may be the difference of the used tags. The size of the tags T25 (720 bp), T18 (606 bp) in the classical two-hybrid assay are much larger than the tags, Sm (36 bp) and Lg (477 bp) used for the luciferase system. Importantly, the use of larger tags might interfere more likely with the studied protein-protein interaction. Furthermore, in the classical two-hybrid assay no linker was included between the tag and the protein.

As the linker functioned to prevent the tag from interfering with proper protein folding and protein interaction, the omission in the classical system may interfere with some protein-protein interactions (Reddy Chichili et al., 2013).

A shift in emission spectra was observed, when looking at the fluorescence of *M. xanthus* cells expressing the bitlucopt luciferase (FITC), in comparison to the 460 nm emission peak (DAPI) for Nluc (Nanoluc; Hall et al., 2012). The difference in emission spectra could be a consequence of the *M. xanthus* cells being on TPM agar, as hard *versus* moist samples can result in a shift in excitation and emission spectra (Pellach et al., 2012). In addition, the changes made to the Nluc luciferase, to create the bitlucopt luciferase, could play a role in the observed shift in emission spectra (Dixon et al., 2016).

Importantly, the luciferase two-hybrid system mostly confirmed the results obtained with the classical two-hybrid assay (**Figure 18**). Using both systems the following interactions could be validated and appeared to represent real protein-protein interactions: MglA and BacM, MglA and BacO, and SofG and BacP were reproducible observed in the luciferase system in *E. coli*. In contrast, the interaction between SofG and MreB could not be confirmed using the luciferase system, which may be explained by the use of differently tagged proteins in these experiments. Moreover, in contradiction with published results (Treuner-Lange et al., 2015) no interaction between MreB and MglA was found using any two-hybrid system. In contrast to MreB, BacM however showed a clear interaction with MglA in all performed assays making this interaction the most robust detected interaction (**Table 9**). In addition, upon removing the C-terminus of BacM (including the proline rich region; BacM$^{\Delta 139\text{-}151}$), a reduction in light was observed.

Table 9 Identification protein-protein interactions using two different two-hybrid assays. ** Protein interactions that still have to be checked.*

Protein-protein interactions	Bacterial two-hybrid system in *E. coli*	Luciferase system in *E. coli*	Luciferase system in *M. xanthus*
MglA-BacM	YES	YES	YES
MglA-BacN	NO	NO	NO
MglA-BacO	YES	YES	YES
MglA-BacP	NO	NO	*
MglA-RomR	NO	NO	NO
MglA-MasK	*	NO	YES
MglA-MglB	*	YES	*
MglA-MreB	NO	NO	NO
SofG-BacP	YES	YES	*

This confirmed the previously identified pulldown result in which MglA was shown to interact with BacM only when the C-terminus was present (**Chapter II Page 46**). Finally, the localization of MglA and BacM in the fluorescence light microscope using the luciferase system showed a clear co-localization of both proteins to subpolar regions of the cell and in the case of BacM$^{(28–128)}$ to a unipolar cluster. Additional clusters were observed for BacM and MglA at mid-cell, while no mid-cell localization was observed when MglA was expressed with BacM$^{(28–128)}$. These mid-cell clusters seemed to occur only when the cell was elongated (**Chapter III 3.3.7 Page 98**).

Besides of BacM, MasK was identified as an interaction partner of MglA using the luciferase system in *M. xanthus* (Thomasson et al., 2002). MasK together with MglA formed light microscopically visible clusters when expressed in *M. xanthus*. These clusters seemed to be located at the cell membrane, indicating that MasK was embedded in the cytoplasmic membrane when it interacted with MglA.

This interaction was similar to the binding behaviour between RasGTPases and protein kinases observed in eukaryotes. For example, Abelson tyrosine-protein kinase (ABL) is known to phosphorylate tyrosine 137 in H-, K-, and NRas (Ting et al., 2015).

In addition, BacO was identified as an interaction partner of both MglA and SofG. Apart from having the DUF583 bactofilin domain, BacO does not share a lot of homology with BacM. Likewise, BacP does not share much homology with BacO outside the bactofilin domain (**Figure 29**). Interestingly, BacO does not contain a proline-rich region in contrast to both BacM and BacP. These results indicated that both MglA and SofG potentially use a similar type of interaction with BacO that differs from the interactions with BacM and BacP.

As all bactofilins contain the conserved DUF583 domain, and in the case of BacO, this domain entails the C-terminus of the protein (**Figure 29**), one option could have been that the DUF583 domain was involved in this interaction. If this would have been the case, we would have expected, based on the conservation of this domain that SofG and MglA would interact with all bactofilins. However, this was not what was observed. Therefore, SofG and MglA are probably both interacting with the N-terminus of BacO. MglA and BacO co-localized diffusively in the cytoplasm in the luciferase-based two-hybrid assay forming poorly visible clusters at both cell poles and the mid cell. Interestingly, this cluster distribution is in line with previous observations using immunofluorescence with an BacO antibody in WT cells (Lin et al., 2017). The observed more diffuse localization in some cells in the luciferase-based assay may be the consequence of the necessary overexpression of BacO in the assay.

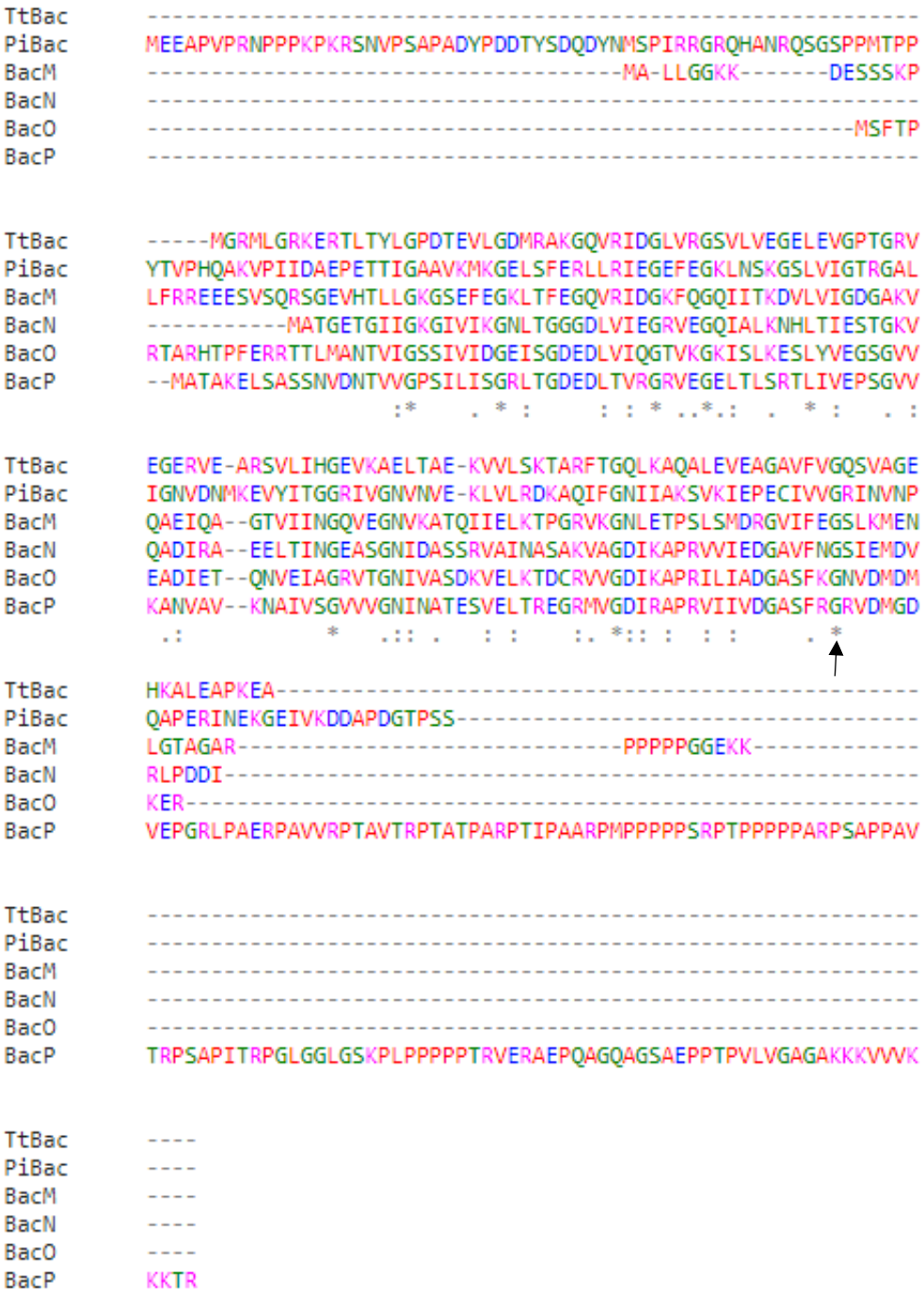

Figure 29. Clustal Omega alignment of T. thermophilus Bactofilin (TTHA1769 or TtBac), P. infestans bactofilin (PITG_07992 or PiBac), M. xanthus bactofilins BacM, BacN, BacO, and BacP. *The DUF583 domain of BacO ends on a guanine leaving a nine-amino acid-long C-terminus (black arrow). An * (asterisk) indicates positions which have a single, fully conserved residue. A : (colon) indicates conservation between groups of strongly similar properties. A . (period) indicates conservation between groups of weakly similar properties.*

Surprisingly, the interaction of SofG with BacP lead to a reduction in light output. This could have been caused by the two proteins interacting in such a way that they inhibited the formation of the SmLg complex. This inhibition of light, like the increase of light, indicates a potential interaction between the two proteins. To clarify this issue, luciferase plasmids would need to be designed in such a way to allow for the C-terminal protein tagging with Sm and Lg. If these constructs would prevent the inhibition of light, the inhibition would have been the result of a non-active luciferase formation during the assay. In extension, systematic tagging of different parts of the two proteins could in theory be used to identify the parts of the protein that are essential for the interaction.

3.5 Conclusion and outlook

The luciferase system allowed for the verification of previously discovered or described protein-protein interactions and the identification of novel such interactions for MglA and SofG. These newly discovered protein interactions included MglA interacting with BacM and BacO and SofG interacting with MglB and BacO. Although the interactions identified with SofG still have to be tested in *M. xanthus*. The identification of BacO as an interaction partner of both MglA and SofG provided another link between the bactofilin cytoskeleton and the Ras-like GTPases indicating that one fundamental role of bactofilins is to act as scaffolds for these important proteins. In this context, it would be interesting to establish whether the link between bactofilins and Ras-like GTPases is conserved in different bacterial species.

The further development of the luciferase system promises considerable advances in our understanding of protein-protein interactions in *M. xanthus*. The development of three additional luciferase plasmids which would allow C-terminal tagging of proteins or combinations of N and C-terminal tagged Sm and Lg bits, would permit screening and identification of additional protein-protein interactions further increasing the versatility of the system. In addition, the optimisation of the system for improved localisation of protein interactions inside the cell would allow to spatially resolve these functional processes.

An article published in 2018 reported the use of a similar luciferase-based system for *in vivo* bioluminescence imaging in mice (Taylor et al., 2018). The authors used the Nanoluc reporter and combined it with eGFP and LSSmOrange creating Lumifluors. These Lumifluors are the brightest bioluminescent signals known to date. Other advantages of the Lumifluors are increased intensity, sensitivity and reduced image acquisition times (Schaub et al., 2015). Combining the bitlucopt subunits with fluorophores might enable the more accurate localisation of these proteins and their interactions in *M. xanthus*.

Chapter IV

4. Biochemical characterisation of BacM and MglA

4.1 Introduction

In this chapter, serendipitously made discoveries will be discussed that were made during experiments that lead to a better understanding of the interplay between MglA and BacM. These discoveries include indications of post-translational modification of MglA, changes in MglA expression levels in bactofilin deletion mutants, attempts to create a ΔBacMΔMglA double mutant, consequences of the overexpression of MglA in *M. xanthus*, and how the overexpression of MglA impacts ΔBacM cells. A lot of these observations were correlated with our current knowledge of Ras and Ras-like proteins from eukaryotic, yeast and bacteria have a lot in common. The experimental results in this chapter combined with the current literature provide new insight into the potential functions of these two proteins and how they impact important processes in *M. xanthus*.

4.2 Materials and Methods

4.2.1 Cloning

MglA was cloned under the pMAT3 plasmid for the controlled expression of MglA in *M. xanthus*. In addition, MglA was cloned into pMR3679 and pMR3651, which added a C-terminal eYFP tag. BacM was cloned into the pSWU30 plasmid. *mglA* and *bacM* genes were amplified using PCR and digested using different restriction enzymes compatible with the target plasmid. The *mglA* gene inserted into pMR3561 was missing a stop codon and was checked using EXPASY translate tool for being in-frame with the eYFP tag. The strains generated and primers used for cloning are listed below (**Table 10**, **Table 11**).

Table 10: Strains used in this chapter

Strains	**Expression**	**Reference**
pMAT3 MglA	*ΔMglA M. xanthus*	This study
pMR3679 MglA	*ΔBacM M. xanthus*	This study
pMR3651 MglA	*ΔBacM M. xanthus*	This study
pSWU30 BacM	*ΔBacM M. xanthus*	This study
ΔBacM	*ΔBacM*	(Koch et al., 2011)
WT (DK1622)	*WT*	(D. Kaiser, 1979)
pET-DUET MglA	Bl21 cells	This study
pET-DUET MglA	Rosetta$_{TM}$ cells	This study

Table 11 Primer list

Plasmid + gene	Description Forward primer (F) Reverse primer (R)	Sequence 5’ to 3’ end
pMR3651/3679 MglA	Mx_MglA_F_NdeI	**ATCGC** *CATATG* ATGTCCTTCATCAATTACTCATC
pMR3651/3679 MglA	Mx_MglA_R_EcoRI	**ATATA** *GAA TTC* TCACCACCCTTCTTGAGCTC

pBJ114 ΔBacM	ΔMXAN_7475 Primer A EcoR-I	**TATAT** *GAA TTC* AAGCAAGTCGCGGACAAG
pBJ114 ΔBacM	ΔMXAN_7475 Primer B	AACGCACGT- GTCCTACTC CTTCCTGAG
pBJ114 ΔBacM	ΔMXAN_7475 Primer C	GAGTAGGAC- ACGTGCGTT CCTGGAAGC
pBJ114 ΔBacM	ΔMXAN_7475 Primer D Xba-I	**TATAT** *TCT AGA* TCTCTTCTTCCTGGTCCA
pSWU30 BacM	Mx_BacM_F_XbaI	**TATAT** *TCT AGA* AAGCAAGTCGCGGACAAG
pSWU30 BacM	Mx_BacM_R_EcoRI	**TATAT** *GAA TTC* TCTCTTCTTCCTGGTCCA
pMAT3 MglA	Mx_MglA_F_XbaI	**TATAT** *TCT AGA* ATGTCCTTCATCAATTACTCATC
pMAT3 MglA	Mx_MglA_R_BamHI	**TATAT** *GGA TCC* TCACCACCCTTCTTGAGCTC

4.2.2 Western blotting

Constituent proteins from cell lysates or subfractions of lysates were separated by SDS-PAGE on a 10-well 4-20% Tris-Glycine gel (Invitrogen). Protein samples were mixed 1:4 with a 4x SDS buffer. These samples were supplemented with 20 mM dithiothreitol (DTT, Sigma). Samples were boiled for 10-15 minutes to denature proteins, loaded onto the SDS gel and run at a 100 volt for 2,5 to 3 hours. Proteins on the SDS gel were transferred to a pre-soaked nitrocellulose membrane (Bio-Rad). This membrane was blocked overnight in 5% powdered fat-free milk dissolved in phosphate buffered saline (PBS). This was done to prevent non-specific adhesion of antibodies to the membrane during blotting. The next day the membrane was washed three times, for 10 minutes each, using 25 ml of PBS-T (phosphate buffer saline with 0.05% TWEEN-20). The primary antibody was applied, which was a rabbit polyclonal MglA antibody (BioServUK) at a dilution of 1:20,000 for 2 hours at room temperature or ON at 4 °C. The membrane was washed three times as described above prior to the addition of Immunopure goat anti-rabbit horseradish peroxidase-conjugated secondary antibody (ThermoScientific). The secondary antibody was added 1:50,000 in PBS-T for 2 hours at room temperature or ON at 4 °C. Visualization of bands was achieved using SuperSignal West Pico chemiluminescent substrate (Thermo Scientific™).

4.2.3 Construction of deletion mutants

In-frame deletion of MXAN_7475 was generated by allelic exchange using the pBJ114 plasmid. The pBJ114 plasmid contains a kanamycin resistance gene and a galactose sensitivity gene. Using PCR a ~500 bp region upstream (AB region) and a ~500 bp region downstream (CD region) of the to be deleted gene were amplified. The PCR products were run on a 1% agarose gel and the bands corresponding to the amplified fragments were gel extracted. The fragments upstream and downstream of the gene were designed to contain a 24 bp region of overlapping sequence.

The overlapping sequence allowed for the linking of the two regions using a second PCR reaction (AD region). This fragment was digested using restriction enzymes compatible with the pBJ114 plasmid and ligated into the pBJ114 plasmid. The AD fragment was checked using sequencing. The AD fragment allowed for the insertion of the plasmid upstream or downstream of the gene. After sequence conformation, 1 µg of the plasmid was introduced into electrocompetent *M. xanthus* ΔMglA cells. Transformants were plated in top agar (0.5%) on CTT and 1.5% agar plates supplemented with 100 µg/mL kanamycin. Removing the kanamycin selection pressure lead to a looping out of the pBJ114 plasmid. When the plasmid was looped out, either the original gene was established, or the gene was replaced with the AD fragment. Colonies were screened for the correct deletion, by plating the cells on both a kanamycin and galactose plate. In theory, the cells should not be able to grow on kanamycin and should grow on galactose, when they have lost the pBJ114 plasmid. However, because galactose is not the most sensitive method, PCR was used in addition to confirm correct deletions.

4.2.4 Growth assays

Cells from three different colonies were grown ON at 32 °C and 200 rpm until OD_{600} = 0.4-0.6. These cells were added to 25 mL of fresh CTT to a starting OD_{600} of 0.05. To these cultures, 50 µM vanillate was added. The OD_{600} was measured at time points T_0 (time of induction), T_1 (1 hour of expression), T_2, T_4, T_8, T_{16}, T_{24}, T_{30}, T_{38}, T_{46}, T_{54}, and T_{62}. The average OD_{600} was calculated for each strain at each time point. Statistical analysis was performed with Prism 7 (GraphPad, Inc.) by two-way ANOVA.

4.3 Results

4.3.1 MglA appears to be post-translationally modified

While isolating MglA from *M. xanthus,* a difference in molecular weight between the *M. xanthus*-expressed MglA *versus* the *E. coli*-expressed MglA band was observed on SDS PAGE (**Figure 30**). MglA expressed in *M. xanthus* ran at a molecular weight that was about 1-2 kDa larger than MglA expressed in *E. coli*. Two different samples of *E. coli* MglA expression strains (**Figure 30**, **Lanes 3/4**) were run next to a non-induced *E. coli* sample (**Figure 30, Lane 5**) to identify the band corresponding to MglA. The difference in molecular weight between MglA expressed in *M. xanthus* WT (DK1622) cells and *E. coli*-overexpressed MglA indicated that the protein was post-translational modified in *M. xanthus*. To confirm the post-translational modification, and to verify that the band observed in WT cells was MglA, we raised an antibody against MglA.

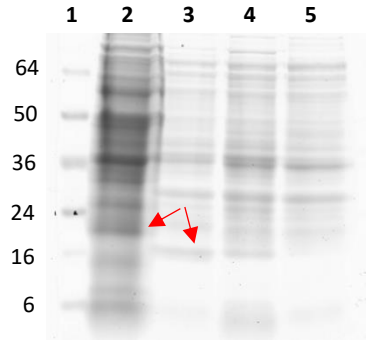

Figure 30. MglA is post-translationally modified in M. xanthus. *Lane 1) See blue prestained protein ladder, Lane 2) WT cells (DK1622), Lane 3) MglA expressed in BL21 cells, Lane 4) MglA expressed in E. coli Rosetta cells, Lane 5) non-induced BL21 E. coli cells. Difference in MglA bands indicated by red arrows. Samples were run on a 4-20% tris/glycine gel. Numbers left from the marker lane correspond to the molecular weight in kilodalton.*

In addition to the MglA antibody, a polyclonal antibody against BacM was raised. Both antibodies were purified and tested for their specificity using Western blots. The ΔMglAB (DK6195) strain, which lacks both MglA and its GAP protein MglB, was used to affinity purify the MglA antibody. The ΔMglA strain was not used because it was unavailable in the lab at the time. Additionally, it turned out that part of the MglA protein was still expressed in the ΔMglA mutant that is used in most *M. xanthus* laboratories (**Chapter V page 157**). The resulting MglA antibody was highly specific, labelling a single band at a molecular weight of about 23 kDa, which was about 2 kDa higher than its calculated molecular weight (**Figure 31 Lane 2**). This MglA band on Western blots ran at a similar height as the MglA band seen in SDS PAGE gels (**Figure 30 Lane 2**). Importantly, the ΔMglAB cell sample which was used as a negative control did not show an MglA-associated band (**Figure 31 Lane 3**). The second used antibody, the anti BacM antibody was developed and purified by Jeffery So (Fallis, 2013).

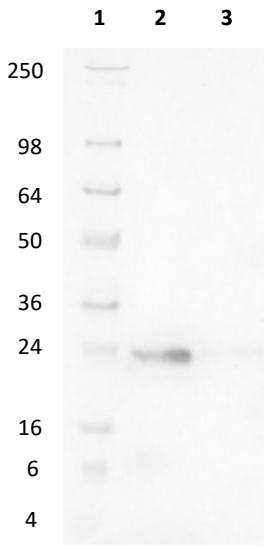

Figure 31. Western blot of MglA using the newly raised anti MglA antibody. *Lane 1: See Blue pre-stained marker; Lane 2: WT cells (DK1622); Lane 3: ΔMglAB (DK6195). Samples were run on a 4-20% tris/glycine gel. Numbers left from the marker lane correspond to the molecular weight in kilodalton.*

A Western blot was done to examine the difference between *M. xanthus* and *E. coli*-expressed MglA. Interestingly, MglA expressed in *E. coli* was lacking the post-translational modification, thereby potentially explaining the aggregation of the protein, when expressed in *E. coli* (**Figure 32**).

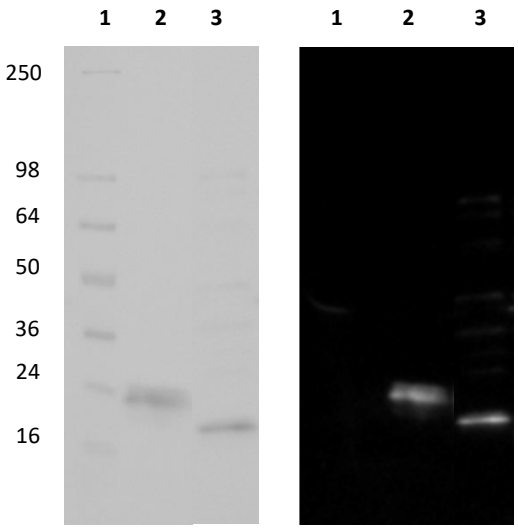

Figure 32. Western blot of E. coli overexpressed MglA and M. xanthus MglA expressed at physiological level. *Lane 1) See blue pre-stained marker, Lane 2) M. xanthus WT cells, Lane 3) pET-DUET1 MglA Rosetta cells. Samples were run on a 4-20% tris/glycine gel prior to Western blotting. Numbers left from the marker lane correspond to the molecular weight in kilodalton.*

As mentioned in **Chapter II page 58**, an attempt was made next to natively isolate MglA from *M. xanthus***.** After the first run over nickel beads, an SDS PAGE gel showed two bands: one around 21 kDa, and one around 23 kDa, the calculated size of MglA (**Figure 33**).

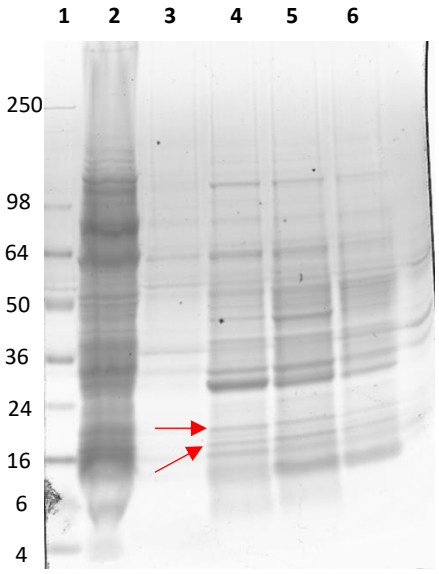

Figure 33. Native isolation of MglA after first round of purification. *Lane 1) See blue pre-stained protein ladder, Lane 2) M. xanthus WT cytoplasmic extract, Lane 3) Elution 1, Lane 4) Elution 2, Lane 5) Elution 3, Lane 6) Elution 4. Two potential MglA bands indicated by red arrows. Samples were run on a 4-20% tris/glycine gel. Numbers left from the marker lane correspond to the molecular weight in kilodalton.*

To verify that both proteins, the 21 and 23 kDa large bands represented different versions of MglA, a Western blot of elution sample 3 was done (**Figure 33**). Using the anti-MglA antibody two different bands in the native MglA isolation were detected, showing that MglA appeared to be post-translationally modified in *M. xanthus* (**Figure 34**). The difference between the MglA bands is similar to the difference that was observed between *M. xanthus*- and *E. coli*-expressed MglA (**Figure 32**). The two observed MglA bands showed about the same intensity on both the SDS PAGE and the Western blot, indicating that the post-translationally modified and non-modified versions of MglA seemed to occur in about equal amounts. The occurrence of these two MglA bands was most likely the result of the isolation procedure during which some of the MglA lost its post-translational modification. In contrast, in WT *M. xanthus* cells only one band was observed indicating that in the cells MglA only occurred in the post-translationally modified state. This interpretation was supported by the observation that only one 23 kDa MglA band was observed when WT cells were probed in a Western blot (**Figure 31**).

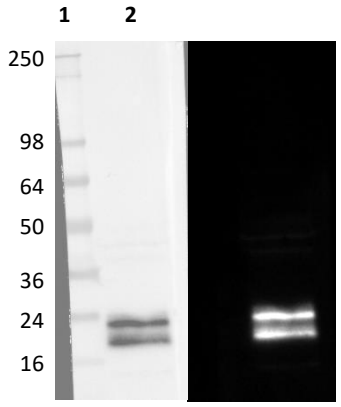

Figure 34. Western blot of a native MglA isolation. *Lane 1) See blue pre-stained ladder, Lane 2) Elution sample 3. MglA sample showing both post-translational modified (upper band) and non-modified (lower band). Numbers left from the marker lane correspond to the molecular weight in kilodalton.*

Although the precise nature of the modification is currently unknown, the observed shift of ca. 1 to 2 kDa between the two MglA bands could be due to a glycosylation, palmitoylation, or phosphorylation. Of these types of modifications, glycosylation, however, seems unlikely, given that most of the observed glycosylation in bacteria has been reported to occur in extracellular and periplasmic proteins, but rarely in cytoplasmic proteins (Nothaft & Szymanski, 2013). Palmitoylation seems more likely, given that the observed MgIA clusters in cells appear to be associated with the cell membrane (Guan & Fierke, 2011). MglA could potentially use these palmityl groups to reversibly attach itself to the membrane in a fashion that mirrors the behaviour of some eukaryotic RasGTPases (Bartels et al., 1999).

4.3.2 The cellular level of MglA depends on the presences of bactofilins

The identified potential interaction between BacM and MglA prompted us to investigate how these two proteins influence each other in various mutant strain backgrounds. These investigations became possible in part due to the newly developed MglA antibody and allowed among others the study whether the presence of BacM in the cell was required for the post-translational modification of MglA.

Another question was whether BacM could play a role in the localisation of MglA potentially targeting the protein to the cell membrane. For this purpose, both ΔBacM and ΔBacNOP cells were studied. No change in post-translational modification of MglA was observed when the bactofilins were missing, but in the absence of BacM or BacNOP the amount of MglA inside the cell was (**Figure 35**). Upon quantification of the MglA bands, a 40-fold reduction in MglA concentration was found between the ΔBacNOP and WT cells, while in ΔBacM cells, the concentration of MglA was even lower showing a 280-fold reduction when compared to WT cells (**Figure 35**).

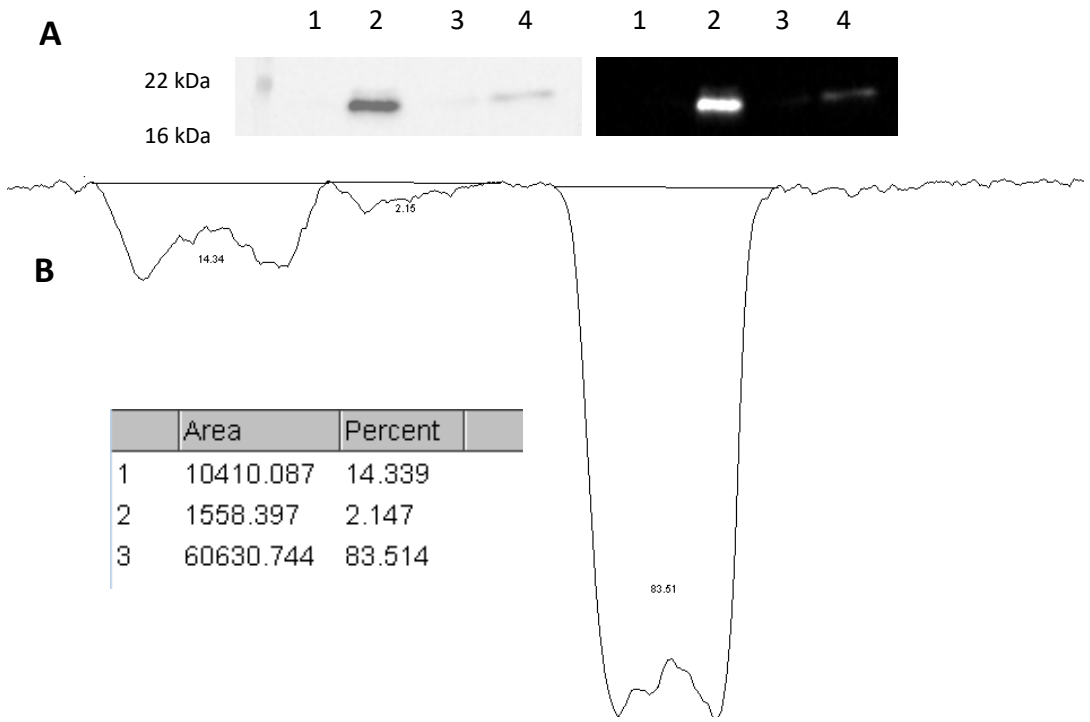

Figure 35. Reduced cellular level of MglA in various bactofilin deletion strains. *(A)Western blot Lane 1 ΔMglAB (DK6195), Lane 2 WT (DK1622), Lane 3 ΔBacM, Lane 4 ΔBacNOP. For each sample 20µl was run from an overnight culture at OD600 ≈ 0.6. (B) Western blot bands were quantified using FIJI* (Schindelin et al., 2012)*. From left to right ΔBacNOP, ΔBacM, WT (DK1622), ΔMglAB (DK6195).*

4.3.3 Generation of a ΔBacM ΔMglA(B) double deletion mutant

All previous reported experiments were performed using either ΔMglA, ΔBacM or ΔMglAB mutant strains. However, using these strains for the experiments posed a problem as the expression of MglA in a ΔBacM strain resulted in an excess of MglA due to the fact that the cells possessed a native copy of the protein.

This excess of MglA had the potential to compromise the observed responses in the cell. To address this problem, an attempt was made to generate a double deletion mutant. Therefore, two approaches were taken: to either delete MglA in a ΔBacM background or to delete BacM in an ΔMglA and ΔMglAB background. Based on the known phenotypes of both the ΔBacM (crooked cell morphology) and ΔMglA (non-motile strain) strains, it was hypothesized that the double deletion would result in non-motile crooked cells. Unfortunately, the generation of the double deletion mutant proved extremely difficult. Numerous attempts were made at deleting either MglA in a ΔBacM background or BacM in a ΔMglA background. However, none of these attempts were successful indicating that a deletion of both genes was lethal to *M. xanthus*. Only when a second copy of MglA was introduced and expressed under a copper-inducible promoter was it possible to delete both MglA and BacM at their original loci. The expression of MglA using the pMAT3 plasmid allowed to precisely control the expression levels of MglA. At relatively high expression levels (250 µM copper) of MglA, the cells died and no double deletion mutants could be obtained (**Figure 36C/D**). On the opposite end, the complete absence of copper lead to all surviving clones retaining BacM (**Figure 36B**). To successfully generate the double mutant, a low to intermediate concentration of copper was used (20 µM), which resulted in the successful recovery of the ΔBacM ΔMglA mutant strain (**Figure 36A**). Despite this success, it turned out that the double deletion mutant showed a much more severe morphological defect than the ΔBacM strain (**Figure 36G/H**). Upon induction with 20 µM copper, the ΔBacM ΔMglA cells were only able to survive for two to three days and were impossible to freeze or to propagate. Once MglA expression was stopped, the cells started showing cluster formation and what appeared like membrane blebbing or secretion along the long axis of the cell (**Figure 36E/F**). The same morphological and physiological results were obtained for the deletion of BacM in the ΔMglAB (DK6195) strain.

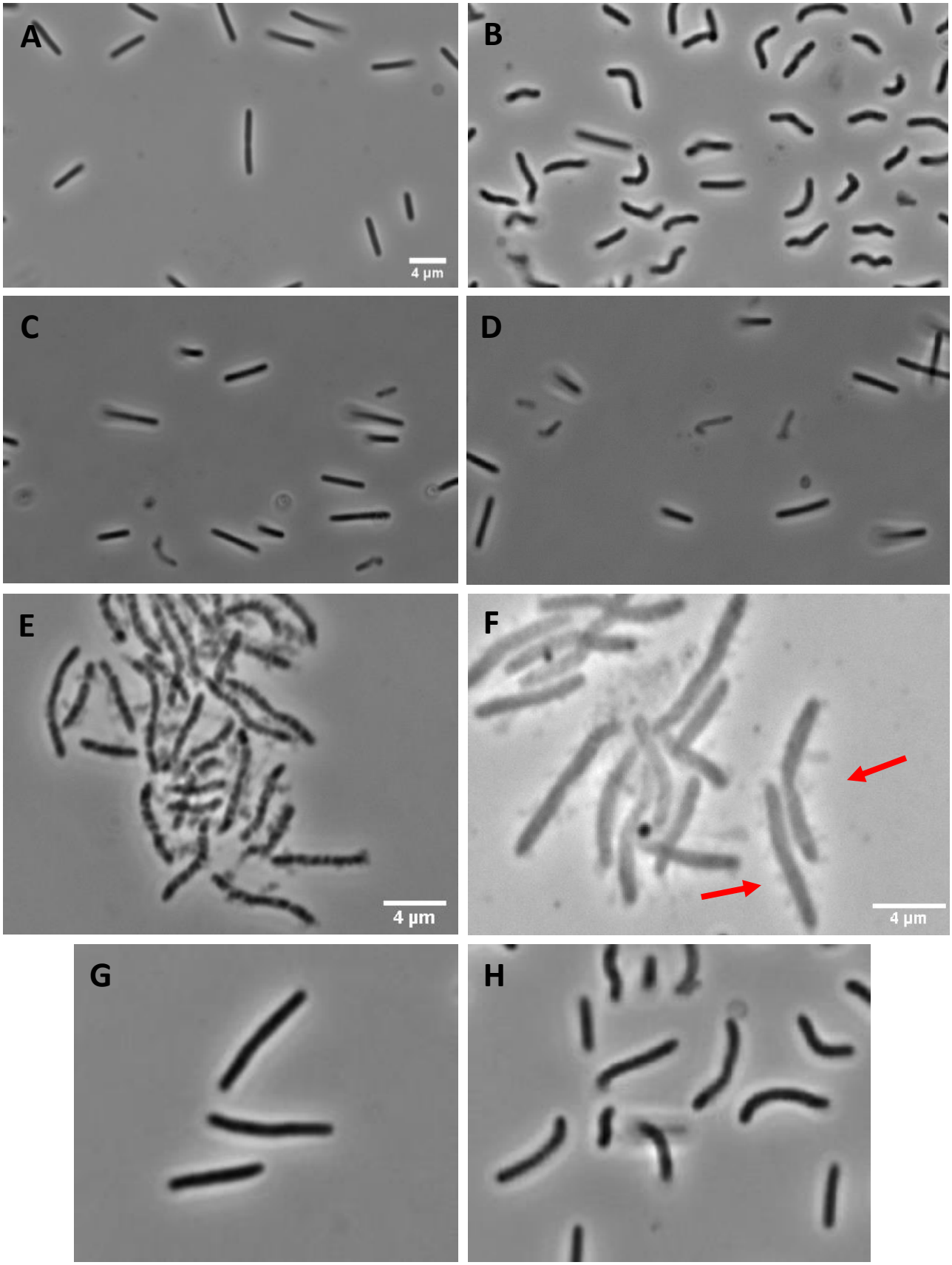

Figure 36. Generation of a ΔBacM ΔMglA double deletion mutant strain. *Deletion of BacM in ΔMglA cells (A) ΔBacMΔMglA double deletion strain grown in the presence of 20 µM copper (B) In the absence of copper no ΔMglA ΔBacM double deletion mutants were obtained (C/D) In the presence of 250 µM copper all the double deletion mutants died due to overexpression of MglA being toxic to ΔBacM cells.(E) ΔBacMΔMglA cells start dying without a second copy of MglA being expressed. (F) ΔBacMΔMglA cells. Membrane blebbing or secretion indicated by red arrows. (G) ΔBacM cells (H) ΔBacMΔMglA cells zoomed in picture from (B). Pictures were taken using a ZEISS AX-10 light microscope with a 100x and 20x lens. (A/B/C/D) see scale bar A.*

4.3.4 Overexpression of MglA in growing ΔMglA(B) cells leads to the formation of elongated cells on hard agar

A serendipitous observation was made while trying to obtain the ΔMglA ΔBacM double deletion mutant. Prolonged overexpression of MglA in ΔMglA(B) *M. xanthus* cells leads to cell elongation. These cells consisted generally of two to three cells attached to one another by a thin cytoplasmic bridge (**Figure 37**). Each extra cell attached to the first often decreased in length, while clear indentations were observed where cell divisions were disrupted. The elongated cells ranged from 10 to 30 µM in length, which was about 2-10 times longer than the average cell length of *M. xanthus* ranging from 3-5 µM (D. Kaiser, 1979).

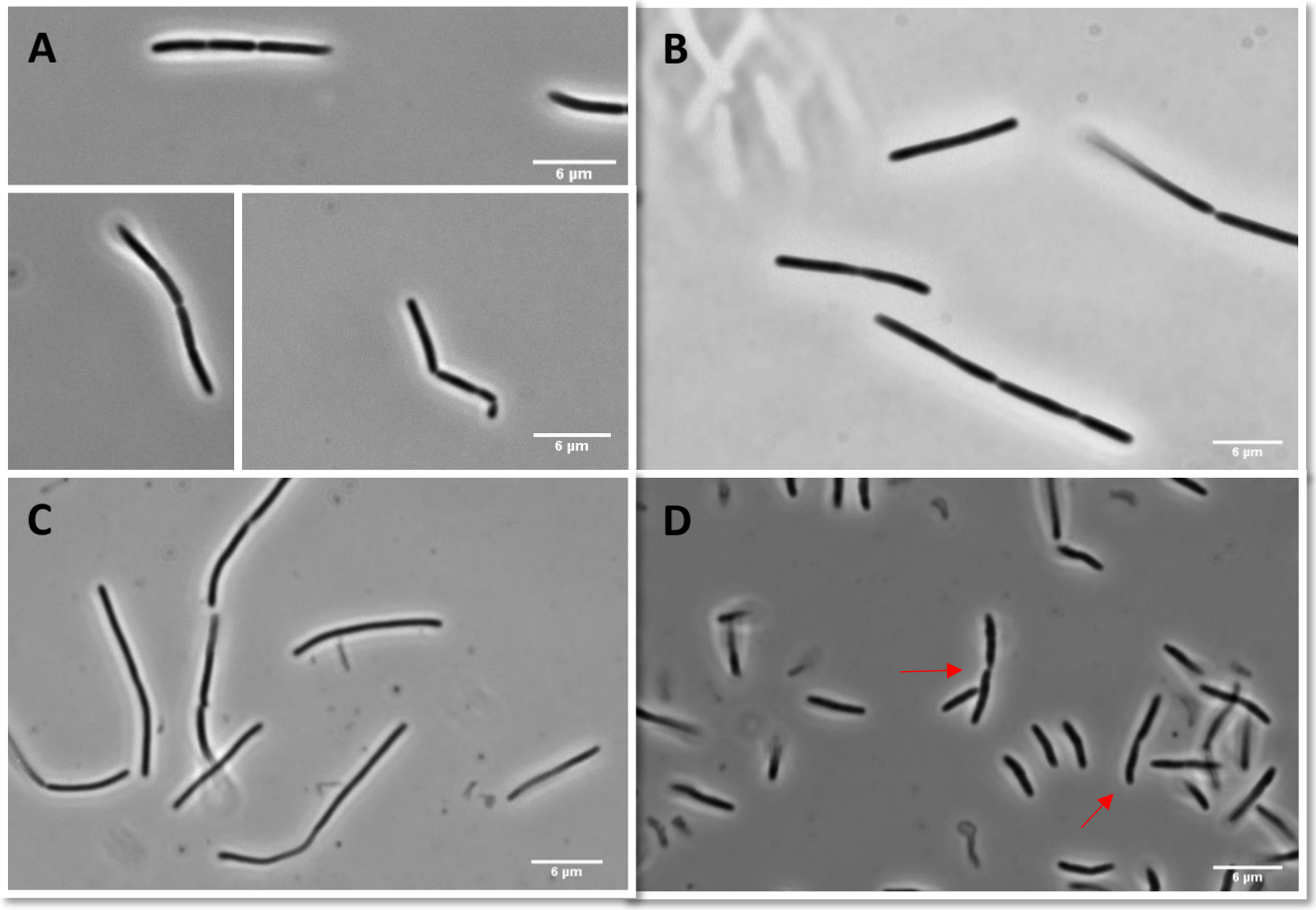

Figure 37. Elongation of ΔMglA(B) M. xanthus cells ater two days of MglA expression on hard agar. *Cells were grown for 2 days on 1.5% agar in the presence of 20 µM copper or 50 µM vanillate. (A) Elongated cells observed in ΔMglAB (DK6195) cells expressing MglA using pMAT3 (20 µM copper). (B) ΔMglA cells expressing MglA using pMAT3 (20 µM copper). (C) ΔMglA cells expressing MglA using pMR3679 (50 µM vanillate). (D) ΔBacM cells expressing MglA using pMR3679 (50 µM vanillate). Double cells observed in ΔBacM cells are indicated by the red arrows. Pictures were taken using a ZEISS AX-10 light microscope with a 100x and 20x lens.*

Several different MglA expression plasmids were used as a control to check that the elongation of the cells was not caused as a result of a random background mutation. The ΔBacM cells overexpressing MglA were mostly singular cells with the occasional double cells (two cells attached to one another, **Figure 37D**). None of the ΔBacM cells showed clear signs of elongation (**Figure 37**). In addition, no discrimination could be made between "double" cells and cells undergoing "normal" cell division. These observations therefore indicated that the absence of BacM prevented cell elongation at increased levels of MglA.

4.3.5 Growth defect caused by the expression of MglA-eYFP in ΔBacM cells

A reduction in growth was observed when overexpressing C-terminally eYFP-tagged MglA in liquid grown ΔBacM cells. To determine whether this growth defect was caused by the expression of MglA or by the presence of the eYFP tag, constructs were made for the overexpression of non-tagged MglA (**Figure 38**). No significant reduction in growth was measured between WT and ΔBacM cells. When expressing MglA in WT cells, a small but statistically insignificant reduction in growth was measured in comparison to WT cells. This small reduction in growth could be attributed to the use of the pMR3679 plasmid and subsequently the presence of kanamycin in the medium and/or the overexpression of MglA. The non-induced MglA ΔBacM cells showed a significant difference in growth in comparison to the induced MglA expression in ΔBacM cells (**Figure 38**), showing that the expression of MglA in ΔBacM cells lead to a growth defect.

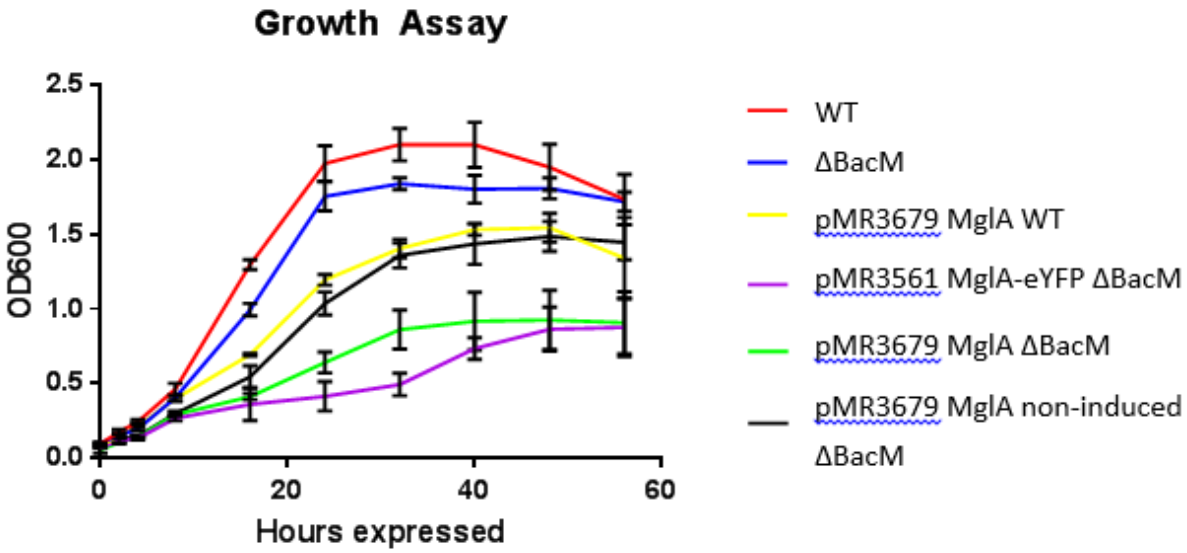

Figure 38. Expression of MglA (eYFP) in ΔBacM cells leads to a reduction in growth when compared to WT or non-induced ΔBacM cells. *Cultures were grown from a starting OD_{600} = 0.05. MglA expression was induced using 50 µM vanillate. Data shown are means ± standard deviation of three biological replicates.*

4.3.6 Expression of a second copy of BacM rescues growth defect caused by the overexpression of MglA in ΔBacM cells

In order to check whether the reduced growth caused by the expression of MglA in ΔBacM cells could be complemented, a second copy of BacM was introduced and expressed using the pSWU30 plasmid. This plasmid contained a tetracycline resistance gene and an *oar* promoter, which was used to moderately overexpress BacM. About twice the amount of BacM was expressed in comparison to WT levels of BacM when using the *oar* promoter in the pSWU30 plasmid (Koch, McHugh, & Hoiczyk, 2011). The expression of a second copy of BacM under the *oar* promoter partly rescued growth in *M. xanthus* (**Figure 39 black line**), showing that the expression of BacM complements the reduced growth defect caused by the overexpression of MglA. That the expression of BacM was not able to fully complement the MglA overexpression could be due to the presence of the pSWU30 plasmid. The cells containing the empty pSWU30 plasmid showed a reduction in growth in comparison to WT cells, indicating that the tetracycline antibiotic is slightly toxic to *M. xanthus*.

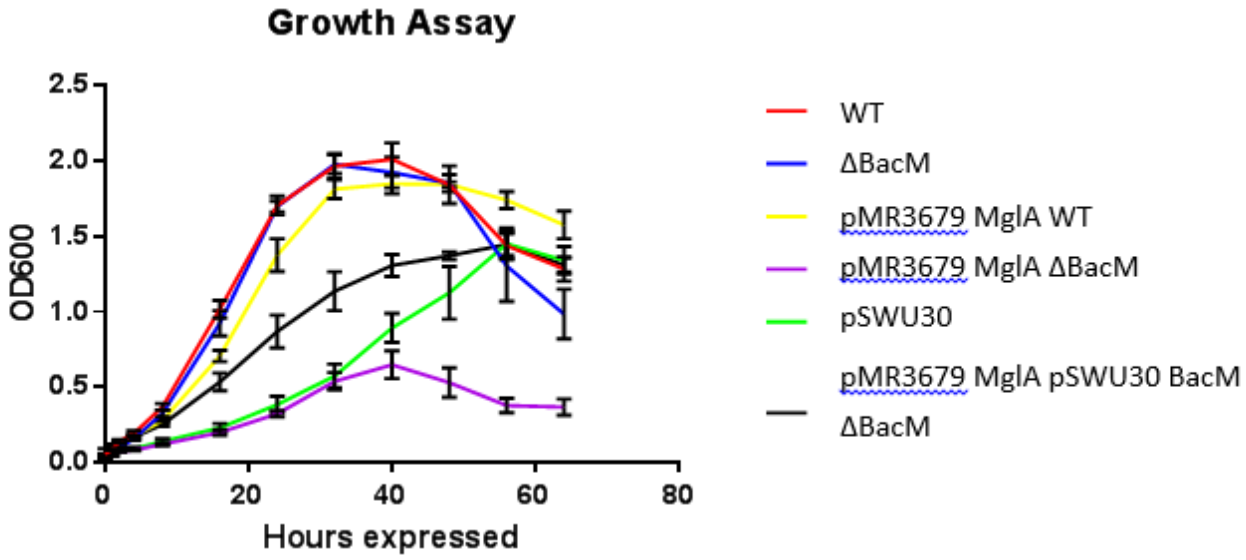

Figure 39. Expression of a second copy of BacM complements the MglA-induced growth defect in the ΔBacM background. *Cultures were grown from a starting OD_{600} = 0.05. MglA expression was induced using 50 µM vanillate. Data shown are means ± standard deviation of three biological replicates.*

4.3.7 The presence of the pSWU30 plasmid is toxic to *M. xanthus* cells

Next, it was checked whether the presence of the pSWU30 plasmid has a toxic effect on *M. xanthus* cell growth. Such an effect would explain why overexpression of BacM and MglA in ΔBacM cells partially complemented the growth defect (**Figure 39**). To investigate this, ΔBacM cells were grown and compared to ΔBacM cells containing an empty pSWU30 plasmid. A strong reduction in cell growth was observed in ΔBacM cells carrying the pSWU30 plasmid, indicating that the presence of the plasmid was toxic to *M. xanthus*. The pSWU30 plasmid contains a tetracycline resistance gene. Tetracycline has previously been shown to be toxic to *M. xanthus* (**Chapter III 3.3.2 page 88**), thereby explaining the observed reduction in growth. Next, an additional second copy of BacM in the pSWU30 plasmid was expressed in the ΔBacM cells. This strain also contained MglA in the pMR3679 plasmid. No significant difference was found between non-induced and induced expression of MglA, indicating that the reduced growth observed in **Figure 39** was not caused by the overexpression of BacM and MglA (**Figure 40**).

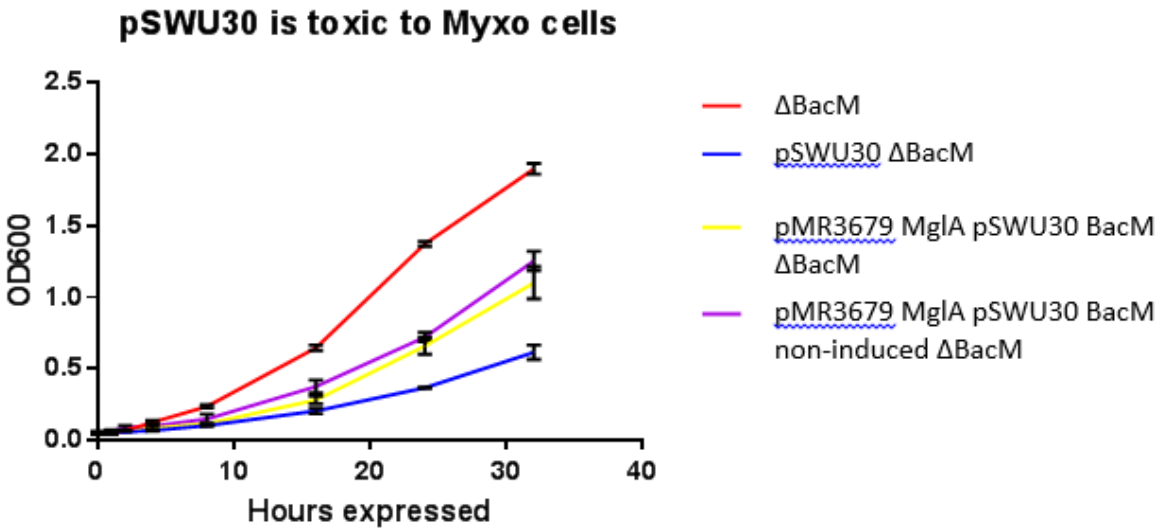

Figure 40. Reduction in growth is a result of the presence of the pSWU30 plasmid. *Cultures were grown from a starting OD_{600} = 0.05. MglA expression was induced using 50 µM vanillate. Data shown are means ± standard deviation of three biological replicates.*

4.3.8 Bioinformatics analysis reveals two hydrophobic regions at the N- and C-terminus of MglA

Upon analysis of the amino acid sequence of MglA two regions were discovered, which appear to be hydrophobic in nature. At the N-terminus of MglA, 10 of the first 18 amino acids are hydrophobic. There are three serines in this region, which could potentially be targeted for prenylation. The prenylation of one or all serines would result in a strongly hydrophobic amino acid cluster (**Figure 41**).

Figure 41 First 18 amino acids MglA potentially containing hydrophobic region. *(yellow) non-polar residues, (purple) serine residues (green) asparagine (blue) positively charged residues (red) negatively charged residues*

The C-terminus of MglA contains an α-helix (α5-helix) (**Figure 42**). Using the programme HeliQuest, the amino acid sequence of this helix was analysed. Interestingly, this analysis indicated that the helix may have a hydrophobic face on one side of the α helix making it an amphipathic helix (**Figure 42**, **see arrow**).

In addition, when looking at the amino acid sequence, it was found to contain an amphipathic lipid packing sensor motif (ALPS) (Drin & Antonny, 2010). Together this could indicate, that this hydrophobic face could be important for the binding to the cytoplasmic membrane (Keskin et al., 2008; Vanni et al., 2013).

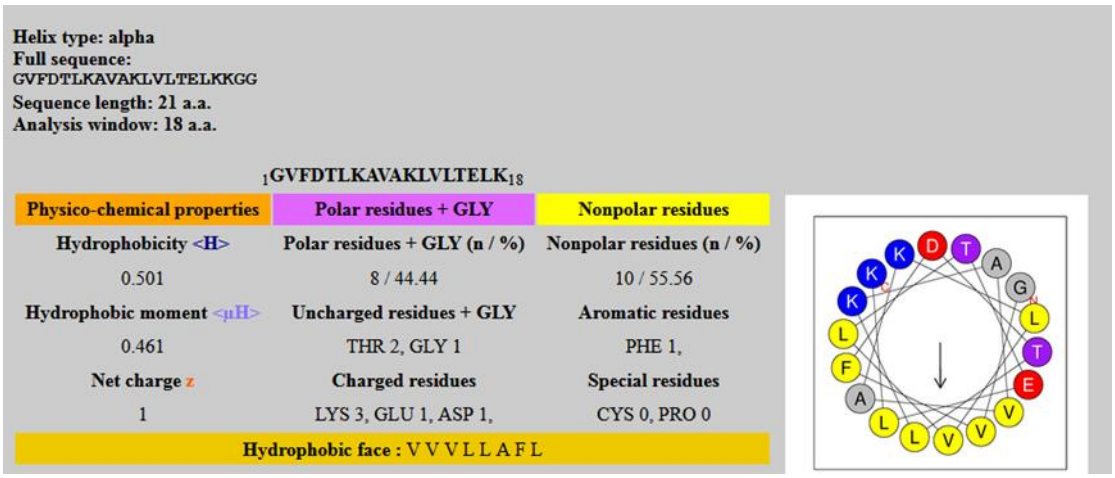

Figure 42 Helical projection of the MglA C-terminal α5-helix*. The projection was generated using the Heliquest software (http://heliquest.ipmc.cnrs.fr), resulting in the identification of a hydrophobic face (see arrow and orange bar). (yellow) non-polar residues, (purple) threonine residues (blue) lysine residues (red) negatively charged residues (grey) alanine and glycine residues.*

4.4 Discussion

The discovery that MgIA is most likely post-translationally modified is highly interesting and important as the identification of the nature of this modification will greatly improve our understanding of the biochemistry of this important protein. In general, post-translational modifications often play roles in cell adaptability, cell cycle control, and metabolism (Grangeasse et al., 2015). More specifically, they often lead to the inhibition or initiation of signalling pathways (Gao & Xu, 2011; Pejaver et al., 2014) or protein translocation processes (Ota et al., 2016; Reuter, Morgan, & Bergmann, 2000) that influence these aforementioned cellular processes. Importantly, eukaryotic Ras GTPases have been reported to often carry post-translational modifications including prenylation, carboxymethylation, palmitoylation, or proteolytic cleavage (Glomset & Farnsworth, 2003). For example, most of the Ras proteins are C-terminally modified and undergo prenylation. This prenylation often takes place at a recognition site called the CAAX motif, in which the X stands for any amino acid. The CAAX motif is recognized by farnesyltransferase that catalyses the transfer of a farnesyl group to the sulfhydryl group of the cysteine, adding a 15- or 20-carbon-long polyisoprene lipid. The protein is then cleaved at the farnesylated cysteine and subsequently carboxymethylated at the exposed carboxyl group (Wui Tan & Rando, 1992). Additionally, several eukaryotic Ras proteins contain upstream cysteines that undergo palmitoylation (Hancock et al., 1989). The palmitoylation of RAS increases the affinity of the protein for membranes by about 100-fold in comparison to the prenylated-only protein (Shahinian & Silvius, 1995). Additionally, palmitoylation is a dynamic and reversible reaction (Bijlmakers & Marsh, 2003). Another example of an eukaryotic Ras protein modification is found in Arf, a Ras protein subfamily that undergoes an N-terminal myristoylation of a glycine residue, which is located next to the starting methionine (Kahn et al., 1988).

Many other eukaryotic signalling proteins are palmitoylated at their N-terminus often in association with myristoylation (Resh, 1999). The prenylation, palmitoylation and myristoylation of these proteins enables them to anchor to the cytoplasmic membrane. At the membrane, they exert their function by interacting with effector kinases like Raf-kinase and PI3-kinase. These interactions in turn then lead to subsequent downstream signalling events (Brunsveld et al., 2009).

Importantly, none of those eukaryotic modifications of Ras proteins has so far been described for any bacterial RasGTPase. Nonetheless, MglA is known to localize to certain protein complexes attached to the membrane (Treuner-Lange et al., 2015). This may indicate that MglA might potentially bind to the membrane and that this could happen in a similar fashion to other eukaryotic Ras proteins with the help of a posttranslational modification. When looking for a CAAX motif in MglA, no such motif was found in the protein sequence. It is therefore unlikely that MglA is prenylated at the C-terminus. Additionally, no N-terminal glycine residue is present, indicating that myristoylation is unlikely to occur. There are only two cysteines and one serine present at the N-terminal region of MglA. The serine is located at the amino acid position 2, while the cysteines are located at positions 13 and 23. A potential palmitoylation of these two cysteines and/or the serine could explain the 1-2 kDa difference observed between PTM MglA and non-PTM-modified MglA. Such a palmitoylation, however, would indicate that the PTM MglA is binding to the cytoplasmic membrane, a process that would contradict the current model that MglA forms a cytosolic complex by binding to MreB and AglZ as part of the focal adhesion complex. These cytosolic complexes in turn are thought to recruit and assemble the Agl-Glt machinery of the focal adhesion complex (Faure et al., 2016).

Following their assembly, the Agl-Glt machineries are proposed to move from the leading cell pole to the lagging cell pole, a movement that is supposed to create the force for A-motility (Faure et al., 2016; Mauriello et al., 2010). If MglA is palmitoylated, then it is likely to bind to the membrane in a fashion similar to eukaryotic Ras proteins, which would make its participation in the focal adhesion complexes and its movement along cytoskeletal proteins more difficult to explain (Brunsveld et al., 2009).

An alternative post-translational modification that could explain the observed shift in in SDS PAGE is glycosylation. However, the N-terminus of MglA does not contain the characteristic bacterial N-glycosylation sequence D/E-Y-N-X-S/T with X and Y being not proline (Kowarik et al., 2006) Additionally, glycosylation has only rarely been described for cytoplasmic bacterial proteins. It therefore seems unlikely that MglA is glycosylated.

Phosphorylation is the most common post-translational modification in signal transduction pathways in all organisms. A primary role of phosphorylation is to act as a switch, turning protein activity or a cellular pathway on or off. This switching between an on or off state often happens in an acute and reversible manner (Hunter, 1995). A phosphorylation-dependent mobility shift of proteins on SDS-PAGE was found to be caused due to decreased binding of SDS (C. R. Lee et al., 2013). This mobility shift is mentioned for both eukaryotic and bacterial proteins (Nam et al., 2005; Wegener & Jones, 1984). The reason for the mobility shift is the negative charge of the phosphate group and the surrounding negatively charged amino acids, leading to a decreased binding of SDS (C. R. Lee et al., 2013). Interestingly, eukaryotic Abelson tyrosine-protein kinase (ABL) has been found to phosphorylate Y_{137} of H-, K-, and NRas, an activation that modulates endocytosis and cytoskeletal remodelling. Crystal structures of un-phosphorylated HRAS (Y137F) in comparison to the phosphorylated HRAS (Y137E) revealed important conformational changes.

Phosphorylation of HRas is therefore essential for protein conformation and function (Ting et al., 2015). In addition, as part of the protein-protein interaction studies of this work it was found that MasK is a tyrosine kinase that interacted with MglA using the luciferase system in *M. xanthus* (**Chapter III 3.3.6 Page 97**). The MglA amino acid sequence has two tyrosine residues Y_{136} and Y_{140}. It is therefore possible that MasK could phosphorylate one or both of these tyrosine residues, leading to a conformational change of MglA. Protein phosphorylation is regarded as an effective way to improve protein solubility, it could therefore explain why MglA without its PTM in *E. coli* aggregates (Hayashi et al., 2008; Li et al., 2003).

In contrast to palmitoylation, phosphorylation of MglA would indicate that the protein most likely is not associated with the membrane, but instead would bind to membrane associated proteins/complexes as suggested by the focal adhesion model.

No 1-2 kDa band-shift was observed in the ΔBacM or ΔBacNOP deletion strains in comparison to the WT (DK1622) MglA band on a Western blot, indicating that the presence of bactofilins is not required for the post-translational modification of MglA. Moreover, the strong reduction in expression of MglA in ΔBacM cells (280-fold) and ΔBacNOP cells (40-fold) indicates that the presence of the bactofilins seems, however, to be essential for the cellular level of MglA.

The expression of two human Ras proteins, KRas and NRas, decreased when their upstream or downstream genes, epidermal growth factor receptor (EGFR) and BRAF respectively, were mutated. Additionally, both KRas plus its upstream EGFR and NRas plus its downstream BRAF were both shown to be mutually exclusive. These findings show that the presence of certain proteins in the Ras signalling pathway is essential for the expression of the RAS proteins itself.

In this paper it was described that the mutation of certain Ras proteins leads to an increase in expression of the same Ras protein and/or others (R. M. Stephens et al., 2017; Unni et al., 2015). In particular, these activation mutations often target amino acids essential for GAP-induced GTP hydrolysis, leading to a constitutively active RAS molecule (Prior et al., 2012). The reduced expression of MglA observed in the ΔBacM and ΔBacNOP strains may suggests a similar Kras/Nras-like link between the bactofilins and MglA. Yet another observation supports such a link. Namely, the failure to generate a double mutant strain ΔBacM ΔMglA. Only when a second copy of MglA was introduced was it possible to delete the first copy of MglA and BacM. These results indicate that BacM and MglA are mutually exclusive, an observation that is in line with the mutual exclusivity found between Kras and EGFR and Nras and BRAF (R. M. Stephens et al., 2017). Together these data support a complex model in which BacM plays a complex role in MglA-induced downstream signalling and MglA gene expression.

An interesting observation was the formation of elongated *M. xanthus* cells upon the overexpression of MglA. As Ras from *S. cerevisiae* is involved in coordinating growth upon improved nutrient conditions, the activation of the Ras/cAMP pathway leads to increased cell sizes (Thevelein & De Winde, 1999). Conversely, inhibition of the Ras pathway leads to G1 cell cycle arrest in *S. cerevisiae* (Kataoka et al., 1985). Under nitrogen starvation, Ras2 in *S. cerevisiae* is activated. Ras2 activates two pathways, the cAMP-dependent PKA pathway and the MAPK pathway. PKA activates the transcriptional activator Flo8 and inactivates the transcriptional repressor Sf11. Both of these contribute to increased expression of Flo11. MAPK inactivates the repressors Dig1 and Dig2. The repression of Dig1 and Dig2 allows Ste12 and Tec1 to activate the expression of Flo11, as well as other proteins involved in cell elongation. Importantly, Flo11 expressional activation also increases cell adhesion and agar invasion (Park & Bi, 2007).

Additionally, cells from *Drosophila* that were lacking Ras were smaller in size, had reduced growth rates, and underwent apoptosis (Prober & Edgar, 2000). Another example is prostate cells expressing active H-ras and adopting an elongated morphology, while the expression of a dominant negative mutant of H-ras causes the cells to become smaller, rounded, and flat (Ghosh et al., 1999).

A reduction in growth was observed when expressing MglA in ΔBacM cells. This observation was expected, given the previously observed reduced expression of MglA in ΔBacM cells making it seem likely that the reduced expression of MglA is a way for *M. xanthus* to compensate for the loss of BacM. Using light microscopy, it was observed that the reduction in growth when expressing MglA in ΔBacM cells was caused by cell lysis through the extensive formation of tubular membrane protrusions.

The expression of Ras proteins in eukaryotes has been correlated with cell survival, including enhanced growth and differentiation. Contrary to this, the expression of some Ras proteins has been linked to certain cell death pathways. These cell death pathways are either apoptotic pathways or novel non-apoptotic death mechanisms (Overmeyer, 2011).

The MglA expression in ΔBacM cells could result in the induction of a non-apoptotic cell death mechanism, a process that may play a role during fruiting body formation.

The GTPase CgtA (member of the Obg-GTP1 subfamily of GTP-binding proteins) from *Vibrio cholera* causes cell elongation when overexpressed in *E. coli* (Shah et al., 2008). A mutant form of the ObgE (CgtA) protein from *E. coli*, containing a one amino acid change (K268I) at the surface of the protein in the G-domain, when expressed in *E. coli,* blocks the cell cycle. The blocking of the cell cycle eventually leads to membrane blebbing and cell death (Dewachter et al., 2017). MglA could potentially have a similar function as ObgE. If MglA is involved in cell cycle progression in *M. xanthus* then this could also explain the impaired motility of the ΔMglA mutant.

Maybe the absence of MglA mimics the cell division state in which *M. xanthus* cells are known to stop moving (Harvey et al., 2014). Contrary to this hypothesis, an *M. xanthus* MglAB mutant strain showed hyper reversal frequencies in comparison to WT (DK1622) cells, thereby indicating that the ΔMglAB strain is still motile and that MglA potentially plays a role in cell reversal (Alfred M. Spormann & Kaiser, 1999).

The elongation of the cells can also be explained by MglA being involved in cell wall synthesis instead of blocking cell cycle progression. Previous work in *Aspergillus fumigatus* suggested the involvement of the Ras pathway in cell wall synthesis (Fortwendel et al., 2009). Likewise, RhoA from *Aspergillus nidulans* was shown to be involved in cell wall synthesis (Guest et al., 2004).

4.5 Conclusion and Outlook

The results discussed in this chapter open up a wide range of questions as to what the precise functions of MglA are. As well as being involved in cellular reversals, cell adhesion, A-motility and S-motility in *M. xanthus,* MglA could additionally play a role in protein expression, cell elongation, cell death, cell cycle progression, or cell wall extension.

Interestingly, a lot of Ras proteins found in eukaryotes and Ras-like GTPases in bacteria show very similar phenotypes to the ones observed in the experiments of this chapter, indicating that MglA might target similar cellular functions as some of these Ras and Ras-like GTPases. Based on the identification of MglA being post-translational modified, the observed localization of MglA to membrane-associated complexes (Treuner-Lange et al., 2015) and the cytoplasmic membrane-binding of both Ras and Ras-like proteins in eukaryotic, yeast and bacterial cells suggests that MglA binds to the cytoplasmic membrane. This binding most likely occurs *via* the palmitoylation of the cysteines/serine residues at the N-terminus of the protein. The palmitoylation allows for the reversible binding of MglA to the membrane (Guan & Fierke, 2011). Additionally, MglA could be phosphorylated at its tyrosine residues. The phosphorylation of MglA seems likely given that H-, K- and NRas are known to be phosphorylated at a tyrosine residue and that phosphorylation increases protein solubility (Ting et al., 2015). It therefore will be interesting to investigate, whether MasK could potentially increase the activity of MglA *via* phosphorylation, which in response could lead to the remodelling of BacM and/or other cytoskeletal proteins.

The identification of MglA being PTM poses a problem in terms of our current understanding of the biochemistry of MglA. All currently known interaction partners of MglA have been identified using yeast two-hybrid assays, *E. coli* two-hybrid assays or have relied on *E. coli* over-expressed MglA. As it now becomes clear that MglA expressed in *E. coli* is lacking the PTM, and all *M. xanthus* MglA is PTM, the currently identified interaction partners for this protein have to be carefully re-evaluated.

Moreover, the observed aggregation of MglA when expressed in *E. coli* may be due to the absence of this PTM. Importantly, the *M. xanthus* luciferase system developed in this work would keep MglA in its physiologically relevant state and thereby circumvent this problem, thereby making a strong case that the identified MglA interaction partners described in this thesis are true biologically relevant partner proteins (**Chapter III, page 76**).

Chapter V

5. Cellular localisation of MglA in the presence and absence of BacM

5.1 Introduction

Two models have been proposed to explain A-motility in *M. xanthus*. One of those two models is based on the secretion of slime using an array of nozzle complexes that are concentrated at both cell poles (Wolgemuth et al., 2002). Theoretic calculations showed that the secretions of slime would be able to account for most of the observed features of A-motility (Wolgemuth et al., 2002). Importantly, during gliding *M. xanthus* was shown to secrete slime at the lagging pole, which could provide the force propelling the cell into the opposite direction (E. Hoiczyk, 2000; Egbert Hoiczyk & Baumeister, 1998). The second model, termed the focal adhesion model is based on the formation of focal areas of contact between the cell surface and the substrate on which the cells move (T. Mignot, 2007). The formation of these focal adhesion complexes starts at the leading cell pole, where they bind at fixed positions to the underlying substrate. As the proteins forming the complexes are envelope-spanning, they are able to connect to the cytoskeleton and upon binding start to move from the leading to the lagging cell pole. This movement is thought to drive the cell forward as the focal adhesion stays anchored in place pushing against the secreted slime (T. Mignot, 2007).

MglA localizes to and plays a crucial role in the formation of these focal adhesion complexes (Mauriello et al., 2010; Treuner-Lange et al., 2015). In 2010, it was shown that a C-terminal YFP-tagged version of MglA formed bipolar and lateral MglA-YFP clusters in *M. xanthus* that co-localised with other components of the focal adhesion complexes.

Likewise, other publications described similar observations, although slightly different experimental conditions were used (Miertzschke et al., 2011; Patryn et al., 2010; Treuner-Lange et al., 2015; Zhang et al., 2012). Based on the previously described interaction between MglA and BacM, different experimental techniques were employed to investigate the cellular localisation of MglA, in the presence and absence of BacM. The employed experimental techniques included fluorescent microscopy, the use of N and C-terminal eYFP-tagged MglA, and immunofluorescence using antibodies against MglA and BacM. The obtained experimental results of these approaches resulted in a re-evaluation of the current two models for gliding motility. In the following, it was investigated whether BacM play a role in MglA cluster formation and arrangement using various *M. xanthus* strains.

5.2 Materials and Methods

5.2.1 Cloning

MglA was cloned into the pMR3651 plasmid, which added a C-terminal eYFP tag, as mentioned in **Materials and Methods Chapter IV**. This plasmid was transformed into ΔMglA, ΔMglAB and ΔBacM cells. The necessary primers for the cloning are listed in **Table 12**.

Table 12 Primer list

Plasmid + gene	Description Forward primer (F) Reverse primer (R)	Sequence 5' to 3' end
pMR3651 MglA	Mx_MglA_F_NdeI	**ATCGC** *CATATG* ATGTCCTTCATCAATTACTCATC
pMR3651 MglA	Mx_MglA_R_EcoRI	**ATATA** *GAA TTC* TCACCACCCTTCTTGAGCTC
-	Upstream F ΔMglA(B)	TGAAGCCCTCATAGGTGA
-	Mx_MglA_R	TCAACCACCCTTCTTGAGCTC
-	Mx_MglA_F	ATGTCCTTCATCAATTAC
-	Downstream R ΔMglA(B)	TCGAAGAGCTCGCGCTTG

5.2.2 Colony-scale swarming assays

Motility of *M. xanthus* on hard agar (1.5%) was determined by measuring the size of swarms after 1-5 days of growth at 32 °C. First, cells were grown ON to mid-log phase in CTT medium. Cells were diluted with CTT medium to 5 x 10^9 cells/mL and 10 µL spots were pipetted onto hard agar. The spots were left under the flowhood for 10 minutes to dry. Afterwards, the plates were covered and wrapped with parafilm, to prevent the agar from drying. The plates were incubated at 32 °C for five days. Each day the diameters of the colonies were measured in millimetres. An average of three independent colonies was measured for each strain.

5.2.3 Adventurous motility assays

For adventurous and social motility assays, time-lapse movies and images were captured of motile cells. Live cells were observed on agar pads using a fluorescent light microscope. Cells were grown in liquid CTT overnight to an OD_{600} of 0.4-0.8. Around 10 µl of this overnight culture was spotted onto a freshly prepared hard or soft agar patch on a glass microscope slide (Fisher Scientific). Agar pads were prepared just before use in a glass assembly. The assembly was prepared by sandwiching two 22 x 22 millimeter ethanol-sterilized #1 thickness cover slips between two standard microscope slides. The cover slips were gently moved to the edges of the slide sandwich to create a square space. Molten agar was carefully injected with a pipette tip into this space and allowed to cool for 5 minutes. The top slide was carefully removed, leaving the agar pad on the bottom slide. This method created an approximately 1 mm thick agar pad with a smooth surface. *M. xanthus* cells were spotted onto the agar pads and covered using a cover slip. Candle wax was molten and used to seal the sides of the cover slip, thereby preventing the sample from drying out. The slides with cells were incubated for at least 60 minutes at 32 °C prior to viewing in the fluorescent microscope.

5.2.4 Fluorescent microscopy

An inverted widefield microscope (Nikon) was used for the acquisition of fluorescent microscopy data. The microscope was equipped with a 100X/1.30 NA oil PH3 objective, an X, Y motorized stage, a sCMOS camera, a light source, filters for green, red, and blue-fluorescent proteins, as well as a temperature-controlled incubation chamber. Prior to using the microscope, the incubation chamber and the microscope were heated to 32 ^{o}C for ~1-2 hours. A drop of high quality immersion oil was added onto the lens of the objective.

The objective lens was swung into the light path and the cells were brought into focus by moving the stage in the Z-direction closer to the objective. For time-lapse experiments the duration was set to 5-10 minutes and a time interval of 10 seconds. Depending on the sample either FITC, DAPI or TxRED was used for the acquisition of fluorescent data. Exposure times were around 100 ms for eYFP-tagged proteins.

5.2.5 Immunofluorescence

Cells were grown in liquid CTT overnight to an OD_{600} of 0.4-0.8. Of this cell culture, 1 ml was centrifuged at 8,000 g for 1 minute. The cell pellet was resuspended in 500 µl of 4% formaldehyde in MKH (8 mM $MgSO_4$, 1 mM $KHPO_4$, 20 mM HEPES pH 8.0). The cells were fixed in this solution for 40 minutes at room temperature. After fixation, the cells were washed twice with 500 µl MKH. The cells were then incubated for 30 minutes with 20 µg/ml lysozyme in MKH (500 µl). The pellet was washed twice with 500 µl MKH. Of the cell suspension, 200 µl was pipetted onto a clean PLL-coated coverslip and spread around. The cells were left on the coverslip for 10 minutes. The liquid was removed and the sample allowed to dry completely. The coverslips were placed in a 6-well plate and the cells were permeabilized by adding 2 ml of 0.2% TritonX-100 in PBS for 30 minutes. The cells were blocked for 20 minutes with PBS containing 0.05% Tween20 and 2% BSA (bovine serum albumin). MglA primary antibody (0.1 µl) was added to 100 µl PBS on clean parafilm. The coverslip was placed facedown onto the drop and left for 1 hour at room temperature. The primary antibody was washed three times with PBSTB (PBS containing 0.05% Tween20 and 2% BSA). The cover slips were labelled with Immunopure goat anti-rabbit horseradish peroxidase-conjugated secondary antibody (ThermoScientific) for 1 hour at room temperature in the dark. All the following steps were performed in the dark. The cover slips were washed three times with PBS. BacM primary antibody (0.1 µl) was added to 100 µl PBS on clean parafilm. The coverslip was placed facedown onto the drop and left for 1 hour at room temperature.

BacM antibody-labelled cells were washed with PBSTB for three times. The cells were labelled with secondary antibody as described above. Cells were washed three times with PBS. The nucleoid was labelled with BisBenzimide at 1 μg/ml in PBS for 20 minutes. The cells were quickly washed with PBS and mounted onto a glass lide with ddH_2O. The corners of the cover slip were covered with nail-polish and allowed to set. Cells were immediately visualized using a fluorescent microscope.

5.3 Results

5.3.1 Expression of C-terminally eYFP-tagged MglA in ΔMglA cells partially rescues spreading on hard agar.

Based on the accumulated evidence supporting an interaction between MglA and BacM (**Chapters II, III and IV**), it was next investigated whether the presence or absence of BacM influences the localisation of MglA. Initially, an eYFP tag was added to the N-terminus of MglA to allow visualisation of the protein *in vivo*. This procedure, however, did not result in a strain in which A-motility was rescued. Even after the addition of different linker regions between the protein and the tag, A-motility was not restored. A similar observation had previously been reported, which suggested that the N-terminus is essential for the function of MglA (Patryn et al., 2010). Next MglA was cloned into the pMR3561 plasmid, which added a small linker region followed by an eYFP-tag to the C-terminus (Iniesta et al., 2012). Whether the MglA-eYFP construct was biological functional was checked by expressing the protein in a *ΔMglA* and *ΔMglAB* background and looking whether the cells were able spread on CTT hard agar (**Figure 43/Figure 45**). This test was based on the observation that cells on hard agar primarily move by A-motility, while S-motility is primarily functional on soft agar (W. Shi & Zusman, 1993). Importantly, the MglA-eYFP was able to partially rescue A-motility. Three different concentrations of vanillate (5, 50, and 500 µM) where used for expression purposes, which will be referred to as low, medium and high induction in the following. These concentrations were based on previously published studies, in which protein expression levels had been studied at different vanillate concentrations (Iniesta et al., 2012). At low induction (5 µM vanillate) motility was restored to 88% of the WT cell level (DK1622), while induction with 500 µM vanillate restored motility only to about 78% indicating that high MglA expression levels resulted in reduced spreading. Two pictures were taken each of a non-induced *ΔMglA* colony, *versus* a 500 µM vanillate-induced *ΔMglA* colony after 3 days of spreading on hard agar at 32^{o}C (**Figure 44**).

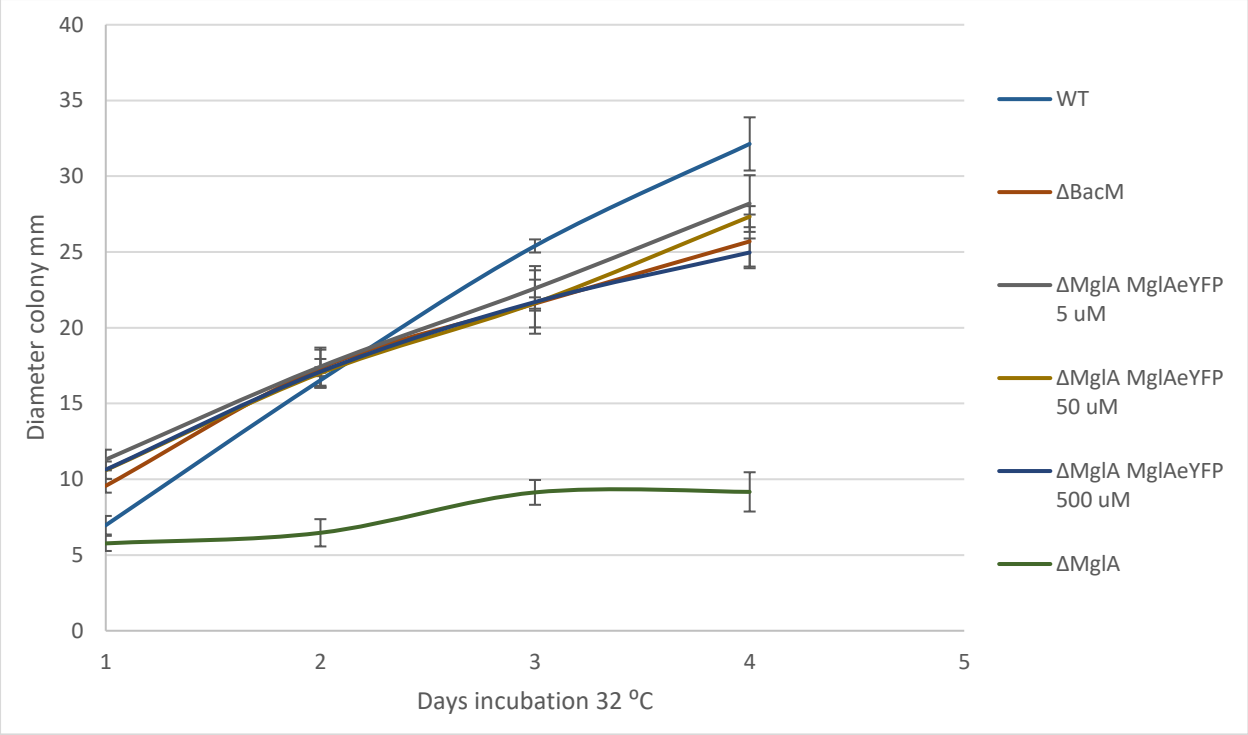

Figure 43. Rescue of spreading on hard agar through expression of MglA-eYFP. *The X-axis shows the days of incubation. The Y-axis the diameter of the colony in mm. ΔMglA cells were induced using 5 µM, 50 µM and 500 µM vanillate. Colonies were grown using a start OD_{600} of 0.1. Data shown are means ± standard deviation of three biological replicates.*

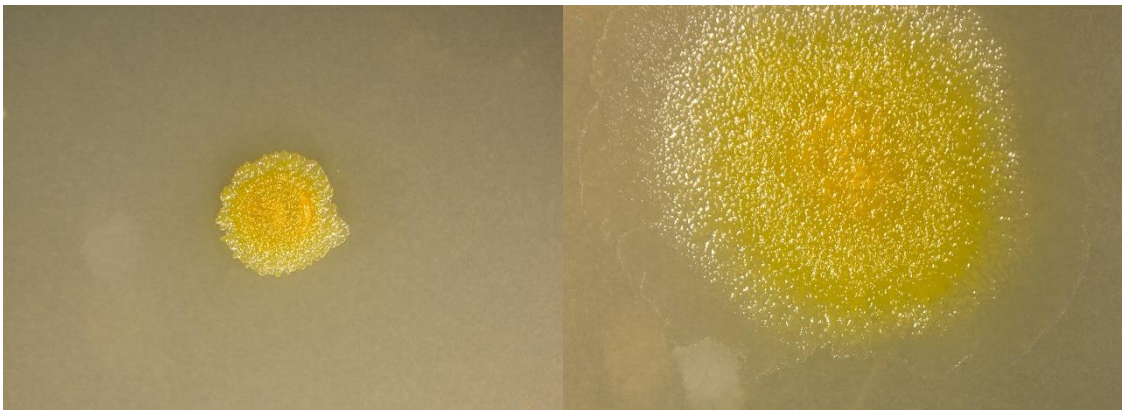

Figure 44. Expression of MglA-eYFP rescues A-motility *(left) ΔMglA colony after 3 days of growth at 32 °C (right) ΔMglA colony after 3 days of growth at 32 °C expressing MglA-eYFP after induction with 500 µM vanillate. Pictures were taken using an Olympus PEN E-PL1 with M.Zuiko Digital 14-42mm Lens camera, at the same magnification.*

5.3.2 MglB plays a role in spreading of *M. xanthus* on hard agar.

Low expression of MglA-eYFP in ΔMglAB (DK6195) cells restored spreading to 60% WT level (**Figure 45**). This was substantially less than the reported rescue at 88% WT level in *ΔMglA* cells at low MglA-eYFP expression. The difference in spreading (28%) indicated that MglB potentially plays an important role in spreading on hard agar.

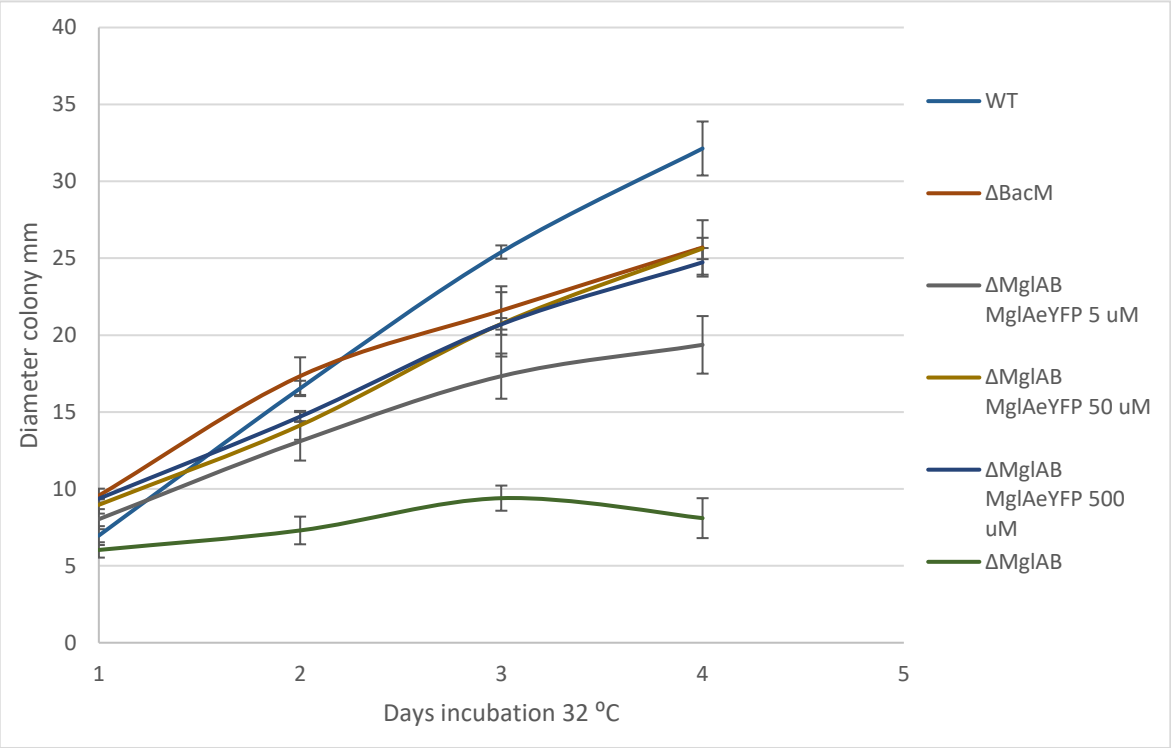

Figure 45. Expression of MglA-eYFP rescues A-motility in the absence of both MglA and MglB. *The X-axis shows the days of incubation. The Y-axis the diameter of the colony in mm. ΔMglAB cells were induced using 5 µM, 50 µM and 500 µM vanillate. Colonies were grown from a starting OD_{600} = 0.1. Data shown are means ± standard deviation of three biological replicates.*

MglB is the GTPase activating protein (GAP) of MglA catalysing the hydrolysis of GTP to GDP (Miertzschke et al., 2011). The GDP-locked form of MglA is known to be the soluble cytoplasmic form, while the GTP-locked form is the active form of the protein that localises to the membrane-associated focal adhesion complexes (Leonardy et al., 2010; Patryn et al., 2010).

As the intrinsic hydrolysis rate of MglA is very low (Patryn et al., 2010), most of the MglA will be in its GTP-bound state in the absence of MglB. At higher concentrations of vanillate (50-500 µM) spreading was restored to 80% WT level and the high expression levels of MglA-eYFP resulted in cells starting to elongate. This elongation was observed in both *ΔMglA* and *ΔMglAB* cells (**Figure 46**) and mirrors the observation of cell elongation after overexpressing of non-tagged MglA (**Chapter IV page 122**).

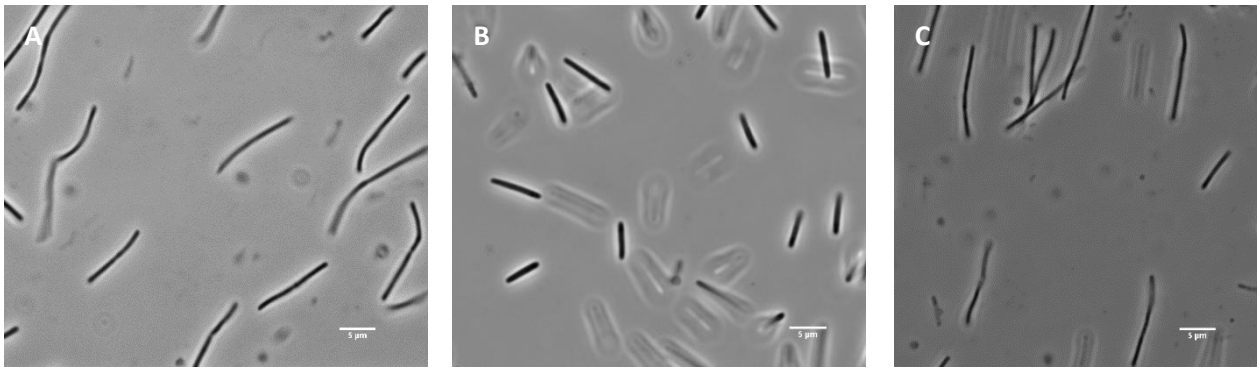

Figure 46. Elongating ΔMglA and ΔMglAB cells after overexpression of MglA-eYFP. *(A) ΔMglA cells expressing MglA-eYFP. (B) WT cells (C) ΔMglAB cells expressing MglA-eYFP. Cells were induced with 500 µM vanillate for 4 days at 32 ^{o}C.*

5.3.3 Elongated cells show evenly distributed MglA-eYFP with less MglA-eYFP at the division site

After 4 days of growth on hard agar, only elongated *M. xanthus* cells were left. The cells that did not show elongation appeared to be not able to survive the overexpression of MglA-eYFP at 500 µM vanillate. Three interesting observations were made, while examining the localization of MglA using fluorescent microscopy. First, MglA-eYFP appeared to localise diffusively throughout the cell with a higher localisation towards both cell poles (**Figure 47**). This confirmed the previously observed localization of MglA and BacM using the luciferase system (**Chapter III 3.3.7 Page 98**). Secondly, the cells lysed *via* membrane blebbing and MglA-eYFP accumulated in the membrane blebs (**Figure 47 A/B red arrow**). Lastly, the localisation of MglA-eYFP at high levels of expression did not seem to be affected by the presence or absence of MglB (**Figure 47**).

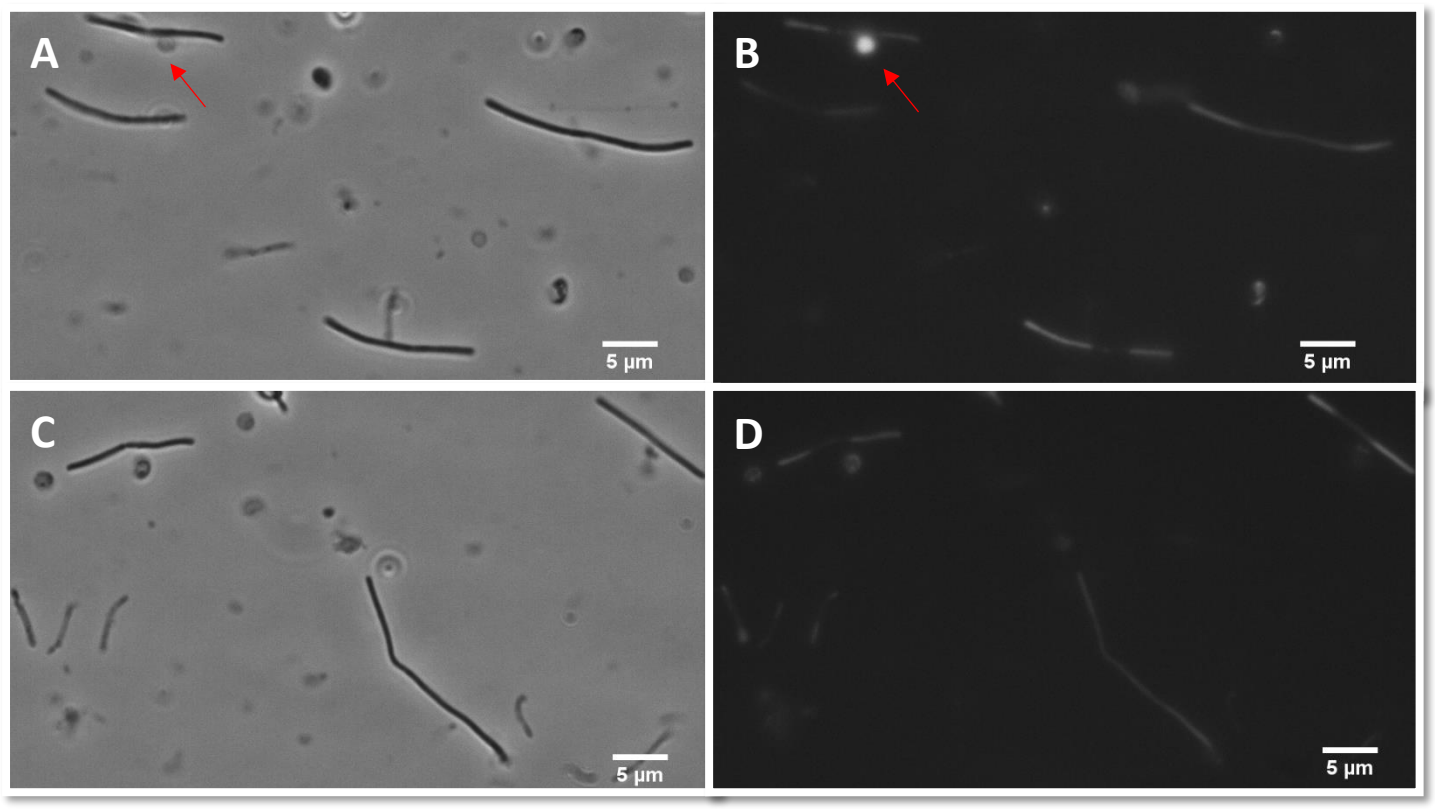

Figure 47. Fluorescent microscopy of elongated M. xanthus cells overexpressing MglA-eYFP in ΔMglA and ΔMglAB cells. *(A/B) ΔMglA cells (red arrow indicates membrane bleb with MglA-eYFP clustering). (C/D) ΔMglAB cells*

5.3.4 MglA-eYFP expression leads to reduced colony spreading on hard agar in ΔBacM cells

Low levels of MglA-eYFP expression in ΔBacM cells on hard agar lead to reduced spreading at 58% of WT level and at 80% of ΔBacM cell level (**Figure 48**). This result confirmed the previously observed reduced growth in ΔBacM cells overexpressing MglA and the observed reduced natural expression of MglA in ΔBacM cells (**Chapter IV pages 118 and 123**). Increasing the expression levels using 50 µM vanillate further reduced the spreading on hard agar. At 500 µM vanillate the colonies showed the same amount of spreading as ΔMglA colonies. Looking at these cells using light microscopy revealed that almost all the cells had died due to membrane blebbing.

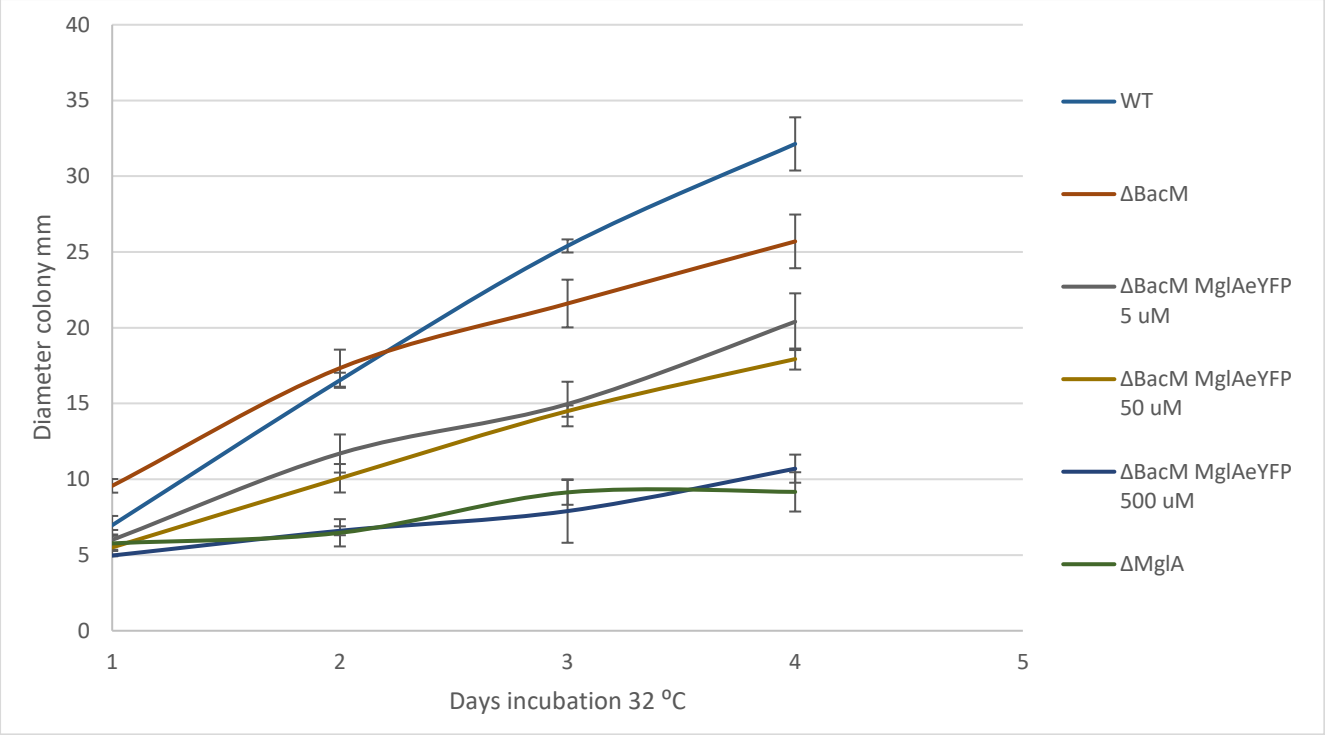

Figure 48. Expression of MglA-eYFP leads to reduced spreading of ΔBacM cells on hard agar *The X-axis shows the days of incubation. The Y-axis the diameter of the colony in mm. ΔBacM cells were induced using 5 µM, 50 µM and 500 µM vanillate. Colonies were grown from a starting OD_{600} = 0.1. Data shown are means ± standard deviation of three biological replicates.*

5.3.5 Fluorescent microscopy reveals a difference in localization of MglA-eYFP in liquid grown cells in the presence and absence of BacM

The expression of MglA-eYFP in ΔBacM cells lead to a reduction in growth (**ChapterIV page 123**) and a reduction in spreading on hard agar. Moreover, the overexpression of MglA-eYFP in ΔBacM cells lead to the formation of membrane blebs and eventually to cell death. This data indicated that BacM might play a role in the proper localization of MglA and that mislocalization of MglA in the absence of BacM leads to toxicity and eventually cell death. To test this hypothesis, the localisation of MglA-eYFP in liquid grown cells was studied. The main difference found between MglA-eYFP expressed in liquid *vs.* agar-grown cells, was that most ΔMglA cells showed fluorescence homogenously dispersed throughout the cell, while ΔBacM cells showed clusters at either one or both cell poles and/or a lateral cluster(s) (**Figure 49E**). At 500 µM vanillate induction some cells showed unipolar clusters in ΔMglA cells. These clusters disappeared when the cells were induced using 50 or 5 µM vanillate (**Figure 49C/D**).

Indicating, that the clusters observed in the ΔMglA cells were a result of the level of overexpression of MglA-eYFP. Thereby, it is important to keep in mind that the 5-50 µM vanillate induction did not lead to cell elongation and that under these expression conditions spreading was almost completely restored in the ΔMglA(B) strain. Large unipolar clusters were observed when overexpressing MglA-eYFP using 500 µM vanillate in ΔBacM cells (**Figure 49F**).

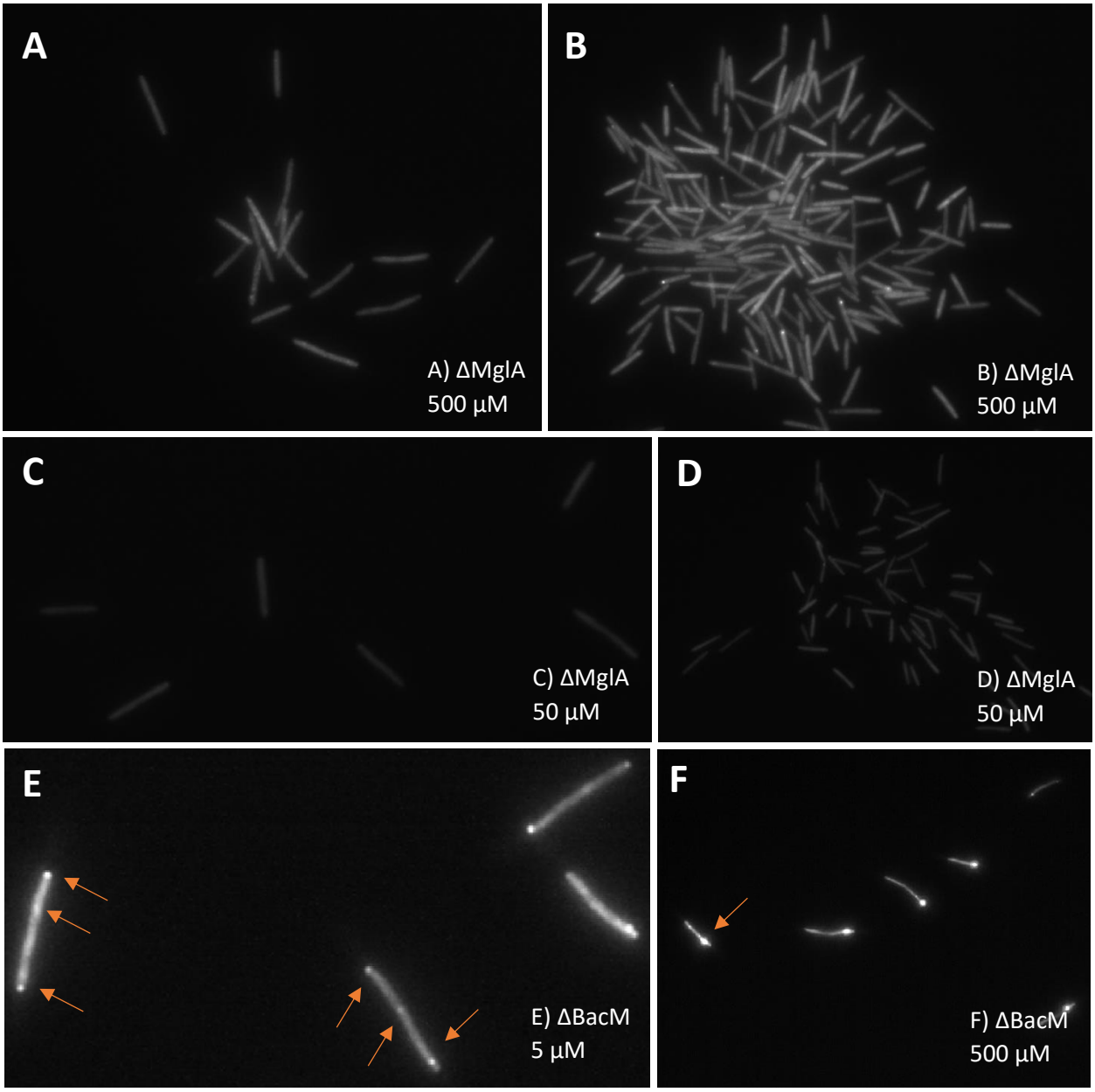

Figure 49. Difference in MglA-eYFP localisation in liquid grown M. xanthus cells. *(A/B) ΔMglA cells induced with 500 µM vanillate, (C/D) ΔMglA cells induced with 5 µM vanillate, (E) ΔBacM cells induced with 5 µM vanillate, (F) ΔBacM cells induced with 500 µM vanillate. Cells were grown until a starting OD_{600} = 0.4-0.6 and induced for 12 hours.*

5.3.6 Fluorescent microscopy shows a difference in localization of MglA-eYFP on hard agar grown cells in the presence and absence of BacM

Medium expression of MglA-eYFP on hard agar resulted in diffuse and unipolar cluster formation in ΔMglA cells. Most cells in groups showed unipolar clusters at the leading cell pole (**Figure 50B**). Cells obstructed in their movement by other cells also formed an MglA cluster at their leading pole (**Figure 51**). These polar clusters disappeared the moment the cell was no longer physically obstructed. Some individual moving cells also showed a cluster forming at the front pole (**Figure 50A**). One possible explanation for the formation of these frontal polar clusters in these cells is, that they are the consequence of force-induced deformation of the membrane, that foster MglA accumulation at the front pole of the cell. The necessary forces may be created by minor elastic deformations of the cell pole when cells were gliding over hard agar. Alternatively, the absence of a slime trail, which could potentially facilitate movement and therefore reduce MglA-eYFP polar cluster formation may foster polar cluster formation (Burchard, 1982; Fontes & Kaiser, 1999). This would explain why some individually moving cells showed a cluster at the front and others did not.

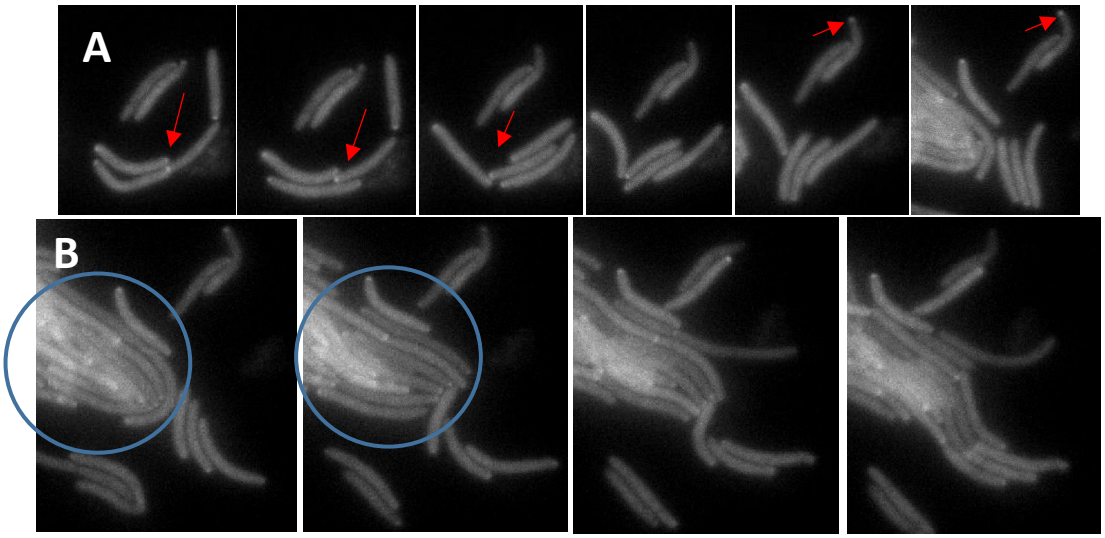

Figure 50. Force-dependent MglA-eYFP unipolar cluster formation. *(A) Front polar cluster in moving cells indicated by red arrows. (B) Cells showing unipolar clusters at the front pole when moving in a group indicated by blue circle. Images were taken every 10 seconds. Cells were induced with 50 µM vanillate and incubated on hard agar.*

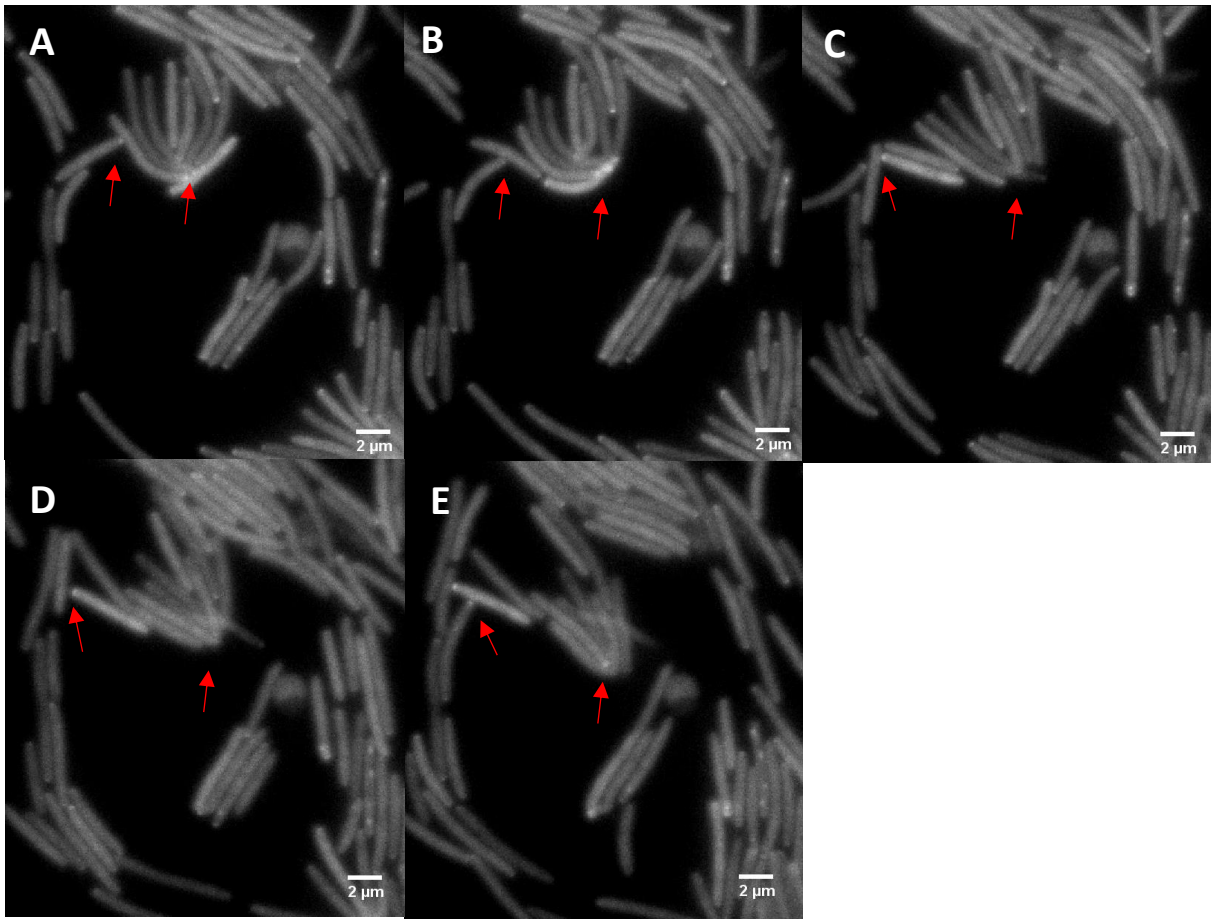

Figure 51. MglA-eYFP expression in a ΔMglA strain. *Cells were induced with 50 µM vanillate and incubated on 1.5% hard agar. MglA cluster formation in cells obstructed in their movement. MglA-eYFP cluster formation, disappearance and reformation are indicated by the red arrows. Images were taken every 10 seconds. Cells were induced with 50 µM vanillate and incubated on hard agar.*

After 12 hours of induction with 500 µM vanillate on hard agar, ΔMglA cells showed mostly bipolar MglA-eYFP clusters and some unipolar clusters (**Figure 52**), showing that the formation of the bipolar clusters is a result of the overexpression of MglA.

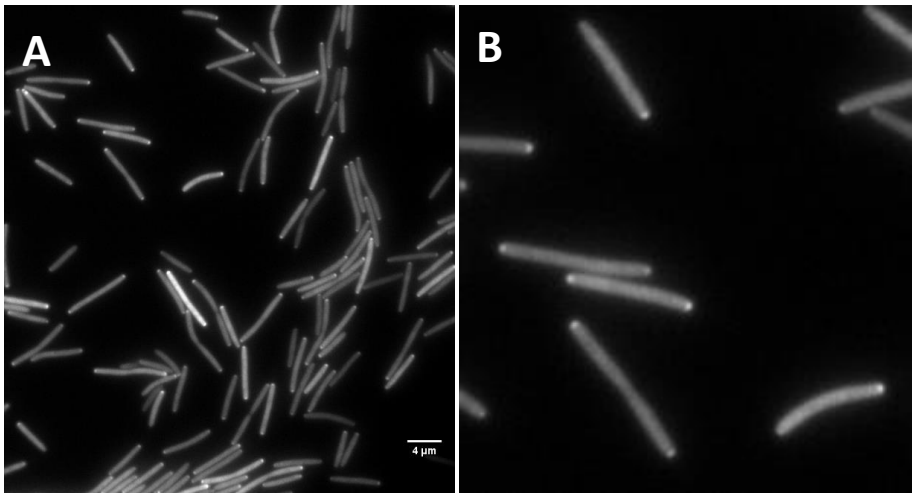

Figure 52. Overexpression of MglA-eYFP using 500 µM vanillate leads to bipolar and unipolar clusters. *(A) ΔMglA cells (B) ΔMglA cells zoomed in showing bipolar and unipolar clusters.*

Low levels of MglA-eYFP expression in ΔBacM cells grown on hard agar resulted in the formation of bipolar clusters (**Figure 53A/B**). The bipolar localisation of MglA-eYFP was the result of the absence of BacM. Indicating that BacM seems to play a role in the prevention of bipolar MglA cluster formation. Certain membrane receptor-induced signalling or membrane curvature could potentially function as a trigger initiating the clustering of MglA. A lot of ΔBacM cells showed membrane blebbing even at as little as 5 µM vanillate induction (**Figure 53C**). Interestingly, these membrane blebs were localised at the poles of the cells.

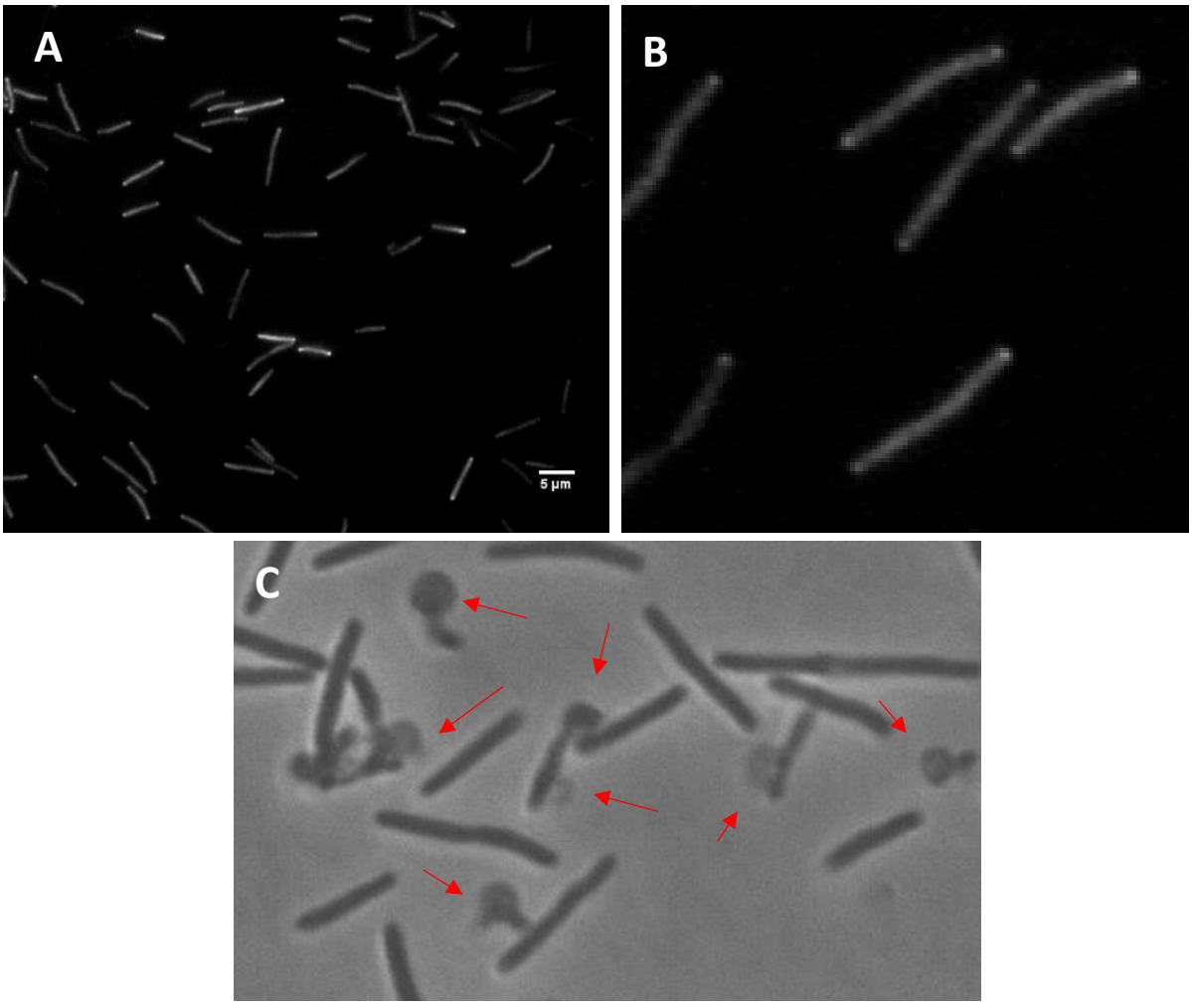

Figure 53. Bipolar cluster formation of MglA-eYFP in ΔBacM cells induced with 5 µM vanillate on hard agar *(A) ΔBacM cells (B) ΔBacM cells zoomed in showing bipolar clusters (C) ΔBacM cells showing mostly polar membrane blebs. Indicated by red arrows.*

Overexpression of MglA-eYFP in ΔBacM cells grown on hard agar resulted in the formation of bipolar and lateral MglA-eYFP clusters (**Figure 54**). Most of these cells died due to membrane blebbing at the cell pole.

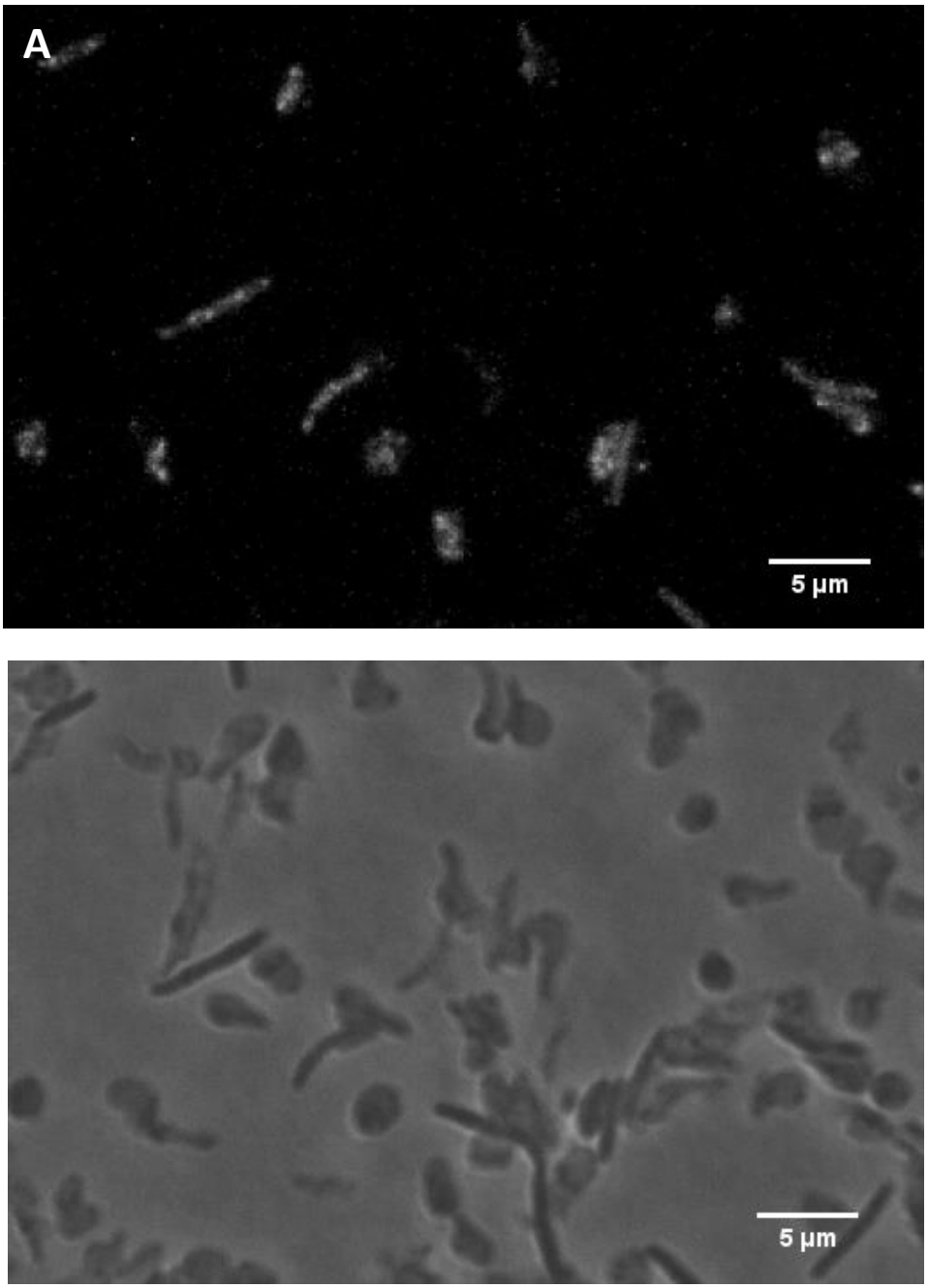

Figure 54. Bipolar and lateral cluster formation of MglA-eYFP in ΔBacM cells induced with 500 µM vanillate on hard agar *(A) ΔBacM cells showing bipolar and lateral clusters (B) ΔBacM cells showing membrane blebs.*

5.3.7 Expression of MglA-eYFP on soft agar-grown cells in the presence and absence of BacM

Medium MglA-eYFP expression in ΔMglA cells grown on soft agar resulted in the formation of unipolar clusters (**Figure 55A**). Most cells, however, showed dispersed fluorescence and no polar clusters. In these cells the clustering of MglA, seemed to correlate with collisions of cells. In the ΔBacM cells bipolar clusters were observed at low MglA-eYFP induction, similarly to when the ΔBacM cells expressed MglA on hard agar (**Figure 55B**). One difference, however, is that these cells had less membrane blebbing, indicating that the hardness of the underlying substratum, in addition to the expression levels, plays a role in membrane blebbing in ΔBacM cells.

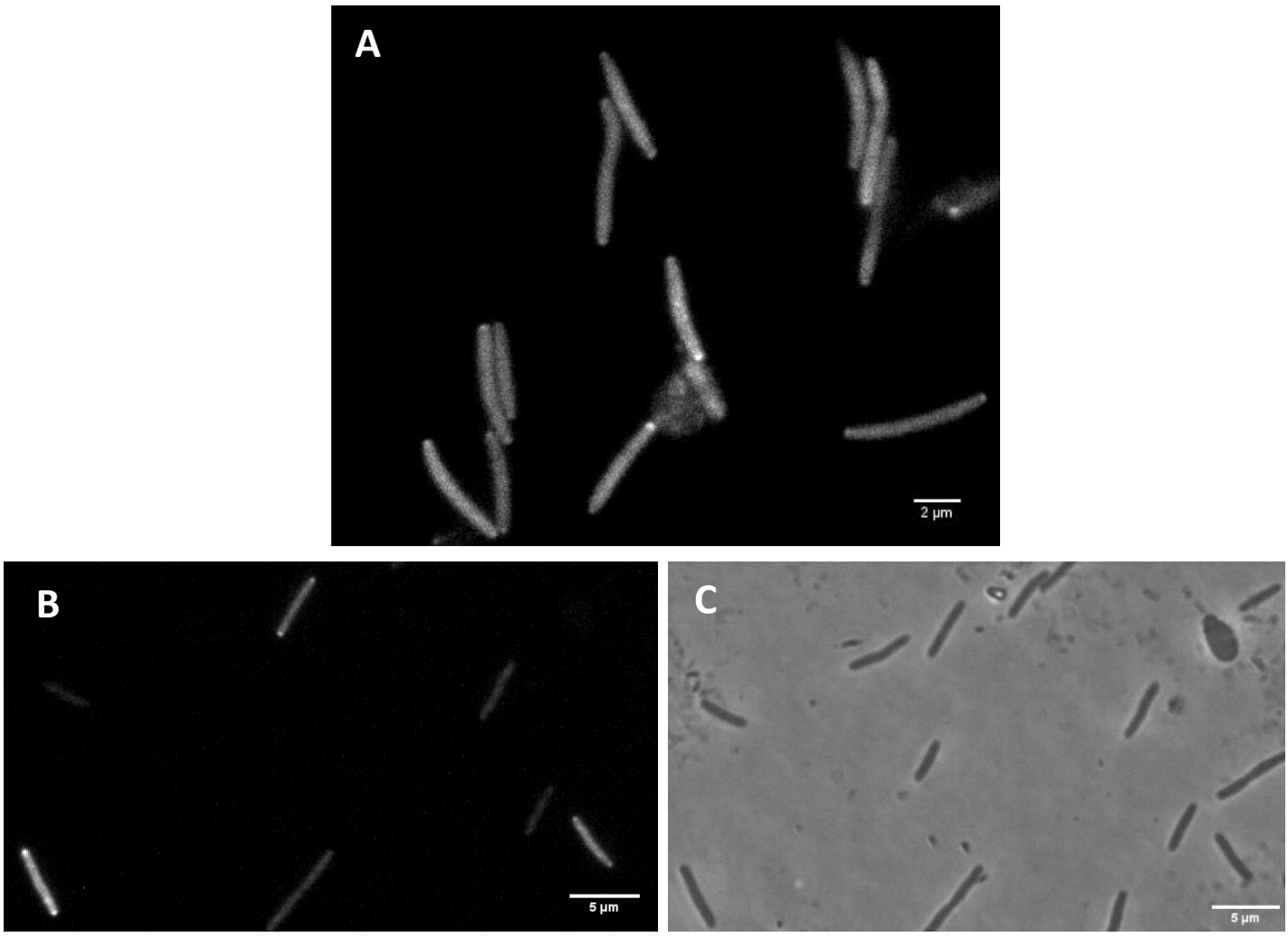

Figure 55. MglA-eYFP expression on soft agar. *(A) MglA-eYFP expression at 50 µM vanillate in ΔMglA cells leads to unipolar cluster formation in some of the cells. (B) MglA-eYFP expression (5 µM vanillate) in ΔBacM cells leading to the formation of bipolar clusters, unipolar clusters and no clusters (C) ΔBacM cells showing less membrane blebbing on soft agar with 5 µM vanillate induced cells.*

To check whether MglA cluster formation was correlated to the hardness of the underlying substratum, MglA-eYFP was expressed (50 µM vanillate) in ΔMglA cells grown on 5% CTT agar. On 5% CTT agar a lot of cells showed bipolar cluster formation of MglA-eYFP, which was identical to the bipolar clusters observed on 1.5% CTT agar (**Figure 56A**). However, half of the ΔMglA cells died within an hour of incubation at 32 ^{o}C on 5% agar. Two types of fluorescent clusters were observed in these cells. Cells that moved a bit slower then physiological WT cell velocity showed bipolar cluster formation. In contrast, damaged or dying cells showed highly reduced velocity and possessed lateral clusters (**Figure 56B**). When measured WT cells were moving with a gliding speed of 6.5 µm/min. and had an average reversal frequency of 1 reversal every 11 min. on 5% agar.

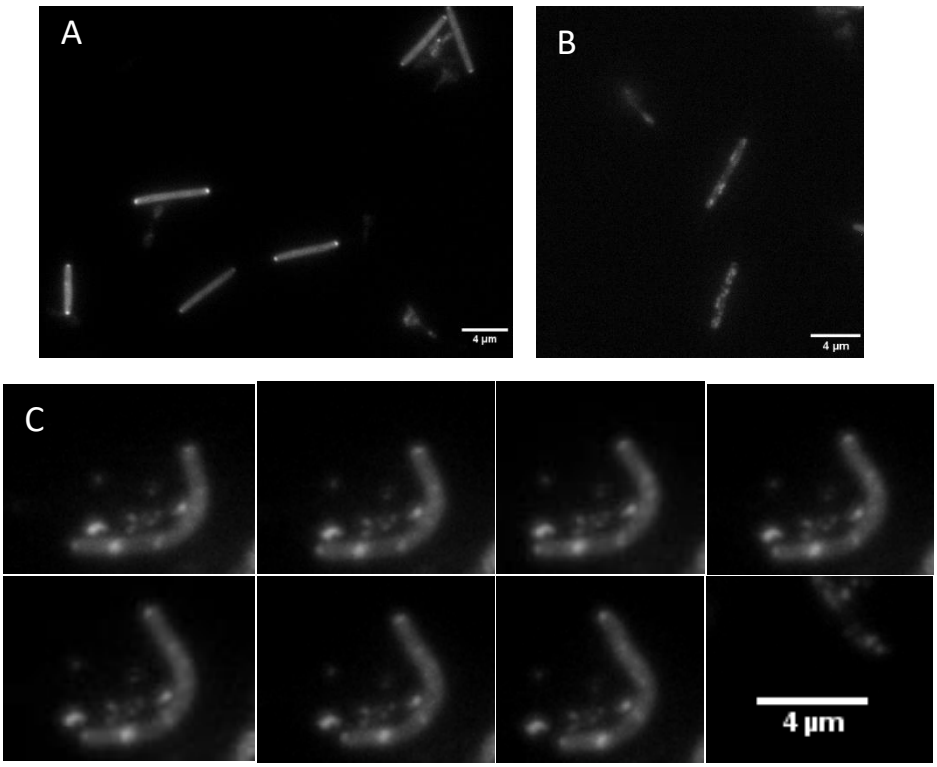

Figure 56. MglA-eYFP cluster formation in ΔMglA cells on 5% agar. *(A) M. xanthus cells showing bipolar clusters (B) Dead M. xanthus cells showing lateral MglA clusters (C) dying cell with bipolar and lateral clusters and reduced gliding motility. Time lapse samples were taken every 10 seconds*

An interesting observation was that dead cells no long showed bipolar clusters, while the dying cells did (**Figure 56B/C**). The average gliding speed of the cells containing bipolar clusters was 3.35 µm/min and the average gliding speed for cells containing lateral clusters was 1.22 µm/min. These speeds are the average of the measurements taken from ten individually gliding cells with bipolar clusters and ten cells with lateral clusters. The cells containing lateral clusters eventually stopped moving and lysed. Thereby, the formation of lateral MglA clusters seemed to be linked to the hardness of the underlying substratum. Additionally, these lateral clusters were correlated with a reduced gliding speed.

Some of the lateral clusters moved while the cell moved forward, while others appeared, disappeared, or remained at fixed positions in the cell (**Figure 57**). The cluster indicated by the green arrow in **Figure 57** stayed at a fixed position near the bend in the cell, as the cell moved forward. A lot of the other clusters, including the one indicated by the blue arrow, seemed to appear and disappear as the cell glided forward. Whether this was the same cluster, or a newly formed cluster due to localised force-induced membrane signals or deformation of the membrane was unclear. These observations cast doubt on previous publications, claiming that MglA localised to focal adhesion clusters which drive motility by moving from the front to back pole (T. Mignot et al., 2007).

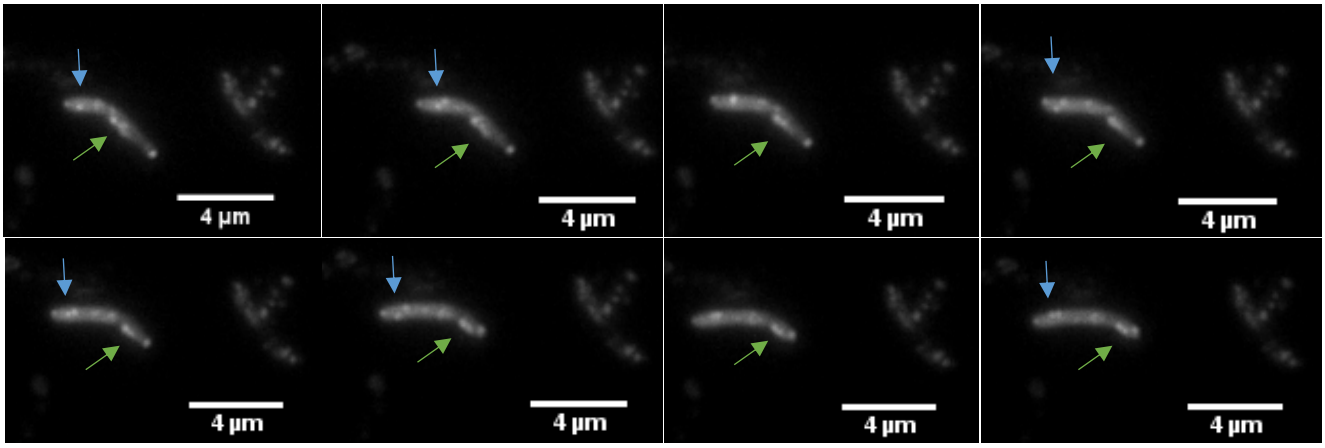

Figure 57. ΔMglA cell with lateral MglA-eYFP clusters. *One of the lateral clusters appears and disappears over time near the front pole (blue arrow) and another cluster travels along the membrane towards the back pole as the cell moves forward (orange arrow)*

After 12 hours of incubation on 5% agar all the cells had died. Leaving behind a pattern of lateral MglA-eYFP clusters (**Figure 58**). These cells did not show any membrane blebbing.

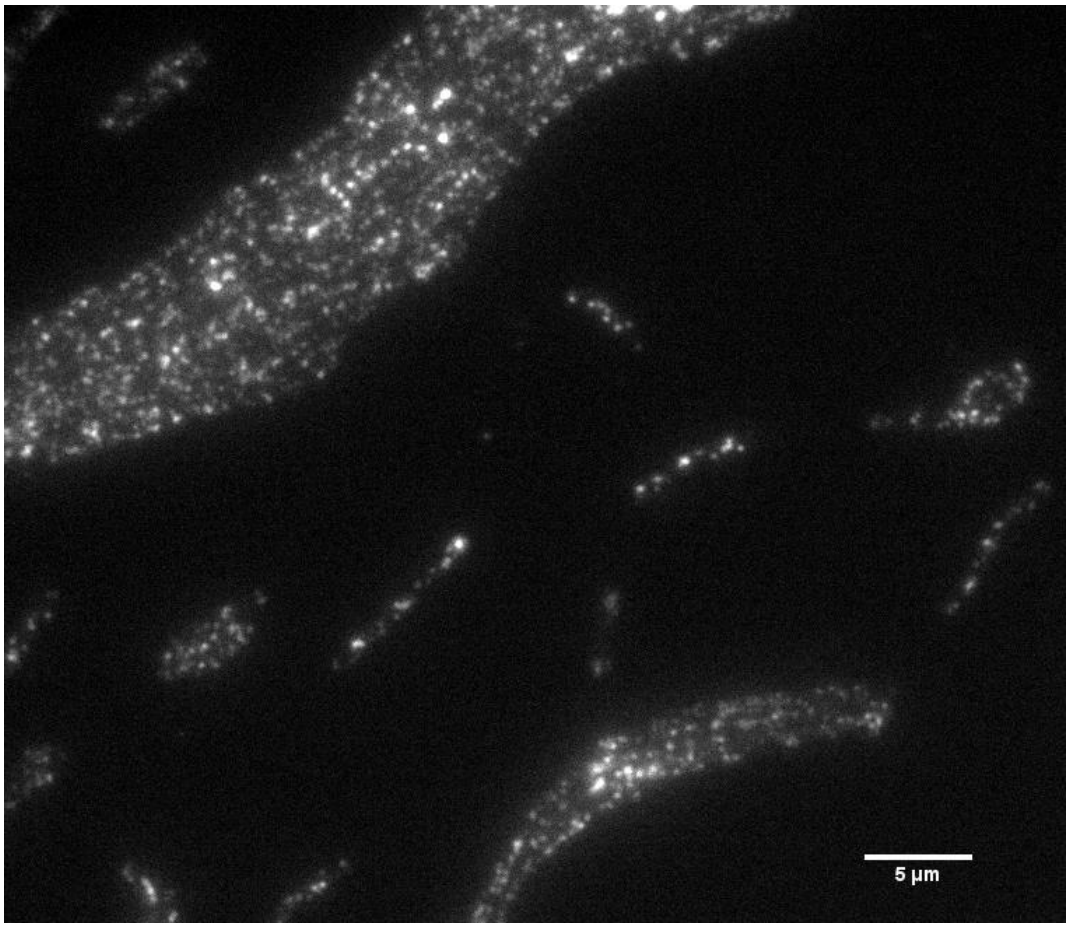

Figure 58. MglA-eYFP lateral cluster formation in dead ΔMglA cells after 12 hours of incubation on 5% CTT agar.

5.3.9 Bipolar cluster formation of MglA-eYFP on hard agar correlates with hyper reversing cells

An interesting observation made during the previously discussed experiments, was the difference in cell reversal frequency observed between different MglA-eYFP expression strains. The most striking difference in reversal frequencies and gliding speed was observed between 50 µM and 500 µM vanillate induction of MglA-eYFP in *ΔMglA* cells. At high expression levels the cells formed bipolar clusters, while at medium expression levels the cells had either no clusters or a unipolar cluster at the leading pole (**Figure 51; Figure 52**).

High induction resulted in cells hyper-reversing with an average frequency of 1 reversal every 40 seconds, while medium induction lead to a cell reversal frequency of 1 reversal every 5 minutes, which was close to the WT reversal frequency of 1 reversal every 7 minutes (A. M. Spormann & Kaiser, 1995). MglA-eYFP expression in a ΔBacM strain lead to the formation of bipolar clusters even at low expression levels (**Figure 53**) and accordingly the cells were hyper-reversing (1 reversal per minute) suggesting that the formation of bipolar clusters appeared to stimulate movement at both cell poles. ΔBacM cells with no MglA-eYFP expression did not hyper-reverse indicating that it is the expression of MglA-eYFP and the formation of bipolar clusters leading to hyper-reversing ΔBacM cells (**Table 13**).

Table 13. Reversal frequencies and speed of ΔMglA and ΔBacM cells expressing MglA-eYFP. *Ten motile cells from each strain were picked and measured using Fiji.*

	Strain:			
Parameter	ΔMglA 50 µM Van.	ΔMglA 500 µM Van.	ΔBacM 0 µM Van.	ΔBacM 5 µM Van.
Average reversal frequency (min^{-1}) (SD)	0.21 (0.2)	1.56 (0.44)	0.18 (0.15)	0.96 (0.31)
Average speed (µm/min) (SD)	6.96 (4.04)	4.61 (2.39)	3.90 (1.06)	1.99 (1.03)

A reduced gliding speed was observed between *ΔMglA* cells expressing high levels of MglA-eYFP (500 µM vanillate) or medium levels (50 µM vanillate). The average gliding speed of WT (DK1622) cells is ca. 4.4 µm/min (Alfred M. Spormann & Kaiser, 1999), which is similar to the gliding speed measured in ΔMglA cells complemented by the expression of MglA-eYFP. A reduction in gliding speed was found at low expression levels of MglA-eYFP in ΔBacM cells. This data indicated that the formation of bipolar clusters lead to hyper-reversing cells and a reduction of the gliding speed of individually moving cells.

5.3.10 Immunofluorescence microscopy showed co-localisation of MglA and BacM

To look at whether MglA and BacM interacted *in vivo* immunofluorescent co-localisation experiments were performed. The control strains in this experiment were: ΔMglA, ΔMglAB, ΔBacM and ΔBacNOP cells. BacM and MglA were stained using BacM- and MglA-specific polyclonal antibodies, which were visualised by a 488 anti-rat and 594 anti-rabbit secondary antibody staining, respectively. Allowing, for the visualisation of BacM using FITC (green fluorescence) and MglA using TxRED (red fluorescence). The nucleoid was stained using bisbenzimide and visualized using DAPI (blue fluorescence). Background fluorescence was checked using WT (DK1622) cells as control, without the use of 2^{nd} antibodies (**Figure 59B**). These cells showed no fluorescent background except for the nucleoid staining with bisbenzimide. An interesting observation was the inability to visualise fluorescently labelled MglA in both the ΔBacM and ΔBacNOP cells. This inability indicated that the absence of bactofilins was linked to a reduced expression of MglA inside the cell (**Figure 59C/D**), thereby confirming the previously identified reduced expression of MglA in a ΔBacM and ΔBacNOP background (**Chapter IV page 118**).

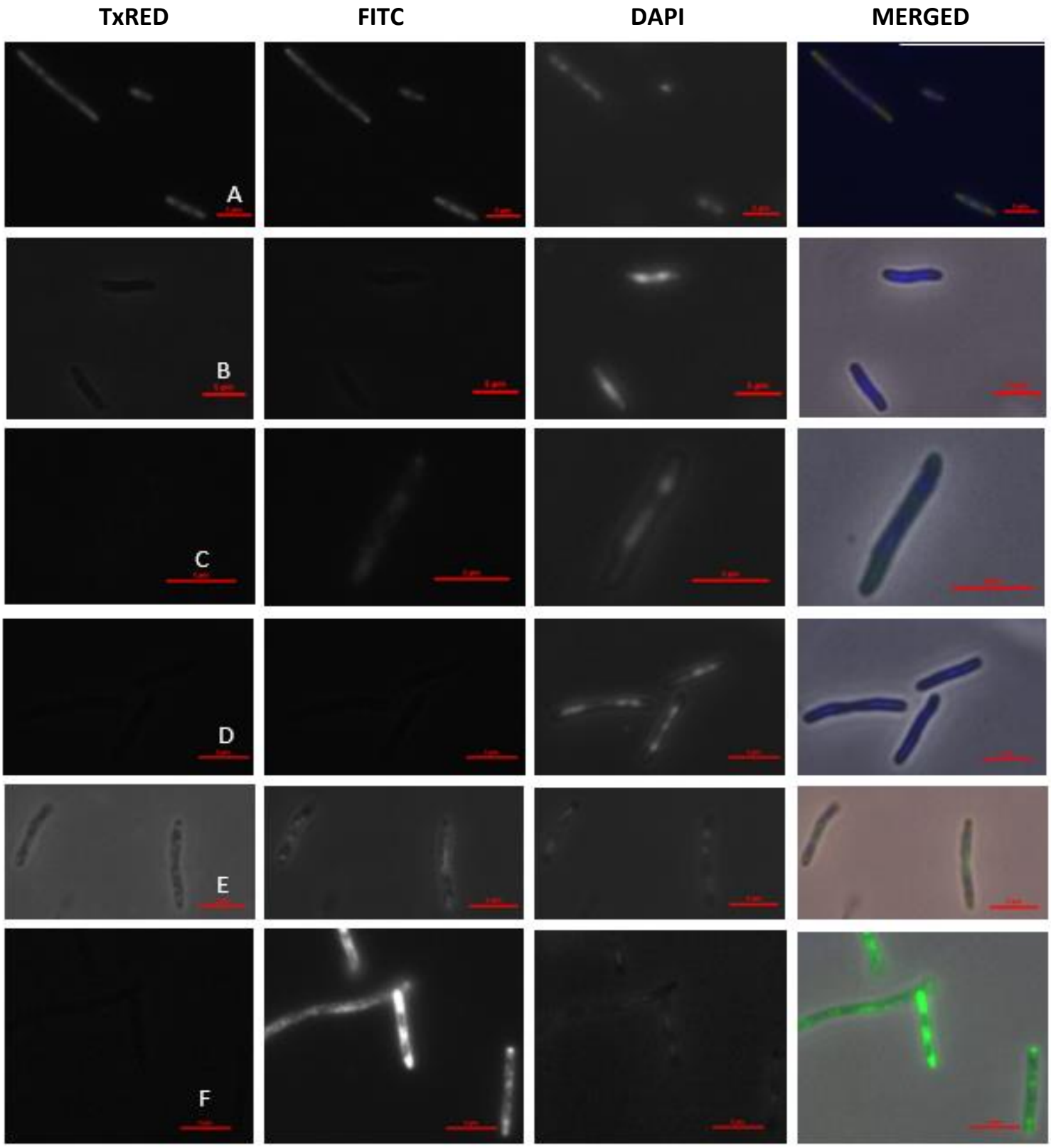

Figure 59. Immunofluorescence microscopy localisation of MglA and BacM. *(A) WT cells (DK1622) (B) WT cells without 2nd antibodies (C) ΔBacNOP cells (D) ΔBacM cells (E) ΔMglA cells (F) ΔMglAB cells (DK6195). (B/C/D/E/F) have an additional brightfield image highlighting the difference in merged pictures when compared to WT cells (A).*

Closer observation of the WT (DK1622) cells showed the two proteins to co-localized in *M. xanthus*. Both proteins were not present in the nucleoid and BacM seemed to additionally form both a cluster at the front and back pole of the cell (**Figure 60**). The absence of an MglA cluster at the pole of the cell was potentially caused by the cells being liquid grown. This confirmed the previous obtained results in which medium level expression of MglA-eYPF (50 µM vanillate) in liquid grown ΔMglA cells, showed no MglA polar cluster formation (**Figure 49**). Interestingly, this result indicated that BacM, except for localising throughout the cell, also clustered at both cell poles. The absence of MglA at both cell poles indicated that a control mechanism seemed to be in place preventing the binding of MglA to the membrane at the cell pole or alternatively to BacM at the cell pole. Alternatively, the high concentration of BacM could potentially lead to thick filament formation physically hindering MglA from binding at the cell pole.

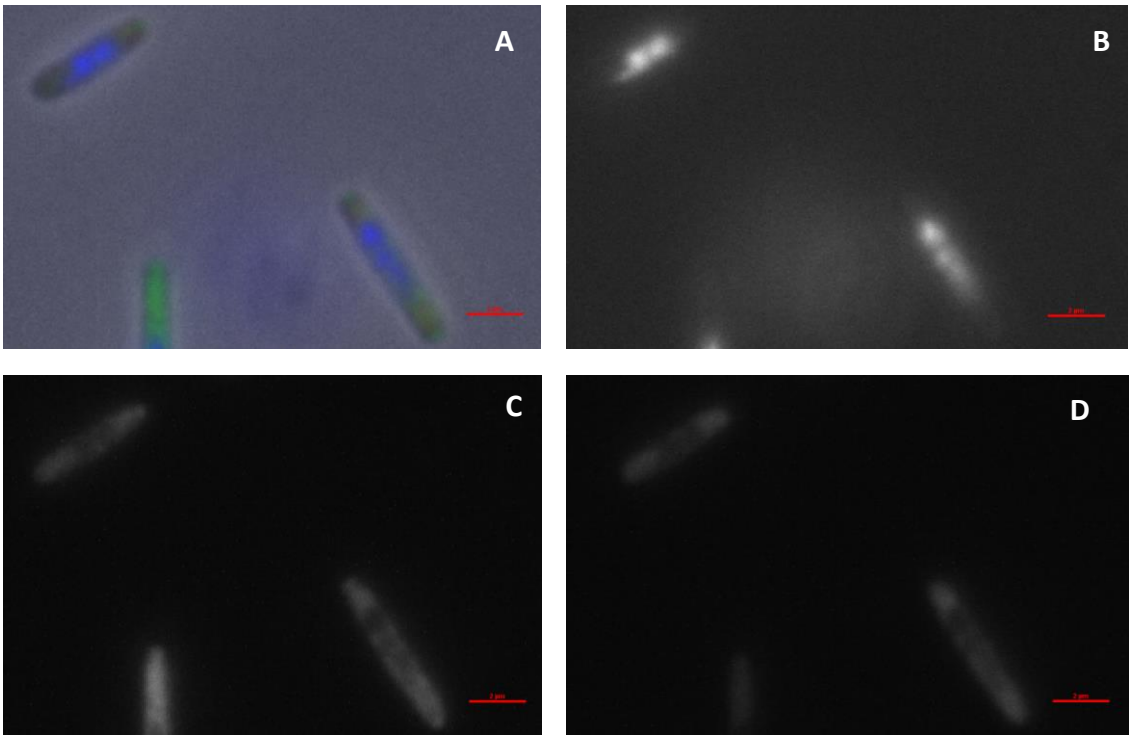

Figure 60. Co-localisation immunofluorescence microscopy of WT cells using a BacM and MglA antibody. *(A) merged picture, (B) DAPI bisbenzimide staining of the nucleoid (C) FITC BacM antibody staining, (D) TxRED MglA antibody staining.*

When looking at the ΔMglA cells, red fluorescence was observed, indicating that the MglA antibody bound, while in the ΔMglAB (DK6195) cells no fluorescence was observed. Therefore, the ΔMglA strain (SA4420) was tested for the presence of MglA. For this purpose, PCRs were set up using two different primer combinations (**Figure 61**; Upstream F ΔMglA(B) with Mx_MglA_R primer downstream (**Lanes 2/3**) Mx_MglA_F and downstream R ΔMglA(B) primers (**Lanes 4/5**)). One primer that bound upstream of the *mglA* gene and a primer binding at the end of the gene. The second combination was a primer binding downstream of the *mglA* gene and a primer that bound at the start of the gene (**Figure 61**). Both primer combinations resulted in a band indicating the presence of the DNA sequence encoding the N- and C-terminal part of MglA. The DNA was extracted from the gel and sequenced revealing that the first and last 20 amino acids of MglA separated by a restriction site were still present in these cells. This may explain why in these cells fluorescence could be detected, as there may still be a truncated form of the protein being expressed. Importantly, the truncated form of the protein did not seem to be biologically functional, as it was not able to complement motility. Nonetheless, it is important to be aware that this truncated form of MglA could influence cellular processes.

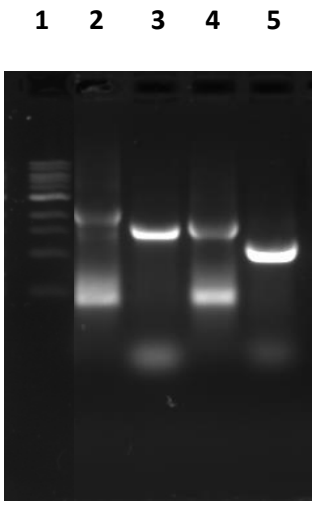

Figure 61. Part of the mglA geneis present in the ΔMglA strain. *Lane 1) 1Kb ladder 2) A-primer with MglA reversed on WT DNA, Lane 3) A-primer with MglA reversed on ΔMglA DNA, Lane 4) D-primer with MglA forward on WT DNA, Lane 5) D-primer with MglA forward on ΔMglA DNA.*

5.4 Discussion

Over the past decade many publications have been published on the localisation and potential function of MglA in *M. xanthus*. One of those papers showed that a cell on hard agar formed bipolar and lateral MglA-YFP clusters (Patryn, Allen, Dziewanowska, Otto, & Hartzell, 2010). Faint polar fluorescence was observed in cells that were claimed to lack MglA-YFP and about 30% of the bends in cells showed an increase in fluorescent intensity. These observations provided evidence for MglA-YFP localising at bends in the cell where it got "stuck" (Patryn et al., 2010). These results differed from our experimental observations. At medium expression level, the ΔMglA cells showed unipolar MglA-eYFP clusters as well as dispersed fluorescence. Higher expression using 500 µM vanillate lead to the formation of bipolar clusters and, when prolonged expressed, cell elongation. Based on the high expression levels, the elongation of cells, and the reduced spreading compared to the 50 µM-induced cells, it was concluded that the high expression (500 µM vanillate) most likely lead to non-biologically relevant concentrations of MglA.

The differences in experimental results for the localisation of MglA-eYFP could be possibly the consequence of the way the cells were prepared. In Patryn et al., 2010 the cells were placed on CTPM 1.5% agar pads or grown in 0.5% (v/v) methylcellulose CTPM broth. These agar patches were covered in polyvinyl film and stored at 4^{o}C. Cells were mixed in TPM medium and placed on the CTPM pads. The slides were then incubated at 33 ^{o}C in the dark for at least 30 minutes (Patryn et al., 2010). In our laboratory, the cells were placed on fresh 1.5% or 0.7% CTT agar. Cells were mixed in CTT medium, placed on these agar patches and incubated at 32 ^{o}C in the dark for at least an hour. The use of CTPM or alternatively storing the agar patches at 4 ^{o}C could potential have an influence on the dryness of the agar patches and therefore localization of MglA.

In the publication were also cells mentioned that contained a faint polar fluorescence, which could indicate that these were actually the more “healthy cells”, with diffusely localised MglA-YFP. The supplemental figures in the paper showed the movement and localisation of six cells possessing lateral MglA-YFP clusters. Upon closer inspection, the average gliding speed of these cells when calculated was found to be around 1 µm/minute. This speed was a lot slower than the published average gliding speed of 4.4 µm/minute (Alfred M. Spormann & Kaiser, 1999). In addition, the gliding speed of these cells was quite similar to the gliding speed of cells showing lateral clusters on 5% agar (1.22 µm/minute). Patryn et al., 2010 also mentioned that MglA localised to bends in the cell, which was also observed in our experiments (**Figure 57**). Minimal induction (5 µM vanillate) of MglA-eYFP in liquid-grown ΔBacM cells lead to the formation of bipolar, unipolar and, in some cells, lateral clusters. Interestingly, ΔBacM cells have a crooked cell morphology and MglA-eYFP seemed to specifically localise to the bends in the cell.

In ΔMglA cells, MglA-eYFP was either dispersed over the cell or localised unipolarly at the front pole of the cell. On hard and soft agar, the localisation of MglA at the front pole of the cell seemed to correlate with the obstruction of the cell, as the front polar cluster was observed in cell groups or when a cell collided head-on with another cell. These results indicated that MglA localised to areas of the cell length where the membrane was deformed or showed curvature. In much the way, some small G-proteins including Ras proteins and their regulators are known to be able to bind to curved membranes (B. Antonny et al., 2005; Hanna et al., 2016; Liang et al., 2018). It could therefore very well be that membrane curvature plays a key role in the membrane localisation of MglA. Alternatively, the localisation of MglA to these sites could also be a result of membrane signalling, a possibility being that it is mechanoreceptor-induced signalling that attracts MglA to these sites (Booth et al., 2007).

The ΔBacM strain was shown to greatly reduce expression levels of MglA (**Chapter IV page 118**) and low amounts of MglA expression in this strain had a negative impact on the spreading of ΔBacM cells. Comparing these results to the fluorescent microscopy data, indicated that the observed bipolar and lateral MglA clusters were responsible for the reduced spreading of *M. xanthus* cells. One possible explanation is that the formation of bipolar MglA clusters reduced motility at the front and back pole of the cell. The difference in the amount of MglA-GTP at the poles and the change in MglA-GTP concentration at the poles over time, could explain the observed hyper-reversing of the cells. Based on these results, BacM seems to play a key role in the localisation of MglA and therefore indirectly a role in motility and cellular reversals.

Importantly, BacM might additionally play a role in the expression or correct localisation of MglB. If MglB does not localise to the lagging pole in the absence of BacM, then this could explain the bipolar cluster formation of MglA. MglB being the GAP protein of MglA is essential for catalysing the hydrolysis of GTP-bound MglA (Miertzschke et al., 2011), thereby preventing the formation of focal adhesion complexes at the rear end of the cell (Y. Zhang et al., 2010). The ΔMglB cells showed a severe defect in swarming on both hard and soft agar, additionally, they were also shown to move at WT velocities and had an increase in cellular reversals (Y. Zhang et al., 2010).

No hyper-reversals were observed for ΔBacM cells, which, however, can be explained by the greatly reduced levels of MglA in these cells. Interestingly, the overexpression of MglA rescued spreading of ΔMglAB cells on hard agar more, than low expression levels. In addition, spreading on hard agar was restored to 88% of WT level when MglA was expressed using 5 µM vanillate, while in the absence of MglB spreading was restored to only 60%. This indicated that the defect in spreading was caused by the absence of MglB and that this defect could be compensated for by overexpressing MglA.

If the only essential form of MglA for A-motility is the GTP-bound form, then one would expect no change or reduced spreading, when overexpressing MglA in ΔMglAB cells in comparison to normal or low expression levels of MglA. This was expected, because the intrinsic hydrolysis of MglA-GTP to MglA-GDP is very low (Patryn et al., 2010). However, the current results indicated that the GDP-bound form of MglA, might also potentially play a role in spreading on hard agar and therefore A-motility. Alternatively, GTP hydrolysis has been shown to be important for the proper functioning of MglA, so it could be that the GTP hydrolysis catalysed by MglB is important for A-motility (S. A. Fremgen et al., 2010).

The observed reduced spreading of ΔBacM cells expressing MglA-eYFP could also be the result of increased binding of focal adhesion complexes to the underlying substratum (Tâm Mignot et al., 2007). The formation of larger or more numerous focal adhesions, could potentially lead to such an increase in cell adherence and, consequentially, a reduction in cell motility. In eukaryotes several Ras proteins have been associated with increased cell surface adhesion (Pollock et al., 2005; Sandri et al., 2012; Secko et al., 2006). In addition, some publications have suggested an inverse relationship between the number of focal adhesion complexes and cell motility in eukaryotic cells (Ilić et al., 1995; Nagasaki et al., 2009; Thompson et al., 2009). Besides the inverse relationship, a biphasic gaussian relationship has been reported for the link between focal adhesion sizes and cell speed (Kim & Wirtz, 2013). If focal adhesion sites in bacteria function similarly to their eukaryotic counterparts, then the formation of large or numerous focal adhesion sites could slow the cell down.

In the paper from Mauriello and co-workers *M. xanthus* cells contained bipolar and lateral MglA-YFP clusters (Mauriello et al., 2010). Genetically, in this strain the original *mglA* gene was replaced by a version that encoded for a C-terminally YFP-tagged protein. The velocity with which these cells moved when measured was around 0.6 µm/min, which is significantly slower than the known average gliding speed of WT (DK1622) cells of 4.4 µm/min (Mauriello et al., 2010; Alfred M. Spormann & Kaiser, 1999).

In addition, another paper looked at the localisation of an N-terminally YFP-tagged version of MglA with an amino acid change at the 82nd position, changing a glutamine to an alanine (Treuner-Lange et al. 2015). This amino acid change locked MglA in its GTP-bound state. Interestingly, the cells shown in this publication have bipolar and lateral MglA clusters and when measured moved with a speed of around 0.8 µm/minute (Treuner-Lange et al., 2015).

These publications together with the here discussed experimental results indicate, that the formation of bipolar and lateral clusters appear to reduce the speed at which these cells glide. This is in contradiction to the focal adhesion model in which one would expect a positive correlation between the number of focal adhesion clusters and the gliding speed of the cell. However, if the main function of these complexes is to attach the cell to the underlying substratum, then the multiple MglA clusters could explain the observed reduced cell speeds.

Cells expressing MglA-eYFP were grown on 5% agar patches to investigate the influence of the hardness of the substratum on MglA cluster formation. After 1 hour of growth at 32^{o}C, two MglA cluster phenotypes were observed. Most of the cells were hyper-reversing and contained bipolar clusters, with an average velocity close to that of WT cells. The other cells showed both bipolar clusters and lateral clusters and moved slower when compared with the cells containing bipolar clusters.

This experiment showed, that the hardness of the underlying substratum played a role in the localisation of MglA. The resulting external physical forces could lead to the activation of certain signals or result in membrane deformations that trigger the formation of MglA clusters at these specific locations. This hypothesis could explain, why as the cell moves forward some of the MglA clusters stay at a fixed position with respect to the underlying substratum. When the membrane is permanently damaged, the MglA cluster should remain fixed at this position, thereby moving forward with the cell. This could explain why some of the lateral clusters observed in ΔMglA cells on 5% agar and in ΔBacM cells on hard agar are not moving from the front to back pole.

Growing the ΔMglA cells overnight on 5% agar caused all the cells to die leaving behind dead cells containing MglA-eYFP clusters. This observation may indicate that the formation of lateral MglA clusters has eventually a toxic effect resulting in cell death.

To verify the observed experimental results, immunofluorescence microscopy was used as an alternative technique to look at the co-localisation of MglA and BacM inside the cell. In both the ΔBacM and ΔBacNOP cells no MglA-related fluorescence was observed. This was in line with the previous findings that MglA was showing very little expression in the bactofilin deletion mutants. In the ΔMglA strain, fluorescence corresponding to the binding of the MglA antibody was observed, but may be explained by the presence of the expressed 40 amino acid-long truncated form of MglA. This truncated version has been deemed biologically non-functional, as it was not able to rescue motility. However, it is possible that the truncated form of the protein may still interact with other cellular protein targets or may disrupt other functions in the cell.

The co-localization of MglA with BacM strengthened the experimental data that had already been collected, proving that these two proteins indeed interact. An interesting observation was the bipolar cluster formation of the immuno-fluorescently labelled BacM. These polar clusters, in addition to the nucleoid, were the only regions were MglA was not co-localising with BacM. This was in contradiction to the observed polar localisation of over-expressed MglA-eYFP in ΔMglA cells. The difference in localisation could be explained, due to the cells being liquid grown and not experiencing physical forces at their cell poles while possessing WT levels of MglA that is, like in WT cells, mostly diffuse in the cytoplasm.

5.5 Conclusion

In this chapter, it was shown that in both, the ΔMglA strain and the ΔBacM strain overexpression of MglA-eYFP lead to bipolar and lateral cluster formation. The formation of these clusters in ΔBacM cells correlated with a reduction in gliding speed, occurrence of hyper-reversing, and reduced spreading on hard agar as well as membrane blebbing and cell death. The same results were obtained for ΔMglA cells when the expression rate was higher and the substratum harder inducing the formation of lateral MglA-eYFP clusters. A correlation was found between the agar concentration and the formation of lateral MglA-eYFP clusters. The higher the agar concentration, the more lateral clusters were formed. This indicated, that a harder substratum causes more membrane deformation that lead to the formation of lateral MglA-eYFP clusters.

Our results in addition to previously published data of cells with lateral MglA clusters, indicate an inverse relationship between these lateral clusters and the gliding speed of the cell. Consequently, these clusters or focal adhesion complexes seem to be important for the attachment of the cell to the underlying substratum (Balagam et al., 2014).

Cells showing the highest spreading rate on hard agar, a normal gliding speed and no hyper-reversing phenotype all had MglA-eYFP diffuse in their cytoplasm. These cells only developed a unipolar cluster when the cell collided with an object at its front pole. Membrane cluster formation is associated with the GTP-bound form of MglA and therefore most of the MglA seems to be in its GDP-bound state.

Taken together these results point towards a membrane curvature or deformation-induced MglA localisation at the front pole of the cell, where it is involved in cell adhesion and regulation of cell reversals. The proper localisation of MglA at the pole seems to depend on the presence of BacM. Without BacM, MglA localises at both poles. The immunofluorescence microscopy data showed two bright polar clusters corresponding to BacM in WT cells. One potential function of these BacM clusters is to prevent MglA from binding to the curved membrane at the poles of the cell.

As over-expression of MglA seemed to correlate with membrane blebbing at the poles of ΔBacM cells. Maybe MglA detects when the cells encounter an object or surface unevenness preventing or reducing forward motion thereby triggering cell reversal.

The results in this chapter question the hypothesis that focal adhesion complexes drive A-motility. Of note, these results do not challenge the slime model, an alternative explanation for the generation of the force driving A-motility. However, if the secretion of slime drives A-motility then the question remains how MglA regulates secretion and cell reversals.

A previously published report showed that an MglA disruption mutant secreted slime at both poles (Yu & Kaiser, 2007) indicating, that MglA is involved in the regulation of polar slime secretion. In addition, disruption of several A-motility genes *gltI, gltC, gltJ, agnB, agnC, aglU* and *cglB* also lead to bipolar slime secretion. Three of these genes *gltI, gltC,* and *gltJ* are part of the focal adhesion complex (Faure et al., 2016). Based on the described literature, it would be important to investigate whether bipolar and lateral localization of MglA, in the absence and presence of BacM, affects the amount and localization of the secreted slime. Future research will be needed to elucidate the function of MglA on slime secretion.

Chapter VI

6. Outlook

In this thesis, the hypothesis of a possible interaction between MglA and BacM was studied using multiple complimentary experimental approaches. The results of these approaches strongly support that the two proteins interact directly with each other through the binding of MglA to the proline-rich C-terminus of BacM, which results in a co-localization of the two proteins. Importantly, the binding and interaction of the two proteins influences a number of cellular responses. In particular, it was observed that MglA more readily forms bipolar and lateral clusters in the absence of BacM, that the cellular reversal frequency increased upon bipolar MglA cluster formation, that the cellular level of MglA was reduced in ΔBacM cells, that the presence of one of the two proteins is essential to *M. xanthus* resulting in double deletions being lethal, and that no elongated cells were observed when MglA is overexpressed in ΔBacM cells. Intriguingly, these experimental results show a remarkable similarity to experimental observations made for Ras or Ras-like proteins in eukaryotic, plant and other bacterial cells (Prober & Edgar, 2000; Guest, Lin, & Momany, 2004; Park & Bi, 2007 Overmeyer, 2011; Dewachter et al., 2017). Along those lines, it was earlier observed that the integration of the *SAR1* gene from *Sacharomyces cerevisiae* into the *M. xanthus* genome, complements the motility-dependent aggregation and fruiting body formation of cells in a ΔMglA strain (P. L. Hartzell, 1997).

In *Sacharomyces cerevisiae,* Sar1 functions in the transport of secretory proteins from the endoplasmatic reticulum, *via* a coat protein complex II (COP-II). (Miller & Schekman, 2013). The formation of the COP-II vesicle is initiated through the activation of Sar1, by its GEF (sec12) (Nakano & Muramatsu, 1989).

Central to the process of COP-II vesicle formation is the fact that Sar1 contains an amphiphatic N-terminal helix, by which it penetrates the ER membranes and induces membrane-curvature (M. C. S. Lee et al., 2005; Long et al., 2010; Settles et al., 2010). Sar1 then interacts with Sec23 and Sec24 to form the pre-budding complex, in which Sec24 interacts with the cargo receptors (X. Bi et al., 2002; Sato & Nakano, 2005). This interaction is followed by the binding of the pre-budding complex to the outer coat complex (Sec31/Sec13), which stimulates the GAP activity of Sec23. The subsequent Sar1 GTP hydrolysis then finalises the process of vesicle formation (Bruno Antonny et al., 2001; X. Bi et al., 2007).

Inspection of the amino acid sequence of MglA reveals no amphiphatic helix at the N-terminus, as the protein starts with a β-sheet (Miertzschke et al., 2011). However, the C-terminal end does contain an α-helix and in addition, contains the necessary amino acids to form an amphipathic lipid packing sensor motif (ALPS) (**Chapter IV 4.8 Page 126**). In other proteins, this motif is involved in the binding to lipids (Drin & Antonny, 2010). Based on the observation that MglA in *M. xanthus* cells forms membrane-located clusters, one likely scenario is that MglA might bind to the membrane *via* its amphipathic α5-helix. Intriguingly, once the pre-budding complex is formed Sar1 interacts with sec31, by binding to its proline rich C-terminal region (Hutchings et al., 2018). Sec31 functions by binding to Sec23 and Sar1, a process that stimulates Sec23-dependent GTP-hydrolysis of Sar1, which leads to the disassembly of the coat complex (Hutchings et al., 2018). Importantly, BacM also interacts *via* its C-terminal proline rich region with MglA and might also conceivingly be involved in the GTP-hydrolysis of MglA. Sar1 is known to be able to sense membrane curvature and binds more avidly to highly curved membranes (Hanna et al., 2016). Similarly, the formation of MglA clusters at the cell poles and bends in the cell, indicates that MglA might also sense membrane curvature and, like Sar1, has a propensity to bind to membranes of high curvature (Patryn et al., 2010).

In addition, insertion of the N-terminal amphipathic α-helix of Sar1 into the membranes of liposomes causes them to form tubules by generating membrane curvature (Bielli et al., 2005; M. C. S. Lee et al., 2005). If MglA functions in the generation of membrane curvature, then this could explain why the ΔBacM cells are vunerable to the expression of MglA, as there is less stimulation of MglA GTP hydrolysis and therefore increased membrane curvature at the MglA clusters. In addition, Sar1 is involved in the secretion of collagen and one of the identified focal adhesion complex proteins (PglI, MXAN_4867) contains a collagen-binding domain (Beiyan Nan et al., 2010). In eukaryotes, collagens are known to be important for cell adhesion and collagen-like proteins are known to be expressed in bacteria (Heino, 2007; Z. Yu et al., 2014). If the MglA clusters are important for the secretion of collagen-like proteins, then this could explain the reduced cell speed observed in *M. xanthus* cells containing lateral MglA clusters (**Chapter V 5.3.9 and Chapter V 5.4 Pages 156 & 162**). In the absence of BacM, MglA expression resulted in bipolar localization, lateral cluster formation, and membrane blebbing, which lead to cell death. Taking into consideration the observed similarities between MglA and Sar1, this indicates that the accumulation of active membrane-bound MglA-GTP could lead to severe lowering of the lipid membrane rigidity (Settles et al., 2010). Based on the Sar1 literature, BacM might potentially be involved in the GTP-hydrolysis of MglA, which would be important for the functioning of MglA (Patryn et al., 2010). In **Chapter V** MglB was found to play a role in colony spreading on hard agar. This experiment together with the Sar1 literature indicates that MglA, MglB and BacM might form a complex similar to the Sec23, Sar1, and Sec31 complex, catalysing the hydrolysis of MglA-GTP to MglA-GDP.

As mentioned in **Chapter IV**, the expression of some Ras proteins is influenced by downstream or upstream proteins in the Ras signalling pathway (R. M. Stephens et al., 2017; Unni et al., 2015). MglA also plays a role in several other important cellular functions including A- and S- motility, cell polarity and cellular reversals. MglA is known to sort the polar localization of PilB/PilT (two ATPases), essential for the extension and retraction of Type-IV pili (Bulyha et al., 2013).

Except for this paper, little is known about how MglA establishes cell polarity and cellular reversals. However, the regulation of dynamic polarity switching of MglA and MglB in *M. xanthus* is important for motility and cellular reversals (Leonardy et al., 2010b).

In the light of the newly discovered results, several aspects of *M. xanthus* biology have to be re-evaluated. For example, the formation and role of the co-called focal adhesion complexes in A-motility model has to be re-assessed. Currently, it is thought that these complexes form a trans-envelope supra-structure and that on the cytoplasmic side these complexes bind to MreB, a process in which MglA serves as the critical connecting link between the complexes and MreB. As the supra-complexes bind to the substrate on the extracellular side of the cells, the front-back movements of these complexes on MreB polymers has been suggested to generate the propulsive force for A-motility. In the light of the here reported results two aspects of this model have to be reversed. First, no evidence was discovered supporting the proposed direct binding of MglA to MreB. In fact, ample support was found suggesting that MglA binds to BacM instead, an observation that is in line with the established interaction of other myxobacterial bactofilins (BacO and P) and small Ras-GTPases (SofG; Bulyha et al., 2013). As a BacM deletion has no influence on A-motility the binding of MglA to BacM appears to not play a direct role in the generation of propulsive force. In contrast, it appears that this binding may provide a platform for MglA attachment and that this in turn may initiate the assembly of the components of the supra-structure trans-envelope complex. Secondly, as described, the suggested primary function of the trans-envelope complexes has been proposed as molecular motors of A-motility. However, some of the newly discovered data call this interpretation in question. Importantly, the lateral MglA clusters described in various publications and in the experiments described in the thesis all appear to result in a significant reduction in gliding, which clearly contradicts their role as motors. So, if not motors, what could the role of the focal adhesion complexes and their interaction with MglA actually be?

Based on the described known role of Sar1, a plausible alternate scenario would be that the outer membrane during its interaction with the substrate sometimes physically attaches to the substrate resulting in the formation of focal adhesions. These structures then function not as motors but rather as brakes. Their occurrence disturbs the cell envelope, which results in the recruitment of MglA to the deformed foci of the membrane at these disturbances. At that location, MglA initiates the assembly of the multi-protein Glt protein machinery (Luciano et al., 2011) that functions to resolve the disturbance and de-tach the outer membrane from the substrate. Importantly, this new assessment makes predictions that can easily be experimentally measured. For example, the number of focal adhesions should correlate with the speed of the cells. Fast moving cells should have less focal adhesions than slower ones. The occurrence of focal adhesion should also correlate with membrane deformation as has been described in **Chapter V 5.3.6 page 149 and 5.3.8 page 153** as large MglA clusters are consistently observed at bends of the cells and at the point of collisions between cells. Importantly, this assessment leaves room that MglA plays other important roles besides of being the organisation centre for the resolution of focal adhesions and the results of this thesis and the literature point to a number of such roles. Polarity determination, cell elongation, and peptidoglycan sculpting are all phenomena that appear to be influenced by MglA. Future research has to show what the molecular mechanism underlying these phenomena are and how MglA orchestrates and regulates them. Most importantly, the presented data show that small Ras GTPases target highly conserved mechanisms such as membrane deformation and that these targets and most likely their underlying mechanisms are conserved from prokaryotes to eukaryotes.

Previous publications showed that the localization of MglA-GTP at the leading cell pole is promoted by the localization of its GAP, MglB at the lagging cell pole (Leonardy et al., 2010; Zhang et al., 2010). Interestingly, MglA and its GEF, the RomR-RomX complex was found to localize in a unipolar or bipolar pattern, with a larger cluster at the lagging pole (Szadkowski et al., 2019). MglB is responsible for the disassembly of the A-motility complex, which occurs after the hydrolysis of MglA-bound GTP (Treuner-Lange et al., 2015a).

Similar to MglB, BacM could theoretically also be involved in the GTP-hydrolysis of MglA based on its similarity with Sar1. GTP-hydrolysis of Sar1 is catalyzed by the binding to the proline-rich domain of Sec31, a domain that shares similarity to the proline-rich C-terminus of BacM (X. Bi et al., 2007) (**Figure 62**). In addition, the MglA-associated phenotypes in a ΔBacM mutant are similar to the phenotypes mentioned in the literature for the ΔMglB mutant (Hartzell, 1997; Keilberg et al., 2012). Based on these observations, a model is proposed, in which BacM's function is to properly localize MglB and/or catalyze GTP-hydrolysis, through the formation of a MglA – MglB – BacM complex (**Figure 63A**).

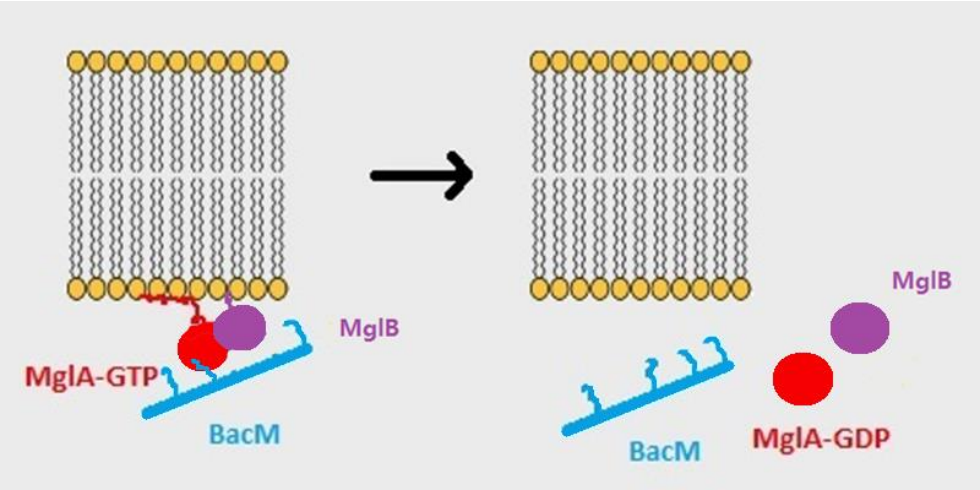

Figure 62. The hydrolysis of MglA-bound GTP is stimulated by the binding of BacM to the MglA – MglB complex.

The loss of BacM in *M. xanthus* cells leads to a crooked cell shape, thereby showing that BacM is essential for the maintenance of the normal cell morphology (Koch et al., 2011). The experiments of this thesis show, that in the absence of BacM, over-expressed MglA localized to both cell poles or formed additional lateral clusters. These clusters seemed to be associated with cell envelope deformations such as bends, indicating that MglA, like Sar1, localizes and binds specifically to areas of membranes that are curved (Patryn et al., 2010; Hanna et al., 2016). Importantly, the clustering of MglA along the cell wall in these cells was found to correlate with a reduced gliding speed, suggesting that the clusters instead of driving A-motility may function as attachment sites that slow the cells down.

MglA is known to be essential for the formation of the Agl-Glt (focal adhesion) complexes (Y. Zhang et al., 2010). The Agl proteins, which are part of the focal adhesion complexes, are known to be involved in the transport of glycan strands across the cell envelope of sporulating cells (Wartel et al., 2013). It is therefore possible, that one of the functions of the focal adhesion complexes is to transport certain proteins or polysaccharides across the cell envelope that are involved in cell attachment explaining why MglA cluster formation leads to a reduced gliding speed (**Figure 63B**).

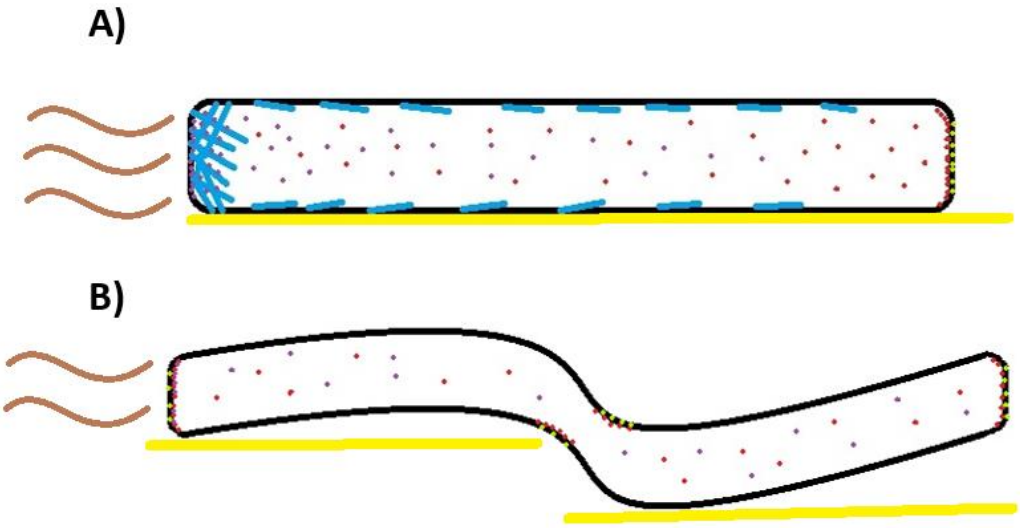

Figure 63. Hypothetical model for the localization of MglA, MglB, BacM and focal adhesion complexes in WT and ΔBacM M. xanthus cells. ***(A)*** *BacM together with MglB are involved in preventing localization of MglA at the backpole of the cell, thereby, leading to reduced cell adhesion at the lagging pole.* ***(B)*** *ΔBacM cells expressing MglA have bipolar and lateral MglA clusters leading to a reduced gliding speed; MglA also forms clusters at bends in the cell. (blue) BacM filaments, (red) MglA, (purple) MglB, (brown) slime, (green) focal adhesion complex (yellow) underlying substrate.*

Whether and how MglA binds to curved membranes remains to be determined. One possibility is that MglA like Sar1 tethers itself to the membrane *via* its amphiphatic α-helix (α5-helix). Another possibility is that the N-terminal serine of MglA is posttranslational modified i.e. prenylated and that this lipid anchors the protein to the membrane (**Figure 64**). Future research will elucidate the nature of the post-translational modification of MglA and how this modification relates to the proteins ability to attach to membranes.

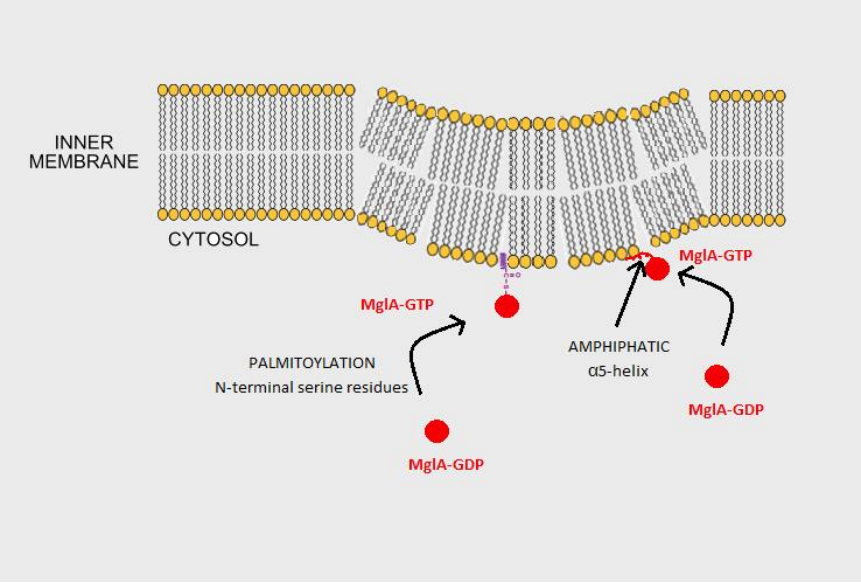

Figure 64. MglA tethering itself to a curved membrane either via its amphiphatic α5-helix or by a palmitoylated N-terminal serine residue.

7. References

Amaral, L., Martins, A., Spengler, G., & Molnar, J. (2014). Efflux pumps of Gram-negative bacteria: What they do, how they do it, with what and how to deal with them. In *Frontiers in Pharmacology: Vol. 4 JAN*. https://doi.org/10.3389/fphar.2013.00168

Anand, B., Verma, S. K., & Prakash, B. (2006). Structural stabilization of GTP-binding domains in circularly permuted GTPases: Implications for RNA binding. *Nucleic Acids Research*, *34*(8), 2196–2205. https://doi.org/10.1093/nar/gkl178

Anraku, Y. (1988). Bacterial Electron Transport Chains. *Annual Review of Biochemistry*, *57*(1), 101–132. https://doi.org/10.1146/annurev.biochem.57.1.101

Antonny, B., Bigay, J., Casella, J.-F., Drin, G., Mesmin, B., & Gounon, P. (2005). Membrane curvature and the control of GTP hydrolysis in Arf1 during COPI vesicle formation. *Biochemical Society Transactions*, *33*(4), 619–622. https://doi.org/10.1042/bst0330619

Antonny, Bruno, Beraud-Dufour, S., Chardin, P., & Chabre, M. (1997). N-terminal hydrophobic residues of the G-protein ADP-ribosylation factor-1 insert into membrane phospholipids upon GDP to GTP exchange. *Biochemistry*, *36*(15), 4675–4684. https://doi.org/10.1021/bi962252b

Antonny, Bruno, Madden, D., Hamamoto, S., Orci, L., & Schekman, R. (2001). Dynamics of the COPII coat with GTP and stable analogues. *Nature Cell Biology*, *3*(6), 531–537. https://doi.org/10.1038/35078500

Argos, P. (1990). An investigation of oligopeptides linking domains in protein tertiary structures and possible candidates for general gene fusion. *Journal of Molecular Biology*, *211*(4), 943–958. https://doi.org/10.1016/0022-2836(90)90085-Z

Arias Del Angel, J. A., Escalante, A. E., Martínez-Castilla, L. P., & Benítez, M. (2018). Cell-fate determination in Myxococcus xanthus development: Network dynamics and novel predictions. *Development Growth and Differentiation*, *60*(2), 121–129. https://doi.org/10.1111/dgd.12424

Ausmees, N., Kuhn, J. R., & Jacobs-Wagner, C. (2003). The bacterial cytoskeleton: an intermediate filament-like function in cell shape. *Cell*, *115*(6), 705–713. http://www.ncbi.nlm.nih.gov/pubmed/14675535

Balagam, R., Litwin, D. B., Czerwinski, F., Sun, M., Kaplan, H. B., Shaevitz, J. W., & Igoshin, O. A. (2014). Myxococcus xanthus Gliding Motors Are Elastically Coupled to the Substrate as Predicted by the Focal Adhesion Model of Gliding Motility. *PLoS Computational Biology*, *10*(5). https://doi.org/10.1371/journal.pcbi.1003619

Banerji, S., & Flieger, A. (2004). Patatin-like proteins: A new family of lipolytic enzymes present in bacteria? In *Microbiology* (Vol. 150, Issue 3, pp. 522–525). https://doi.org/10.1099/mic.0.26957-0

Barlowe, C., Orci, L., Yeung, T., Hosobuchi, M., Hamamoto, S., Salama, N., Rexach, M. F., Ravazzola, M., Amherdt, M., & Schekman, R. (1994). COPII: A membrane coat formed by Sec proteins that drive vesicle budding from the endoplasmic reticulum. *Cell*, *77*(6), 895–907. https://doi.org/10.1016/0092-8674(94)90138-4

Bartels, D. J., Mitchell, D. A., Dong, X., & Deschenes, R. J. (1999). Erf2, a Novel Gene Product That Affects the Localization and Palmitoylation of Ras2 in Saccharomyces cerevisiae . *Molecular and Cellular Biology*, *19*(10), 6775–6787. https://doi.org/10.1128/mcb.19.10.6775

Baxter, J. C., & Funnell, B. E. (2014). Plasmid Partition Mechanisms. *Microbiology Spectrum*, *2*(6).

https://doi.org/10.1128/microbiolspec.plas-0023-2014

Beck, R., Sun, Z., Adolf, F., Rutz, C., Bassler, J., Wild, K., Sinning, I., Hurt, E., Brügger, B., Béthune, J., & Wieland, F. (2008). Membrane curvature induced by Arf1-GTP is essential for vesicle formation. *Proceedings of the National Academy of Sciences of the United States of America*, *105*(33), 11731–11736. https://doi.org/10.1073/pnas.0805182105

Bhat, S., Zhu, X., Patel, R. P., Orlando, R., & Shimkets, L. J. (2011). Identification and localization of Myxococcus xanthus porins and lipoproteins. *PLoS ONE*, *6*(11). https://doi.org/10.1371/journal.pone.0027475

Bhattacharya, N., O'Donnell, J., & Stagg, S. M. (2012). The structure of the Sec13/31 COPII cage bound to Sec23. *Journal of Molecular Biology*, *420*(4–5), 324–334. https://doi.org/10.1016/j.jmb.2012.04.024

Bi, E. F., & Lutkenhaus, J. (1991). FtsZ ring structure associated with division in Escherichia coli. *Nature*, *354*(6349), 161–164. https://doi.org/10.1038/354161a0

Bi, X., Corpina, R. A., & Goldberg, J. (2002). Structure of the Sec23/24-Sar1 pre-budding complex of the COPII vesicle coat. *Nature*, *419*(6904), 271–277. https://doi.org/10.1038/nature01040

Bi, X., Mancias, J. D., & Goldberg, J. (2007). Insights into COPII Coat Nucleation from the Structure of Sec23•Sar1 Complexed with the Active Fragment of Sec31. *Developmental Cell*, *13*(5), 635–645. https://doi.org/10.1016/j.devcel.2007.10.006

Bielli, A., Haney, C. J., Gabreski, G., Watkins, S. C., Bannykh, S. I., & Aridor, M. (2005). Regulation of Sar1 NH 2 terminus by GTP binding and hydrolysis promotes membrane deformation to control COPII vesicle fission. *Journal of Cell Biology*, *171*(6), 919–924. https://doi.org/10.1083/jcb.200509095

Bijlmakers, M. J., & Marsh, M. (2003). The on-off story of protein palmitoylation. In *Trends in Cell Biology* (Vol. 13, Issue 1, pp. 32–42). https://doi.org/10.1016/S0962-8924(02)00008-9

Blackhart, B. D., & Zusman, D. R. (1985). "Frizzy" genes of Myxococcus xanthus are involved in control of frequency of reversal of gliding motility. *Proceedings of the National Academy of Sciences*, *82*(24), 8767–8770. https://doi.org/10.1073/pnas.82.24.8767

Blair, K. M., Mears, K. S., Taylor, J. A., Fero, J., Jones, L. A., Gafken, P. R., Whitney, J. C., & Salama, N. R. (2018). The Helicobacter pylori cell shape promoting protein Csd5 interacts with the cell wall, MurF, and the bacterial cytoskeleton. *Molecular Microbiology*, *110*(1), 114–127. https://doi.org/10.1111/mmi.14087

Bland, N. D., Pinney, J. W., Thomas, J. E., Turner, A. J., & Isaac, R. E. (2008). Bioinformatic analysis of the neprilysin (M13) family of peptidases reveals complex evolutionary and functional relationships. *BMC Evolutionary Biology*, *8*(1). https://doi.org/10.1186/1471-2148-8-16

Booth, I. R., Edwards, M. D., Black, S., Schumann, U., & Miller, S. (2007). Mechanosensitive channels in bacteria: Signs of closure? In *Nature Reviews Microbiology* (Vol. 5, Issue 6, pp. 431–440). https://doi.org/10.1038/nrmicro1659

Bork, P., Sander, C., & Valencia, a. (1992). An ATPase domain common to prokaryotic cell cycle proteins, sugar kinases, actin, and hsp70 heat shock proteins. *Proceedings of the National Academy of Sciences of the United States of America*, *89*(16), 7290–7294. https://doi.org/10.1073/pnas.89.16.7290

Bos, J. L., Rehmann, H., & Wittinghofer, A. (2007). GEFs and GAPs: Critical Elements in the Control of Small G Proteins. *Cell*, *129*(5), 865–877. https://doi.org/10.1016/j.cell.2007.05.018

Bos, J., Rehmann, H., & Wittinghofer, A. (2007). GEFs and GAPs : Critical Elements in the Control of Small G Proteins. *Cell*, 865–877. https://doi.org/10.1016/j.cell.200

Boussadia, O., Amiot, F., Cases, S., Triqueneaux, G., Jacquemin-Sablon, H., & Dautry, F. (1997). Transcription of unr (upstream of N-ras) down-modulates N-ras expression in vivo. *FEBS Letters*, *420*(1), 20–24. https://doi.org/10.1016/S0014-5793(97)01479-8

Boyartchuk, V. L., Ashby, M. N., & Rine, J. (1997). Modulation of ras and a-factor function by carboxyl-terminal proteolysis. *Science*, *275*(5307), 1796–1800. https://doi.org/10.1126/science.275.5307.1796

Bradbeer, C. (1993). The proton motive force drives the outer membrane transport of cobalamin in Escherichia coli. *Journal of Bacteriology*, *175*(10), 3146–3150. https://doi.org/10.1128/jb.175.10.3146-3150.1993

Briegel, A., Dias, D. P., Li, Z., Jensen, R. B., Frangakis, A. S., & Jensen, G. J. (2006). Multiple large filament bundles observed in Caulobacter crescentus by electron cryotomography. *Molecular Microbiology*, *62*(1), 5–14. https://doi.org/10.1111/j.1365-2958.2006.05355.x

Brunsveld, L., Waldmann, H., & Huster, D. (2009). Membrane binding of lipidated Ras peptides and proteins - The structural point of view. In *Biochimica et Biophysica Acta - Biomembranes* (Vol. 1788, Issue 1, pp. 273–288). https://doi.org/10.1016/j.bbamem.2008.08.006

Bullock, H. A., Shen, H., Boynton, T. O., & Shimkets, L. J. (2018). Fatty acid oxidation is required for Myxococcus xanthus development. *Journal of Bacteriology*, *200*(10). https://doi.org/10.1128/JB.00572-17

Bulyha, I., Lindow, S., Lin, L., Bolte, K., Wuichet, K., Kahnt, J., van der Does, C., Thanbichler, M., & Søgaard-Andersen, L. (2013). Two Small GTPases Act in Concert with the Bactofilin Cytoskeleton to Regulate Dynamic Bacterial Cell Polarity. *Developmental Cell*, *25*(2), 119–131. https://doi.org/10.1016/j.devcel.2013.02.017

Burchard, R. P. (1982). Trail following by gliding bacteria. *Journal of Bacteriology*, *152*(1), 495–501.

Buss, J., Coltharp, C., Huang, T., Pohlmeyer, C., Wang, S. C., Hatem, C., & Xiao, J. (2013). In vivo organization of the FtsZ-ring by ZapA and ZapB revealed by quantitative super-resolution microscopy. *Molecular Microbiology*, *89*(6), 1099–1120. https://doi.org/10.1111/mmi.12331

Bustamante, V. H., Martínez-Flores, I., Vlamakis, H. C., & Zusman, D. R. (2004). Analysis of the Frz signal transduction system of Myxococcus xanthus shows the importance of the conserved C-terminal region of the cytoplasmic chemoreceptor FrzCD in sensing signals. *Molecular Microbiology*, *53*, 1501–1513. https://doi.org/10.1111/j.1365-2958.2004.04221.x

Bustelo, X. R., Sauzeau, V., & Berenjeno, I. M. (2007). GTP-binding proteins of the Rho/Rac family: Regulation, effectors and functions in vivo. In *BioEssays* (Vol. 29, Issue 4, pp. 356–370). https://doi.org/10.1002/bies.20558

Cabeen, M. T., & Jacobs-Wagner, C. (2010). The Bacterial Cytoskeleton. *Http://Dx.Doi.Org/10.1146/Annurev-Genet-102108-134845*.

Cabr??, E. J., S??nchez-Gorostiaga, A., Carrara, P., Ropero, N., Casanova, M., Palacios, P., Stano, P., Jim??nez, M., Rivas, G., & Vicente, M. (2013). Bacterial division proteins FtsZ and ZipA induce vesicle shrinkage and cell membrane invagination. *Journal of Biological Chemistry*, *288*(37), 26625–26634. https://doi.org/10.1074/jbc.M113.491688

Carlier, M. F. (1992). Nucleotide hydrolysis regulates the dynamics of actin filaments and microtubules. In *Philosophical transactions of the Royal Society of London. Series B, Biological*

sciences (Vol. 336, Issue 1276, pp. 93–97). https://doi.org/10.1098/rstb.1992.0048

Carlos Amor, J., Harrison, D. H., Kahn, R. A., & Ringe, D. (1994). Structure of the human ADP-ribosylation factor 1 complexed with GDP. *Nature*, *372*(6507), 704–708. https://doi.org/10.1038/372704a0

Cascales, E., Buchanan, S. K., Duche, D., Kleanthous, C., Lloubes, R., Postle, K., Riley, M., Slatin, S., & Cavard, D. (2007). Colicin Biology. *Microbiology and Molecular Biology Reviews*, *71*(1), 158–229. https://doi.org/10.1128/MMBR.00036-06

Chang, Y. W., Rettberg, L. A., Treuner-Lange, A., Iwasa, J., Søgaard-Andersen, L., & Jensen, G. J. (2016). Architecture of the type IVa pilus machine. *Science*, *351*(6278). https://doi.org/10.1126/science.aad2001

Charbon, G., Cabeen, M. T., & Jacobs-Wagner, C. (2009). Bacterial intermediate filaments: In vivo assembly, organization, and dynamics of crescentin. *Genes and Development*, *23*(9), 1131–1144. https://doi.org/10.1101/gad.1795509

Chavrier, P., & Goud, B. (1999). The role of ARF and Rab GTPases in membrane transport. *Current Opinion in Cell Biology*, *11*(4), 466–475. https://doi.org/10.1016/S0955-0674(99)80067-2

Chen, Y., Bjornson, K., Redick, S. D., & Erickson, H. P. (2004). A rapid fluorescence assay for FtsZ assembly indicates cooperative assembly with a dimer nucleus. *Biophysical Journal*, *88*(1), 505–514. https://doi.org/10.1529/biophysj.104.044149

Clausen, M., Jakovljevic, V., Søgaard-Andersen, L., & Maier, B. (2009). High-force generation is a conserved property of type IV pilus systems. *Journal of Bacteriology*. https://doi.org/10.1128/JB.00396-09

Cotter, C. R., Schüttler, H. B., Igoshin, O. A., & Shimkets, L. J. (2017). Data-driven modeling reveals cell behaviors controlling self-organization during Myxococcus xanthus development. *Proceedings of the National Academy of Sciences of the United States of America*, *114*(23), E4592–E4601. https://doi.org/10.1073/pnas.1620981114

Coulombe, P. a, & Wong, P. (2004). Cytoplasmic intermediate filaments revealed as dynamic and multipurpose scaffolds. *Nature Cell Biology*, *6*(8), 699–706. https://doi.org/10.1038/ncb0804-699

Curtis, P. D., Atwood, J., Orlando, R., & Shimkets, L. J. (2007). Proteins associated with the Myxococcus xanthus extracellular matrix. *Journal of Bacteriology*, *189*(21), 7634–7642. https://doi.org/10.1128/JB.01007-07

d'Enfert, C., Gensse, M., & Gaillardin, C. (1992). Fission yeast and a plant have functional homologues of the Sar1 and Sec12 proteins involved in ER to Golgi traffic in budding yeast. *The EMBO Journal*, *11*(11), 4205–4211. https://doi.org/10.1002/j.1460-2075.1992.tb05514.x

Daniel, R. A., & Errington, J. (2003). Control of cell morphogenesis in bacteria: Two distinct ways to make a rod-shaped cell. *Cell*, *113*(6), 767–776. https://doi.org/10.1016/S0092-8674(03)00421-5

Das, S., & Lambright, D. G. (2016). Membrane Trafficking: An Endosome Tether Meets a Rab and Collapses. In *Current Biology* (Vol. 26, Issue 20, pp. R927–R929). https://doi.org/10.1016/j.cub.2016.08.056

David, M., Petit, D., & Bertoglio, J. (2012). Cell cycle regulation of Rho signaling pathways. In *Cell Cycle* (Vol. 11, Issue 16, pp. 3003–3010). https://doi.org/10.4161/cc.21088

de Franceschi, N., Hamidi, H., Alanko, J., Sahgal, P., & Ivaska, J. (2015). Integrin traffic-the update. In *Journal of Cell Science* (Vol. 128, Issue 5, pp. 839–852). https://doi.org/10.1242/jcs.161653

Dempwolff, F., Reimold, C., Reth, M., & Graumann, P. L. (2011). Bacillus subtilis MreB orthologs self-organize into filamentous structures underneath the cell membrane in a heterologous cell system. *PLoS ONE*, *6*(11). https://doi.org/10.1371/journal.pone.0027035

Deng, X., Gonzalez Llamazares, A., Wagstaff, J., Hale, V. L., Cannone, G., McLaughlin, S. H., Kureisaite-Ciziene, D., & Löwe, J. (2019). Bactofilins form non-polar filaments that bind to membranes directly. *BioRxiv*, 617639. https://doi.org/10.1101/617639

Denham, E. L., Ward, P. N., & Leigh, J. A. (2008). Lipoprotein signal peptides are processed by Lsp and Eep of Streptococcus uberis. *Journal of Bacteriology*, *190*(13), 4641–4647. https://doi.org/10.1128/JB.00287-08

Deretic, V., Saitoh, T., & Akira, S. (2013). Autophagy in infection, inflammation and immunity. In *Nature Reviews Immunology* (Vol. 13, Issue 10, pp. 722–737). https://doi.org/10.1038/nri3532

Dermardirossian, C., Schnelzer, A., & Bokoch, G. M. (2004). Phosphorylation of RhoGDI by Pak1 mediates dissociation of Rac GTPase. *Molecular Cell*, *15*(1), 117–127. https://doi.org/10.1016/j.molcel.2004.05.019

Dewachter, L., Verstraeten, N., Jennes, M., Verbeelen, T., Biboy, J., Monteyne, D., Pérez-Morga, D., Verstrepen, K. J., Vollmer, W., Fauvart, M., & Michiels, J. (2017). A mutant isoform of ObgE causes cell death by interfering with cell division. *Frontiers in Microbiology*, *8*(JUN). https://doi.org/10.3389/fmicb.2017.01193

Dey, A., Vassallo, C. N., Conklin, A. C., Pathak, D. T., Troselj, V., & Wall, D. (2016). Sibling rivalry in Myxococcus xanthus is mediated by kin recognition and a polyploid prophage. *Journal of Bacteriology*, *198*(6), 994–1004. https://doi.org/10.1128/JB.00964-15

Diekmann, Y., Seixas, E., Gouw, M., Tavares-Cadete, F., Seabra, M. C., & Pereira-Leal, J. B. (2011). Thousands of Rab GTPases for the cell biologist. *PLoS Computational Biology*, *7*(10). https://doi.org/10.1371/journal.pcbi.1002217

Dixon, A. S., Schwinn, M. K., Hall, M. P., Zimmerman, K., Otto, P., Lubben, T. H., Butler, B. L., Binkowski, B. F., MacHleidt, T., Kirkland, T. A., Wood, M. G., Eggers, C. T., Encell, L. P., & Wood, K. V. (2016). NanoLuc Complementation Reporter Optimized for Accurate Measurement of Protein Interactions in Cells. *ACS Chemical Biology*, *11*(2), 400–408. https://doi.org/10.1021/acschembio.5b00753

Dominguez-Escobar, J., Chastanet, A., Crevenna, A. H., Fromion, V., Wedlich-Soldner, R., & Carballido-Lopez, R. (2011). Processive Movement of MreB-Associated Cell Wall Biosynthetic Complexes in Bacteria. *Science*, *333*(July), 225–228. https://doi.org/10.1126/science.1203466

Dominguez, R., & Holmes, K. C. (2011). Actin structure and function. *Annual Review of Biophysics*, *40*(April), 169–186. https://doi.org/10.1146/annurev-biophys-042910-155359

Donaldson, J. G., & Jackson, C. L. (2011). ARF family G proteins and their regulators: Roles in membrane transport, development and disease. In *Nature Reviews Molecular Cell Biology* (Vol. 12, Issue 6, pp. 362–375). https://doi.org/10.1038/nrm3117

Drin, G., & Antonny, B. (2010). Amphipathic helices and membrane curvature. In *FEBS Letters* (Vol. 584, Issue 9, pp. 1840–1847). https://doi.org/10.1016/j.febslet.2009.10.022

El Andari, J., Altegoer, F., Bange, G., & Graumann, P. L. (2015). Bacillus subtilis bactofilins are essential for flagellar hook- and filament assembly and dynamically localize into structures of less than 100 nm diameter underneath the cell membrane. *PLoS ONE*, *10*(10). https://doi.org/10.1371/journal.pone.0141546

Erickson, H. P., Anderson, D. E., & Osawa, M. (2010). FtsZ in Bacterial Cytokinesis: Cytoskeleton and Force Generator All in One. *Microbiology and Molecular Biology Reviews*, *74*(4), 504–528. https://doi.org/10.1128/mmbr.00021-10

Erickson, Harold P. (1997). FtsZ, a tubulin homologue in prokaryote cell division. In *Trends in Cell Biology* (Vol. 7, Issue 9, pp. 362–367). https://doi.org/10.1016/S0962-8924(97)01108-2

Errington, J. (2015). Bacterial morphogenesis and the enigmatic MreB helix. *Nat Rev Micro*, *13*(4), 241–248. https://doi.org/10.1038/nrmicro3398

Esue, O., Rupprecht, L., Sun, S. X., & Wirtz, D. (2010). Dynamics of the bacterial intermediate filament crescentin in vitro and in vivo. *PloS One*, *5*(1), e8855. https://doi.org/10.1371/journal.pone.0008855

Etienne-Manneville, S., & Hall, A. (2002). Rho GTPases in cell biology. In *Nature* (Vol. 420, Issue 6916, pp. 629–635). https://doi.org/10.1038/nature01148

Fallis, A. . (2013). 済無No Title No Title. *Journal of Chemical Information and Modeling*, *53*(9), 1689–1699. https://doi.org/10.1017/CBO9781107415324.004

Faure, L. M., Fiche, J. B., Espinosa, L., Ducret, A., Anantharaman, V., Luciano, J., Lhospice, S., Islam, S. T., Tréguier, J., Sotes, M., Kuru, E., Van Nieuwenhze, M. S., Brun, Y. V., Théodoly, O., Aravind, L., Nollmann, M., & Mignot, T. (2016). The mechanism of force transmission at bacterial focal adhesion complexes. *Nature*, *539*(7630), 530–535. https://doi.org/10.1038/nature20121

Favini-Stabile, S., Contreras-Martel, C., Thielens, N., & Dessen, A. (2013). MreB and MurG as scaffolds for the cytoplasmic steps of peptidoglycan biosynthesis. *Environmental Microbiology*, *15*(12), 3218–3228. https://doi.org/10.1111/1462-2920.12171

Feniouk, B. A., Suzuki, T., & Yoshida, M. (2007). Regulatory interplay between proton motive force, ADP, phosphate, and subunit ε in bacterial ATP synthase. *Journal of Biological Chemistry*, *282*(1), 764–772. https://doi.org/10.1074/jbc.M606321200

Fenton, A. K., & Gerdes, K. (2013). Direct interaction of FtsZ and MreB is required for septum synthesis and cell division in Escherichia coli. *The EMBO Journal*, *32*(13), 1953–1965. https://doi.org/10.1038/emboj.2013.129

Filippi, M. D., Harris, C. E., Meller, J., Gu, Y., Zheng, Y., & Williams, D. A. (2004). Localization of Rac2 via the C terminus and aspartic acid 150 specifies superoxide generation, actin polarity and chemotaxis in neutrophils. *Nature Immunology*, *5*(7), 744–751. https://doi.org/10.1038/ni1081

Fletcher, D. A., & Mullins, R. D. (2010). Cell mechanics and the cytoskeleton. *Nature*, *463*(7280), 485–492. https://doi.org/10.1038/nature08908

Fontes, M., & Kaiser, D. (1999). Myxococcus cells respond to elastic forces in their substrate. *Proceedings of the National Academy of Sciences*, *96*(14), 8052–8057. https://doi.org/10.1073/pnas.96.14.8052

Forget, M. A., Desrosiers, R. R., Gingras, D., & Béliveau, R. (2002). Phosphorylation states of Cdc42 and RhoA regulate their interactions with Rho GDP dissociation inhibitor and their extraction from biological membranes. *Biochemical Journal*, *361*(2), 243–254. https://doi.org/10.1042/0264-6021:3610243

Fortwendel, J. R., Juvvadi, P. R., Pinchai, N., Perfect, B. Z., Alspaugh, J. A., Perfect, J. R., & Steinbach, W. J. (2009). Differential effects of inhibiting chitin and 1,3-β-D-glucan synthesis in Ras and calcineurin mutants of Aspergillus fumigatus. *Antimicrobial Agents and Chemotherapy*, *53*(2), 476–482. https://doi.org/10.1128/AAC.01154-08

Fremgen, S. A., Burke, N. S., & Hartzell, P. L. (2010). Effects of site-directed mutagenesis of mglA on motility and swarming of Myxococcus xanthus. *BMC Microbiology*, *10*. https://doi.org/10.1186/1471-2180-10-295

Fremgen, S., Williams, A., Furusawa, G., Dziewanowska, K., Settles, M., & Hartzell, P. (2013). MasABK Proteins Interact with Proteins of the Type IV Pilin System to Affect Social Motility of Myxococcus xanthus. *PLoS ONE*, *8*(1). https://doi.org/10.1371/journal.pone.0054557

Fu, G., Bandaria, J. N., Le Gall, A. V., Fan, X., Yildiz, A., Mignot, T., Zusman, D. R., & Nan, B. (2018). MotAB-like machinery drives the movement of MreB filaments during bacterial gliding motility. *Proceedings of the National Academy of Sciences*, 201716441. https://doi.org/10.1073/pnas.1716441115

Galicia, C., Lhospice, S., Varela, P. F., Trapani, S., Zhang, W., Navaza, J., Herrou, J., Mignot, T., & Cherfils, J. (2019). MglA functions as a three-state GTPase to control movement reversals of Myxococcus xanthus. *Nature Communications*. https://doi.org/10.1038/s41467-019-13274-3

GAO, J., & XU, D. (2011). *CORRELATION BETWEEN POSTTRANSLATIONAL MODIFICATION AND INTRINSIC DISORDER IN PROTEIN*. 94–103. https://doi.org/10.1142/9789814366496_0010

Garner, E. C., Bernard, R., Wang, W., Zhuang, X., Rudner, D. Z., & Mitchison, T. (2011a). Coupled, circumferential motions of the cell wall synthesis machinery and MreB filaments in B. subtilis. *Science (New York, N.Y.)*, *333*(6039), 222–225. https://doi.org/10.1126/science.1203285

Garner, E. C., Bernard, R., Wang, W., Zhuang, X., Rudner, D. Z., & Mitchison, T. (2011b). Coupled, circumferential motions of the cell wall synthesis machinery and MreB filaments in B. subtilis. *Science (New York, N.Y.)*, *333*(6039), 222–225. https://doi.org/10.1126/science.1203285

Gasser, B., Saloheimo, M., Rinas, U., Dragosits, M., Rodríguez-Carmona, E., Baumann, K., Giuliani, M., Parrilli, E., Branduardi, P., Lang, C., Porro, D., Ferrer, P., Tutino, M., Mattanovich, D., & Villaverde, A. (2008). Protein folding and conformational stress in microbial cells producing recombinant proteins: A host comparative overview. In *Microbial Cell Factories* (Vol. 7). https://doi.org/10.1186/1475-2859-7-11

Ghosh, P. M., Ghosh-Choudhury, N., Moyer, M. L., Mott, G. E., Thomas, C. A., Foster, B. A., Greenberg, N. M., & Kreisberg, J. I. (1999). Role of RhoA activation in the growth and morphology of a murine prostate tumor cell line. *Oncogene*, *18*(28), 4120–4130. https://doi.org/10.1038/sj.onc.1202792

Glomset, J. A., & Farnsworth, C. C. (2003). Role of Protein Modification Reactions in Programming Interactions Between Ras-Related GTPases and Cell Membranes. *Annual Review of Cell Biology*, *10*(1), 181–205. https://doi.org/10.1146/annurev.cb.10.110194.001145

Goldman, B. S., Nierman, W. C., Kaiser, D., Slater, S. C., Durkin, A. S., Eisen, J. A., Eisen, J., Ronning, C. M., Barbazuk, W. B., Blanchard, M., Field, C., Halling, C., Hinkle, G., Iartchuk, O., Kim, H. S., Mackenzie, C., Madupu, R., Miller, N., Shvartsbeyn, A., … Kaplan, H. B. (2006). Evolution of sensory complexity recorded in a myxobacterial genome. *Proceedings of the National Academy of Sciences of the United States of America*, *103*(41), 15200–15205. https://doi.org/10.1073/pnas.0607335103

Gómez-Santos, N., Glatter, T., Koebnik, R., Świątek-Połatyńska, M. A., & Søgaard-Andersen, L. (2019). A TonB-dependent transporter is required for secretion of protease PopC across the bacterial outer membrane. *Nature Communications*, *10*(1). https://doi.org/10.1038/s41467-019-09366-9

Grangeasse, C., Stülke, J., & Mijakovic, I. (2015). Regulatory potential of post-translational modifications in bacteria. *Frontiers in Microbiology*, *6*(MAY).

https://doi.org/10.3389/fmicb.2015.00500

Graumann, P. L. (2004). Cytoskeletal elements in bacteria. In *Current Opinion in Microbiology* (Vol. 7, Issue 6, pp. 565–571). https://doi.org/10.1016/j.mib.2004.10.010

Graumann, P., & Marahiel, M. A. (1996). Some like it cold: Response of microorganisms to cold shock. In *Archives of Microbiology* (Vol. 166, Issue 5, pp. 293–300). https://doi.org/10.1007/s002030050386

Guan, X., & Fierke, C. A. (2011). Understanding protein palmitoylation: Biological significance and enzymology. In *Science China Chemistry* (Vol. 54, Issue 12, pp. 1888–1897). https://doi.org/10.1007/s11426-011-4428-2

Guest, G. M., Lin, X., & Momany, M. (2004). Aspergillus nidulans RhoA is involved in polar growth, branching, and cell wall synthesis. *Fungal Genetics and Biology*, *41*(1), 13–22. https://doi.org/10.1016/j.fgb.2003.08.006

Hale, C. A., & De Boer, P. A. J. (1999). Recruitment of ZipA to the septal ring of Escherichia coli is dependent on FtsZ and independent of FtsA. *Journal of Bacteriology*, *181*(1), 167–176.

Hall, M. P., Unch, J., Binkowski, B. F., Valley, M. P., Butler, B. L., Wood, M. G., Otto, P., Zimmerman, K., Vidugiris, G., MacHleidt, T., Robers, M. B., Benink, H. A., Eggers, C. T., Slater, M. R., Meisenheimer, P. L., Klaubert, D. H., Fan, F., Encell, L. P., & Wood, K. V. (2012). Engineered luciferase reporter from a deep sea shrimp utilizing a novel imidazopyrazinone substrate. *ACS Chemical Biology*, *7*(11), 1848–1857. https://doi.org/10.1021/cb3002478

Hancock, J. F., Magee, A. I., Childs, J. E., & Marshall, C. J. (1989). All ras proteins are polyisoprenylated but only some are palmitoylated. *Cell*, *57*(7), 1167–1177. https://doi.org/10.1016/0092-8674(89)90054-8

Hanna, M. G., Mela, I., Wang, L., Henderson, R. M., Chapman, E. R., Edwardson, J. M., & Audhya, A. (2016). Sar1 GTPase activity is regulated by membrane curvature. *Journal of Biological Chemistry*, *291*(3), 1014–1027. https://doi.org/10.1074/jbc.M115.672287

Hartzell, P., & Kaiser, D. (1991a). Function of MglA, a 22-kilodalton protein essential for gliding in Myxococcus xanthus. *Journal of Bacteriology*, *173*(23), 7615–7624.

Hartzell, P., & Kaiser, D. (1991b). Upstream gene of the mgl operon controls the level of MglA protein in Myxococcus xanthus. *Journal of Bacteriology*, *173*(23), 7625–7635. https://doi.org/10.1128/jb.173.23.7625-7635.1991

Hartzell, P. L. (1997). Complementation of sporulation and motility defects in a prokaryote by a eukaryotic GTPase. *Proceedings of the National Academy of Sciences of the United States of America*, *94*(18), 9881–9886. https://doi.org/10.1073/pnas.94.18.9881

Harvey, C. W., Madukoma, C. S., Mahserejian, S., Alber, M. S., & Shrout, J. D. (2014). Cell division resets polarity and motility for the bacterium Myxococcus xanthus. *Journal of Bacteriology*, *196*(22), 3853–3861. https://doi.org/10.1128/JB.02095-14

Hay, N. A., Tipper, D. J., Gygi, D., & Hughes, C. (1999). A novel membrane protein influencing cell shape and multicellular swarming of Proteus mirabilis. *Journal of Bacteriology*, *181*(7), 2008–2016. http://www.pubmedcentral.nih.gov/articlerender.fcgi?artid=93611&tool=pmcentrez&rendertype=abstract

Hayashi, Y., Li, C. P., Enomoto, H., Ibrahim, H. R., Sugimoto, Y., & Aoki, T. (2008). Improvement of functional properties of ovotransferrin by phosphorylation through dry-heating in the presence

of pyrophosphate. *Asian-Australasian Journal of Animal Sciences*, *21*(4), 596–602. https://doi.org/10.5713/ajas.2008.70501

Heino, J. (2007). The collagen family members as cell adhesion proteins. In *BioEssays* (Vol. 29, Issue 10, pp. 1001–1010). https://doi.org/10.1002/bies.20636

Herrmann, H., & Aebi, U. (2004). Intermediate filaments: molecular structure, assembly mechanism, and integration into functionally distinct intracellular Scaffolds. *Annual Review of Biochemistry*, *73*, 749–789. https://doi.org/10.1146/annurev.biochem.73.011303.073823

Hodgkin, J., & Kaiser, D. (1977). Cell to cell stimulation of movement in nonmotile mutants of Myxococcus. *Proceedings of the National Academy of Sciences of the United States of America*, *74*(7), 2938–2942. https://doi.org/10.1073/pnas.74.7.2938

Hodgkin, Jonathan, & Kaiser, D. (1979). Genetics of gliding motility in Myxococcus xanthus (Myxobacterales): Two gene systems control movement. *Molecular and General Genetics MGG*, *171*(2), 177–191. https://doi.org/10.1007/BF00270004

Holden, S. J., Pengo, T., Meibom, K. L., Fernandez Fernandez, C., Collier, J., & Manley, S. (2014). High throughput 3D super-resolution microscopy reveals Caulobacter crescentus in vivo Z-ring organization. *Proceedings of the National Academy of Sciences*, *111*(12), 4566–4571. https://doi.org/10.1073/pnas.1313368111

Holmes, K. C., Popp, D., Gebhard, W., & Kabsch, W. (1990). Atomic model of the actin filament. In *Nature* (Vol. 347, Issue 6288, pp. 44–49). https://doi.org/10.1038/347044a0

Hope, M. J., Bally, M. B., Webb, G., & Cullis, P. R. (1985). Production of large unilamellar vesicles by a rapid extrusion procedure. Characterization of size distribution, trapped volume and ability to maintain a membrane potential. *BBA - Biomembranes*. https://doi.org/10.1016/0005-2736(85)90521-8

Hosking, E. R., Vogt, C., Bakker, E. P., & Manson, M. D. (2006). The Escherichia coli MotAB Proton Channel Unplugged. *Journal of Molecular Biology*, *364*(5), 921–937. https://doi.org/10.1016/j.jmb.2006.09.035

Hsia, K. C., & Hoelz, A. (2010). Crystal structure of α-COP in complex with ε-COP provides insight into the architecture of the COPI vesicular coat. *Proceedings of the National Academy of Sciences of the United States of America*, *107*(25), 11271–11276. https://doi.org/10.1073/pnas.1006297107

Huecas, S., Llorca, O., Boskovic, J., Martfn-Benito, J., Valpuesta, J. M., & Andreu, J. M. (2008). Energetics and geometry of FtsZ polymers: Nucleated self-assembly of single protofilaments. *Biophysical Journal*, *94*(5), 1796–1806. https://doi.org/10.1529/biophysj.107.115493

Huecas, S., Ramírez-Aportela, E., Vergoñós, A., Núñez-Ramírez, R., Llorca, O., Díaz, J. F., Juan-Rodríguez, D., Oliva, M. A., Castellen, P., & Andreu, J. M. (2017). Self-Organization of FtsZ Polymers in Solution Reveals Spacer Role of the Disordered C-Terminal Tail. *Biophysical Journal*, *113*(8), 1831–1844. https://doi.org/10.1016/j.bpj.2017.08.046

Hunter, T. (1995). Protein kinases and phosphatases: The Yin and Yang of protein phosphorylation and signaling. In *Cell* (Vol. 80, Issue 2, pp. 225–236). https://doi.org/10.1016/0092-8674(95)90405-0

Hutagalung, A. H., & Novick, P. J. (2011). Role of Rab GTPases in membrane traffic and cell physiology. In *Physiological Reviews* (Vol. 91, Issue 1, pp. 119–149). https://doi.org/10.1152/physrev.00059.2009

Hutchings, J., Stancheva, V., Miller, E. A., & Zanetti, G. (2018). Subtomogram averaging of COPII assemblies reveals how coat organization dictates membrane shape. *Nature Communications*, *9*(1). https://doi.org/10.1038/s41467-018-06577-4

Hyman, A. A., Salser, S., Drechsel, D. N., Unwin, N., & Mitchison, T. J. (1992). Role of GTP hydrolysis in microtubule dynamics: information from a slowly hydrolyzable analogue, GMPCPP. *Molecular Biology of the Cell*, *3*(10), 1155–1167. https://doi.org/10.1091/MBC.3.10.1155

Ilić, D., Furuta, Y., Kanazawa, S., Takeda, N., Sobuet, K., Nakatsuji, N., Nomura, S., Fujimoto, J., Fujimoto, J., Yamamoto, T., & Aizawa, S. (1995). Reduced cell motility and enhanced focal adhesion contact formation in cells from FAK-deficient mice. In *Nature* (Vol. 377, Issue 6549, pp. 539–544). https://doi.org/10.1038/377539a0

Imada, K., Shiota, M., Kohashi, K., Kuroiwa, K., Song, Y. H., Sugimoto, M., Naito, S., & Oda, Y. (2013). Mutual regulation between Raf/MEK/ERK signaling and Y-box-binding protein-1 promotes prostate cancer progression. *Clinical Cancer Research*, *19*(17), 4638–4650. https://doi.org/10.1158/1078-0432.CCR-12-3705

Inclán, Y. F., Vlamakis, H. C., & Zusman, D. R. (2007). FrzZ, a dual CheY-like response regulator, functions as an output for the Frz chemosensory pathway of Myxococcus xanthus. *Molecular Microbiology*, *65*(1), 90–102. https://doi.org/10.1111/j.1365-2958.2007.05774.x

Ingerson-Mahar, M., & Gitai, Z. (2012). A growing family: The expanding universe of the bacterial cytoskeleton. In *FEMS Microbiology Reviews* (Vol. 36, Issue 1, pp. 256–267). https://doi.org/10.1111/j.1574-6976.2011.00316.x

Iniesta, A. A., García-Heras, F., Abellón-Ruiz, J., Gallego-García, A., & Elías-Arnanz, M. (2012). Two systems for conditional gene expression in Myxococcus xanthus inducible by isopropyl-β-d-thiogalactopyranoside or vanillate. *Journal of Bacteriology*, *194*(21), 5875–5885. https://doi.org/10.1128/JB.01110-12

Iwatsuki, H., & Suda, M. (2010). Seven kinds of intermediate filament networks in the cytoplasm of polarized cells: structure and function. *Acta Histochemica et Cytochemica*, *43*(2), 19–31. https://doi.org/10.1267/ahc.10009

Izaurralde, E., Kutay, U., Von Kobbe, C., Mattaj, L. W., & Görlich, D. (1997). The asymmetric distribution of the constituents of the Ran system is essential for transport into and out of the nucleus. *EMBO Journal*, *16*(21), 6535–6547. https://doi.org/10.1093/emboj/16.21.6535

Jackson, K. M., Schwartz, C., Wachter, J., Rosa, P. A., & Stewart, P. E. (2018). A widely conserved bacterial cytoskeletal component influences unique helical shape and motility of the spirochete Leptospira biflexa. *Molecular Microbiology*, *108*(1), 77–89. https://doi.org/10.1111/mmi.13917

Jakovljevic, V., Leonardy, S., Hoppert, M., & Søgaard-Andersen, L. (2008). PilB and PilT are ATPases acting antagonistically in type IV pilus function in Myxococcus xanthus. *Journal of Bacteriology*, *190*(7), 2411–2421. https://doi.org/10.1128/JB.01793-07

Jeffers, M., Paciucci, R., & Pellicer, A. (1990). Characterization of unr; a gene closely linked to N-ras. *Nucleic Acids Research*, *18*(16), 4891–4899.

Jenkins, C., Samudrala, R., Anderson, I., Hedlund, B. P., Petroni, G., Michailova, N., Pinel, N., Overbeek, R., Rosati, G., & Staley, J. T. (2002). Genes for the cytoskeletal protein tubulin in the bacterial genus Prosthecobacter. *Proc Natl Acad Sci U S A*, *99*(26), 17049–17054. https://doi.org/10.1073/pnas.012516899

Jiang, S. Y., & Ramachandran, S. (2006). Comparative and evolutionary analysis of genes encoding small GTPases and their activating proteins in eukaryotic genomes. *Physiological Genomics*,

24(3), 235–251. https://doi.org/10.1152/physiolgenomics.00210.2005

Jim??nez, M., Martos, A., Vicente, M., & Rivas, G. (2011). Reconstitution and organization of Escherichia coli proto-ring elements (FtsZ and FtsA) inside giant unilamellar vesicles obtained from bacterial inner membranes. *Journal of Biological Chemistry*, *286*(13), 11236–11241. https://doi.org/10.1074/jbc.M110.194365

Jones, L. J. F., Carballido-López, R., & Errington, J. (2001). Control of Cell Shape in Bacteria. *Cell*, *104*(6), 913–922. https://doi.org/10.1016/S0092-8674(01)00287-2

Jones, P. G., Krah, R., Tafuri, S. R., & Wolffe, A. P. (1992). DNA gyrase, CS7.4, and the cold shock response in Escherichia coli. *Journal of Bacteriology*, *174*(18), 5798–5802. https://doi.org/10.1128/jb.174.18.5798-5802.1992

Ka, F. L., Baron, R., Ali, B. R., Magee, A. I., & Seabra, M. C. (2007). Rab GTPases containing a CAAX motif are processed post-geranylgeranylation by proteolysis and methylation. *Journal of Biological Chemistry*, *282*(2), 1487–1497. https://doi.org/10.1074/jbc.M605557200

Kahn, R. A., Goddard, C., & Newkirk, M. (1988). Chemical and immunological characterization of the 21-kDa ADP-ribosylation factor of adenylate cyclase. *Journal of Biological Chemistry*, *263*(17), 8282–8287.

Kaimer, C., & Zusman, D. R. (2016). Regulation of cell reversal frequency in Myxococcus xanthus requires the balanced activity of CheY-like domains in FrzE and FrzZ. *Molecular Microbiology*, *100*(2), 379–395. https://doi.org/10.1111/mmi.13323

Kaiser, D. (1979). Social gliding is correlated with the presence of pili in Myxococcus xanthus. *Proceedings of the National Academy of Sciences*, *76*(11), 5952–5956. https://doi.org/10.1073/pnas.76.11.5952

Kaiser, D, Manoil, C., & Dworkin, M. (1979). Myxobacteria: Cell Interactions, Genetics, and Development. *Annual Review of Microbiology*, *33*(1), 595–639. https://doi.org/10.1146/annurev.mi.33.100179.003115

Kaiser, Dale, & Crosby, C. (1983). Cell movement and its coordination in swarms of myxococcus xanthus. *Cell Motility*. https://doi.org/10.1002/cm.970030304

Karl, D. M. (1978). Determination of GTP, GDP, and GMP in Cell and Tissue Extracts. *Methods in Enzymology*, *57*(C), 85–94. https://doi.org/10.1016/0076-6879(78)57011-0

Kataoka, T., Powers, S., Cameron, S., Fasano, O., Goldfarb, M., Broach, J., & Wigler, M. (1985). Functional homology of mammalian and yeast RAS genes. *Cell*, *40*(1), 19–26. https://doi.org/10.1016/0092-8674(85)90304-6

Keilberg, D., Wuichet, K., Drescher, F., & Søgaard-Andersen, L. (2012). A Response Regulator Interfaces between the Frz Chemosensory System and the MglA/MglB GTPase/GAP Module to Regulate Polarity in Myxococcus xanthus. *PLoS Genetics*, *8*(9). https://doi.org/10.1371/journal.pgen.1002951

Keskin, O., Gursoy, A., Ma, B., & Nussinov, R. (2008). Principles of protein-protein interactions: What are the preferred ways for proteins to interact? In *Chemical Reviews* (Vol. 108, Issue 4, pp. 1225–1244). https://doi.org/10.1021/cr040409x

Ki, L., & Ying, H. (2009). RanGTPase: A key regulator of nucleocytoplasmic trafficking. In *Molecular and Cellular Pharmacology* (Vol. 1, Issue 3, pp. 148–156). https://doi.org/10.4255/mcpharmacol.09.19

Kim, D. H., & Wirtz, D. (2013). Focal adhesion size uniquely predicts cell migration. *FASEB Journal*,

27(4), 1351–1361. https://doi.org/10.1096/fj.12-220160

Kjeldgaard, M., Nyborg, J., & Clark, B. F. C. (1996). The GTP binding motif: Variations on a theme. In *FASEB Journal* (Vol. 10, Issue 12, pp. 1347–1368).

Klinkert, K., Rocancourt, M., Houdusse, A., & Echard, A. (2016). Rab35 GTPase couples cell division with initiation of epithelial apico-basal polarity and lumen opening. *Nature Communications*, *7*. https://doi.org/10.1038/ncomms11166

Koch, M. K., Mchugh, C. a., & Hoiczyk, E. (2011). BacM, an N-terminally processed bactofilin of Myxococcus xanthus, is crucial for proper cell shape. *Molecular Microbiology*, *80*(4), 1031–1051. https://doi.org/10.1111/j.1365-2958.2011.07629.x

Kowarik, M., Young, N. M., Numao, S., Schulz, B. L., Hug, I., Callewaert, N., Mills, D. C., Watson, D. C., Hernandez, M., Kelly, J. F., Wacker, M., & Aebi, M. (2006). Definition of the bacterial N-glycosylation site consensus sequence. *EMBO Journal*, *25*(9), 1957–1966. https://doi.org/10.1038/sj.emboj.7601087

Kruse, T., Bork-Jensen, J., & Gerdes, K. (2005). The morphogenetic MreBCD proteins of Escherichia coli form an essential membrane-bound complex. *Molecular Microbiology*, *55*(1), 78–89. https://doi.org/10.1111/j.1365-2958.2004.04367.x

Kühn, J., Briegel, A., Mörschel, E., Kahnt, J., Leser, K., Wick, S., Jensen, G. J., & Thanbichler, M. (2010). Bactofilins, a ubiquitous class of cytoskeletal proteins mediating polar localization of a cell wall synthase in Caulobacter crescentus. *The EMBO Journal*, *29*(2), 327–339. https://doi.org/10.1038/emboj.2009.358

LaBreck, C. J., Conti, J., Viola, M. G., & Camberg, J. L. (2019). MinC N- and C-Domain interactions modulate ftsz assembly, division site selection, and minD-dependent oscillation in Escherichia coli. *Journal of Bacteriology*, *201*(4). https://doi.org/10.1128/JB.00374-18

Lancero, H., Brofft, J. E., Downard, J., Birren, B. W., Nusbaum, C., Naylor, J., Shi, W., & Shimkets, L. J. (2002). Mapping of Myxococcus xanthus social motility dsp mutations to the dif genes. *Journal of Bacteriology*. https://doi.org/10.1128/JB.184.5.1462-1465.2002

Lancero, H. L., Castaneda, S., Caberoy, N. B., Ma, X., Garza, A. G., & Shi, W. (2005). Analysing protein - Protein interactions of the Myxococcus xanthus Dif signalling pathway using the yeast two-hybird system. *Microbiology*, *151*(5), 1535–1541. https://doi.org/10.1099/mic.0.27743-0

Lang, P., Gesbert, F., Delespine-Carmagnat, M., Stancou, R., Pouchelet, M., & Bertoglio, J. (1996). Protein kinase A phosphorylation of RhoA mediates the morphological and functional effects of cyclic AMP in cytotoxic lymphocytes. *The EMBO Journal*, *15*(3), 510–519. https://doi.org/10.1002/j.1460-2075.1996.tb00383.x

Lange, A., Mills, R. E., Lange, C. J., Stewart, M., Devine, S. E., & Corbett, A. H. (2007). Classical nuclear localization signals: Definition, function, and interaction with importin α. In *Journal of Biological Chemistry* (Vol. 282, Issue 8, pp. 5101–5105). https://doi.org/10.1074/jbc.R600026200

Larsen, R. A., Cusumano, C., Fujioka, A., Lim-Fong, G., Patterson, P., & Pogliano, J. (2007). Treadmilling of a prokaryotic tubulin-like protein, TubZ, required for plasmid stability in Bacillus thuringiensis. *Genes and Development*, *21*(11), 1340–1352. https://doi.org/10.1101/gad.1546107

Lebowitz, P. F., Davide, J. P., & Prendergast, G. C. (1995). Evidence that farnesyltransferase inhibitors suppress Ras transformation by interfering with Rho activity. *Molecular and Cellular Biology*, *15*(12), 6613–6622. https://doi.org/10.1128/mcb.15.12.6613

Lee, C. R., Park, Y. H., Kim, Y. R., Peterkofsky, A., & Seok, Y. J. (2013). Phosphorylation-dependent mobility shift of proteins on SDS-PAGE is due to decreased binding of SDS. *Bulletin of the Korean Chemical Society*, *34*(7), 2063–2066. https://doi.org/10.5012/bkcs.2013.34.7.2063

Lee, M. C. S., Orci, L., Hamamoto, S., Futai, E., Ravazzola, M., & Schekman, R. (2005). Sar1p N-terminal helix initiates membrane curvature and completes the fission of a COPII vesicle. *Cell*, *122*(4), 605–617. https://doi.org/10.1016/j.cell.2005.07.025

Leighton, T. L., Yong, D. H., Howell, P. L., & Burrows, L. L. (2016). Type IV Pilus Alignment Subcomplex Proteins PilN and PilO Form Homo- and Heterodimers in Vivo. *Journal of Biological Chemistry*. https://doi.org/10.1074/jbc.M116.738377

Leonardy, S., Miertzschke, M., Bulyha, I., Sperling, E., Wittinghofer, A., & Søgaard-Andersen, L. (2010a). Regulation of dynamic polarity switching in bacteria by a Ras-like G-protein and its cognate GAP. *The EMBO Journal*, *29*, 2276–2289. https://doi.org/10.1038/emboj.2010.114

Leonardy, S., Miertzschke, M., Bulyha, I., Sperling, E., Wittinghofer, A., & Søgaard-Andersen, L. (2010b). Regulation of dynamic polarity switching in bacteria by a Ras-like G-protein and its cognate GAP. *The EMBO Journal*, *29*(14), 2276–2289. https://doi.org/10.1038/emboj.2010.114

Li, C. P., Salvador, A. S., Ibrahim, H. R., Sugimoto, Y., & Aoki, T. (2003). Phosphorylation of Egg White Proteins by Dry-Heating in the Presence of Phosphate. *Journal of Agricultural and Food Chemistry*, *51*(23), 6808–6815. https://doi.org/10.1021/jf030043+

Li, Y., Sun, H., Ma, X., Lu, A., Lux, R., Zusman, D., & Shi, W. (2003). Extracellular polysaccharides mediate pilus retraction during social motility of *Myxococcus xanthus*. *Proceedings of the National Academy of Sciences of the United States of America*, *100*(9), 5443–5448. https://doi.org/10.1073/pnas.0836639100

Liang, H., Mu, H., Jean-Francois, F., Lakshman, B., Sarkar-Banerjee, S., Zhuang, Y., Zeng, Y., Gao, W., Nissley, D. V, Gorfe, A. A., Zhao, W., & Zhou, Y. (2018). Membrane curvature sensing of the lipid-anchored K-Ras small GTPases. *BioRxiv*. https://doi.org/10.1101/492710

Licking, E., Gorski, L., & Kaiser, D. (2000). A Common Step for Changing Cell Shape in Fruiting Body and Starvation-Independent Sporulation of Myxococcus xanthus. *Journal of Bacteriology*, *182*(12), 3553–3558. https://doi.org/10.1128/JB.182.12.3553-3558.2000

Lilly, W. W., Stajich, J. E., Pukkila, P. J., Wilke, S. K., Inoguchi, N., & Gathman, A. C. (2008). An expanded family of fungalysin extracellular metallopeptidases of Coprinopsis cinerea. *Mycological Research*, *112*(3), 389–398. https://doi.org/10.1016/j.mycres.2007.11.013

Lin, L., Osorio Valeriano, M., Harms, A., Søgaard-Andersen, L., & Thanbichler, M. (2017). Bactofilin-mediated organization of the ParABS chromosome segregation system in Myxococcus xanthus. *Nature Communications*, *8*(1). https://doi.org/10.1038/s41467-017-02015-z

Liu, Y., Kahn, R. A., & Prestegard, J. H. (2009). Structure and Membrane Interaction of Myristoylated ARF1. *Structure*, *17*(1), 79–87. https://doi.org/10.1016/j.str.2008.10.020

Loepfe, C., Raimann, E., Stephan, R., & Tasara, T. (2010). Reduced host cell invasiveness and oxidative stress tolerance in double and triple csp gene family deletion mutants of listeria monocytogenes. *Foodborne Pathogens and Disease*, *7*(7), 775–783. https://doi.org/10.1089/fpd.2009.0458

Long, K. R., Yamamoto, Y., Baker, A. L., Watkins, S. C., Coyne, C. B., Conway, J. F., & Aridor, M. (2010). Sar1 assembly regulates membrane constriction and ER export. *Journal of Cell Biology*, *190*(1), 115–128. https://doi.org/10.1083/jcb.201004132

Loose, M., & Mitchison, T. J. (2014). The bacterial cell division proteins FtsA and FtsZ self-organize into dynamic cytoskeletal patterns. *Nature Cell Biology*, *16*(1), 38–46. https://doi.org/10.1038/ncb2885

Los, D. A. (2004). The effect of low-temperature-induced DNA supercoiling on the expression of the desaturase genes in synechocystis. *Cellular and Molecular Biology (Noisy-Le-Grand, France)*, *50*(5), 605–612.

Löwe, J., & Amos, L. A. (1998). Crystal structure of the bacterial cell-division protein FtsZ : Abstract : Nature. *Nature*, *391*(6663), 203–206. https://doi.org/10.1038/34472

Lu, A., Cho, K., Black, W. P., Duan, X. Y., Lux, R., Yang, Z., Kaplan, H. B., Zusman, D. R., & Shi, W. (2005). Exopolysaccharide biosynthesis genes required for social motility in Myxococcus xanthus. *Molecular Microbiology*. https://doi.org/10.1111/j.1365-2958.2004.04369.x

Lu, L., Horstmann, H., Ng, C., & Hong, W. (2001). Regulation of Golgi structure and function by ARF-like protein 1 (Arl1). *Journal of Cell Science*, *114*(24), 4543–4555.

Luciano, J., Agrebi, R., Le Gall, A. V., Wartel, M., Fiegna, F., Ducret, A., Brochier-Armanet, C., & Mignot, T. (2011). Emergence and modular evolution of a novel motility machinery in bacteria. *PLoS Genetics*, *7*(9). https://doi.org/10.1371/journal.pgen.1002268

Lyu, Z., Coltharp, C., Yang, X., & Xiao, J. (2016). Influence of FtsZ GTPase activity and concentration on nanoscale Z-ring structure in vivo revealed by three-dimensional Superresolution imaging. *Biopolymers*, 725–734. https://doi.org/10.1002/bip.22895

Maloney, P. C., Kashket, E. R., & Wilson, T. H. (1974). A Protonmotive Force Drives ATP Synthesis in Bacteria. *Proceedings of the National Academy of Sciences*, *71*(10), 3896–3900. https://doi.org/10.1073/pnas.71.10.3896

Manson, M. D., Tedesco, P., Berg, H. C., Harold, F. M., & Van der Drift, C. (1977). A protonmotive force drives bacterial flagella. *Proceedings of the National Academy of Sciences*, *74*(7), 3060–3064. https://doi.org/10.1073/pnas.74.7.3060

Margolin, W. (2009). Sculpting the Bacterial Cell. In *Current Biology* (Vol. 19, Issue 17). https://doi.org/10.1016/j.cub.2009.06.033

Marinissen, M. J., Chiariello, M., & Gutkind, J. S. (2001). Regulation of gene expression by the small GTPase Rho through the ERK6 (p38γ) MAP kinase pathway. *Genes and Development*, *15*(5), 535–553. https://doi.org/10.1101/gad.855801

Martin, S., & Parton, R. G. (2008). Characterization of Rab18, a Lipid Droplet-Associated Small GTPase. In *Methods in Enzymology* (Vol. 438, pp. 109–129). https://doi.org/10.1016/S0076-6879(07)38008-7

Martinez-Canamero, M., Munoz-Dorado, J., Farez-Vidal, E., Inouye, M., & Inouye, S. (1993). Oar, a 115-kilodalton membrane protein required for development of Myxococcus xanthus. *Journal of Bacteriology*, *175*(15), 4756–4763. https://doi.org/10.1128/jb.175.15.4756-4763.1993

Martos, A., Raso, A., Jiménez, M., Petrášek, Z., Rivas, G., & Schwille, P. (2015). FtsZ polymers tethered to the membrane by ZipA are susceptible to spatial regulation by min waves. *Biophysical Journal*, *108*(9), 2371–2383. https://doi.org/10.1016/j.bpj.2015.03.031

Marzesco, A. M., Dunia, I., Pandjaitan, R., Recouvreur, M., Dauzonne, D., Benedetti, E. L., Louvard, D., & Zahraoui, A. (2002). The small GTPase Rab13 regulates assembly of functional tight junctions in epithelial cells. *Molecular Biology of the Cell*, *13*(6), 1819–1831. https://doi.org/10.1091/mbc.02-02-0029

Mateos-Gil, P., Paez, A., Hörger, I., Rivas, G., Vicente, M., Tarazona, P., & Vélez, M. (2012). Depolymerization dynamics of individual filaments of bacterial cytoskeletal protein FtsZ. *Proceedings of the National Academy of Sciences of the United States of America*, *109*(21), 8133–8138. https://doi.org/10.1073/pnas.1204844109

Mattick, J. S. (2002). Type IV Pili and Twitching Motility. *Annual Review of Microbiology*. https://doi.org/10.1146/annurev.micro.56.012302.160938

Maurer-Stroh, S., Washietl, S., & Eisenhaber, F. (2003). Protein prenyltransferases. In *Genome Biology* (Vol. 4, Issue 4). https://doi.org/10.1186/gb-2003-4-4-212

Mauriello, E. M. F., Mouhamar, F., Nan, B., Ducret, A., Dai, D., Zusman, D. R., & Mignot, T. (2010). Bacterial motility complexes require the actin-like protein, MreB and the Ras homologue, MglA. *The EMBO Journal*, *29*(2), 315–326. https://doi.org/10.1038/emboj.2009.356

Michaelson, D., Ali, W., Chiu, V. K., Bergo, M., Silletti, J., Wright, L., Young, S. G., & Philips, M. (2005). Postprenylation CAAX processing is required for proper localization of ras but not Rho GTPases. *Molecular Biology of the Cell*, *16*(4), 1606–1616. https://doi.org/10.1091/mbc.E04-11-0960

Miertzschke, M., Koerner, C., Vetter, I. R., Keilberg, D., Hot, E., Leonardy, S., Søgaard-Andersen, L., & Wittinghofer, A. (2011). Structural analysis of the Ras-like G protein MglA and its cognate GAP MglB and implications for bacterial polarity. *The EMBO Journal*, *30*(20), 4185–4197. https://doi.org/10.1038/emboj.2011.291

Mignot, T. (2007). The elusive engine in Myxococcus xanthus gliding motility. In *Cellular and Molecular Life Sciences* (Vol. 64, Issue 21, pp. 2733–2745). https://doi.org/10.1007/s00018-007-7176-x

Mignot, T., Shaevitz, J. W., Hartzell, P. L., & Zusman, D. R. (2007). Evidence That Focal Adhesion Complexes Power Bacterial Gliding Motility. *Science*, *315*(5813), 853–856. https://doi.org/10.1126/science.1137223

Mignot, Tâm, Shaevitz, J. W., Hartzell, P. L., & Zusman, D. R. (2007). Evidence That Focal Adhesion Complexes Power Bacterial Gliding Motility. *Science*, *315*(5813). http://science.sciencemag.org/content/315/5813/853.full

Militello, R. D., Munafó, D. B., Berón, W., López, L. A., Monier, S., Goud, B., & Colombo, M. I. (2013). Rab24 is Required for Normal Cell Division. *Traffic*, *14*(5), 502–518. https://doi.org/10.1111/tra.12057

Miller, E. A., & Schekman, R. (2013). COPII - a flexible vesicle formation system. In *Current Opinion in Cell Biology* (Vol. 25, Issue 4, pp. 420–427). https://doi.org/10.1016/j.ceb.2013.04.005

Milner, D. S., Till, R., Cadby, I., Lovering, A. L., Basford, S. M., Saxon, E. B., Liddell, S., Williams, L. E., & Sockett, R. E. (2014). Ras GTPase-Like Protein MglA, a Controller of Bacterial Social-Motility in Myxobacteria, Has Evolved to Control Bacterial Predation by Bdellovibrio. *PLoS Genetics*, *10*(4). https://doi.org/10.1371/journal.pgen.1004253

Moeck, G. S., & Coulton, J. W. (1998). TonB-dependent iron acquisition: Mechanisms of siderophore-mediated active transport. In *Molecular Microbiology* (Vol. 28, Issue 4, pp. 675–681). https://doi.org/10.1046/j.1365-2958.1998.00817.x

Mohammadi, T., Karczmarek, A., Crouvoisier, M., Bouhss, A., Mengin-Lecreulx, D., & Den Blaauwen, T. (2007). The essential peptidoglycan glycosyltransferase MurG forms a complex with proteins involved in lateral envelope growth as well as with proteins involved in cell division in Escherichia coli. *Molecular Microbiology*, *65*(4), 1106–1121. https://doi.org/10.1111/j.1365-2958.2007.05851.x

Mosyak, L., Zhang, Y., Glasfeld, E., Haney, S., Stahl, M., Seehra, J., & Somers, W. S. (2000). The bacterial cell-division protein ZipA and its interaction with an FtsZ fragment revealed by X-ray crystallography. *The EMBO Journal*, *19*(13), 3179–3191. https://doi.org/10.1093/emboj/19.13.3179

Müller, S., Strack, S. N., Ryan, S. E., Shawgo, M., Walling, A., Harris, S., Chambers, C., Boddicker, J., & Kirby, J. R. (2016). Identification of functions affecting predatorprey interactions between Myxococcus xanthus and Bacillus subtilis. *Journal of Bacteriology*, *198*(24), 3335–3344. https://doi.org/10.1128/JB.00575-16

Na Pombejra, S., Jamklang, M., Uhrig, J. P., Vu, K., & Gelli, A. (2018). The structure-function analysis of the Mpr1 metalloprotease determinants of activity during migration of fungal cells across the blood-brain barrier. *PLoS ONE*, *13*(8). https://doi.org/10.1371/journal.pone.0203020

Nachury, M. V., & Weis, K. (1999). The direction of transport through the nuclear pore can be inverted. *Proceedings of the National Academy of Sciences of the United States of America*, *96*(17), 9622–9627. https://doi.org/10.1073/pnas.96.17.9622

Nagasaki, A., Kanada, M., & Uyeda, T. Q. (2009). Cell adhesion molecules regulate contractile ring-independent cytokinesis in Dictyostelium discoideum. *Cell Research*, *19*(2), 236–246. https://doi.org/10.1038/cr.2008.318

Nakano, A., & Muramatsu, M. (1989). A novel GTP-binding protein, sar1p, is involved in transport from the endoplasmic reticulum to the Golgi apparatus. *Journal of Cell Biology*, *109*(6 I), 2677–2691. https://doi.org/10.1083/jcb.109.6.2677

Nam, T. W., Park, Y. H., Jeong, H. J., Ryu, S., & Seok, Y. J. (2005). Glucose repression of the Escherichia coli sdhCDAB operon, revisited: Regulation by the CRP·cAMP complex. *Nucleic Acids Research*, *33*(21), 6712–6722. https://doi.org/10.1093/nar/gki978

Nan, B., Chen, J., Neu, J. C., Berry, R. M., Oster, G., & Zusman, D. R. (2011). Myxobacteria gliding motility requires cytoskeleton rotation powered by proton motive force. *Proceedings of the National Academy of Sciences*, *108*(6), 2498–2503. https://doi.org/10.1073/pnas.1018556108

Nan, Beiyan, Bandaria, J. N., Guo, K. Y., Fan, X., Moghtaderi, A., Yildiz, A., & Zusman, D. R. (2015). The polarity of myxobacterial gliding is regulated by direct interactions between the gliding motors and the Ras homolog MglA. *Proceedings of the National Academy of Sciences*, *112*(2), E186–E193. https://doi.org/10.1073/pnas.1421073112

Nan, Beiyan, Mauriello, E. M. F., Sun, I. H., Wong, A., & Zusman, D. R. (2010). A multi-protein complex from Myxococcus xanthus required for bacterial gliding motility. *Molecular Microbiology*, *76*(6), 1539–1554. https://doi.org/10.1111/j.1365-2958.2010.07184.x

Nothaft, H., & Szymanski, C. M. (2013). Bacterial protein n-glycosylation: New perspectives and applications. In *Journal of Biological Chemistry* (Vol. 288, Issue 10, pp. 6912–6920). https://doi.org/10.1074/jbc.R112.417857

Nudleman, E., & Kaiser, D. (2004). Pulling together with type IV pili. In *Journal of Molecular Microbiology and Biotechnology*. https://doi.org/10.1159/000077869

Oliveira Paiva, A. M., Friggen, A. H., Qin, L., Douwes, R., Dame, R. T., & Smits, W. K. (2019). The Bacterial Chromatin Protein HupA Can Remodel DNA and Associates with the Nucleoid in Clostridium difficile. *Journal of Molecular Biology*, *431*(4), 653–672. https://doi.org/10.1016/j.jmb.2019.01.001

Ota, M., Gonja, H., Koike, R., & Fukuchi, S. (2016). Multiple-Localization and Hub Proteins. In *PLoS ONE* (Vol. 11, Issue 6). https://doi.org/10.1371/journal.pone.0156455

Overmeyer, J. H. (2011). Death pathways triggered by activated Ras in cancer cells. *Frontiers in Bioscience*, *16*(1), 1693. https://doi.org/10.2741/3814

Palsdottir, H., Remis, J. P., Schaudinn, C., O'Toole, E., Lux, R., Shi, W., McDonald, K. L., Costerton, J. W., & Auer, M. (2009). Three-dimensional macromolecular organization of cryofixed myxococcus xanthus biofilms as revealed by electron microscopic tomography. *Journal of Bacteriology*, *191*(7), 2077–2082. https://doi.org/10.1128/JB.01333-08

Papke, B., Schmick, M., Vartak, N., & Bastiaens, P. (2014). Chapter 8: Ras Superfamily Small G Proteins: Biology and Mechanisms 1. In *Wittinghofer, A (ed). Book Title: Ras Superfamily Small G Proteins: Biology and Mechanisms 1*. https://doi.org/10.1007/978-3-7091-1806-1

Parish, J. (1985). Myxobacteria: Development and Cell Interactions. *Biochemical Education*, *13*(2), 91. https://doi.org/10.1016/0307-4412(85)90045-7

Park, H.-O., & Bi, E. (2007). Central Roles of Small GTPases in the Development of Cell Polarity in Yeast and Beyond. *Microbiology and Molecular Biology Reviews*, *71*(1), 48–96. https://doi.org/10.1128/mmbr.00028-06

Parry, D. A. D. (2005). Microdissection of the sequence and structure of intermediate filament chains. In *Advances in Protein Chemistry* (Vol. 70, pp. 113–142). https://doi.org/10.1016/S0065-3233(05)70005-X

Pasqualato, S., Renault, L., & Cherfils, J. (2002). Arf, Arl, Arp and Sar proteins: A family of GTP-binding proteins with a structural device for "front-back" communication. *EMBO Reports*, *3*(11), 1035–1041. https://doi.org/10.1093/embo-reports/kvf221

Pathak, D. T., Wei, X., Dey, A., & Wall, D. (2013). Molecular Recognition by a Polymorphic Cell Surface Receptor Governs Cooperative Behaviors in Bacteria. *PLoS Genetics*, *9*(11). https://doi.org/10.1371/journal.pgen.1003891

Patryn, J., Allen, K., Dziewanowska, K., Otto, R., & Hartzell, P. L. (2010). Localization of MglA, an essential gliding motility protein in Myxococcus xanthus. *Cytoskeleton*, *67*(5), 322–337. https://doi.org/10.1002/cm.20447

Pejaver, V., Hsu, W. L., Xin, F., Dunker, A. K., Uversky, V. N., & Radivojac, P. (2014). The structural and functional signatures of proteins that undergo multiple events of post-translational modification. *Protein Science*, *23*(8), 1077–1093. https://doi.org/10.1002/pro.2494

Pellach, M., Goldshtein, J., Ziv-Polat, O., & Margel, S. (2012). Functionalised, photostable, fluorescent polystyrene nanoparticles of narrow size-distribution. *Journal of Photochemistry and Photobiology A: Chemistry*, *228*(1), 60–67. https://doi.org/10.1016/j.jphotochem.2011.11.012

Perkins-Balding, D., Ratliff-Griffin, M., & Stojiljkovic, I. (2004). Iron transport systems in Neisseria meningitidis. *Microbiology and Molecular Biology Reviews : MMBR*, *68*(1), 154–171. http://www.ncbi.nlm.nih.gov/pubmed/15007100%0Ahttp://www.pubmedcentral.nih.gov/articlerender.fcgi?artid=PMC362107

Pfeffer, S., & Aivazian, D. (2004). Targeting Rab GTPases to distinct membrane compartments. In *Nature Reviews Molecular Cell Biology* (Vol. 5, Issue 11, pp. 886–896). https://doi.org/10.1038/nrm1500

Phadtare, S. (2004). Recent developments in bacterial cold-shock response. *Current Issues in Molecular Biology*, *6*(2), 125–136. http://www.ncbi.nlm.nih.gov/pubmed/15119823

Phadtare, S. (2011). Unwinding activity of cold shock proteins and RNA metabolism. In *RNA Biology* (Vol. 8, Issue 3, pp. 394–397). https://doi.org/10.4161/rna.8.3.14823

Pichoff, S., & Lutkenhaus, J. (2005). Tethering the Z ring to the membrane through a conserved membrane targeting sequence in FtsA. *Molecular Microbiology*, *55*(6), 1722–1734. https://doi.org/10.1111/j.1365-2958.2005.04522.x

Pichoff, S., & Lutkenhaus, J. (2007). Identification of a region of FtsA required for interaction with FtsZ. *Molecular Microbiology*, *64*(4), 1129–1138. https://doi.org/10.1111/j.1365-2958.2007.05735.x

Pilhofer, M., Ladinsky, M. S., McDowall, A. W., Petroni, G., & Jensen, G. J. (2011). Microtubules in Bacteria: Ancient tubulins build a five-protofilament homolog of the eukaryotic cytoskeleton. *PLoS Biology*, *9*(12). https://doi.org/10.1371/journal.pbio.1001213

Pollard, T. D., & Cooper, J. A. (2009). Actin, a central player in cell shape and movement. *Science (New York, N.Y.)*, *326*(5957), 1208–1212. https://doi.org/10.1126/science.1175862

Pollock, C. B., Shirasawa, S., Sasazuki, T., Kolch, W., & Dhillon, A. S. (2005). Oncogenic K-RAS is required to maintain changes in cytoskeletal organization, adhesion, and motility in colon cancer cells. *Cancer Research*, *65*(4), 1244–1250. https://doi.org/10.1158/0008-5472.CAN-04-1911

Prieto-Sánchez, R. M., & Bustelo, X. R. (2003). Structural basis for the signaling specificity of RhoG and Rac1 GTPases. *Journal of Biological Chemistry*, *278*(39), 37916–37925. https://doi.org/10.1074/jbc.M301437200

Prior, I. A., Lewis, P. D., & Mattos, C. (2012). A comprehensive survey of ras mutations in cancer. In *Cancer Research* (Vol. 72, Issue 10, pp. 2457–2467). https://doi.org/10.1158/0008-5472.CAN-11-2612

Prober, D. A., & Edgar, B. A. (2000). Ras1 promotes cellular growth in the Drosophila wing. *Cell*, *100*(4), 435–446. https://doi.org/10.1016/S0092-8674(00)80679-0

Rajagopala, S. V, Titz, B., Goll, J., Parrish, J. R., Wohlbold, K., McKevitt, M. T., Palzkill, T., Mori, H., Finley Jr., R. L., & Uetz, P. (2007). The protein network of bacterial motility. *Molecular Systems Biology*, *3*, 128. https://doi.org/10.1038/msb4100166

Raskin, D. M., & de Boer, P. A. (1999). Rapid pole-to-pole oscillation of a protein required for directing division to the middle of Escherichia coli. *Proceedings of the National Academy of Sciences of the United States of America*, *96*(9), 4971–4976. https://doi.org/10.1073/pnas.96.9.4971

Reddy Chichili, V. P., Kumar, V., & Sivaraman, J. (2013). Linkers in the structural biology of protein-protein interactions. In *Protein Science* (Vol. 22, Issue 2, pp. 153–167). https://doi.org/10.1002/pro.2206

Reichenbach, H., & Dworkin, M. (1981). The Order Myxobacterales. In *The Prokaryotes*. https://doi.org/10.1007/978-3-662-13187-9_20

Reid, R. A., Moyle, J., & Mitchell, P. (1966). Synthesis of adenosine triphosphate by a protonmotive force in rat liver mitochondria. *Nature*, *212*(5059), 257–258. https://doi.org/10.1038/212257a0

Resh, M. D. (1999). Fatty acylation of proteins: New insights into membrane targeting of myristoylated and palmitoylated proteins. In *Biochimica et Biophysica Acta - Molecular Cell Research* (Vol. 1451, Issue 1, pp. 1–16). https://doi.org/10.1016/S0167-4889(99)00075-0

Reuter, C. W., Morgan, M. A., & Bergmann, L. (2000). Targeting the Ras signaling pathway: a rational, mechanism-based treatment for hematologic malignancies? *Blood*, *96*(5), 1655–1669. http://www.ncbi.nlm.nih.gov/pubmed/10961860

Rojas, A. M., Fuentes, G., Rausell, A., & Valencia, A. (2012). The Ras protein superfamily: Evolutionary tree and role of conserved amino acids. In *Journal of Cell Biology* (Vol. 196, Issue 2, pp. 189–201). https://doi.org/10.1083/jcb.201103008

Rolbetzki, A., Ammon, M., Jakovljevic, V., Konovalova, A., & Søgaard-Andersen, L. (2008). Regulated Secretion of a Protease Activates Intercellular Signaling during Fruiting Body Formation in M. xanthus. *Developmental Cell*, *15*(4), 627–634. https://doi.org/10.1016/j.devcel.2008.08.002

Rudack, T., Xia, F., Schlitter, J., Kötting, C., & Gerwert, K. (2012). The role of magnesium for geometry and charge in GTP hydrolysis, revealed by quantum mechanics/Molecular mechanics simulations. *Biophysical Journal*, *103*(2), 293–302. https://doi.org/10.1016/j.bpj.2012.06.015

Salje, J., van den Ent, F., de Boer, P., & Löwe, J. (2011). Direct Membrane Binding by Bacterial Actin MreB. *Molecular Cell*, *43*(3), 478–487. https://doi.org/10.1016/j.molcel.2011.07.008

Sandri, C., Caccavari, F., Valdembri, D., Camillo, C., Veltel, S., Santambrogio, M., Lanzetti, L., Bussolino, F., Ivaska, J., & Serini, G. (2012). The R-Ras/RIN2/Rab5 complex controls endothelial cell adhesion and morphogenesis via active integrin endocytosis and Rac signaling. *Cell Research*, *22*(10), 1479–1501. https://doi.org/10.1038/cr.2012.110

Sato, K., & Nakano, A. (2005). Dissection of COPII subunit-cargo assembly and disassembly kinetics during Sar1p-GTP hydrolysis. *Nature Structural and Molecular Biology*, *12*(2), 167–174. https://doi.org/10.1038/nsmb893

Schaub, F. X., Reza, M. S., Flaveny, C. A., Li, W., Musicant, A. M., Hoxha, S., Guo, M., Cleveland, J. L., & Amelio, A. L. (2015). Fluorophore-NanoLuc BRET reporters enable sensitive In Vivo optical imaging and flow cytometry for monitoring tumorigenesis. *Cancer Research*, *75*(23), 5023–5033. https://doi.org/10.1158/0008-5472.CAN-14-3538

Schauer, K., Gouget, B., Carrière, M., Labigne, A., & De Reuse, H. (2007). Novel nickel transport mechanism across the bacterial outer membrane energized by the TonB/ExbB/ExbD machinery. *Molecular Microbiology*, *63*(4), 1054–1068. https://doi.org/10.1111/j.1365-2958.2006.05578.x

Schauer, K., Rodionov, D. A., & de Reuse, H. (2008). New substrates for TonB-dependent transport: do we only see the "tip of the iceberg"? In *Trends in Biochemical Sciences* (Vol. 33, Issue 7, pp. 330–338). https://doi.org/10.1016/j.tibs.2008.04.012

Schindelin, J., Arganda-Carreras, I., Frise, E., Kaynig, V., Longair, M., Pietzsch, T., Preibisch, S., Rueden, C., Saalfeld, S., Schmid, B., Tinevez, J. Y., White, D. J., Hartenstein, V., Eliceiri, K., Tomancak, P., & Cardona, A. (2012). Fiji: An open-source platform for biological-image analysis. In *Nature Methods* (Vol. 9, Issue 7, pp. 676–682). https://doi.org/10.1038/nmeth.2019

Schumacher, D., Bergeler, S., Harms, A., Vonck, J., Huneke-Vogt, S., Frey, E., & Søgaard-Andersen, L. (2017). The PomXYZ Proteins Self-Organize on the Bacterial Nucleoid to Stimulate Cell Division. *Developmental Cell*, *41*(3), 299-314.e13. https://doi.org/10.1016/j.devcel.2017.04.011

Schweins, T., & Wittinghofer, A. (1994). GTP-Binding Proteins: Structures, interactions and relationships. *Current Biology*, *4*(6), 547–550. https://doi.org/10.1016/S0960-9822(00)00122-6

Secko, D. M., Siu, C. H., Spiegelman, G. B., & Weeks, G. (2006). An activated Ras protein alters cell adhesion by dephosphorylating Dictyostelium DdCAD-1. *Microbiology*, *152*(5), 1497–1505. https://doi.org/10.1099/mic.0.28709-0

Settles, E. I., Loftus, A. F., McKeown, A. N., & Parthasarathy, R. (2010). The vesicle trafficking protein Sar1 lowers lipid membrane rigidity. *Biophysical Journal*, *99*(5), 1539–1545. https://doi.org/10.1016/j.bpj.2010.06.059

Shah, S., Das, B., & Bhadra, R. K. (2008). Functional analysis of the essential GTP-binding-protein-coding gene cgtA of Vibrio cholerae. *Journal of Bacteriology*, *190*(13), 4764–4771. https://doi.org/10.1128/JB.02021-07

Shahinian, S., & Silvius, J. R. (1995). Doubly-Lipid-Modified Protein Sequence Motifs Exhibit Long-Lived Anchorage to Lipid Bilayer Membranes. *Biochemistry*, *34*(11), 3813–3822. https://doi.org/10.1021/bi00011a039

Shalaeva, D. N., Cherepanov, D. A., Galperin, M. Y., Golovin, A. V., & Mulkidjanian, A. Y. (2018). Evolution of cation binding in the active sites of P-loop nucleoside triphosphatases in relation to the basic catalytic mechanism. *ELife*, *7*. https://doi.org/10.7554/eLife.37373

Shao, J., Sheng, H., DuBois, R. N., & Beauchamp, R. D. (2000). Oncogenic Ras-mediated cell growth arrest and apoptosis are associated with increased ubiquitin-dependent cyclin D1 degradation. *Journal of Biological Chemistry*, *275*(30), 22916–22924. https://doi.org/10.1074/jbc.M002235200

Shi, C., Fricke, P., Lin, L., Chevelkov, V., Wegstroth, M., Giller, K., Becker, S., Thanbichler, M., & Lange, A. (2015). Atomic-resolution structure of cytoskeletal bactofilin by solid-state NMR. *Science Advances*, *1*(11), e1501087. https://doi.org/10.1126/sciadv.1501087

Shi, W., & Zusman, D. R. (1993). The two motility systems of Myxococcus xanthus show different selective advantages on various surfaces (gliding bacterium/swarming/fruiting/video microscopy). In *Proc. Natl. Acad. Sci. USA* (Vol. 90). http://www.pnas.org/content/pnas/90/8/3378.full.pdf

Shih, Y.-L., & Rothfield, L. (2006). The bacterial cytoskeleton. *Microbiology and Molecular Biology Reviews : MMBR*, *70*(3), 729–754. https://doi.org/10.1128/MMBR.00017-06

Sit, S. T., & Manser, E. (2011). Rho GTPases and their role in organizing the actin cytoskeleton. In *Journal of Cell Science* (Vol. 124, Issue 5, pp. 679–683). https://doi.org/10.1242/jcs.064964

Sliusarenko, O., Zusman, D. R., & Oster, G. (2007). The motors powering A-motility in Myxococcus xanthus are distributed along the cell body. *Journal of Bacteriology*, *189*(21), 7920–7921. https://doi.org/10.1128/JB.00923-07

Sodergren, E., & Kaiser, D. (1983). Insertions of Tn5 near genes that govern stimulatable cell motility in Myxococcus. *Journal of Molecular Biology*, *167*(2), 295–310. https://doi.org/10.1016/S0022-2836(83)80337-4

Söderström, B., Badrutdinov, A., Chan, H., & Skoglund, U. (2018). Cell shape-independent FtsZ dynamics in synthetically remodeled bacterial cells. *Nature Communications*, *9*(1). https://doi.org/10.1038/s41467-018-06887-7

Spoerner, M., Herrmann, C., Vetter, I. R., Kalbitzer, H. R., & Wittinghofer, A. (2001). Dynamic properties of the Ras switch I region and its importance for binding to effectors. *Proceedings of the National Academy of Sciences of the United States of America*, *98*(9), 4944–4949. https://doi.org/10.1073/pnas.081441398

Spormann, A. M., & Kaiser, A. D. (1995). Gliding movements in Myxococcus xanthus. *Journal of Bacteriology*, *177*(20), 5846–5852. https://doi.org/10.1128/jb.177.20.5846-5852.1995

Spormann, A M. (1999). Gliding motility in bacteria: insights from studies of Myxococcus xanthus. *Microbiology and Molecular Biology Reviews : MMBR*, *63*(3), 621–641. http://www.pubmedcentral.nih.gov/articlerender.fcgi?artid=103748&tool=pmcentrez&rendertype=abstract

Spormann, Alfred M., & Kaiser, D. (1999). Gliding mutants of Myxococcus xanthus with high reversal frequencies and small displacements. *Journal of Bacteriology*, *181*(8), 2593–2601.

Stephens, K., Hartzell, P., & Kaiser, D. (1989). Gliding motility in Myxococcus xanthus: mgl locus, RNA, and predicted protein products. *Journal of Bacteriology*, *171*(2), 819–830. https://doi.org/10.1128/jb.171.2.819-830.1989

Stephens, R. M., Yi, M., Kessing, B., Nissley, D. V., & McCormick, F. (2017). Tumor RAS gene expression levels are influenced by the Mutational status of RAS genes and both Upstream and Downstream RAS Pathway genes. *Cancer Informatics*, *16*. https://doi.org/10.1177/1176935117711944

Stricker, J., Maddox, P., Salmon, E. D., & Erickson, H. P. (2002). Rapid assembly dynamics of the Escherichia coli FtsZ-ring demonstrated by fluorescence recovery after photobleaching. *Proceedings of the National Academy of Sciences of the United States of America*, *99*(5), 3171–3175. https://doi.org/10.1073/pnas.052595099

Sun, M., Wartel, M., Cascales, E., Shaevitz, J. W., & Mignot, T. (2011). Motor-driven intracellular transport powers bacterial gliding motility. *Proceedings of the National Academy of Sciences of the United States of America*. https://doi.org/10.1073/pnas.1101101108

Swulius, M. T., & Jensen, G. J. (2012). The helical mreb cytoskeleton in Escherichia coli MC1000/pLE7 is an artifact of the N-terminal yellow fluorescent protein tag. *Journal of Bacteriology*, *194*(23), 6382–6386. https://doi.org/10.1128/JB.00505-12

Sycuro, L. K., Pincus, Z., Gutierrez, K. D., Biboy, J., Stern, C. a., Vollmer, W., & Salama, N. R. (2010). Peptidoglycan crosslinking relaxation promotes helicobacter pylori's helical shape and stomach colonization. *Cell*, *141*(5), 822–833. https://doi.org/10.1016/j.cell.2010.03.046

Szadkowski, D., Harms, A., Carreira, L. A. M., Wigbers, M., Potapova, A., Wuichet, K., Keilberg, D., Gerland, U., & Søgaard-Andersen, L. (2019). Spatial control of the GTPase MglA by localized RomR–RomX GEF and MglB GAP activities enables Myxococcus xanthus motility. *Nature Microbiology*. https://doi.org/10.1038/s41564-019-0451-4

Szoka, F., & Papahadjopoulos, D. (1980). Comparative properties and methods of preparation of lipid vesicles (liposomes). In *Annual review of biophysics and bioengineering*. https://doi.org/10.1146/annurev.bb.09.060180.002343

Szwedziak, P., Wang, Q., Bharat, T. A. M., Tsim, M., & L??we, J. (2014). Architecture of the ring formed by the tubulin homologue FtsZ in bacterial cell division. *ELife*, *3*, e04601. https://doi.org/10.7554/eLife.04601

Szwedziak, P., Wang, Q., Bharat, T. A. M., Tsim, M., Löwe, J., Adams, D., Errington, J., Agulleiro, J., Fernandez, J., Amat, F., Moussavi, F., Comolli, L., Elidan, G., Downing, K., Horowitz, M., Begg, K., Nikolaichik, Y., Crossland, N., Donachie, W., … Woldringh, C. (2014). Architecture of the ring formed by the tubulin homologue FtsZ in bacterial cell division. *ELife*, *3*, e04601. https://doi.org/10.7554/eLife.04601

Takhar, H. K., Kemp, K., Kim, M., Howell, P. L., & Burrows, L. L. (2013). The platform protein is essential for type IV pilus biogenesis. *Journal of Biological Chemistry*. https://doi.org/10.1074/jbc.M113.453506

Taylor, A., Sharkey, J., Plagge, A., Wilm, B., & Murray, P. (2018). Multicolour in Vivo Bioluminescence Imaging Using a NanoLuc-Based BRET Reporter in Combination with Firefly Luciferase. *Contrast Media and Molecular Imaging*, *2018*. https://doi.org/10.1155/2018/2514796

Ten Klooster, J. P., Jaffer, Z. M., Chernoff, J., & Hordijk, P. L. (2006). Targeting and activation of Rac1

are mediated by the exchange factor β-Pix. *Journal of Cell Biology*, *172*(5), 759–769. https://doi.org/10.1083/jcb.200509096

Thevelein, J. M., & De Winde, J. H. (1999). Novel sensing mechanisms and targets for the cAMP-protein kinase A pathway in the yeast Saccharomyces cerevisiae. In *Molecular Microbiology* (Vol. 33, Issue 5, pp. 904–918). https://doi.org/10.1046/j.1365-2958.1999.01538.x

Thomasson, B., Link, J., Stassinopoulos, A. G., Burke, N., Plamann, L., & Hartzell, P. L. (2002). MgLA, a small GTPase, interacts with a tyrosine kinase to control type IV pili-mediated motility and development of Myxococcus xanthus. *Molecular Microbiology*, *46*(5), 1399–1413. https://doi.org/10.1046/j.1365-2958.2002.03258.x

Thompson, O., Moore, C. J., Hussain, S.-A., Kleino, I., Peckham, M., Hohenester, E., Ayscough, K. R., Saksela, K., & Winder, S. J. (2009). Modulation of cell spreading and cell-substrate adhesion dynamics by dystroglycan. *Journal of Cell Science*, *123*(1), 118–127. https://doi.org/10.1242/jcs.047902

Ting, P. Y., Johnson, C. W., Fang, C., Cao, X., Graeber, T. G., Mattos, C., & Colicelli, J. (2015). Tyrosine phosphorylation of RAS by ABL allosterically enhances effector binding. *FASEB Journal*, *29*(9), 3750–3761. https://doi.org/10.1096/fj.15-271510

Treuner-Lange, A., Macia, E., Guzzo, M., Hot, E., Faure, L. M., Jakobczak, B., Espinosa, L., Alcor, D., Ducret, A., Keilberg, D., Castaing, J. P., Lacas Gervais, S., Franco, M., Søgaard-Andersen, L., & Mignot, T. (2015a). The small G-protein MglA connects to the MreB actin cytoskeleton at bacterial focal adhesions. *The Journal of Cell Biology*, *210*(2). http://jcb.rupress.org/content/210/2/243

Treuner-Lange, A., Macia, E., Guzzo, M., Hot, E., Faure, L. M., Jakobczak, B., Espinosa, L., Alcor, D., Ducret, A., Keilberg, D., Castaing, J. P., Lacas Gervais, S., Franco, M., Søgaard-Andersen, L., & Mignot, T. (2015b). The small G-protein MglA connects to the MreB actin cytoskeleton at bacterial focal adhesions. *The Journal of Cell Biology*, *210*(2), 243–256. https://doi.org/10.1083/jcb.201412047

Typas, A., Banzhaf, M., Gross, C. a., & Vollmer, W. (2011). From the regulation of peptidoglycan synthesis to bacterial growth and morphology. *Nature Reviews Microbiology*, *10*(2), 123–136. https://doi.org/10.1038/nrmicro2677

Unni, A. M., Lockwood, W. W., Zejnullahu, K., Lee-Lin, S. Q., & Varmus, H. (2015). Evidence that synthetic lethality underlies the mutual exclusivity of oncogenic KRAS and EGFR mutations in lung adenocarcinoma. *ELife*, *4*(JUNE), 1–23. https://doi.org/10.7554/eLife.06907

Van den Ent, F., Amos, L. A., Löwe, J., Ent, F. Van Den, Amos, L. A., & Lo, J. (2001). Prokaryotic origin of the actin cytoskeleton. *Nature*, *413*(6851), 39–44. https://doi.org/10.1038/35092500

van den Ent, F., Izoré, T., Bharat, T. A. M., Johnson, C. M., & Löwe, J. (2014). Bacterial actin MreB forms antiparallel double filaments. *ELife*, *2014*(3). https://doi.org/10.7554/eLife.02634

van den Ent, F., Johnson, C. M., Persons, L., de Boer, P., & Löwe, J. (2010). Bacterial actin MreB assembles in complex with cell shape protein RodZ. *The EMBO Journal*, *29*(6), 1081–1090. https://doi.org/10.1038/emboj.2010.9

van Teeffelen, S., Wang, S., Furchtgott, L., Huang, K. C., Wingreen, N. S., Shaevitz, J. W., & Gitai, Z. (2011). The bacterial actin MreB rotates, and rotation depends on cell-wall assembly. *Proceedings of the National Academy of Sciences*, *108*(38), 15822–15827. https://doi.org/10.1073/pnas.1108999108

Vanni, S., Vamparys, L., Gautier, R., Drin, G., Etchebest, C., Fuchs, P. F. J., & Antonny, B. (2013).

Amphipathic lipid packing sensor motifs: Probing bilayer defects with hydrophobic residues. *Biophysical Journal*, *104*(3), 575–584. https://doi.org/10.1016/j.bpj.2012.11.3837

Vasa, S., Lin, L., Shi, C., Habenstein, B., Riedel, D., Kühn, J., Thanbichler, M., & Lange, A. (2015). β-Helical architecture of cytoskeletal bactofilin filaments revealed by solid-state NMR. *Proceedings of the National Academy of Sciences*, *112*(2), E127–E136. https://doi.org/10.1073/pnas.1418450112

Vassallo, C., Pathak, D. T., Cao, P., Zuckerman, D. M., Hoiczyk, E., & Wall, D. (2015). Cell rejuvenation and social behaviors promoted by LPS exchange in myxobacteria. *Proceedings of the National Academy of Sciences of the United States of America*, *112*(22), E2939–E2946. https://doi.org/10.1073/pnas.1503553112

Wachi, M., Doi, M., Tamaki, S., Park, W., Nakajima-Iijima, S., & Matsuhashi, M. (1987). Mutant isolation and molecular cloning of mre genes, which determine cell shape, sensitivity to mecillinam, and amount of penicillin-binding proteins in Escherichia coli. *Journal of Bacteriology*, *169*(11), 4935–4940. https://doi.org/10.1073/pnas.0921

Wade, R. H. (2009). On and around microtubules: An overview. In *Molecular Biotechnology* (Vol. 43, Issue 2, pp. 177–191). https://doi.org/10.1007/s12033-009-9193-5

Wall, D., Kolenbrander, P. E., & Kaiser, D. (1999). The Myxococcus xanthus pilQ (sglA) gene encodes a secretin homolog required for type IV pilus biogenesis, social motility, and development. *Journal of Bacteriology*.

Wang, Z., Wang, S., & Wu, Q. (2014). Cold shock protein A plays an important role in the stress adaptation and virulence of Brucella melitensis. In *FEMS Microbiology Letters* (Vol. 354, Issue 1, pp. 27–36). https://doi.org/10.1111/1574-6968.12430

Wartel, M., Ducret, A., Thutupalli, S., Czerwinski, F., Le Gall, A. V., Mauriello, E. M. F., Bergam, P., Brun, Y. V., Shaevitz, J., & Mignot, T. (2013). A Versatile Class of Cell Surface Directional Motors Gives Rise to Gliding Motility and Sporulation in Myxococcus xanthus. *PLoS Biology*, *11*(12). https://doi.org/10.1371/journal.pbio.1001728

Wegener, A. D., & Jones, L. R. (1984). Phosphorylation-induced Mobility Shift in Phospholamban in Sodium Dodecyl Sulfate-Polyacrylamide Gels. *The Journal of Biological Chemistry*, *259*(3), 1834–1841.

White, C. L., Kitich, A., & Gober, J. W. (2010). Positioning cell wall synthetic complexes by the bacterial morphogenetic proteins MreB and MreD. *Molecular Microbiology*, *76*(3), 616–633. https://doi.org/10.1111/j.1365-2958.2010.07108.x

Whitworth, D. E., Millard, A., Hodgson, D. A., & Hawkins, P. F. (2008). Protein-protein interactions between two-component system transmitter and receiver domains of Myxococcus xanthus. *Proteomics*, *8*(9), 1839–1842. https://doi.org/10.1002/pmic.200700544

Williamson, M. P. (1994). The structure and function of proline-rich regions in proteins. *Biochemical Journal*, *297*(Pt 2), 249–260. https://doi.org/061/7

Wolgemuth, C., Hoiczyk, E., Kaiser, D., & Oster, G. (2002). How Myxobacteria Glide. *Current Biology*, *12*(5), 369–377. https://doi.org/10.1016/S0960-9822(02)00716-9

Wu, L. J., & Errington, J. (2012). Nucleoid occlusion and bacterial cell division. *Nat Rev Microbiol*, *10*(1), 8–12. https://doi.org/10.1038/nrmicro2671

Wui Tan, E., & Rando, R. R. (1992). Identification of an Isoprenylated Cysteine Methyl Ester Hydrolase Activity in Bovine Rod Outer Segment Membranes. *Biochemistry*, *31*(24), 5572–5578.

https://doi.org/10.1021/bi00139a021

Yamamoto, T., Taya, S., & Kaibuchi, K. (1999). Ras-induced transformation and signaling pathway. In *Journal of Biochemistry* (Vol. 126, Issue 5, pp. 799–803). https://doi.org/10.1093/oxfordjournals.jbchem.a022519

Yang, Y. J., Singh, R. P., Lan, X., Zhang, C. S., Li, Y. Z., Li, Y. Q., & Sheng, D. H. (2018). Genome editing in model strain myxococcus xanthus DK1622 by a site-specific Cre/loxP recombination system. *Biomolecules*, *8*(4). https://doi.org/10.3390/biom8040137

Yankovskaya, V., Horsefield, R., Törnroth, S., Luna-Chavez, C., Miyoshi, H., Léger, C., Byrne, B., Cecchini, G., & Iwata, S. (2003). Architecture of succinate dehydrogenase and reactive oxygen species generation. *Science*, *299*(5607), 700–704. https://doi.org/10.1126/science.1079605

Yu, R., & Kaiser, D. (2007). Gliding motility and polarized slime secretion. *Molecular Microbiology*, *63*(2), 454–467. https://doi.org/10.1111/j.1365-2958.2006.05536.x

Yu, Z., An, B., Ramshaw, J. A. M., & Brodsky, B. (2014). Bacterial collagen-like proteins that form triple-helical structures. *Journal of Structural Biology*, *186*(3), 451–461. https://doi.org/10.1016/j.jsb.2014.01.003

Zeytuni, N., & Zarivach, R. (2012). Structural and functional discussion of the tetra-trico-peptide repeat, a protein interaction module. In *Structure* (Vol. 20, Issue 3, pp. 397–405). https://doi.org/10.1016/j.str.2012.01.006

Zhang, X., & Bremer, H. (1995). Control of the Escherichia coli rrnB P1 promoter strength by ppGpp. *Journal of Biological Chemistry*, *270*(19), 11181–11189. https://doi.org/10.1074/jbc.270.19.11181

Zhang, Y., Franco, M., Ducret, A., & Mignot, T. (2010). A bacterial ras-like small GTP-binding protein and its cognate GAP establish a dynamic spatial polarity axis to control directed motility. *PLoS Biology*, *8*(7). https://doi.org/10.1371/journal.pbio.1000430

Zhang, Y., Guzzo, M., Ducret, A., Li, Y.-Z., & Mignot, T. (2012). A Dynamic Response Regulator Protein Modulates G-Protein–Dependent Polarity in the Bacterium Myxococcus xanthus. *PLoS Genetics*, *8*(8), e1002872. https://doi.org/10.1371/journal.pgen.1002872

Zieske, K., & Schwille, P. (2014). Reconstitution of self-organizing protein gradients as spatial cues in cell-free systems. *ELife*, *3*, e03949. https://doi.org/10.7554/eLife.03949

Zuckerman, D. M., Boucher, L. E., Xie, K., Engelhardt, H., Bosch, J., & Hoiczyk, E. (2015). The Bactofilin Cytoskeleton Protein BacM of Myxococcus xanthus Forms an Extended β-Sheet Structure Likely Mediated by Hydrophobic Interactions. *Plos One*, *10*(3), e0121074. https://doi.org/10.1371/journal.pone.0121074